# Investigation of Methods and Metrics

# for

# Improved Benchmarking of Photocatalytic Carbon Dioxide Reduction

Elizabeth Rose Bache Bay

Submitted for the degree of Doctor of Philosophy

Heriot-Watt University

School of Engineering and Physical Science

November 2017

# ABSTRACT

Solar fuel production utilizing carbon dioxide through the process of photocatalysis is an attractive method to sustainably generate energy carriers. Research into photocatalytic $CO_2$ reduction has however been challenged by low conversion. To enable progress, this thesis works through the challenges of benchmarking, to address experimental conditions and results reporting. Starting with a literature survey to identify parameters affecting photoreduction, and assess key terms reported, crucial challenges are isolated. These challenges are limited benchmarking, experimental standardization, and the dual term challenge. Terms are proposed to address critical limitations in data interpretation, and a list is proposed for benchmark-necessary reporting. Two sets of identical experimental condition tests were conducted focusing on gas phase experiments conducted with titanium dioxide-based photocatalysts, with commercially available catalysts, including an anatase $TiO_2$, P25, and Mirkat 211, and modified samples, including doping, structure order, and calcination. To investigate metrics comparisons Mirkat 211 and Au doped $TiO_2$ are explored further for interaction effects and regime identification with the results analyzed three ways: through unitary product formation, photonic yield, and an extended rate normalization. Benchmarking of the Mirkat 211, through single variable experiments, and Au doped $TiO_2$, through a design of experiments, is assessed as compared to the existing literature. In conclusion, the importance of greater context of regimes is emphasized, identification of the importance of the reaction length, irradiance, and catalyst loading experimental variables is ranked, the catalytic versus photonic quantification compared, and recommendations for improving the experimental set up and necessary experimental reporting for photocatalysis are given.

# DEDICATION

This thesis is dedicated

To my Mother,

for encouraging me even though I was far from home.

And to my Father,

for every time I was given the weekly Science section of the LA Times.

# ACKNOWLEDGEMENTS

My deep gratitude goes to the Institute of Mechanical, Process and Energy Engineering [IMPEE] and the school of Engineering and Physical Sciences [EPS] for the Fees Only Scholarship, and to the Center for Innovation in Carbon Capture and Storage [CICCS] (recently renamed the Research Centre for Carbon Solutions [RCCS]) for enabling my research.

My most sincere appreciation goes to my primary supervisor Prof. Mercedes Maroto-Valer for her guidance, insight, and for the privilege of this amazing opportunity. My other supervisors have also been crucial to my progress; Dr. Jan-Willem Bos for his willingness to discuss the more abstract questions of PhD completion, Dr. Eva Sanchez Fernandez for her extensive expertise, clarity, and drive.

Thank you, thank you to Alberto Olivo and Warren Thompson. You both have wonderful PhD work ahead of you and I hope you can give it all your brilliance.

Thanks Dr. Oluwafunmilola Ola for her aid with the MS and testing rig and day-to-day operations. And gratitude to Yolanda Fernandez Diez for support, enthusiasm, and discussion.

I thank Curtis L. Abbott and Richard Kinsella for substantial technical support with gases and rig construction.

Thank you to my amazing editors and crucial companions on the way; Muhammad Farooq, Joy Godfrey and Ann Forsyth.

My overwhelming gratefulness goes to everyone in the CICCS team for always being willing to discuss research and analytical issues and having a wealth of helpful suggestions and tips. Thank you my friends. Thank you Luc.

Thank you Gutowski for encouragement in the direction of the pursuit of a PhD and the logic to motivate. And to Keane for the brilliant Master's Viva that challenged me to go further.

My thanks also to everyone on the Athena SWAN EPS self-assessment team and my Mechanical Engineering Tutoring students for both giving me hope and energy to show up and do the work.

Thank you Rosie.

Thank you to my family. Kathryn, thank you for checking in and making sure I got that full first draft done, Christopher, Alexander, Christopher and Theodore, Sara and Stephen, Annette and Andy and Nick, Eleanor and Michael, Dorothy and Rodney, and all the people who hold me up with love.

And always Jonathan, who chose me. I wouldn't have made it here without you.

In my Mother's words: "Dear God, thank you for the gift of memory so that we can know history. Thank you for the gift of reason so that we can understand how things work. Thank you for feelings so that we can know what is important. Thank you, God, for these gifts that bring us closer to you."

# DECLARATION STATEMENT

ACADEMIC REGISTRY
**Research Thesis Submission**

| | | | |
|---|---|---|---|
| Name*:* | Elizabeth Rose Bache Bay | | |
| School/PGI: | EPS | | |
| Version: *(i.e. First, Resubmission, Final)* | Final | Degree Sought: | PhD, Chemical Engineering |

**Declaration**

In accordance with the appropriate regulations I hereby submit my thesis and I declare that:

1) the thesis embodies the results of my own work and has been composed by myself
2) where appropriate, I have made acknowledgement of the work of others and have made reference to work carried out in collaboration with other persons
3) the thesis is the correct version of the thesis for submission and is the same version as any electronic versions submitted*.
4) my thesis for the award referred to, deposited in the Heriot-Watt University Library, should be made available for loan or photocopying and be available via the Institutional Repository, subject to such conditions as the Librarian may require
5) I understand that as a student of the University I am required to abide by the Regulations of the University and to conform to its discipline.
6) I confirm that the thesis has been verified against plagiarism via an approved plagiarism detection application e.g. Turnitin.

* *Please note that it is the responsibility of the candidate to ensure that the correct version of the thesis is submitted.*

| | | | |
|---|---|---|---|
| Signature of Candidate*:* | | Date: | |

**Submission**

| | |
|---|---|
| Submitted By *(name in capitals):* | ELIZABETH ROSE BACHE BAY |
| Signature of Individual Submitting: | |
| Date Submitted: | |

**For Completion in the Student Service Centre (SSC)**

| | | | |
|---|---|---|---|
| Received in the SSC by *(name in capitals):* | | | |
| Method of Submission (*Handed in to SSC; posted through internal/external mail*): | | | |
| E-thesis Submitted (***mandatory for final theses***) | | | |
| Signature: | | Date: | |

# TABLE OF CONTENTS

# LIST OF TABLES

# LIST OF FIGURES

# LIST OF ABBREVIATIONS

| | |
|---|---|
| Apparent quantum yield | AQY |
| Appearance potential soft ionization | APSI |
| Atmospheric mass | AM |
| Brunauer-Emmett-Teller | BET |
| Carbon dioxide Capture and Storage | CCS |
| Carbon dioxide Capture and Utilization | CCU |
| Carbon dioxide equivalent | $CO_2e$ |
| Centre for Innovation in Carbon Capture and Storage | CICCS |
| Conduction band | CB |
| Design of Experiments | DoE |
| Diffuse reflectance infrared Fourier transform spectroscopy | DRIFTS |
| Electron paramagnetic resonance | EPR |
| Electron volt | eV |
| Evaporation induced self assembly | EISA |
| Fourier transform infrared spectroscopy | FTIR |
| Gas chromatography | GC |
| Incident photo to charge carrier energy | IPCE |
| Intergovernmental Panel on Climate Change | IPCC |
| Internal quantum efficiency | IQE |
| International Union of Pure and Applied Chemistry | IUPAC |
| Kubelka-Munk | KM |
| Layered double hydroxides | LDH |
| Mass Spectrometer | MS |
| Montmorillonite | MMT |
| Multiple ion detection | MID |
| Parts per million | ppm |
| Parts per million by volume | ppmv |
| Photoreduction quantum efficiency | PQE |
| Quantum efficiency | QE |
| Quantum yield index | QYI |
| Quartz inert capillary | QIC |

| | |
|---|---|
| Scanning tunneling microscopes | STM |
| Secondary electron multiplier | SEM |
| Turn over frequency | TOF |
| Turn over number | TON |
| Turn over productivity | TOP |
| Two dimensional | 2D |
| Ultra violet | UV |
| Ultra violet and visible spectrometry | UV-vis |
| United Kingdom | UK |
| United States of America | USA |
| Valence band | VB |
| Volumetric rate of photon absorption | VRPA |

# LIST OF SYMBOLS

| Name | Symbol |
|---|---|
| Absorbed radiant density | $\langle L^{a}_{p,\lambda}(t)\rangle_V$ |
| Activation energy | $E_t$ |
| Adsorption constant of binding constant | K |
| Angstrom | Å |
| Apparent activation energy | $E_a$ |
| Apparent conversion | $X^A$ |
| Apparent quantum yield | AQY |
| Area of light irradiation | $A_{proj}$ |
| Cell potential | E |
| Chemical reaction rate | $r_c$ |
| Concentration | C |
| Conversion | X |
| Damköhler number I | Da |
| Damköhler number II | DaII |
| Electron /trapped electron | $e^-$ / $e^-_{tr}$ |
| Experimental reaction rate | R |
| Faraday's constant | F |
| Gibbs free energy | ΔG |
| Heat of adsorption | $Q_a$ |
| Heat of desorption | $Q_p$ |
| Hole/ trapped electron | $h^+$ / $h^+_{tr}$ |
| Incident light intensity or irradiance | $I_{int}$ |
| Initial concentration | $C_o$ |
| Interfacial area | a |
| Kinetic constant | $k_C$ |
| Limiting reagent concentration | A |
| Mass transport reaction rate | $r_M$ |
| Number of electrons | $n_e$ |
| Optimum mass | $m_{opt}$ |

| | |
|---|---|
| Photon efficiency | $\xi$ |
| Photon flow in reaction medium | $q_{\rho,\lambda}$ |
| Photon flow within photocatalyst | $q^{a}_{\rho,\lambda}$ |
| Photoreduction quantum efficiency | PQE |
| Plank's constant | h |
| Product distribution | $ |
| Quantum efficiency | $\Phi(\Delta\lambda)$ |
| Quantum yield | $\Phi$ |
| Quantum yield index | QYI |
| Radiation chemical yield | G |
| Rate constant | k |
| Reaction order | n |
| Reaction rate | r |
| Residence time | $\tau$ |
| Selectivity | S |
| Spectral photon flux | $q^{0}_{n,\rho,\lambda}$ |
| Speed of light | c |
| Turn Over Frequency | TOF |
| Turn Over Number | TON |
| Unitary production | $U_P$ |
| Unitary productivity | $\dot{U}_p$ |
| Volume | V |
| Wavelength | $\lambda$ |
| Yield | y |

# LIST OF PUBLICATIONS BY THE CANDIDATE

## Presentations at conferences/meetings:

E. R. B. Bay, M. Maroto-Valer, 3rd UK Solar Fuels Network Symposium, "Understanding of photocatalytic reduction of carbon dioxide in context of reactor design", January 2015, Heriot Watt University, Edinburgh, UK

E. R. B. Bay, O. Ola, M. Maroto-Valer, 13th International Conference on Carbon Dioxide Utilization, "Normalization of product results in photocatalytic reduction of $CO_2$", July 2015, University Town National University of Singapore, Singapore

E. R. B. Bay, M. Maroto-Valer, Chemistry in Energy Conference, "Challenges and Solution Strategy in Photocatalytic Reduction of $CO_2$", July 2015, Heriot Watt University, Edinburgh, UK

E. R. B. Bay, O. Ola, J-W.G. Bos and M. Maroto-Valer, 3rd IMPEE Conference Competition, "How did the Material perform? Normalization of photocatalytic reduction of $CO_2$", August 2015, Heriot Watt University, Edinburgh, UK

E. R. B. Bay, O. Ola, J-W.G. Bos and M. Maroto-Valer, Carbon Dioxide Utilisation Faraday Discussion "Understanding factors affecting products formation in photocatalytic reduction of carbon dioxide" (poster), September 2015, University of Sheffield, Sheffield, UK

A. Olivo, E. R. B. Bay, W. Thompson, E. Sanches Fernandes, R. Trofimovaite, S. Kumar, A. F. Lee, M. Maroto-Valer, 14$^{th}$ International Conference on Carbon Dioxide Utilization, "Solar Fuels from Photocatalytic Reduction of $CO_2$ *via* Engineering Innovation", September 2016, University of Sheffield, Sheffield, UK

A. Olivo, E.R.R. Bay, E. Sanchez Fernandez, W. Thompson, M. Maroto-Valer, E. Ghedini, M. Signoretto, 4th IMPEE Conference Competition, "The search for the golden age of $CO_2$ photoreduction", September 2016, Heriot Watt University, Edinburgh, UK

W. Thompson, E.R.B. Bay, E. Sanchez Fernandez, M. Maroto-Valer, A. Olivo, 4th IMPEE Conference Competition, "Reactor design, kinetics and process optimization towards solar fuels", September 2016, Heriot Watt University, Edinburgh, UK

A. Olivo, E. R. B. Bay, W. Thompson, E. Sanches Fernandes, E. Lesnik, X. Luo, M. Maroto-Valer, CRITICAT Advanced Photocatalysis Workshop, "Solar Fuels from Photocatalytic Reduction of $CO_2$ *via* Engineering Innovation", December 2016, Heriot Watt University, Edinburgh, UK

E. Sanchez Fernandez, W. Thompson, X. Luo, E. R. B. Bay, A. Olivo and M. M. Maroto-Valer, 15$^{th}$ International Conference on Carbon Dioxide Utilization, "The impact of kinetics on catalysts benchmarking in $CO_2$ photo-reduction", July 2017, Shanghai Advanced Research Institute of Chinese Academy of Sciences (SARI-CAS) and ShanghaiTech University (ShanghaiTech), Shanghai, China.

A. Olivo, M. Signoretto, E. R. B. Bay, W. Thompson, M. Maroto-Valer, "$CO_2$ conversion to solar fuels: importance of reaction conditions for significant assessment of photocatalytic performances", August 2017, Proceeding of EUROPACAT 2017, Florence, Italy.

# CHAPTER 1 – INTRODUCTION

This chapter discusses the challenges of climate change that give impetus to reducing carbon dioxide ($CO_2$) emissions and targets for future $CO_2$ atmospheric concentrations (section 1.1). Some strategies to reduce $CO_2$ emissions are considered including Carbon dioxide Capture and Storage (CCS) and Carbon dioxide Capture and Utilization (CCU). Various utilization options are considered with photoreduction having potential for energy savings (section 1.2). This chapter introduces and explains the particular concern of results comparison for $CO_2$ photoreduction, as it potentially hinders the progress in this field by not enabling benchmarking across laboratory analysis (section 1.3). To demonstrate how this thesis addresses the challenges of benchmarking the aim and objectives are laid out followed by the thesis structure (section 1.4).

## 1.1 The challenge of climate change, 2050 Targets and Energy Security

The greenhouse effect is caused by solar radiation's absorption by specific gases in Earth's atmosphere. This absorbed radiation is dissipated as heat. Heat, from solar radiation, is retained by the atmosphere, as seen in Figure 1.1. The radiation interacts with the atmosphere with various wavelengths being reflected, and other wavelengths absorbed, and energy being transferred to water, atmosphere, and the earth surface (Figure 1.1). This heat is natural and necessary to sustain life on earth; however, anthropogenic contributions to the concentration of greenhouse gases are causing widespread environmental changes. Current human activities that increase $CO_2$ levels center on combustion of fossil fuels for transport and industry. Other anthropogenic sources of greenhouse gases include agriculture, deforestation, fossil fuel production, industrial processes, water treatment and wastewater [1]. As of 2010 the breakdown of global greenhouse gas emissions by economic sector suggested transportation at 14% of emissions, energy and heat production at 35%, industry 21%, agriculture forestry and land use 24%, and buildings contributing 6% of emissions [1].

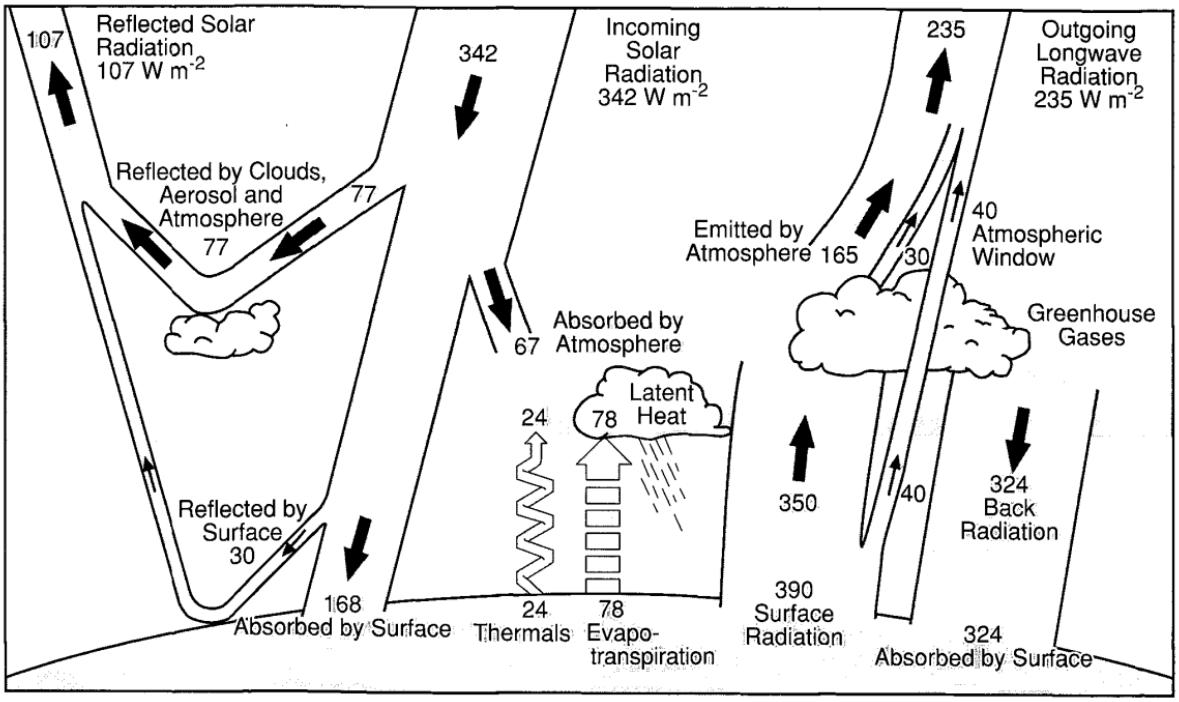


Figure 1.1 The greenhouse gas effect from back radiation, with the larger radiation and energy balance including reflection and latent heat, from Trenberth *et al.* [2].

The impacts of climate change that are of greatest concern include changes in local temperatures, rainfall patterns, sea water levels and extreme weather patterns resulting in floods and droughts [1, 3]. Thus, there is motivation to move towards the reduction in the use of fossil fuels and the development of smart technologies to overcome traditional fuels utilization drawbacks. A focus is made on $CO_2$ as it is often the largest component of greenhouse gases produced, and thus, has the largest climate change impact.

An example of the distribution of greenhouse gas sources is given using the greenhouse gas emissions for the UK in 2015. For the UK, the total emissions for 2015 were 495.7 million metric tons $CO_2$ equivalent ($CO_2e$, which is the global warming impact of any gas in terms of amounts of $CO_2$ which would have the same heating potential) [4]. Reducing $CO_2$ emissions is the focus of a large amount of legislation, global agreements, and research. However, to effectively reduce the threat of climate change legislation requires widespread action and the use of operative research.

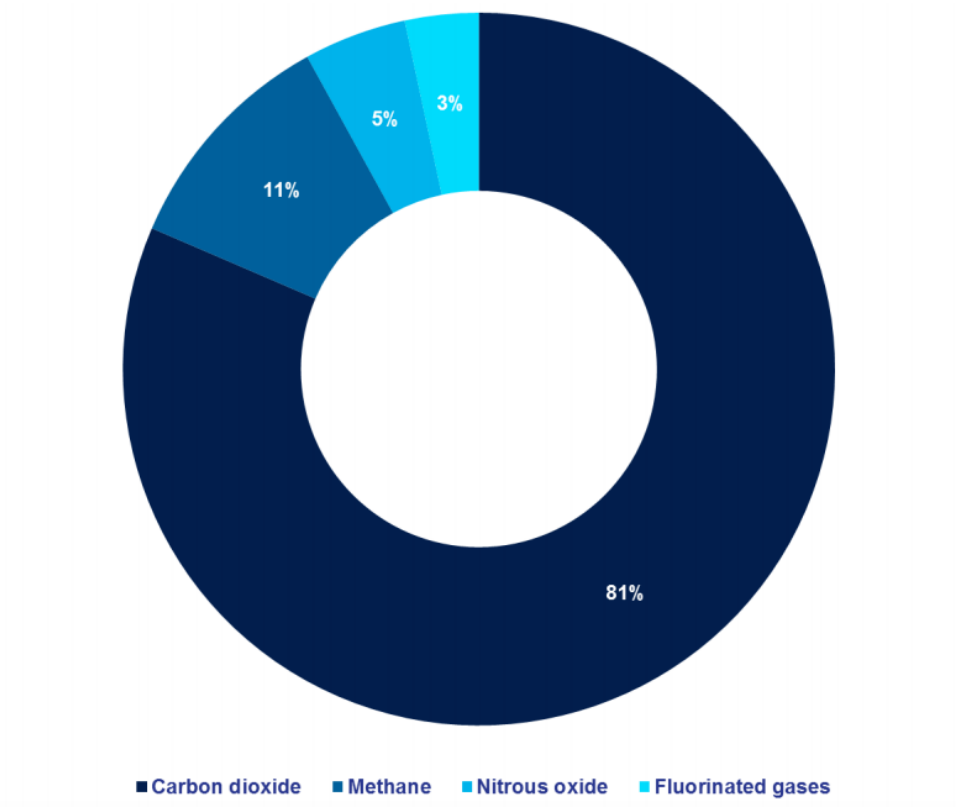


Figure 1.2 The composition of total gas emissions that contribute to climate change, produced in 2015 by the UK from [4].

The second largest produced gas in Figure 1.2 is methane, which is roughly 26 times as effective at absorbing infrared (IR) radiation as $CO_2$, however, with shorter lifetimes [5]. Methods for methane gas collection for emissions reduction are particularly attractive as methane can be utilized as a fuel. Methane utilization includes human and animal waste management and landfill gas capture for electricity generation [6-8]. This methane has been temporarily diverted from the atmosphere, reducing climate change impacts. The success of such projects coupled with the increasing cost of the environmental impacts of fossil fuels may increase the demand for sustainably sourced methane.

Looking globally at $CO_2$ emissions, it can be seen in Figure 1.3 that global emissions from fossil fuel and industry are growing and that the majority of these emissions are coming from coal and oil, with the USA having a disproportionately large

per person figure for emissions relative to the rest of the world. It is also noteworthy that the emissions in China have grown substantially since the early 2000's.

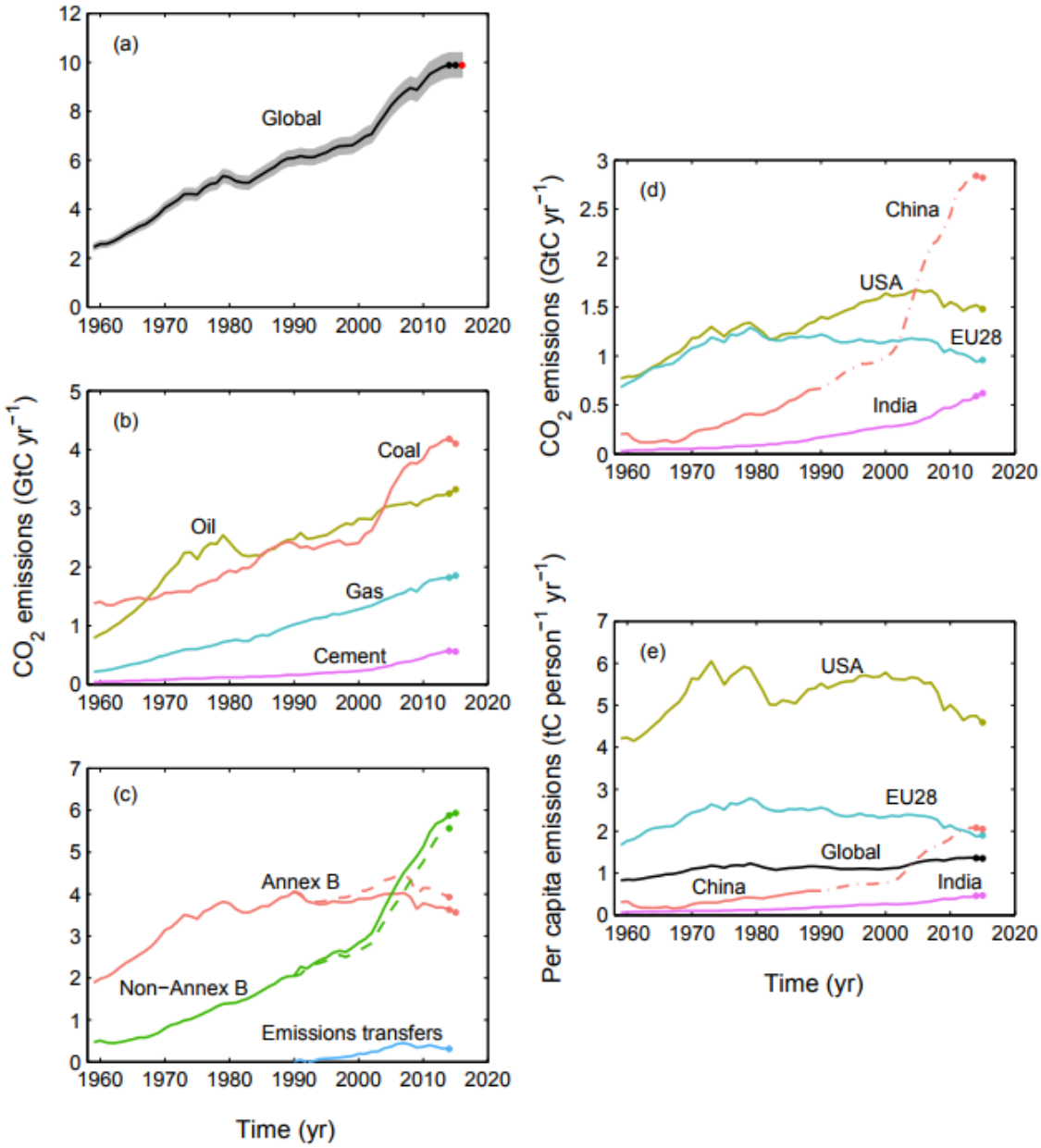


Figure 1.3 Fossil fuel and industry $CO_2$ emissions viewed in various ways; (a) the emissions global total including uncertainty shaded in grey (±5%) with a Gross Domestic Product projection (red dot) to 2016, (b) fuel type make up of global emissions, (c) emissions based on the Annex designation of the Kyoto Protocol with territorial emissions a solid line, consumption emissions a dashed line and the transfer of emissions from non-Annex B to Annex B countries at the bottom, (d) shows the territorial $CO_2$ emissions for the European Union and the 28 countries represented as of 2012, and the top three emitters by country: the USA, China, and India and plot (e) gives the previous territorial emissions with the Global emissions as a per capita figure [9].

The rising concerns over the pace and effectiveness of current measures to limit climate change are caused by the growing cognizance of the ongoing repercussions of current emissions. A temperature rise of 1.5°C was agreed upon as the goal for limiting

warming by the Paris Agreement. This is a significant change from the 2°C goal, as mentioned in the Copenhagen Accord in 2009 [10]. Only one degree of temperature rise is available to stay within agreed limits, as there is roughly a 0.5°C temperature increase documented for the early 2000's, as shown in Figure 1.4 [11]. Considering the 1.5°C expected temperature rise in relation to $CO_2e$ emissions, stabilization at 450 parts per million by volume (ppmv) $CO_2e$ greenhouse gas concentrations in the atmosphere has been found to offer a 46% chance of not exceeding 2°C rise in global temperature [12-14]. Hansen and colleagues would argue that a level of 350 ppm $CO_2$ is necessary to maintain relative equilibrium in earth's climate; however, this does not quantify the impact of non-$CO_2$ greenhouse gases [15]. The comparison of temperature, and then conflation of $CO_2$ and $CO_2e$ emissions concentrations, complicates political discussions. For a broader approach, Anderson and Bows compare the timing of the emissions peaks and intensity of emissions reduction programs and predicted concentration stabilization. This gives insight on the timing and ability to stabilize the greenhouse gas concentrations in the atmosphere [12]. For example, they discuss a scenario with an emissions peak in 2020, requiring either stabilization at 550 or 650 ppmv $CO_2e$ that would require annual reductions of 6% or 3% in overall emissions requiring 9% or 3.5% reductions in energy and process emissions, respectively. Both of these scenarios are not predicted to limit warming below 2°C. When taking into consideration that the Paris Agreement calls for peak emissions to occur as soon as possible and then net-zero emissions necessary in the second half of the century, there is a need for approximately 800 gigatons of $CO_2$ avoided emissions by 2050 to meet the International Energy Agency's two-degree scenario [16].

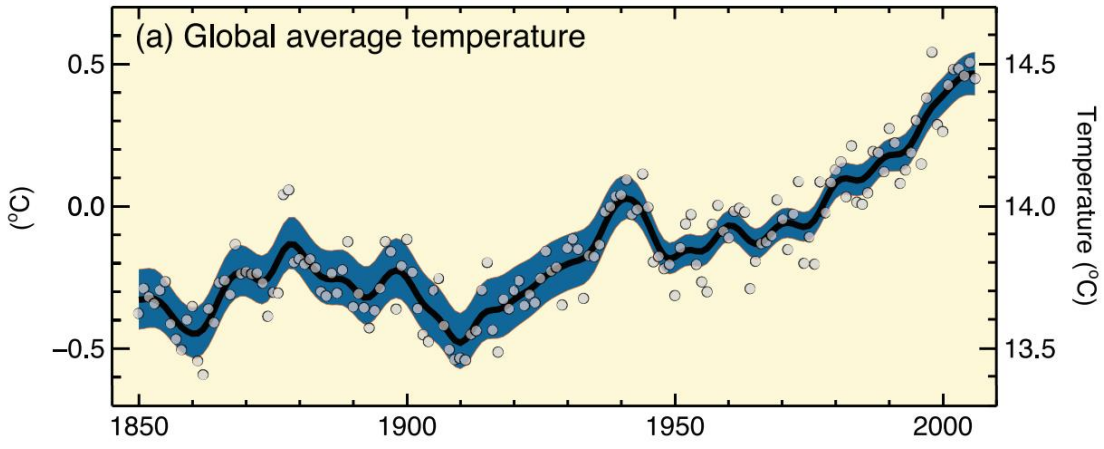


Figure 1.4 Global average surface temperature with circles being yearly values and smooth curves decadal averages, reproduced from Solomon *et al.* [11].

Rates of annual reduction in emissions in these headlines are not seen in our current economic structures unless they coincide with economic recession [17]. A similar reduction of 5.2% per year for a decade has only come from economic regression and output reduction, as seen in the Soviet Union [17]. These headlines suggest the immediate need for a robust response to the predicted future temperature increases. In the UK there are 4 year targets for emissions reductions; however, it is all predicated on net emissions being reduced, not eradicated, and the current legislation ends in 2027 [18].

Attempts to encourage action around $CO_2$ reductions include political targets. In the UK, as in other developed countries, legislation aims to reduce the amount of $CO_2$ released to the atmosphere, for example, the UK's greenhouse gas emissions target of at least an 80% reduction (from the 1990 baseline) in emissions by 2050. The EU targets include a goal of 20% emissions cut by 2020 and a similar reduction of 80-95% by 2050 as compared to 1990 levels [18]. One approach in achieving these emission reduction targets is to utilize greater capacity of renewable energy.

David MacKay, Chief Scientific Advisor to the UK Department of Energy and Climate Change 2010-2014, discussed the questions of energy consumption and energy supply. He made his comparisons by considering land areas of various countries. Figure 1.5 shows graphically the issues of sourcing energy with increasing demand and is a reminder of the necessity for a multiplicity of solutions to the climate change challenge. The premise is that the area available to the population is also the area that energy would be sourced from. Therefore, renewable energy options are viable only if they provide the energy density required by the population in their available area. This figure also shows that countries are increasing demand for energy over time, as population densities increase and energy consumption per person increases.

In Figure 1.5 the point size for a country is proportional to land area (except for areas less than 38000 $km^2$ (e.g. Belgium), which are shown by a fixed smallest point size to ensure visibility). Line segments to centers of circles show 15 years shift in position (from 1990 to 2005) for Australia, Libya, the USA, Sudan, Brazil, Portugal, China, India, Bangladesh, the UK and the Republic of Korea. The straight lavender lines with slope -1 are contours of equal power consumption per unit area, while the green lines show rough energy production numbers for different green energy options [19]. The significance of this graph is in pointing to challenges in supplying energy to meet demand, including the impact of local environment on renewable energy options. Renewables do not always produce the amount of energy they are rated to produce, due to shifting conditions, and thus, the plot should be a guide. This plot also does not address issues of energy storage.

There is a need for many solutions to the questions of energy sourcing and energy storage as populations and energy demand are not stagnant.

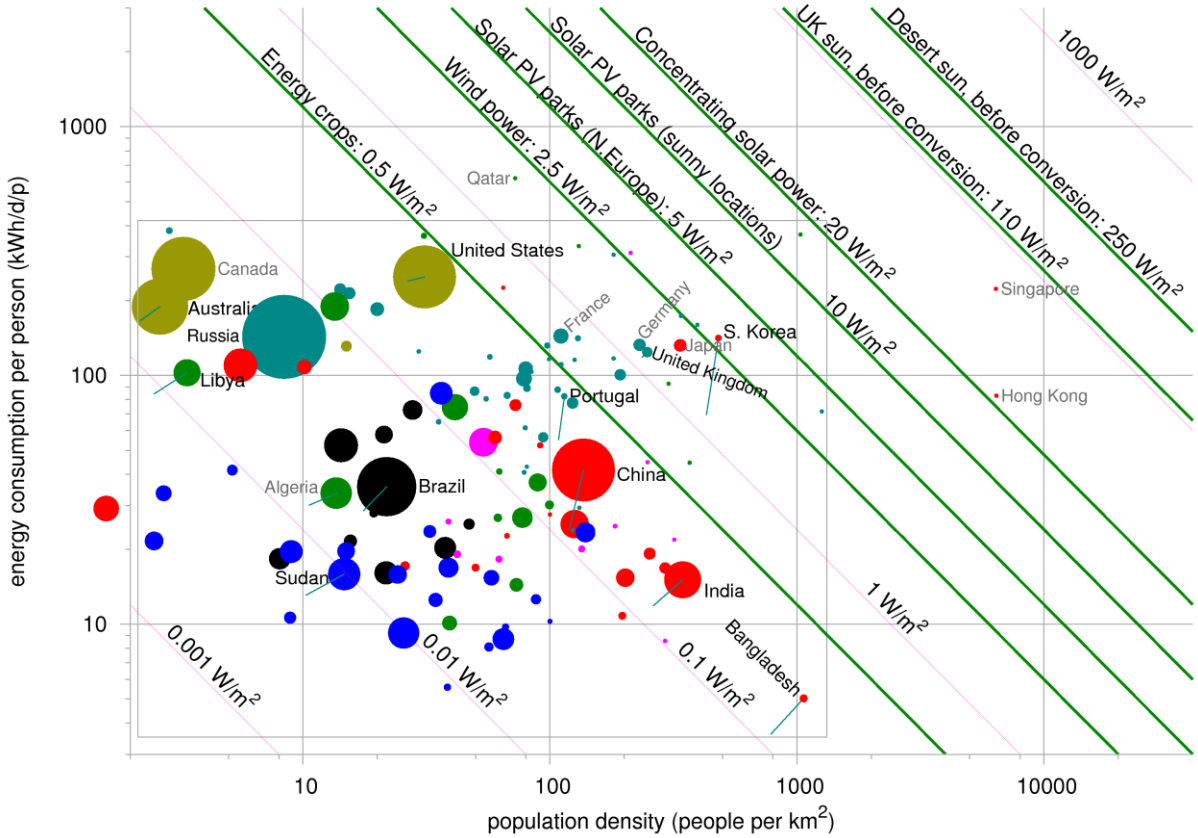


Figure 1.5 David MacKay's power consumption per person versus population density plot, in 2005 [19].

The complexity of balancing energy demand and energy consumption means that strategies for addressing climate change need to be robust and diverse. Strategies to reduce the emission of $CO_2$ and other greenhouse gases include increasing the energy efficiency of current technology and infrastructure, and low carbon technology such as renewable energy technology, for example photovoltaic and wind energy. In the energy sector, and for electricity production in particular, a shift to greater production from nuclear power and renewable energy sources is being pursued along with mitigation technology that captures carbon dioxide. Renewable energy from wind and solar are intermittent energy supplies and thus requires load shifting through demand side adjustments or energy storage for enabling supply side energy provisions. Hydropower is site dependent and limited by natural water cycles; however, it can be used by controlled deployment. Biomass suffers from a low energy density. Hydrocarbons as energy carriers remains preferable due to entrenched infrastructure investments making current energy production and industrial developments economically favorable. Therefore, progressing options of $CO_2$ storage or utilization becomes pragmatic.

### 1.2 Carbon Dioxide Capture and Utilization

Carbon dioxide Capture and Storage (CCS) has been a focus of the energy sector and is becoming a focus of the industrial sector when emissions cannot be avoided. To enable the industrial usage of fossil fuels without the release of $CO_2$, research and development have been oriented toward the capture of $CO_2$ and its long term storage. $CO_2$ capture is often limited to flue gases from large stationary sources of $CO_2$ such as power generation sites and cement manufacturing sites due to the difficulty of gas collection and separation from air. $CO_2$ capture has three main options available: pre-combustion, post-combustion or oxy combustion (Figure 1.6).

In pre-combustion processes, $CO_2$ is removed from the fuel through steam reforming, producing syngas. Post-combustion processes focus on removing $CO_2$ from the flue gas. Oxy combustion is a process where fuel is burned with pure $O_2$ often combined with $CO_2$ to moderate the combustion temperature and thus resulting in a higher concentration of $CO_2$ in the flue gas. The main focus has been on post-combustion processes that capture $CO_2$ through chemical absorption *via* scrubbers using aqueous amines or surface immobilized amines [20-22]. This is because to implement pre-combustion or pure oxy combustion requires a power plant to be built to accommodate the technology, whereas post-combustion can be retrofitted to existing plants.

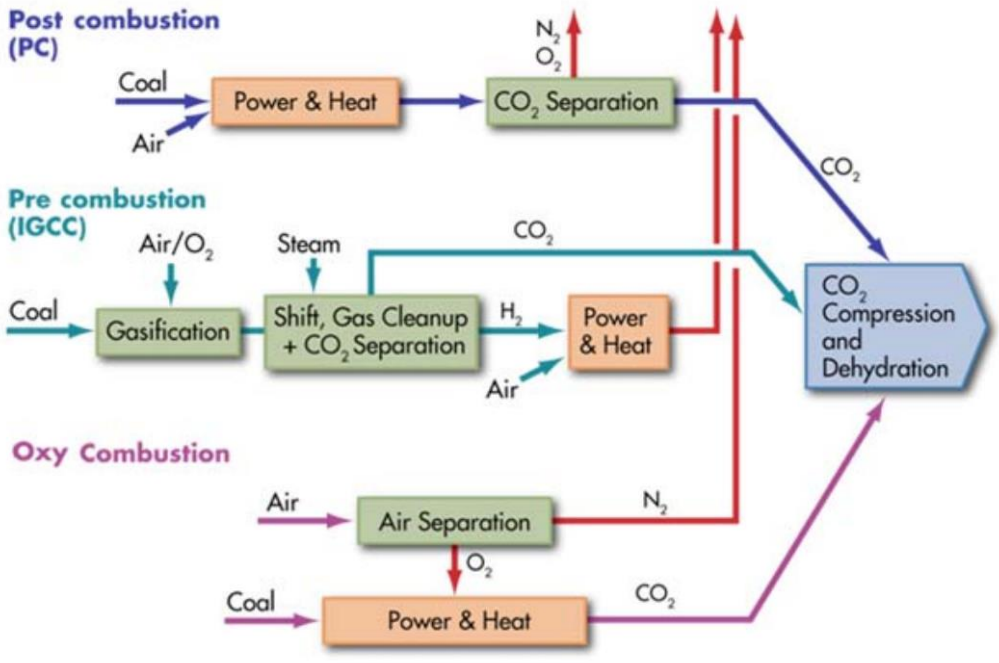


Figure 1.6 Schematic showing fuel and gas flows occurring in the three carbon capture processes from Global CCS Institute [23].

$CO_2$ capture introduces added costs to energy production. An increase in economic feasibility is pursued within Carbon Dioxide Capture and Utilization (CCU)

research. CCU takes the captured $CO_2$ and instead of this being transported for long term storage, the gas is used as a resource. Once purified, $CO_2$ can be used immediately for certain applications and in other cases is modified chemically or biologically.

$CO_2$ has many direct industrial uses for example within the food industry for carbonation in soft drinks, horticulture, and as a packaging gas, and within the energy industry for enhanced oil recovery, or as a chemical precursor for bulk chemicals, particularly in the production of urea, also as a protective gas in fire extinguishers [24]. It can even be used for refrigeration [25]. $CO_2$ can also be utilized through its conversion into carbon-based products. Products made from $CO_2$ include bulk and fine chemicals, solid inorganic and polymeric materials, hydrocarbons and fuels, as well as carbon-mineral oxides, such as $MgCO_3$ and $CaCO_3$ formed from reactions with silicates for use in building materials and permanent long term storage of $CO_2$ [25].

Due to the energy penalty of the incorporation of $CO_2$ into industrial processes (the replacement energy deriving mainly from fossil fuels) and the short timescales of $CO_2$ containment, with the exclusion of mineralization, utilization is not often considered to be of a large enough scale to address climate change $CO_2$ mitigation [25]. The Intergovernmental Panel on Climate Change (IPCC) roughly estimated the yearly turnover in industrial applications of $CO_2$ was 152.6 Mt per year [26], against 35.5 Gt $CO_2$ emissions per year [16]. CCS and CCU both reduce emissions, with the potential scale of storage and mineralization being large enough to coincide with continued fossil fuel usage. CCS has the potential for greater long-term storage and removal of $CO_2$ from the carbon cycle. CCU, on the other hand, has the potential for generating income to offset the investment necessary to employ capture technology.

In the case of fuels production, fossil fuels are still relatively abundant and low cost, therefore fuel from captured $CO_2$ needs to be converted utilizing an efficient, inexpensive process. Importantly, $CO_2$ utilization will also need to avoid net $CO_2$ emissions in order to be a viable technology of the $CO_2$ capture and $CO_2$ reduction processes. This requires the energy input in the reaction to come from renewable sources [26].

Hydrocarbons can also be produced from $CO_2$ through photocatalytic reactions, thermal hydrogenation, or electrochemical reduction, although these processes are not commercially viable yet [27]. There is also work being undertaken on photoelectrocatalytic reduction of $CO_2$ [28]. Each process, however, has its drawbacks: Hydrogenation and electrochemical reduction sacrifice energy either in the formation of $H_2$, or the use of electric current, which increases the energy consumption of these

processes [29, 30]. In particular, hydrogenation is unsustainable because it utilizes $H_2$ that is almost entirely (96%) produced from fossil fuel steam reforming, and work on bioethanol and bioglycerol steam reforming is not near commercialization [31, 32]. Electricity is still generated primarily from fossil fuels. Energy conversion processes are additional opportunities for energy loss due to inefficient conversion; therefore, the photoreduction process directly utilizing solar radiation is the preferred process to optimize for sustainability. This, along with cost competitive demands on solar fuels, makes photoreduction an attractive process. Song has estimated that an annual global demand for $CO_2$ for the production of chemicals and materials could be as much as 0.36-3.6 gigametric tons, and for synthetic liquid fuels 3.6-36 gigametric tones, comparable to over 25 gigametric tons of global emissions [24].

### 1.3 Artificial Photosynthesis and $CO_2$ Photoreduction

Photosynthesis is a vital natural process that converts $CO_2$ and water into oxygen and glucose [33]. On its own, photosynthesis is an effective and sustainable way to convert $CO_2$ into valuable products. However, in 1998 it was only capturing 30% of $CO_2$ emissions [34]. As fossil fuel energy sources are major causes of greenhouse gas emissions and $CO_2$ is the most widely produced greenhouse gas, it is immediately evident that increased photosynthesis is beneficial. There is also plenty of room in natural photosynthesis for improvement. The performance of chlorophyll is highly efficient in absorbing photons; however, the overall performance of photosynthesis is in the area of 4.6-6%, calculated based on the energy stored in biomass relative to the total initial solar energy incident. This can be seen in Figure 1.7, with only 46 and 60 kJ final energy being stored in plant mater from an initial 1000 kJ of energy from the sun. These numbers are specific to chloroplastic NADP-malic enzyme. As shown below in Figure 1.7, there is a variety of energy losses, from the inability of the active enzyme to absorb wavelengths outside the absorbance spectrum, to light reflection, and a large portion of energy is lost during carbohydrate synthesis. This carbohydrate synthesis process is the area in which photocatalysis could ideally improve upon nature. To obtain the numbers shown in Figure 1.7, Zhu, Long and Ort used a temperature of 30°C and atmospheric concentration of 380 ppm of $CO_2$ giving a theoretical maximum photosynthetic energy conversion [35].

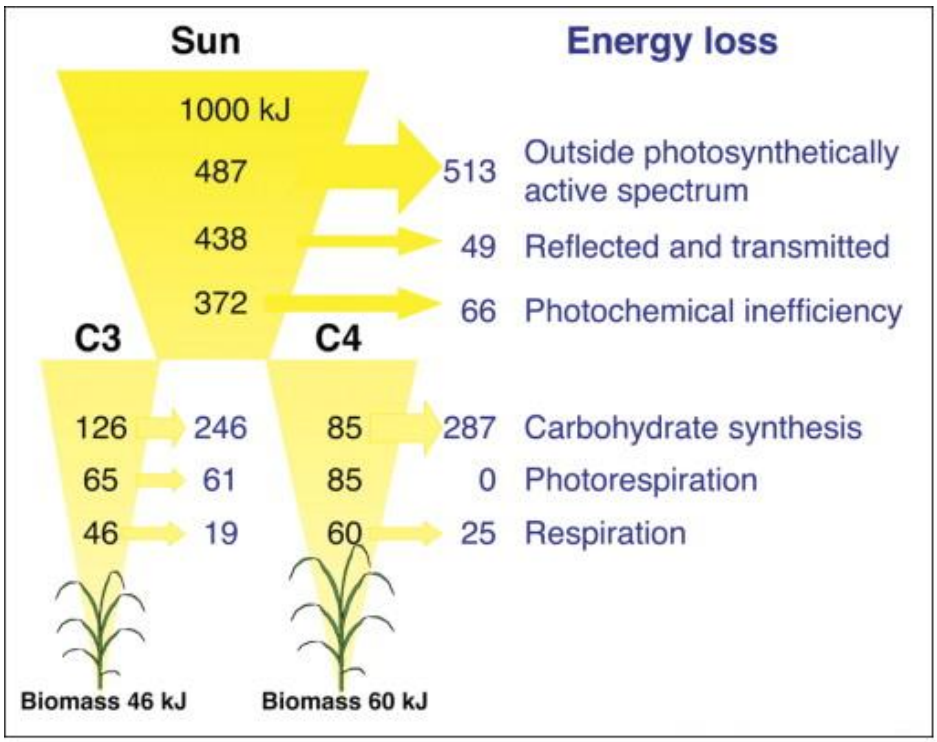


Figure 1.7 Energy losses in natural photosynthesis, particularly the energy loss in product synthesis resulting in the low energy efficiency of creating biomass from Zhu *et al.* [35].

Artificial photosynthesis builds on natural photosynthesis, attempting to produce industrially applicable and storable fuels. The complex activities completed in photosynthesis to convert $CO_2$ and $H_2O$ into molecules of growth have captivated people as they attempt to mimic the process, in particular with photocatalysis [36, 37]. The idea of artificial photosynthesis has been heavily linked to the production of hydrogen, however other fuels such as methanol, methane, alkanes, alcohols and aldehydes can be produced [27, 33, 38, 39]. Some success has been found with hybrid systems, for example Dan Nocera's artificial leaf produces various fuels and products including polyhydroxybutyrate (a biopolymer), isopropanol and alcohols at an efficiency of 10% with a pure $CO_2$ feedstock, and 3 to 4% using air [40]. The artificial leaf utilizes a water-splitting catalyst and hydrogen-oxidizing bacterium in aerobic conditions.

Natural photosynthesis and its analysis gives a place for artificial photosynthesis to start. In the case of photosynthesis, the tradeoff has been to facilitate a kinetically challenging electron build-up to enable a more thermodynamically favorable reaction and product formation. In one case, to facilitate this discussion, figures of the photosynthesis structure included bond distances and figures of the kinetics included charge transfer timings [41]. When this time scale view is considered for the recombination of excitons in $TiO_2$, with most charge carriers recombining within a nanosecond [42], it is clear that the charge carrier lifetimes need to be matched to the kinetics of the reaction for

photocatalytic $CO_2$ reduction to be successful. And Ohtani reinforces this point when he asserts that the reaction rate is governed by an unknown intrinsic rate of recombination [43].

Artificial photosynthesis, particularly photocatalytic $CO_2$ reduction, aims to improve the products available from the $CO_2$ reduction process. $CO_2$ photoreduction by means of photocatalysis consists of heterogeneous reactions under light illumination utilizing semiconductive materials. These reactions are conducted in various reactors either in gas or liquid phase. These reactions are performed using light driven catalysts that transfer energy necessary for $CO_2$ reduction. The current product results of these processes are low in the range of μmoles of products, such as 3 $\mu mol/g_{catalyst}$ of $CH_3OH$ [44], or 550 $\mu mol/g_{catalyst}$ $CH_4$ production observed [45]. Because artificial photosynthesis builds on natural photosynthesis, energy comparisons between the two can gauge improvement. To be able to compare the photocatalytic results to the efficiency of the photosynthesis process, the light energy input to the photocatalytic reaction testing would need to be known as well as the energy embodied in the products detected. The ability to calculate efficiency greatly benefits comparisons, even if it is understood that the energy necessary to promote the process is much greater than the energy embodied in the product [46]. Work has been conducted to assess the source of low production yields and explain the low efficiency observed, examples are discussed in the following paragraphs.

Ohtani found that the photo(electro)chemical reactions were driven by electrical or chemical bias and irreversible charge separation [47]. Low efficiencies may be a result of insufficient reaction driving force. Another concern is brought up by Yang and colleagues tracking the source of the carbon in the product gases, and thus acknowledging that the carbon can come from either the gas used for testing or impurities in the photocatalyst [48]. The way to address these concerns is through reporting detailed analysis of experimental considerations and results.

Kondratenko and associates asserted that there is a significant challenge to commercialize photocatalysis for $CO_2$ reduction, including the material efficiency and the reactor design [27]. Often confusion over results and reporting conversion measurements leaves photocatalysis open to unwarranted criticisms that would be avoidable with more thorough and thoughtful testing and reporting. As reporting of material efficiency is not consistent, comprehensive or normalized for the reactor design, one possibility to address the commercialization challenge would be insightful benchmarking. Therefore, a critical step to improve the efficiencies of catalyst performance will be through data and results

that are comparable. In this way, information can be better understood and utilized for improved photocatalyst design.

There is a wide range of opportunity going forward when the conditions of experimental work are understood. This includes the development of evaluation of mass transport in the photocatalytic reactor system [49, 50], assessment of capture and conversion using a single material [51-53], and eventually, life cycle analysis of the process [54, 55], considering purity of $CO_2$ feedstock, and realistic feedstock options along with selectivity for combustible gas outputs. Focusing on benchmarking and assessing results brings this work closer. In the work of photoreduction of $CO_2$ the connections between results and process are still being revealed.

### *1.3.1 Comparability of $CO_2$ photoreduction tests and limits on benchmarking*

Results of photocatalytic performance for the reduction of $CO_2$ are varied, with a multitude of units, as there is no agreed figure of merit. Current work appears to be focused on identifying material performance, with the hope that a high performance will then be taken up for commercial development. This work is important for screening materials, and has proven the $CO_2$ photoreduction process time and again. However, these results can limit wider comparison when terms are not standard and various information (for example, catalyst concentration and substrate to catalyst ratio) are omitted. To represent the concerns over the variation in reporting, two diverse examples are discussed below. In one case, the quantum efficiency and relative product yield rate are reported. In the other the most common reported result of product yield is reported. In trying to clarify and compare these samples crucial concerns are raised that apply to a large body of photocatalytic research.

The first example reviews results presented by Singh and colleagues [33]. They have investigated the band-gap energies of $TiO_2$ to yield selective products from tuning "the energetic alignment of band-edge states" [33]. Their work in identifying the density of states and photocatalytic activity through selectivity for $C_2H_6$ gave insight into origins of performance improvements. They tested a $TiO_2$ and copper indium sulfide [CIS] nanocrystal composite [33]. Their results were reported with a wider context and irradiance quantification that is uncommon, as illustrated in Figure 1.8, below.

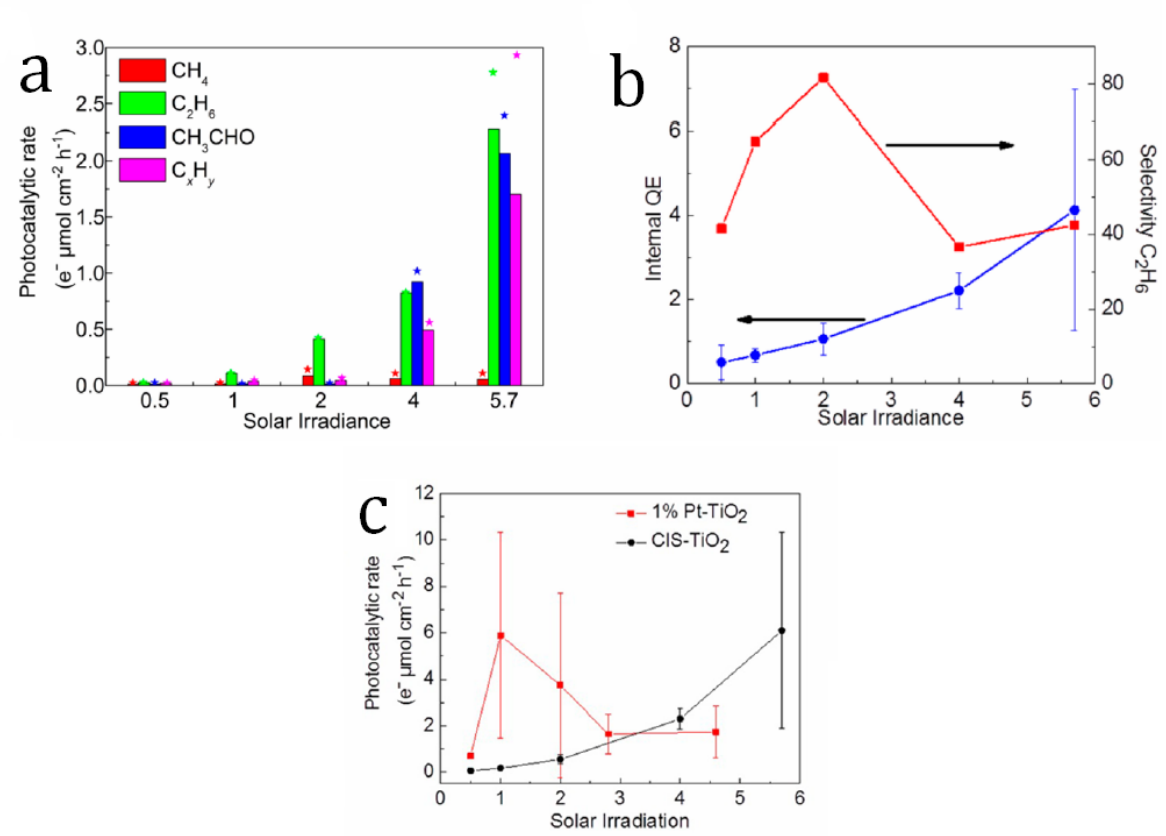


Figure 1.8 Results of photocatalytic reduction of $CO_2$ and water on a $TiO_2$ nanoparticles with copper-indium sulfide nanocrystals attached including a) chemical composition of products of photocatalytic process b) yields and selectivity of those products and c) the relationship between fuel production and rate of photogeneration from Singh *et al.* [33].

The second case is work done by Tahir and Amin on montmorillonite (MMT) layers dispersed in $TiO_2$ and the impact on photocatalytic performance [56]. They propose that the MMT shortens charge transport with adequate absorption and improved $TiO_2$ surface behavior [56]. Their tests were conducted with 20% MMT loading and reported in terms of amount of product detected normalized by amount of catalyst used and experiment time with typical units of µmole/gh.

As shown in Figure 1.8, internal quantum efficiency and selectivity for $C_2H_6$ are reported along with photocatalytic rate. These represent the light and catalytic performance of the material. This can be contrasted with the more common reported product formation in Figure 1.9. The largest difference that can be seen is that the photocatalytic rate from Singh's work included the electrons used for the formation of the products. This differs greatly from the product amounts themselves being reported by Tahir and Amin (Figure 1.9). Secondly, all the results reported by Singh are shown as a function of the solar irradiance and not as a function of time or amount of catalyst tested,

thus, highlighting the importance of the solar contribution to the photocatalytic process, that can be unintentionally omitted elsewhere.

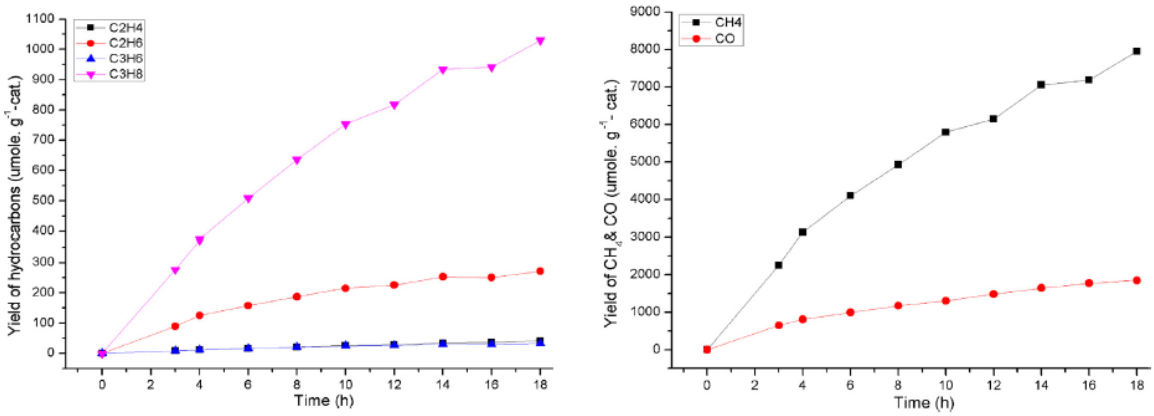


Figure 1.9 Results of photocatalytic $CO_2$ and water reduction conducted with a MMT loading of 20% in $TiO_2$ from Tahir and Amin [56].

The usage of a per area measurement by Singh is very different from a per amount of catalyst measurement that Tahir and Amin use. However, with appropriate catalyst dispersion data the units can be converted. This is hindered when incomplete reporting makes data conversion impossible. The challenge then becomes deciding what information it is necessary to be reported to enable meaningful comparisons across reactor systems and reaction conditions. As shown in Table 1.1 there is a wide range of terms and units currently in use. This view of the units and all the various related terms given in the table can be misleading as not all the terms quantify the same thing. With the percentage results the terms used calculate unique attributes of the process. For the μmole, and μmole derived results however, there is less distinction between the terms. Focusing on benchmarking is an opportunity to improve how results are presented, and many have highlighted the need for work on this challenge.

Table 1.1 Metric names and units from $CO_2$ photoreduction literature.

| *Metric Term* | *Units* |
|---|---|
| *Selectivity [33, 57-59], relative peak areas [60], quantum yield [58, 61], quantum efficiency [59], apparent quantum yield [62], conversion [57], molar balance [57], turn over productivity [58]* | % |
| *Internal Quantum Yield [33]* | Unit-less |
| *Product evolution amount [63], production of product [64]* | μmole, (nmole as corrected by surface area ratios [64]) |
| *Yield of product [65, 66], production [44, 61, 67, 68], yield [59, 62, 69], turn over number [70], amount evolved [71], concentration [72]* | μmole/g |
| *Amount evolved [71]* | μmole/$cm^2$ |
| *Product produced or photocatalytic activity [73]* | μmole/$m^2$h |
| *Yield of product [56], specific rate [74], yield rate [58, 59, 75], product yield [76], product rate [77], yield [78, 79], production rate [68, 80], production coefficients [72]* | μmole/gh |
| *Photocatalytic rate [33]* | $e^-$ μmole/$cm^2$h |
| *Yield [58, 59]* | ppm |

Benchmarking issues have been discussed in various literature reviews. Indrakanti *et al.* described it this way: "Although it would be more instructive to compare the conversion efficiencies and quantum yields of various $TiO_2$ –based catalysts, often such data is not readily available" [81]. The lack of data may be due to the complexity of testing the process as Dhakshinamoorthy *et al.* point out that "… the present situation in the field is confusing and it is difficult to compare the performances of difference catalysts due to the large variability in the type of light, pH of the solution, $CO_2$ pressure and other experimental conditions that determine the final productivity of the photocatalyst…"

[82]. The challenge may be finding an appropriate results term. Kondratenko *et al.* reiterate the challenge as; "Making a valid quantitative comparison of catalytic performance in $CO_2$ reduction is … difficult because of the following issues: 1… [A] large variety of illumination sources was used… 2. Another relevant parameter to evaluate photocatalytic performance is the effectivity of the catalyst to convert light into chemical energy" [27]. And more recently Chen *et al.* write; "To date, there is no standard protocol for evaluating photocatalytic performance, or single parameter that enables quantitative benchmarking of $CO_2$ conversion efficiencies to specific carbon-containing solar fuels or chemicals" [83].

Clearly the experimental process is complex and terms used to quantify the process are not evaluating the conversion of light energy to chemical energy in a clear way alongside assessing the rate of the reaction. These criticisms may come from the challenge of not being able to collate all relevant experimental conditions, an inability to identify and relate experimental causations to product formation, a limitation of current terms available to quantify the process, or further issues not yet identified. However, this challenge appears not to have been resolved. Value is seen in enabling benchmarking.

Recently Bligaard *et al.* published a perspective on benchmarking recommendations for four areas of catalytic research [84]. They were not able to focus on photocatalysis, however, they recognize a widespread need for agreed standards of quantitative comparison, and they encourage discussion and data sharing, and in particular assessing benchmarking tools. The benefits of improving benchmarking include "accelerating discovery, refining understanding, and promoting the application of better catalysts" [84]. Protocol development, reactor refinement, and standardization has also been addressed for photoelectrochemical water splitting [85-87]. And recommendations for the standardization of photocatalytic air purification have been discussed [88].

Benchmarking is the use of standard tests to compare performance between materials or the use of a standard material to compare performance between experimental systems. Currently the limit of benchmarking within $CO_2$ photoreduction has been the use of benchmarking materials like P25 or unmodified synthesized materials. However, the performance of the benchmarking materials varies, the full interaction of light with material and with reactor are not currently quantified, and the assessment of optimal reaction conditions is often limited or incomplete. Thus, a $CO_2$ photoreduction benchmarking discussion requires a wider scope.

### *1.3.2 Attempts to address benchmarking challenges*

Some contributions have been made to address $CO_2$ photoreduction benchmarking challenges in particular; These include a review article [81], International Union of Pure and Applied Chemistry (IUPAC) recommendations [89], and an article from editors outlining best practices [90]. This review article, [81], focuses on titanium based photocatalysts for $CO_2$ reduction, calls the product amount normalized by amount of catalyst used, and the length of the experiment (μmole/gh), specific rate (as opposed to product yield), and works towards understanding an economic goal for the material performance. However, it fails to bridge the gap between the experimental complexity, material intricacy, and reaction dynamics with a recommendation of a figure of merit.

IUPAC recommendations focus on the influence of light on nomenclature and how results should be reported (which is covered in more detail in Chapter 2). They propose four separate terms to quantify the light performance for various conditions. This, however, does not address issues around experimental setup and process to accompany the terminology recommendations, even as it builds on previous work clarifying quantum yields [91]. Buriak, Kamat, and Schanze, as editors, recommend good practice, and in particular connect terms such as efficient and efficiency to the lack of disclosure of experimental conditions and analytical data [90]. There appears to be a problem of naming and then integrating the appropriate complexity into reported results and experimental standards. These contributions do not address the benchmarking challenge because they do not identify the missing data or conditions necessary for benchmarking to be successful.

Other significant contributions to the benchmarking discussion on $CO_2$ photoreduction come from Herrmann [92] and Ohtani [43]. Both work at clarifying aspects of photocatalysis that impact the photoconversion. Herrmann's contribution to analyzing parameters that effect photoreduction is discussed in more detail in Chapter 2, section 2.7. And indeed, Ohtani covers a wide range of pertinent information from thermodynamics to kinetics to quantum efficiency. Ohtani goes so far as to articulate the problem anew, writing in the section on Activity, "Known: Rate of photocatalytic reactions under given conditions, i.e. relative photocatalytic activity and general empirical tends. Unknown: Intrinsic photocatalytic activity, overall kinetic equation, and true correlation between physical or structural properties and photocatalytic reaction rate." To start to tackle the challenge of finding the true correlation between the material attributes and photocatalytic reaction rate there needs to be more work understanding the photocatalytic experimental test. When it is appreciated that variability in light sources,

photocatalytic materials, and reactor designs are conflated in the results reporting, then the work of disentangling the influences of each can begin.

This thesis starts from the premise that the complexity of the problem is large enough to warrant serious consideration. Effort will be placed on being specific with variables and results in the complex $CO_2$ photoreduction system.

### 1.4 Aim and Objectives

The **aim** of this thesis is to improve $CO_2$ photocatalytic reduction research by addressing the issue of benchmarking results. This comparability is limited by unknown reaction conditions and hindered by unquantified reactor parameters. To address this challenge, this thesis aims to quantify the effectiveness of current benchmarking by comparing the variation of results from literature, with the variation of results that can be obtained in experimental conditions. In particular this thesis compares results from P25 and Au modified $TiO_2$ samples from literature with experimental results from Mirkat 211, a commercially available anatase $TiO_2$, and Au doped $TiO_2$, a highly promising modification [93]. With these results, this thesis tests the effectiveness of a newly proposed extended yield normalization for use as a singular figure of merit.

The **first objective** is to assess current understanding of results reporting and the context of the photocatalytic process, which generates these results. This objective includes in-depth understanding of the efficiency terms reported and results used to quantify the process. This allows for challenges to benchmarking to be identified as well as a consideration of the limitations of current practice.

The **second objective** is to quantify the current benchmarking with the comparison of two photocatalytic material performances, each varying experimental parameters. This thesis carries out two key pieces of work demonstrating the applicability of two tools: the statistical approach represented by the design of experiments; and the parameter based approach of testing regimes. This allows for exploration of the dual term challenge posed by quantifying the light and catalytic performance separately. And lastly, this thesis quantifies the current effectiveness of identical experimental condition bench-marking by comparing literature results ranges with results ranges that can be obtained with varying experimental conditions in the lab.

The first objective, to assess the current understanding of results reported and their context, is covered in Chapters 2 and 3 of this thesis. Chapter 2 focuses on materials

modifications research relative to a commercial standard or lab synthesized unmodified material in independent labs and the parameters affecting photoreduction. Therefore, Chapter 2 gives general background on photocatalysis and starts linking modifications to expected performance and results.

Chapter 3 builds on this work delving much deeper into the specific results reported and the specifics of the research conducted. This enables a larger challenge of figure of merit and necessary experimental conditions to be developed and considered, that may be difficult to recognize when immersed in materials improvement. Therefore, Chapter 3 goes further, giving specifics relevant to $CO_2$ photoreduction and the current reporting of the contexts that limit them. This starts the discussion of results gathering in the second objective with Chapter 3 also finalizing recommendations of results terms.

Then consideration turns to practical, lab-implemented, testing. The current form of benchmarking with identical experimental conditions and assessment of the results based on materials modifications is discussed, in Chapter 4, relative to the range of performance found in literature.

In Chapter 5, $AuTiO_2$ is investigated with a statistical approach of the design of experiments to observe interactions of reaction parameters. Results of Mirkat experiments in Chapter 6 follow a discussion and proposal of testing regimes that work through parameters as single variable variance experiments. Chapter 7 revisits the dual term challenge and benchmarking questions from a perspective of analyzing experimental results. The work presented confirms the influence of experimental regimes on results, highlights the importance of complete results processing, demonstrates a limited or "fuzzy" benchmark of Mirkat with $AuTiO_2$ and compares this to current benchmarking practice. Finally, conclusions are presented in Chapter 8, stressing agreeing procedure and relative parameter influence, the utility of the extended normalization, and conclusions about benchmarking in $CO_2$ photoreduction and photocatalysis.

# CHAPTER 2 – INTRODUCTION TO PHOTOCATALYSIS, CARBON DIOXIDE PHOTOREDUCTION, AND THE PARAMETERS AFFECTING PHOTOCONVERSION

In this chapter, the basics of photoreduction are laid out starting with the definition of photoreduction and thermodynamics of $CO_2$ reduction in section 2.1. The use of semiconductors for photocatalysis is discussed in section 2.2 focusing in on $TiO_2$ as a promising abundant material. Then materials modifications are reviewed in terms of improving $TiO_2$ performance in section 2.3 covering light response, hydrophobicity and charge carrier lifetimes. These materials modifications are discussed relative to the assessment of the performance improvement. This is followed by section 2.4 discussing photoreduction reaction mechanisms of $CO_2$. This chapter concludes with section 2.5 and parameters affecting $CO_2$ photoreduction and conversion to solar fuels are discussed, including catalyst loading, material properties and dispersion, along with the light provided to the reaction, reactor properties, and operating conditions including reactant concentrations, temperature and pressure. Section 2.6 concludes with a scope of study diagram linking the discussion to the thesis specifics.

## 2.1 $CO_2$ Photoreduction and Thermodynamics of $CO_2$ reduction

$CO_2$ photoreduction by means of photocatalysis was noted in literature in 1911, in an article discussing the light reaction in uranium salt and oxalic acid mixtures [94]. In 1921, an article about the synthesis of formaldehyde and carbohydrates from $CO_2$ and water was published also using the term photocatalysis. Interestingly, the article references previous research in a quest to understand photosynthesis [95]. Kondratenko and Indrakanti put the advent of photocatalysis in the 1970s [81], however Herrmann cites a Doerfler and Hauffe article printed in 1964 as the first reference [96] and more review into early photocatalysis has been conducted [97, 98].

Photoreduction is a term used to describe a light driven process for the reduction of a molecule or chemical compound, and in particular, $CO_2$ photoreduction refers to $CO_2$ reduction to C-based compounds, such as $C_1$ compounds (for example methane, methanol, methyl amines, formaldehyde, and formate) and $C_2$ compounds (for example ethanol, acetate, methylformate and acetaldehyde) [81, 99]. Attempts to improve photoreduction include using a photocatalyst.

Photocatalysis describes research on a light driven reaction in which a catalyst is used. Serpone and colleagues would describe photocatalysis as a process in which a material and photons accelerate a reaction without specification of mechanism [100]. This can be contrasted with catalysis, which specifies a thermodynamically favored reaction, however, kinetically slow, with improved kinetics through use of a catalyst [101]. However, in the case of photocatalysis, the reaction does not need to be thermodynamically favorable, as the photons provide energy to the reaction. The photoconversion of $CO_2$ is a many step reaction process where the specific mechanism, and particularly reaction intermediates, are still being discovered and further consensus on the fundamental reaction pathways is necessary. This has led to the use of the term "photocatalysis" regardless of specific reaction mechanisms [101].

To enable the photoreaction of $CO_2$ with water the assistance of a photocatalytic material and the input of solar energy radiation is required due to $CO_2$ being a highly stable molecule, as shown in Figure 2.1 below. Thermodynamics are seen from the Gibbs free energy of the reaction, where a negative Gibbs free energy implies that the reaction will proceed, also referred to as a spontaneous reaction [47]. $CO_2$ has a large negative Gibbs free energy [$\Delta G^o$] as compared to $CH_4$, which means that the former requires a larger energy input to be decomposed. If looking at the difference in Gibbs free energy, there needs to be a 444.7 kJ/mol input of energy to move from $CO_2$ to $CH_4$ on the chart, which is calculated without considering the source and energy necessary to "acquire" four H atoms from water splitting.

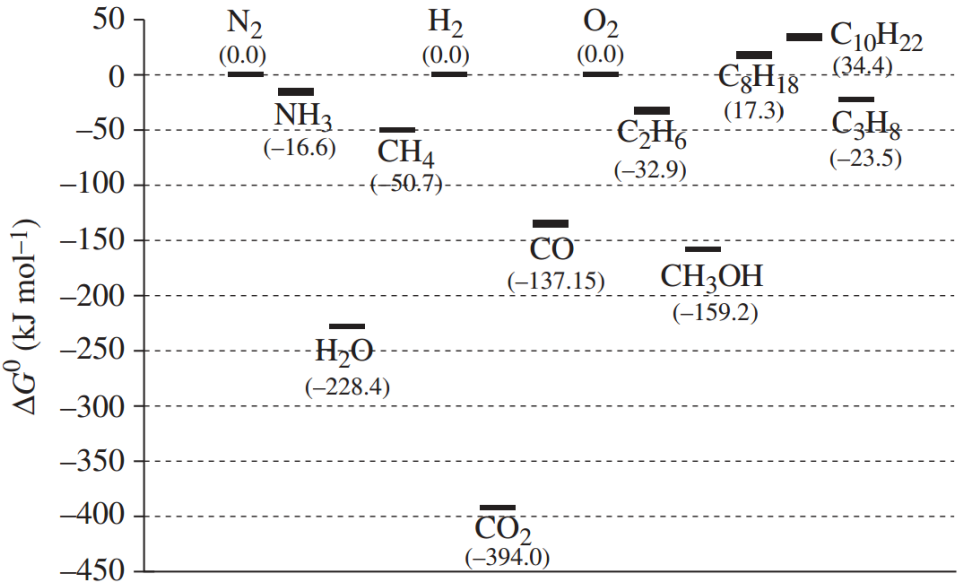


Figure 2.1 $CO_2$ and related chemicals Gibbs free energy of formation from Jiang *et al.* [102].

This comparison of a catalyst with a photocatalyst, is presented in Figure 2.2 showing activation energy barriers. Processes b and d reflect traditional catalytic expectations where the product is more stable than the reagents. In the case of a and c, the activation energy is greater than the Gibbs free energy which means that energy in the form of either heat, electricity or photons must be supplied. Catalysis with endothermic reactions is done at high temperature, or with an electrocatalyst or photocatalyst. This shift in activation energy proves the assistance of a photocatalyst, while also acknowledging the energy input necessary to form the products. Relatively high activation energy does however prevent reverse reactions. So whereas all scenarios represented (a, b, c and d of Figure 2.2) are catalysis, for $CO_2$ photoreduction with the use of a photocatalyst the representing figure is figure d. The case for catalysis in general is contrasted with the case for photocatalysis, showing that if the activation energy shift can be proved, photocatalytic behavior can be proved.

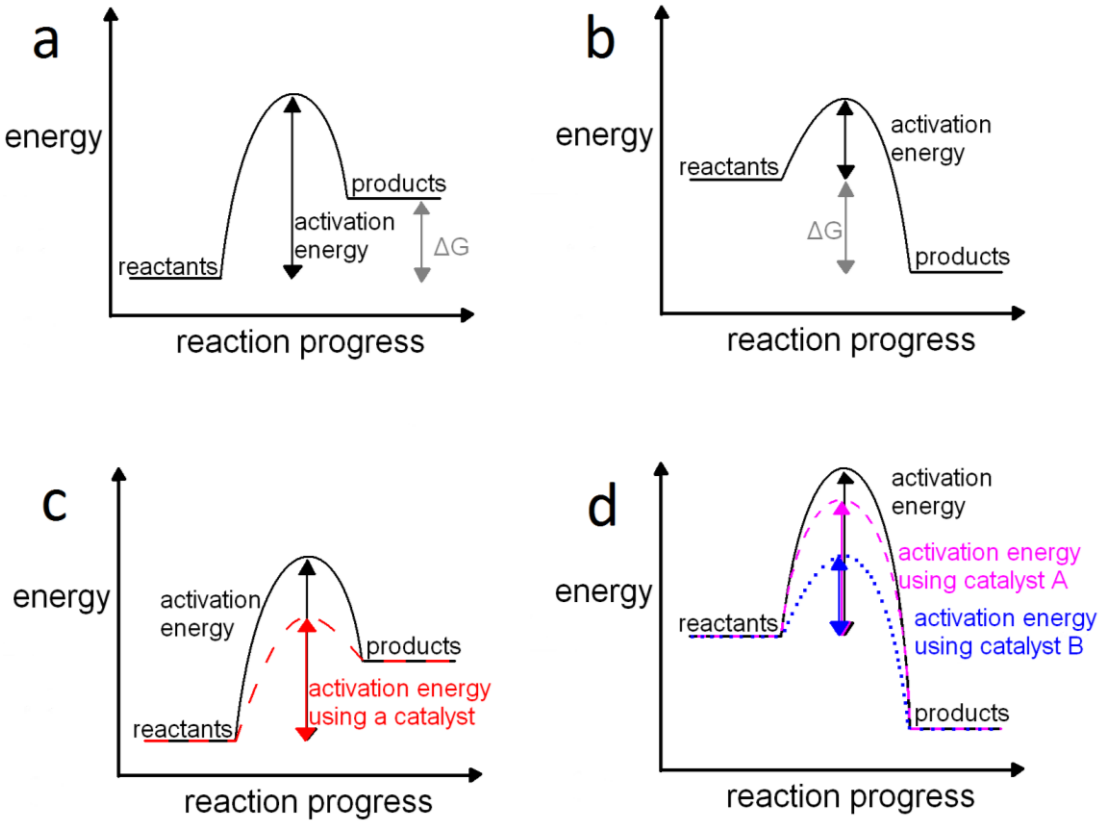


Figure 2.2 Energy of reactions, (a) of a endothermic, thermodynamically unfavorable process with a positive ΔG (in grey), (b) of a exothermic, thermodynamically favorable process with a negative ΔG (in grey), (c) of a photocatalyzed process that still requiring a net increase in energy of the products showing the impact of the photocatalyst (red dashed line), and (d) of a catalyzed process with catalyst A (pink dashed) and catalyst B (blue dotted line).

These thermodynamically specific requirements of photocatalysis mean that the measurements of the processes are going to be different. Understanding why they are

different and learning from catalysis comparisons of performance would greatly improve photocatalysis research. Thus, the implications of catalysis are important to consider when analyzing photocatalytic performance in the context of developing rigorous standardized procedures and for the catalytic nature of the process to be quantified.

Methods for photoreduction, as discussed by Wang and colleagues, include semiconductors or transition metal oxides, metal organic complexes, biological systems typically utilizing algae, and hybrid systems of enzyme activated organic/biological hybrids [103]. Semiconductors have been commonly utilized in photoreduction and make up the bedrock of $CO_2$ photocatalytic work.

## 2.2 Photoreduction using Semiconductors

Semiconductors are attractive as photocatalysts, as they are stable and do not degrade in the presence of photons and reactants; thus fulfilling one catalysis requirement. Another specification of catalysis is that this catalyst material is not changed by the reaction [101]. They promote electrons that would then be available to the reactants adsorbed to the semiconductor. There is a debate over the role of semiconductors as catalysts or as assistants to the reaction [100]. The semiconductor behavior is complex, with formation and transfer of electrons and holes such that catalytic terminology and performance can be difficult to apply or relate to the reaction [104]. As Serpone points out, Childs and Ollis in 1980 wanted to term the behavior "semiconductor-assisted photoreactions" [100, 105]. This debate is due to low catalytic performance where the expectation is for the turn over number (the number of molecules that a catalytic site can convert to product) to be greater than 1 [100].

As described elsewhere [106], the assumed mechanism for photocatalysis is depicted below in Figure 2.3. The valence band is shown with electrons in ground state that when excited by a photon, can jump to the conduction band. This promotion to an excited state occurs only if the energy of the photon is greater than the energy barrier of the band gap. The excited electrons that did not recombine with holes would then be available to travel to the surface and react with substrates [107]. The position of the valence band is sufficiently oxidizing if it is below the redox potential of the reactant or substrate to be oxidized (if the substrate is more anodic) and the sufficiently reductive conduction band is higher than the redox potential of the reactant or substrate to be reduced (if the substrate is more cathodic) [47].

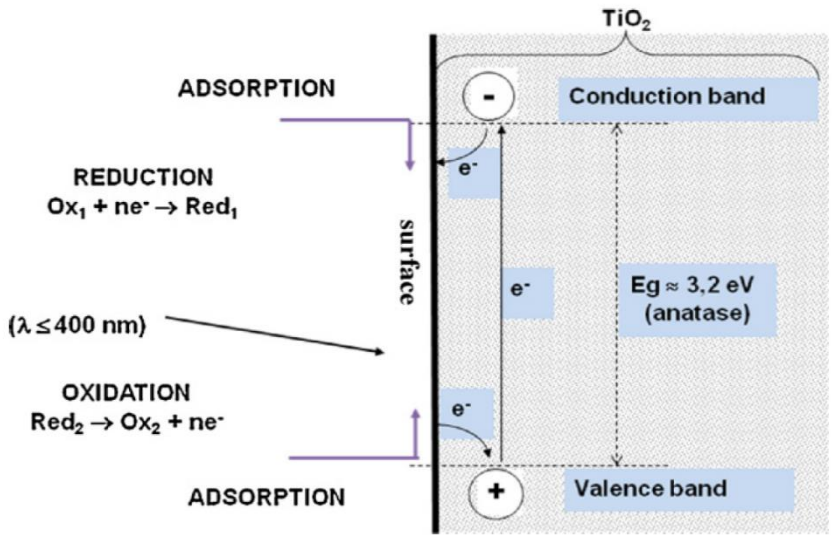


Figure 2.3 Electron energy band diagram for anatase titanium dioxide showing electron energy increasing upwards, from Herrmann [92].

The free energy of reaction (ΔG) of the reaction is the difference between the redox potential of the substrate to be reduced and the redox potential of the substrate to be oxidized [47]. In $CO_2$ reduction, a multistep process is simplistically explained by the oxidation of $H_2O$ and the reduction of $CO_2$. Some of the proposed reactions for the conversion of $CO_2$, with varying amounts of necessary electrons, along with their redox potentials (in respect to a normal hydrogen electrode at pH of 7) are listed below in Equations 2.1 through 2.9 [81, 107]. The relationship of ΔG with the cell potential (E) as measured in volts is ΔG =-nFE, with n being the number of moles of electrons from the balanced redox reaction and F Faraday's constant; 96,485 coulomb/mol. Redox tests are conducted in liquid phase and the more positive the number the more likely reduction will occur, while the more negative the more likely oxidation:

| | | |
|---|---|---|
| $H_2O \rightarrow ½\ O_2 + 2H^+ + 2e^-$ | 0.82 V | (Equation 2.1) |
| $2H^+ + 2e^- \rightarrow H_2$ | -0.41 V | (Equation 2.2) |
| $CO_2 + e^- \rightarrow CO_2^{*-}$ | -1.90 V | (Equation 2.3) |
| $CO_2 + H^+ + 2e^- \rightarrow HCO_2$ | -0.49 V | (Equation 2.4) |
| $CO_2 + 2H^+ + 2e^- \rightarrow CO + H_2O$ | -0.53 V | (Equation 2.5) |
| $CO_2 + 2H^+ + 2e^- \rightarrow HCOOH$ | -0.61 V | (Equation 2.6) |
| $CO_2 + 4H^+ + 4e^- \rightarrow HCHO + H_2O$ | -0.48 V | (Equation 2.7) |
| $CO_2 + 6H^+ + 6e^- \rightarrow CH_3OH + H_2O$ | -0.38 V | (Equation 2.8) |
| $CO_2 + 8H^+ + 8e^- \rightarrow CH_4 + 2H_2O$ | -0.24 V | (Equation 2.9) |

As can be seen above, the redox potential is smallest for the production of methane [$CH_4$]. Single electron excitement [$CO_2^{*-}$] is widely considered an initiating step to the photoreduction processes and would therefore determine the energy barrier to be overcome [81]. Thus, while methane production is thermodynamically preferable, the 8 electron reaction is challenged by kinetics.

The energy levels necessary for the reactions can then be compared to the semiconductor band gap energy. Figure 2.4 can be used to assess the energy levels of the band gap edges and their expected abilities for redox and oxidation of reactants. As can be seen in Figure 2.4, the conduction band and valence band positions of $TiO_2$ are at sufficient energy levels for the formation of $CH_4$.

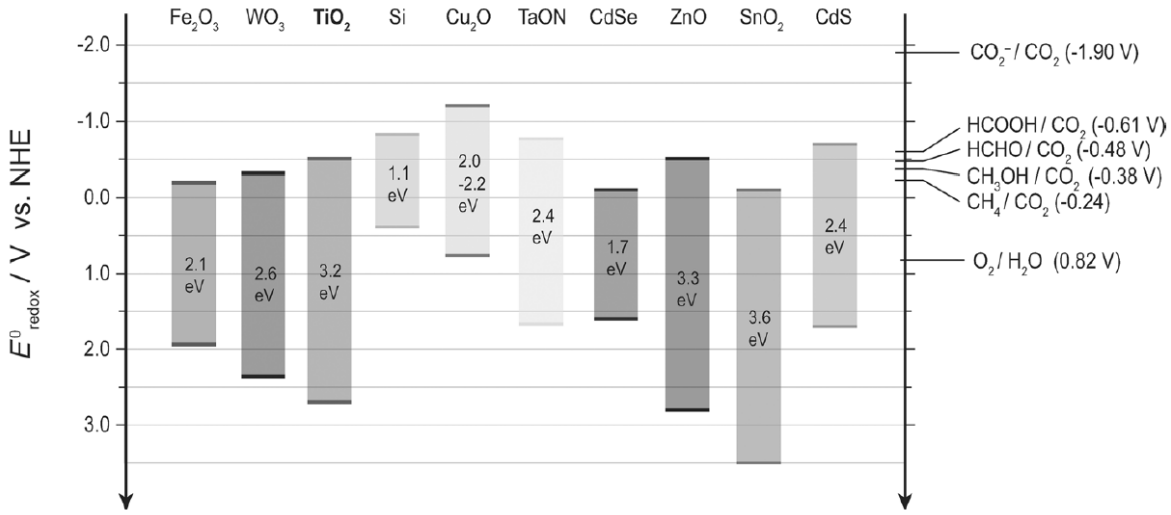


Figure 2.4 Band gap energies for various semiconductor photocatalysts showing conduction band and valence band potentials relative to redox potentials of compounds involved in $CO_2$ reduction at pH 7 from Habisreutinger *et al.* [107].

Materials such as metal oxides ($ZrO_2$, $Ga_2O_3$, and $Ta_2O_5$), mixed metal oxide semiconductors ($CaFe_2O_4$, $NaNbO_3$, $ZnGa_2O_4$, and $Zn_2GeO_4$), layered double hydroxides (LDH, Zn/Al LDH, Zn/Ga LDH, Mg/In LDH, CuZnGa-LDH, and Mg/Al LDH) [108], and graphene-based semiconductor photocatalysts have been used for $CO_2$ photoreduction [109]. Even as there are many alternate materials to $TiO_2$ that are currently utilized for photoreduction, for the purposes of results comparison $TiO_2$ provides the widest collection of work to analyze.

### 2.3 $TiO_2$ as a photocatalyst and modifications of $TiO_2$ performance

$TiO_2$ is a highly attractive photocatalyst due to its observed UV photocatalytic activity, non-toxicity, abundance (making up 0.63 wt% of the earth's crust it is the ninth most

abundant element [110, 111]), low cost, electronic properties and high molecular stability [112-114]. This has led to $TiO_2$ receiving a wide breadth of attention making it one of the most studied photocatalysts for $CO_2$ reduction [81, 82, 114-117]. Thus, it is the focus of this benchmarking study.

Interestingly, $TiO_2$ based materials are also used as catalysts for $CO_2$ reduction, however, this is done in the presence of $H_2$ for direct hydrogenation, and not $H_2O$ typically used in photocatalysis as otherwise high temperatures would be necessary [118, 119]. $TiO_2$ has three crystal phases that naturally occur at atmospheric pressure [120], rutile with an approximately 3.0 eV band gap, anatase with an approximate band gap of 3.4 eV, and brookite with an approximate band gap of 3.3 eV in bulk [121], and 3.0, 3.19 and 3.11 eV respectively for nanocrystals [122]. Rutile and anatase have a tetragonal crystal system, and brookite is rhombohedral [123].

More work has been done in the liquid phase for reactions and surfaces [124], however, these do not directly apply to gas phase because the reactant concentrations are significantly different and $CO_2$ forms low concentrations of carbonic acid ($H_2CO_3$) in water which usually dissociate to bicarbonates and carbonates. These dynamics make performance of photocatalysts hard to quantify and difficult to improve. Thus, there is a challenge to look more critically at the performance of photocatalysts, utilizing understandings from catalysis to engage with photocatalytic research practice.

$TiO_2$ was first used in photocatalysis for hydrogen production from water in 1972 [116]. According to Indrakanti, the first case of photocatalytic $CO_2$ reduction was published in 1979 [81]. Photocatalytic production of simple carbon based compounds such as formic acid and formaldehyde was conducted by Inoue and associates [125]. The results of their study are summarized in Table 2.1.

Table 2.1 provides the same information that is reported now and could be packaged into the results seen in section 1.4.1. For example, the amount of product is given relative to reaction time (illumination period) and amount of catalyst used. Thus, this table of results holds information identical to the $\mu mol/(g_{catalyst}\, h)$. Perhaps it suggests that the information gathered is chosen for historic reasons.

Table 2.1 Product yield results in moles from first photocatalytic $CO_2$ reduction [125].

| ***Catalyst (1.0g/100 ml water)*** | ***Illumination period (h)*** | ***Yields of Products:*** | ***HCHO ($x10^{-3}$ M)*** | ***$CH_3OH$ ($x10^{-4}$ M)*** |
|---|---|---|---|---|
| ***$TiO_2$*** | 7.0 | | 1.1 | 2.3 |
| ***$TiO_2$*** | 14.0 | | 1.8 | 7.8 |
| ***$TiO_2$*** | 30.0 | | 1.8 | 14.6 |
| ***$TiO_2$**** | 7.0 | | 0.0 | 0.0 |
| ***ZnO*** | 7.0 | | 1.2 | 3.5 |
| ***CdS*** | 7.0 | | 2.0 | 11.7 |
| ***GaP*** | 7.0 | | 1.0 | 11.0 |
| ***SiC*** | 7.0 | | 1.0 | 53.5 |
| ***$WO_3$*** | 7.0 | | 0.0 | 0.0 |

* $TiO_2$ suspension was illuminated with light of wavelengths longer than 500 nm.

In the decades that have followed this early experiment using $TiO_2$ for photocatalytic reduction of $CO_2$ there has been a struggle to improve the photocatalytic performance of $TiO_2$. This has coincided with difficulties in understanding how to report effectively improvements in photocatalytic performance. In this chapter, particular focus is paid to the photocatalytic limitations of $TiO_2$ and the various solutions that have been attempted since this study. A major line of study is materials modifications.

Modifications of $TiO_2$ are made in an attempt to either increase selectivity in product production or advance photocatalytic behavior, such as selectivity or product yield. Limitations of $TiO_2$ photocatalytic behavior include limited light activity, hydrophilic behavior, and rapid electron hole recombination. Each of these challenges has been the focus of research, as described here.

### *2.3.1 Addressing Light Activity*

$TiO_2$ is active as a photocatalyst under UV light irradiation. This is a limited range of the solar radiation available, and thus, limits the full potential of the photocatalytic activity. Lowering the band-gap energy of $TiO_2$ would allow a greater range of solar radiation to promote electrons. There are still uncertainties as to whether modifications to the band-gap of $TiO_2$ directly improve the overall photocatalytic behavior. This is due to the energy of the resulting electrons being lower, and thus, not as capable of providing the energy

needed thermodynamically for $CO_2$ reduction. Nguyen, Vu and Do argue for increasing the number of photo-generated carriers which overall is significant to initiating the conversion [106]. However, there is also the resulting shift in the absolute energy positions that could impact the oxidation and reduction potential of excitons. Therefore, verification testing of improvement in photocatalytic performance for $CO_2$ reduction, with lower band-gap energy catalysts, is still necessary.

#### *2.3.1.1 Defining the limits: Light absorption*

The band gap of $TiO_2$ is 3.2 eV, corresponding to 388 nm wavelength [112]. The semiconductor absorbs incoming wavelengths of 388 nm or less, as the shorter wavelengths have greater energy (Figure 2.5). Decreasing the band-gap energy enables lower energy photons to excite an electron. This lower energy corresponds to an increase in the wavelength.

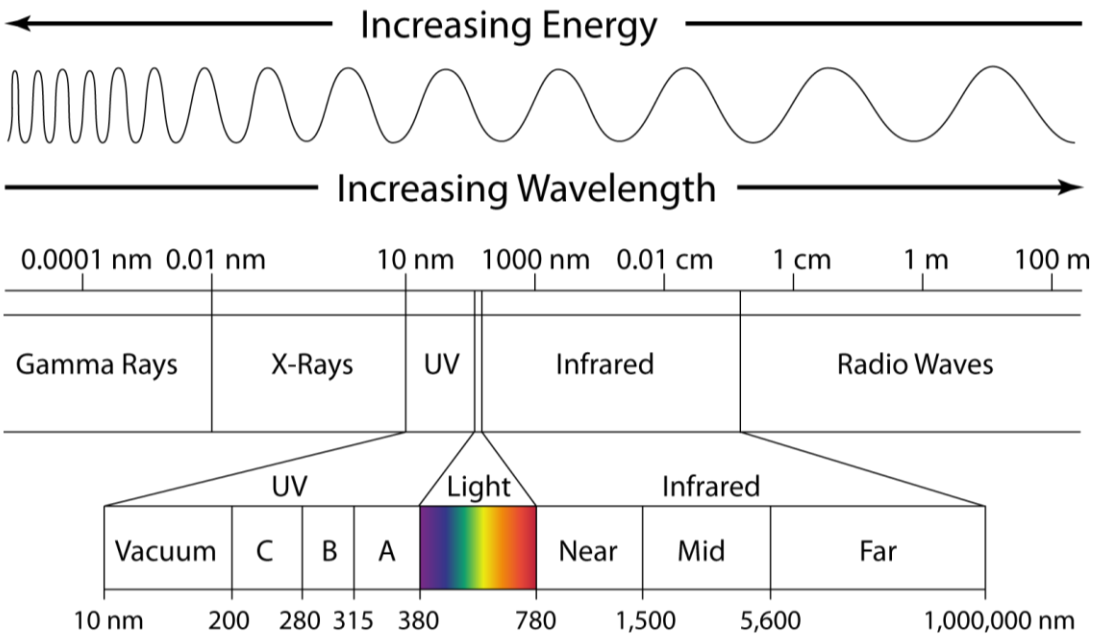


Figure 2.5 Electromagnetic spectrum, reproduced from Pool [126].

A decrease in the band gap to incorporate visible light would make approximately 50% of solar energy available to the photocatalytic process, as opposed to the UV light at approximately 4% of available radiated solar energy [127]. The reason for this substantial increase in solar energy can be seen in Figure 2.6, which shows the solar irradiation intensities along the electromagnetic spectrum. The peak intensity is clearly within the visible light spectrum.

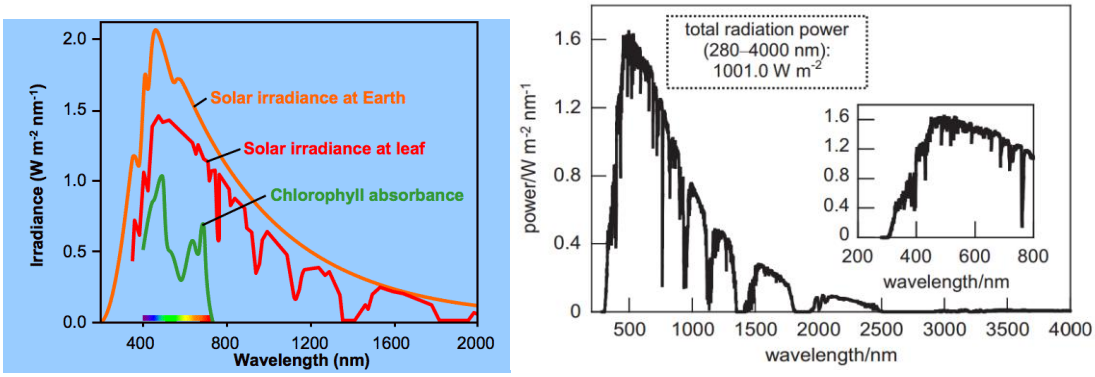


Figure 2.6 Solar radiation spectrum, from Koning [128] (right), and then the solar radiation spectrum at atmospheric mass (AM) of 1.5 (left) wish a zoomed in box of ultraviolet and visible light, from Vinyard *et al.* [43].

Therefore, many attempts have been made to lower the band-gap energy of $TiO_2$ based photocatalysts, as described below.

### *2.3.1.2 Opportunities: modifications to improve light absorption in the visible range*

The modifications attempted to improve light electron excitation include metal ion doping [39], semiconductor composites like $CeO_2$-$TiO_2$ [129], quantum dots [130, 131], hybridized structures such as carbon nanotubes grown on Ni doped $TiO_2$ [132], nanotube structure of $TiO_2$ [133], dye sensitizing [134], and dye sensitizing including up-conversion nanoparticles [135]. However, the most studied modification for improved visible light absorption is nitrogen doping [136-142]. Accumulating defects in $TiO_2$ [143] has been claimed to improve light absorption.

Surface area and light penetration improvements are often discussed in terms of improved light efficiency. Similar reasons were found for the improvement presented of a $CeO_2$-$TiO_2$ composite with 2D hexagonal structure. In this case, it was claimed that the large surface area increased light harvesting [129]. There are unclear lines of differentiation of improvement of the photocatalyst light activity and physical properties that are desirable from a reaction kinetics standpoint. An improvement in physical access of photons to the surface of the catalyst, may not really lead to an improvement in efficiency if the mass of the catalyst had been optimized for the amount of light. Thus, it needs to be quantified and clear when there is an improvement in quantum efficiency, or material performance, relative to a reaction parameter optimization. This will be investigated further within this thesis.

### *2.3.2 Addressing Hydrophobicity*

For photocatalytic reactions to be successful reactants must interact with the photocatalyst surface. The behavior of water and $CO_2$ on the surface of $TiO_2$ influences the success of photoreduction and catalytic activity.

#### *2.3.2.1 Defining the limits: Hydrophilic behavior*

$H_2O$ and $TiO_2$ interaction is significant to the reduction of $CO_2$ to valuable products. This is because the $H_2O$ provides the $H^+$ or $H^-$ to the reaction. There is a need to allow for the $H^+$ or $H^-$ generation and for the $CO_2$ dissociation on the photocatalyst surface. UV light induced hydrophilicity has been observed for $TiO_2$, where the contact angle of the water becomes almost zero under UV light irradiation [114]. Water droplets, with a regular contact angle on a dark surface, under UV light exposure, spread to coat the whole surface. This is shown in Figure 2.7, where the hydrophilicity impedes the surface interaction with $CO_2$ by removing it from the surface [116]. $CO_2$ adsorption on the catalyst surface lowers the energy of the reaction, thus this water induced separation from the surface becomes a barrier to the reaction. Thus, this behavior can limit $CO_2$ reduction especially when water is made abundant to the reaction [115].

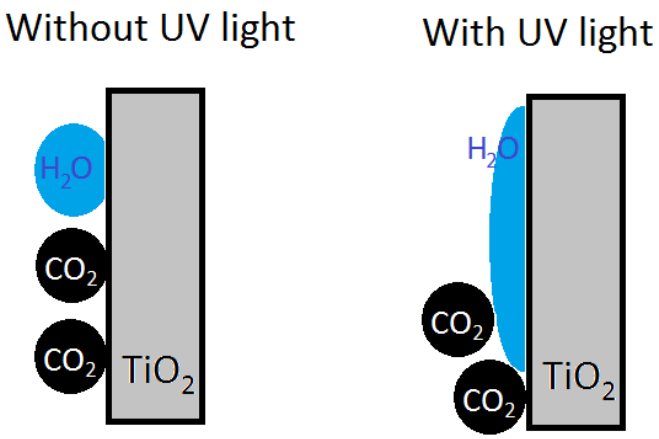


Figure 2.7 Depiction of water interactions with the $TiO_2$ surface. On the right depicts no light and on the left the light interaction with the $TiO_2$ and water induces a low contact angle and shows surface "cleaning". Figure made based on figure by Dr. Yolanda Fernandez Diez.

#### *2.3.2.2 Opportunities: modifications to improve hydrophobicity*

A MgO-$TiO_2$ composite was used for its good $CO_2$ adsorption and was found to improve CO formation and catalyst life time. The comparison to similar shaped materials with

lower $CO_2$ adsorption enabled the conclusion that a source of the improvement was the $CO_2$ adsorption [144].

A review of the published literature has not provided straightforward methods to improve hydrophobicity. Reactant gas ratios of $CO_2$ and water were varied by Tahir and Amin; however, the findings suggested that higher $CO_2$ partial pressure limited $CO_2$ reduction [145]. A change in partial pressure of $CO_2$ from 0.04 bar up to 0.06 bar reduced $CH_4$ production by 50 $\mu mole/g_{catalyst}$ and reduced production of CO by roughly 500 $\mu mole/g_{catalyst}$ [145]. This result is contrary to expected $H_2O$ and $CO_2$ interactions, where the water would adhere to the catalyst surface more actively and limit $CO_2$ reduction. This is most likely due to the reaction being in the gas phase. Studies that utilize gas phase reactors with either gas bubblers, or standing water at the base of the reactor, to maintain water vapor levels, limit the cleaning effect of water by inhibiting water droplet formation. In this way, perhaps, the competition for reaction sites is limited. This may be the reason some studies have moved away from liquid phase reactions and instead use gas phase reactants. In this thesis gas phase testing will be used.

### *2.3.3 Addressing Charge carrier lifetimes (electron hole recombination)*

Photocatalysis depends on electrons providing energy to the $CO_2$ molecules for reduction. The lifetimes of these electrons and the available pathways for energy dissipation greatly influence the success of reduction, and therefore, longer lifetimes are desired.

#### *2.3.3.1 Defining the limits: Charge separation*

A critical challenge in using $TiO_2$ is the charge dynamics. As photocatalysis relies on the energy of excited electrons to enable reactions the lifetime of the electrons greatly influences the reaction. Rapid electron-hole recombination on the order of two to three times faster than other electron transfer processes makes interaction with reactants difficult [81].

This same issue can be seen biologically. In nature, electron tunneling is used to separate charge carriers. In the case of photosynthesis, the distance that the electron travels for transfer from chlorophyll to the reaction center or within and between reaction centers is critical. The length has to be less than 14 angstroms (Å) to be faster than enzymatic transfers, and is found to be less than 6 Å in the case of redox chlorins in the core of reaction centers [146]. At this distance, tunneling times of electrons are 10 picoseconds or less. This spacing and multiple chains for the electron to tunnel across,

allow the electron to travel to specific sites for reaction purposes. In this way, photosynthetic enzymes create charge carrier separation.

In comparison, the size of atoms is on the order of a few Å. Thus, $TiO_2$ particles need to have effective paths for electron transport to reactants, or significant assistance from effective charge carrier traps. In these ways, the electrons would be available to provide energy to the reaction.

#### *2.3.3.2 Opportunities: charge carrier dynamics*

$CeO_2$-$TiO_2$ composite with 2D hexagonal structure increases efficiency by increasing charge separation [129]. The resulting improvement in performance was attributed to the electronic conductivity of the graphitic carbon. The use of bicrystalline $TiO_2$ as a mix of anatase and brookite [147], montmorillonite $TiO_2$ nanocomposites [56], trinary nancomposites such as MgO/Pt-$TiO_2$ [148], Ag loaded $TiO_2$ [149], and Cu loading [150] are all photocatalyst modification attempts at more effective charge separation. Arguments supporting increased charge separation revolve around electronic pathways enabling charges to last longer. These longer life charge carriers are then available to be effective in photoreduction. The charge transfer to reactants is also an area to improve with attempts including exposing the {100} facet of $TiO_2$ [151]. Methanol has also been used as a hole scavenger in reactions with Ag doped bicrystalline $TiO_2$ [152]. The hole scavenging limits recombination. Work has been done using magnets to lengthen the life of electron-hole pairs [153 Li, Zou, Au].

For this thesis, charge carrier dynamics will not be investigated further. Instead, focus will remain on attempts to quantify overall performance resulting from the whole photocatalytic process, including this dynamic charge carrier behavior.

### *2.3.4 Materials matrix and the assessment of the effect of materials modifications*

Since specific improvements to the photocatalytic process are intended from modifications, results analysis would benefit from clear links of improvement based on goal. To structure this thinking Table 2.2 is given below correlating material and experimental modifications to the expected improvement. Light and catalytic behavior can then be quantified separately, it becomes necessary to be specific about what results should improve.

Table 2.2 Modification of $TiO_2$ materials organized by type of modification and the goal or expected influence of the modification.

| | *Light Absorption (modifying bandgap)* | *Charge Carrier Lifetimes* | *Hydrophilic Behavior* |
|---|---|---|---|
| *Defects* | | Oxygen vacancies, multiple crystal phases [154], particle size | Crystal facet [154] |
| *Lattice Substitution* | Nitrogen doping [136-142], anion doping, (including iodine, carbon) | Cu doping [150], metal doping [155] | |
| *Multiple Materials / Composite* | Dye sensitization, depositing Au particles [154], dual semiconductor materials [155] | Montmorillonite $TiO_2$, Pt on the surface [154] | MgO-$TiO_2$ |
| *Morphology* | Quantum dots [154] | Nano rods | |

Table 2.2 allows for materials to be understood both in terms of the material complexity and what outcome is expected. For improvement of light absorption there would be expected a corresponding improvement in quantum efficiency. With improved charge carrier lifetimes, it would be expected to improve both quantum efficiency and reaction rate. The improvement of hydrophilic behavior would improve reaction rate. With the identification of tests that measure the material for reaction rate and quantum efficiency it becomes possible to see if modifications improve performance in the ways expected.

## 2.4 Mechanisms of $CO_2$ Photoreduction

> "*Because reaction mechanisms are at the heart of our fundamental understanding of catalysis, it is a grand challenge to examine all the elementary steps of a reaction and to determine how the rate of each correlates with the structure of the catalyst.*"
>
> - Thomas Bligaard *et al.*, 2016, [84]

Reaction mechanisms have been studied using theoretical calculations, microscopic and spectroscopicly with scanning tunneling microscopes (STM), diffuse reflectance infrared Fourier transform spectroscopy (DRIFTS) and electron paramagnetic resonance (EPR) [156]. Liu and Li break down the reaction mechanisms into three sections covering the $CO_2$ behavior, charge transfer, and pathways to product formation [156]. For photoreduction, Liu and Li state that $CO_2$ behavior includes the processes of adsorption, activation with an electron and dissociation of C—O bond, while also acknowledging $CO_2^-$ formation and spontaneous dissociation. Charge transfer focuses on charge separation and then transfer, with this behavior being dependent on crystal phase and defect disorder. Then the discussion of pathways to product formation focuses on the rate limiting step, intermediates and product selectivity. Debate over the rate limiting step have culminated in two views, one being the rate limiting step is activation of reactants through charge transfer, and the other being reactant dynamics of adsorption on the surface of the catalyst [156] . The rate limiting step may not be the correct model, and this could be revisited in relation to steady state approximations instead [157, 158]. Importantly, Yuan *et al.* point out the crucial impact the surface reactions have on the overall efficiency of the process, trying to link the cause to outcome and instigating an important shift in focus away from the specifics of the material, but instead acknowledging an impact on conversion process [159].

Figure 2.8 shows a proposed mechanism of $CO_2$ adsorption and reduction on $TiO_2$ [160]. On the left of Figure 2.8 are the three routes of $CO_2$ adsorption through reaction with a surface free OH group and converting to bicarbonate (1), attaching to an oxygen vacancy becoming carbonate (2), and then chemisorption to the surface and the resulting equilibrium (3). The right side of Figure 2.8 shows the reduction of $CO_2$ by surface adsorbed hydrogen. The proposed mechanisms, such as shown in Figure 2.8, include

oxygen vacancies. It should be noted that modeling of anatase $TiO_2$ has found that electron transfer to reactants is much more likely to occur at an oxygen vacancy at the surface than from the conduction band of $TiO_2$ [161]. Liu et.al. found that oxygen vacancies increased photoreduction activity [162]. This implies that surface defects are photocatalytically active sites and that the energy transfer of the electron is more complicated than the simplistic band gap model implies. Modeling also suggests that oxygen vacancies are difficult to produce and require more energy than one excited electron to generate [163]. This means that as a catalytic active site the performance of oxygen vacancies is expected to be low. The search for CO in product gases, such as found in Table 2.3, may be in reference to non-catalytic behavior and instead interactions with carbon based surface contaminants [156]. Within the photoreduction process and related reaction phenomena many reaction mechanisms are possible with a variety of products developed which can participate in further photoreduction.

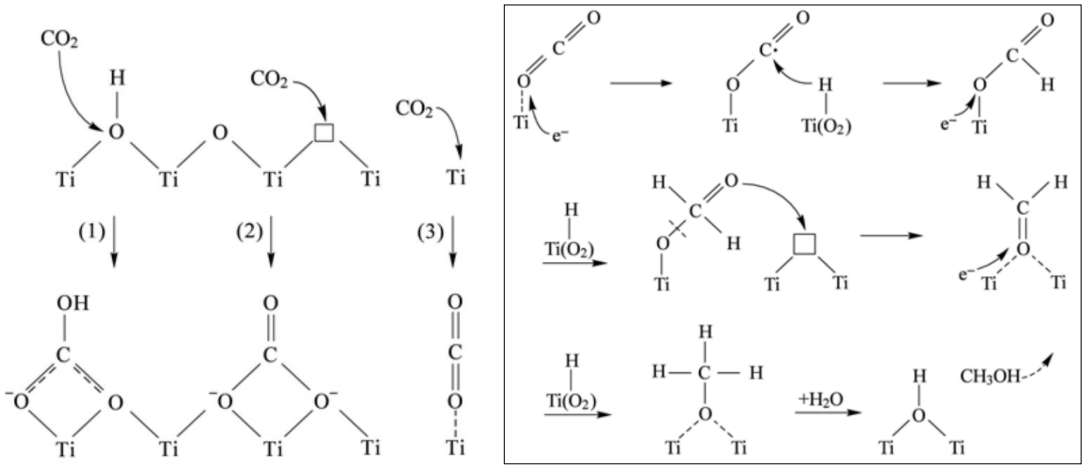


Figure 2.8 The mechanism of $CO_2$ adsorption left and $CO_2$ reduction right boxed as proposed by Wu and Huang, indicating more than one Ti site is necessary for $CO_2$ photoreduction from [160]. Empty boxes within figure indicate vacant site.

An example of mechanisms that provides a larger mechanism process for interpreting intermediates and products is Shkrob *et al.* argument that the formation of methane follows a "Glyoxal cycle" (Figure 2.9) [99]. This figure shows a cycle of $CO_2$ fixation, which includes even two processes they refer to as short cuts that don't include radical or redox chemistry. In this case, the mechanism shown in Figure 2.9 was proved half way through the use of Electron paramagnetic resonance (EPR) limiting which species could be observed, however they argue that the transformations would be readily completed. This introduces many interesting questions, such as the impact of the reaction shortcuts, particularly in terms of the energy economy of the formation route, and light

interactions that are not photocatalytic. Do various routes to CO limit the impact of focusing on CO detection to represent photoreduction? Is it enough as Liu and Li suggest for photoillumination to enhance the desired reaction [156]?

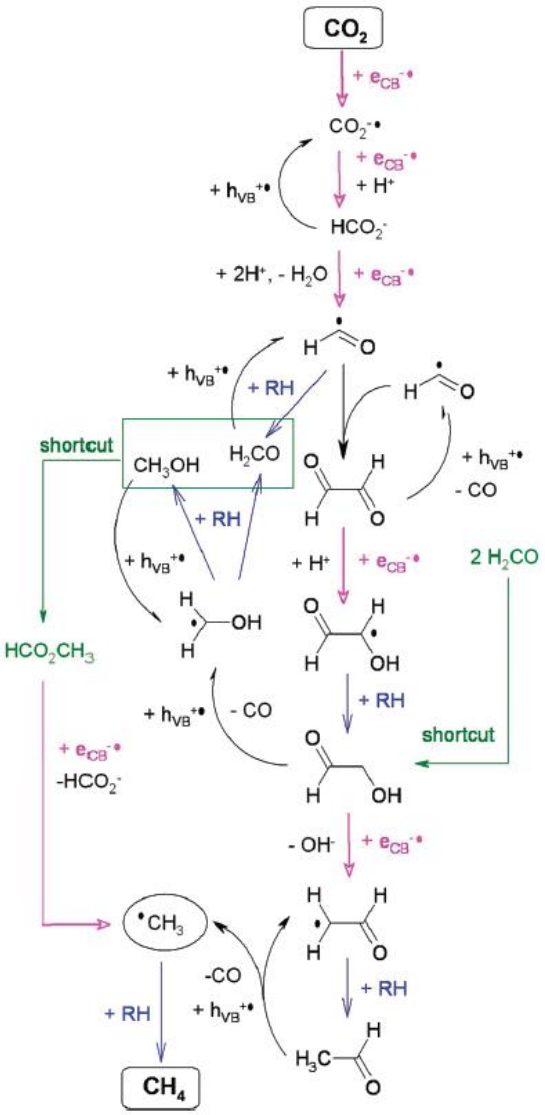


Figure 2.9 The Glyoxal cycle that is proposed for the formation of methane. RH refers to the generic donor of H atoms often water, from Shkrob *et al.* [99].

The mechanism discussion is complex. There is work suggesting that accessibility of the surface may be a source of deactivation, with the competition of $H_2O$ molecules limiting the adsorption of $CO_2$ [147]. Depending on the desired product, gas phase or liquid phase may be better suited based on reaction mechanism [164]. In $CO_2$ photoreduction there are disparate goals and concerns and findings. Knowing reaction mechanisms enable all possible products to be identified; this assists comparisons of catalysts across modifications. As modifications directly impact reaction mechanisms, it becomes necessary for comparability purposes to be able to report results to investigate the effect of reaction mechanism. This is only possible if the effect of external

experimental parameters are understood and controlled, and is more wholly encompassed if both the photonic and catalytic performance are reported.

The review done by Liu and Li, is able to provide proposed or possible reaction pathways for the formation of carbon monoxide and methane, and points out these vary depending on crystal phase, prevalence and types of defects, and electronic structure of the catalyst [156]. This wide diversity can be seen in Table 2.3 through the various intermediates and products being found in the literature. Table 2.3 covers a range of $TiO_2$ modifications and measured products with the usual focus on $CH_4$ visible due to product frequency, and $CH_3OH$ (methanol) the second most prevalent term followed by CO (carbon monoxide). It is important to notice what is being chosen to be quantified as part of the product formation results. The tracking of hydrogen and oxygen lower in the table indicates attempts at assessing the contribution of water to the formation of products.

Table 2.3 Tabulated review of literature reaction intermediates (absorbed species on the surface of the photocatalyst) and products for the reduction of $CO_2$ by photocatalysis, reproduced from [156].

| *Catalysts* | *Reaction intermediates* | *Products* | *Reaction Media* | *References* |
|---|---|---|---|---|
| *$TiO_2$-anatase* | H•, $CH_3$•, OH• | $CH_4$, $CH_3OH$ | NaOH solution | [165] |
| *$TiO_2$-brookite* | $CO_2$•, HCOOH | CO, $CH_4$ | $H_2O$ vapor | [162] |
| *$TiO_2$-P25* | $HCOO^-$, $CO_3^{2-}$ | $CH_4$ | $H_2O$ solution | [166] |
| *Ti-MCM-41* | $O^-$, OH• | CO | $H_2O$ vapor | [167] |
| *Ti-SBA-15* | CO, HCOH | $CH_4$, $C_2H_4$, $C_2H_6$ | $H_2O$ vapor | [168] |
| *CuTi/$SiO_2$* | - | CO, $CH_4$ | $H_2O$ vapor | [169] |
| *CuTi/5A* | $CO_2$•, COOH•, $CH_3OH$ | $CH_4$, $CH_3OH$, $CH_3COOH$, COOH-COOH | Alkaline solution | [170] |
| *Pt/$TiO_2$* | $HCO_3^-$ | $CH_4$ | $H_2O$ vapor | [171] |
| *Au/$TiO_2$* | - | $CH_4$, $C_2H_6$, HCHO, CH3OH | $H_2O$ vapor | [172] |
| *Pd/$TiO_2$* | $CO_3^{2-}$, $CO_2$(aq), $H_2CO_3$ | $CH_4$, $C_2H_6$, $C_3H_8$ | $Na_2CO_3$ solution | [173] |
| *N-$TiO_2$* | H•, $CH_3$• $HCO_2$•, $CH_3O_2$• | HCOOH, HCHO, $CH_3OH$, $CH_4$ | $KHCO_3$ solution | [174] |
| *$FeTiO_3$/$TiO_2$* | $H_2CO_3$, $HCO_2$•, HCOOH | $CH_3OH$ | $NaHCO_3$ solution | [175] |
| *CuO/$TiO_2$* | C residue | $CH_4$ | $H_2O$ vapor | [48] |
| *CuO-$TiO_2$* | HCOOH, HCHO | $HCOOCH_3$ | $CH_3OH$ solution | [176] |
| *CuOx/$TiO_2$* | $CO_2$•, $HCO_3^-$ | CO, $CH_4$ | $H_2O$ vapor | [177] |
| *AgBr/$TiO_2$* | $CO_2$•, C•, $CH_3$• | $CH_4$, $CH_3OH$, CO, $CH_3CH_2OH$ | $KHCO_3$ solution | [178] |
| *Pt-Cu/$TiO_2$* | CO, OH• | CO, $H_2$, $CH_4$, olefin, branched paraffin, alkanes | $H_2O$ vapor | [179] |

| *Catalysts* | *Reaction intermediates* | *Products* | *Reaction Media* | *References* |
|---|---|---|---|---|
| *Ag/ALa$_4$Ti$_4$O$_{17}$ (A: Ca, Sr, Ba)* | - | CO, HCOOH, $H_2$, $O_2$ | $H_2O$ vapor | [180] |
| *Cu-I/TiO$_2$* | H•, CO•, C• | CO, $CH_4$, $CH_3Cl$ | $H_2O$ vapor | [181] |
| *Ni-N/TiO$_2$* | - | $CH_3OH$ | NaOH, $Na_2SO_3$ solution | [182] |
| *M-N/TiO$_2$ (M: Pt, Au, Ag)* | C residues | $CH_4$ | $H_2O$ vapor | [137] |

The level of understanding of photocatalytic mechanisms may have implications for products reporting. The current range of intermediates, indicating a diversity of reaction mechanisms, and diversity of products found challenge results reporting; examples of greater variety in products show that lab practices may be limited, and product totals will not encompass the whole of results of the photocatalytic process. To address this complexity some articles focus on specific products, such as CO [61, 71] and $CH_4$ [68, 183-187] while others display the wide range of products [69]. One of the widest being the reporting of CO, $CH_4$, $CH_3OH$, $C_2H_6$, $C_2H_4$, $C_3H_6$ and $C_3H_8$ [58]. This bounds the capacity of the analysis, fewer products tracked limiting the scope to selectivity for specific products, while a wider range of products is more inclined to analyze overall $CO_2$ conversion.

It can be seen in Figure 2.9 that intermediates and final products for the production of methane are a larger body of chemicals than found in Table 2.3. Meaning that even though molecules such as $CH_3OH$ are measured as products, they have potential for further reactions and these products may not be easily detected. Some intermediates are short lived. In fact, the photocatalytic process can be accompanied by many phenomena that challenge detection or widen the range of products including photoreforming, product condensation on the photocatalyst surface (or within the rig), and competitive reactions. Therefore, investigations into the specifics of the surface interactions during photocatalysis and the proposed chemical processes are vitally important and will over time greatly improve the $CO_2$ reduction research. What this means to current experimental work is that researchers need to be more discerning about and descriptive of the rig specifications and analysis measures taken to address the challenges of having a wide and overlapping product range and getting products to detection.

## 2.5 Parameters affecting $CO_2$ Photoreduction and Conversion

This discussion focuses on the effect of operational parameters on $CO_2$ photoconversion. There can be a lack of normalization of the reactor and light in reported terms, and even a lack of reporting these parameters in a consistent way. Therefore, parameters that influence testing and conversion results are reviewed here to assess current practice. These factors include catalyst specifics, light source utilized, reactor design, and the operating conditions which include temperature and pressure. Rate is the obvious way to measure the impact in varying the operational parameters and is utilized throughout this discussion. It becomes clear for further discussion and experimental work that the use of specific rate is crucial to exploring the reaction conditions and implementing benchmarking.

### *2.5.1 Catalyst*

The amount of catalyst used has direct impact on the ability to benchmark product formation results. The challenge here is to quantify catalytic sites for the photocatalytic process and utilize terms such as turn over frequency (TOF) to measure conversion. This review is not focusing on all catalyst properties that improve performance, but instead, on the catalyst properties that need to be understood to quantify photocatalyst performance. Therefore, the following sections discuss how mass of catalyst used, the morphology, and the specific surface area of the catalyst are important to consider because they influence the light accessibility to the catalytic active sites. It will be shown that the testing results are fundamentally impacted when light and catalytic activity are not acknowledged in the rig design and experimental set up.

#### *2.5.1.1 Mass of catalyst /catalyst loading*

The mass of the catalyst in the reactor can be optimized for the incident photons, as shown in Figure 2.10 [96]. This means that the rate and quantum yield results could be optimized for the amount of catalyst. Optimization is preferable if mass of photocatalyst is to be used to normalize conversion. Colina-Márquez *et al.* optimized catalyst loading from modeling and calculations for heterogeneous liquid reactors of tubular or compound parabolic collector shape by using the local volumetric rate of photon absorption (VRPA) as representative of solar radiation absorption and finding the maximum when varying concentration [188]. This optimization varies as a function of scattering albedo, which is defined as the ratio scattering to total extinction. Then, to normalize for the reactor radius

they used optical thickness and apparent optical thickness, a term they coined for normalizing scattering and light interactions of photocatalysts to the reactor radius [188]. Ollis reported that for gas phase reactors there is a limitation on light accessibility and when the optical density of the catalyst particle is greater than 1-2 (unit-less number) only illuminated mass or surface area should be compared [157]. This optimum mass can be found experimentally. As suggested in Figure 2.10, the optimum mass ($m_{opt}$) for the reactor configuration and light provided can be found by varying mass. Zhao *et al.* discussed the mass of catalyst used in their gas phase reactor and found that there is a point at which additional catalyst no longer increases production rate. They found that the performance of 100mg of catalyst is equal to the performance of 200mg of catalyst, both producing roughly 0.22 µmol/h of CO [147].

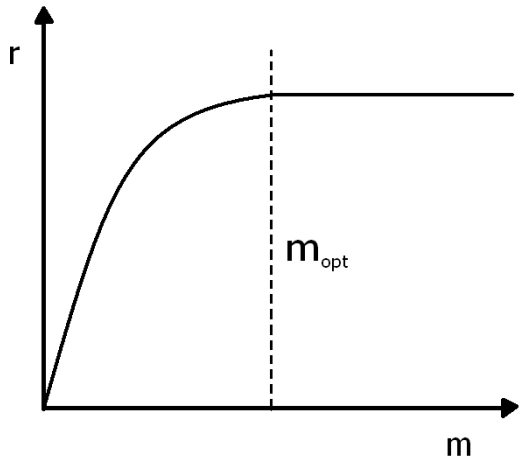


Figure 2.10. Expected plot for the reaction rate (r) as a function of mass (m), modified from Herrmann [96].

Acknowledgement of the mass of the catalyst is done through reporting µmol/$g_{catalyst}$h, i.e. the amount of product per the amount of catalyst and time of testing. And the mass can be discussed in terms of an intrinsic metric such as catalyst concentration or catalyst to substrate ratio. In this case, it is discussed in terms of reporting mass thereby enabling the use of intrinsic metrics. Results such as quantum efficiency might benefit from being gathered from the initial linear range of the plot (Figure 2.10). Moreover, kinetic law of the material performance would benefit from being gathered in the saturated mass range of testing, particularly if not normalized for amount of catalyst used. Therefore, the mass would not limit or modify the reaction rate, and would also not act as a penalty in the rate calculation. Mass of photocatalyst loading is explored with both $AuTiO_2$ and Mirkat experimental work in chapters 5 and 6.

### *2.5.1.2 Morphology and Surface Area of Catalyst*

Morphology can relate to a catalytic material's shape, size, volume, surface, structure and crystallinity. Historically, Brunauer-Emmett-Teller (BET) specific surface area has been reported on the assumption that the number of active sites is proportional to the surface area [189]. This specific surface area, however, is not used in current practices to normalize product formation results. As discussed in section 3.1.1 on product yield, the $CO_2$ photoreduction results are often reported per mass of catalyst. The implications of reporting considering specific surface area need to be understood.

The identification of active sites allows for catalytic behavior to be quantified. The morphology of the catalyst affects the availability of atoms to the surface and the electronic properties at the surface, and therefore, impacts the number of active sites. Most photocatalytic testing is conducted with nanoparticles, which are usually polycrystalline and already challenging to identify active sites with; however, some research has been conducted with nanorods and other particle morphologies [132, 133]. Modifications affecting porosity or structure including nanorods add complexity to quantifying catalytic behavior because of changes to active sites and added complexities to light interactions. The challenge for catalyst measurements has been the photon dependency of active sites. For example, active sites may be generated when activated by photons, however they cannot be defined as such because catalytic performance becomes unquantifiable using TOF due to the extremely short life of the charge separation. Serpone *et al.* discussed the generation and extinction of active sites and the challenges in identifying the number of active sites [100]. They also made the point that the active sites need to be identified irrespective of whether they have been excited or activated by a photon [100].

Even as the BET surface area of $TiO_2$ is often reported, suggesting that it is catalytically active on the entire surface, when doping and modifications are done to improve performance, these modified sites may become active sites for the reaction if co-catalysts are added. In general, promoters are not active themselves, but instead increase $TiO_2$ activity. Therefore, too high promoter loading will lead to lower activity from covering a high fraction of the surface. Results reporting $\mu mol/g_{catalyst}h$ take into account the whole mass of the catalyst irrespective of doping metals or active sites.

Attempts have been made to quantify active sites through approximating the number of surface atoms by multiplying the number of crystal lattice atoms per area by the surface area of the solid photocatalyst [104]. This enables the turnover number to be determined; however, reactions occurring at a steady state of charge (exciton or hole

formation) at the photocatalyst surface [104], require continuous systems not yet widely available or understood in this context. Thus, the procedures for TOF measurements are not necessarily practical and accessible.

Effectively active sites should be a function of illuminated surface area. Illuminated surface area would also quantify the area of the reactor devoted to catalyst loading and provide a way to normalize results for the size of the reactor. Illuminated surface area is discussed and used when analyzing results in this thesis.

### *2.5.2 Light Source*

Light source quantification is crucial to determining quantum efficiency measurements. The light source is also the input of energy for the reaction to proceed, and thus, is the input by which to assess the energy conversion to products of the process. Understanding the light sources used for testing and the information reported are crucial to quantifying the effectiveness of photocatalysis. Discussion of the characteristics of light used for testing is presented here.

Light flux, or really photon flux, is used to quantify the incoming light unit (Equation 2.10). Efficiency can then be measured from how many photons are successful in the photocatalytic reaction.

$$photon\ flux = \frac{number\ of\ photons}{time\ (s)\ \times\ area\ (m^2)} \qquad \text{Equation 2.10}$$

Light intensity is irradiance or the power per area ($W/m^2$ Equation 2.11). Measurements of irradiance of light sources are taken to understand the intensity of the light which activates the photocatalytic reaction. Light entering a reactor however, loses intensity the further it travels in the reactor. This occurs due to emitted light from a source spreading such that the intensity becomes less as a function of the distance it travels as sown in Equation 2.11.

$$Intensity = \frac{source\ strength\ power}{A\ of\ sphere, (radius\ length\ going\ from\ source\ to\ catalyst)} = \frac{S}{4\pi r^2} \qquad \text{Equation 2.11}$$

A represents the surface area in Equation 2.11. There is also a consideration that the catalyst will reflect light, and some of that light will be again reflected back to the catalyst and some will be dissipated. The distance that light travels in reactor designs should be kept constant for testing and should be reported with results. As it is difficult to identify the intensity of the light that is available at the photocatalytic material, it is appropriate to report incident or external quantum efficiency.

The IUPAC Glossary of terms defines measurements that address some of the information about the light supplied in the definition of terms [89]. In the case of measurements calculated using incident light, the term "photonic" is used, absorbed light then utilizes "quantum". In the case of measurements using a monochromatic light source the term "yield" is used, and a wavelength spectra source is assigned the term "efficiency". In summary, the related measurements are quantum yield (absorbed and monochromatic), quantum efficiency (absorbed and wavelength range), photonic yield (incident and monochromatic), and photonic efficiency (incident and wavelength range) [89]. This addresses some of the variability in testing and reporting procedure.

To be specific, Quantum yield [Φ] (relative to flux of absorbed photons, $q^{a}_{n,p,\lambda}$, – superscript a - in monochromatic radiation – subscript n, for molar amount, p, photon, λ, wavelength, A is the absorbance of the wavelength, and x is the chosen quantity for tracking reaction progress) is defined in Equation 2.12 [89]:

$$\Phi\ (\lambda) = \frac{number\ of\ events}{number\ of\ photons\ absorbed} = \frac{{}^{dx}/_{dt}}{q^{0}_{n,p,\lambda}[1-10^{-A}]} \qquad \text{Equation 2.12}$$

It can be calculated as an average [89]:

$$\Phi_{Ph\rightarrow cat}(\lambda) = \frac{{}^{dn}/_{dt}}{\langle L^{a}_{p,\lambda}(t)\rangle_{V}} \qquad \text{Equation 2.13}$$

The term n refers to a measure of concentration of product formation or reactant consumed (i.e. number of events). Where $\langle L^{a}_{p,\lambda}(t)\rangle_{V}$ is the absorbed (spectral) photon flux density defined by the equation (in this case the x is a designation of position, so the absorbed flux is a function of position and time x) [89]:

$$\langle L^a_{p,\lambda}(t)\rangle_V = \frac{1}{V}\int_0^V L^a_\lambda(x,t)dV \qquad \text{Equation 2.14}$$

The absorbed photon flux density is an integral per time interval of the whole volume of monochromatic light entering the system averaged per volume.

Returning to the term x, within quantum yield, as a measure of concentration of product formation or reactant consumed (i.e. number of events). Otherwise, quantum yield can be defined as an integral; Quantum efficiency [$\Phi\ (\Delta\lambda)$] (relative to absorbed photons in a range of wavelengths) [89]:

$$\Phi\ (\Delta\lambda) = \frac{\int_{\lambda_1}^{\lambda_2}\frac{dn(\lambda)}{dt}d\lambda}{\int_{\lambda_1}^{\lambda_2} q^0_{n,p,\lambda}\,[1-10^{-A(\lambda)}]d\lambda} \qquad \text{Equation 2. 15}$$

However, this is for a homogeneous system (as opposed to the heterogeneous system in this study), where A is the absorbance depending on the wavelength [$\lambda$]; A takes into account the fraction of absorbed photons. The term x (representing disappearing reagent or formed products) is a measure of the reaction process and is wavelength-dependent. Photocatalytic activity can be used as a synonym for both quantum yield and quantum efficiency.

Photonic yield (relative to incident photons in monochromatic radiation) has been given no symbol and is found in terms of $q^0_{n,p,\lambda}$ [89]:

$$photonic\ yield = \frac{dn/_{dt}}{q^0_{n,p,\lambda}} \qquad \text{Equation 2.16}$$

Photonic efficiency [$\xi$] (relative to incident photons in a range of wavelengths) is defined as [89]:

$$\xi = \frac{dn/_{dt}}{\int_{\lambda_1}^{\lambda_2} q^0_{n,p,\lambda}d\lambda} \qquad \text{Equation 2.17}$$

This is in terms of chemical amounts such as moles, with the term $q^0_{n,p,\lambda}$ being the spectral photon flux (units being mol/sec). These two terms have also been referred to as photocatalytic efficiency.

Effective radiation catalytic activity, or radiation chemical yield (G), is less commonly used and represents the number of reacted molecules, or formed products, by a 100 eV energy radiation.

Herrmann has proposed a relationship between the reaction rate in photocatalysis and the radiant flux demonstrating increased recombination at high flux (Figure 2.11) [96]. Lab tested reaction rate (R) shows the behavior of catalytic conversion as proportionally dependent on radiant flux in either a linear or square root manner.

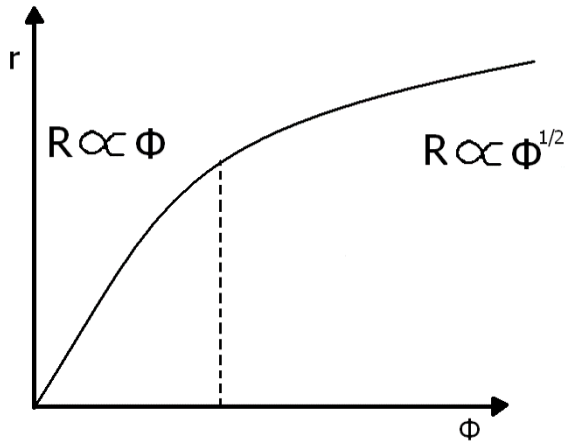


Figure 2.11 Reaction rate (r) shown as a proportional function of radiant flux (Φ), modified from Herrmann [96].

Light sources used for photocatalytic reduction of $CO_2$ include UV light lamps [149, 190] such as high pressure mercury lamps [191, 192], other mercury lamps [56, 145, 193], and UV-visible spectrum lamps [132, 152] including Xenon arc lamps [129, 133, 147, 148, 151, 194, 195].

The usage of a monolith was stated to have higher yield rates due to "higher illuminated surface area and efficient light utilization" [193]. This brings to the fore the necessity to use optimal amounts of catalyst relative to light provided. This improvement would not be as significant if optimization of the mass of the catalyst had already been accounted for, particularly relative to the illuminated surface area.

For the purposes of testing, using the optimum wavelength is appropriate if the reaction is for indoor use, i.e. artificially illuminated reactors [196]. $CO_2$ photoreduction, for the production of solar fuels, would ideally be commercially conducted using solar radiation, and therefore, the band gap energy of the catalyst would not impact the choice of light source. This is because the light source is fixed as solar. Moreover, the light used for testing needs to be normalized and understood in the context of solar irradiation. In the case of solar photovoltaic panels, the ideal band-gap energy for a single

semiconductor was identified as 1.34 eV based on the solar spectrum and is known as the Shockley-Queisser limit [197]. This is another way of expressing the desire to utilize a larger portion of the solar spectrum, as discussed in section 2.5.1.1. This value is much lower than that of $TiO_2$, 3.2 eV, demonstrating the desire to lower the band gap energy of the catalyst for the purpose of solar fuels [107]. However, it should be kept in mind that this has been surpassed by including multiple energy level pathways such as utilizing multiple semiconductors together [198]. In this thesis, irradiation is reported, however, experiments with a solar standard are not conducted.

### *2.5.3 Reactor*

$CO_2$ photoreduction is relatively unstandardized, in part because photoreactors can vary greatly in size, shape and volume. These photoreactor differences can lead to a large variety of flow patterns in the reactors. Common materials used in $CO_2$ photoreduction include quartz [118, 119] and stainless steel [56, 191, 192], while Pyrex glass is suitable for near-UV, and quartz glass is needed for UV [189].

Reactors can be designed for batch reactions, or as a continuous process with constant flow of reactants and products. To optimize contact in large scale reactors, stirred tank photoreactors and fluidized bed photoreactors can be utilized for liquid and gas phase reactants, respectively [189]. In photoreator design, lamp and reactant configurations are important due to radiation emission and absorption and fluid dynamics interaction. There are many reactor configurations in relation to light geometries available. These can be seen in relation to reactor design below in Table 2.4. Light geometries available include: immersion well, where the light source is immersed in the suspension; annular, where the light source is encased within a central cylinder with the suspension in a coaxial cylinder around it; multilamp options with many lights surrounding the reactor cylinder; elliptical, where both the light source and reactants are encased in elliptical reflecting chamber; film type, where reactants form a thin liquid on reactor walls; and flat wall photoreactor, where light from a single direction or parallel beam radiation field is used to illuminate reactants under a flat transparent wall of the reactor [189].

Reactors can also facilitate different catalyst supports as suggested by variants of fixed bed designs in Table 2.4 [199]. Within reactors used for $CO_2$ photoreduction, catalysts can be supported on the bottom of the reactor, quartz plates, glass fibers or glass fiber filters [147, 152], Teflon holders [148], and ceramic monoliths [112, 193]. Other expansions of the photoreactor design have included dye-sensitized film [134], twin

reactors [194], and a hydrogel-embedded microfluidic network [190].

Table 2.4 Reactor designs and light geometries that are available [199].

| *Reactor Design* | *Light and Reactor Geometry* |
|---|---|
| *Fluidized and slurry reactor (multiphase)* | Immersion well, annular, multilamp, elliptical |
| *Fixed bed reactor* | Film type, flat wall |
| *Variants of fixed bed designs* | Monolith reactor, optical fiber reactor |

### *2.5.4 Operating Conditions*

The operating conditions under which $CO_2$ photoreduction tests are run will certainly impact on the results, and particularly the comparability of the results. This section discusses the effect of reactant concentrations, temperature and pressure of the reaction. Considerations for photocatalysis may also include length of reaction and whether sacrificial agents or dyes are used. Unfortunately, these conditions are generally not sufficiently monitored or reported, as discussed below. In this thesis, reactant concentrations, temperature, and pressure are monitored and reported, however not varied for further analysis. The length of reaction, particularly for batch reactions conduced herein are varied.

#### *2.5.4.1 Reactant Concentrations*

As discussed above regarding the mass of catalysis (section 3.3.1.1), semiconductor activation by a photon provides active sites that can be generated and then extinguished, and therefore, the number of active sites can change. To use a reaction rate model, a constant number of active sites are assumed during illumination. The reaction rate as a function of reactant concentrations can be found experimentally (as long as light intensity is kept constant) by varying concentration of reactant; with expected results as shown in Figure 2.12. This information could be used to optimize the amount of $CO_2$ necessary to maintain the reaction rate and may have implications for the purity of the $CO_2$ feedstock.

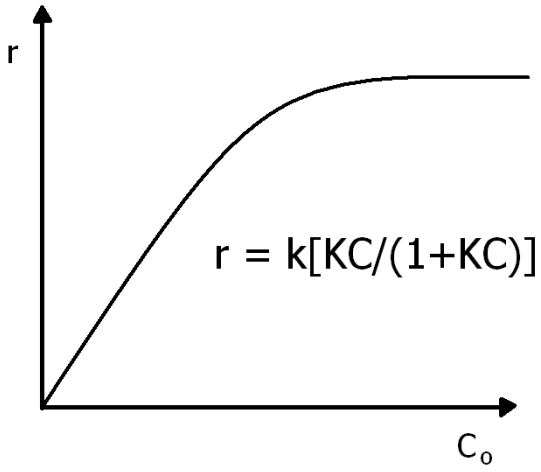


Figure 2.12. Expected plot showing the rate of reaction (r) as a function of initial concentration of reactant ($C_o$), with resultant rate equation as a function of adsorption constant (K), apparent first order rate constant (k) and reactant concentration (C), modified from Herrmann [96].

Currently, reactions are carried out in excess of $CO_2$, with $CO_2$ and $H_2O$ (reactant) concentrations having an unknown impact on reaction rate [107]. However, some work has been done to identify reaction rate dependencies. Reaction rate as a function of initial concentration of reactants is model dependent. With the Langmuir-Hinshelwood model, the rate of a catalytic reaction is dependent on the rate constant $k$, the apparent binding constant $K$, and the reactant concentration C, as seen in Equation 2.18 [200]:

$$rate = \frac{kKC}{(1 + KC)} \qquad \text{Equation 2.18}$$

Ollis used this model for photocatalytic kinetics for homogenous reactors and warned that the approximations that make this model applicable can be misunderstood. Ollis found that the intensity dependence of k and K were applicable to the pseudo-steady state approximation and not the slow-step approximation in the case of photocatalysis [157]. The pseudo-steady state can be due to numerous things including mass transfer, light transfer, and limiting intermediates. Therefore, even though the Langmuir adsorption model only applies to heterogeneous catalysis, the equation can appear to match the observed behavior. This means that a rate-determining step may not be an applicable model in this case. This is in agreement with Murzin's work that the steady state approach should be applied in cases of heterogeneous photocatalysis [158]. This means that without thorough investigation of rate dependence, or experimental investigation and modification to ensure adequate light and mass transfer, that the mechanism cannot be easily inferred from the rate relationship.

Questions of carbon residues on the catalyst and their impact on the photocatalytic process have been raised in the literature [48]. Yang and colleagues performed tests using isotopically labelled $^{13}CO_2$ allowing them insight into the source of the carbon. They concluded that CO observed in photocatalytic reactions could be formed from a reaction of the $CO_2$ with the surface carbon residues [48]. Performance of mass balance calculations on photocatalytic reactions would be an option to provide necessary information to support production rates. Thus, it is also important to consider mass balance of the reactants and products, as this would provide information about the source of carbon. Tests where amounts of reactants and products could be measured accurately would allow for confirmation that the source of carbon in the products was from $CO_2$ and not from any residual carbon on the surface of the photocatalyst [201]. Blank tests run without catalyst, light, and $CO_2$ respectively verify carbon residues are not the source for products as well. In this thesis, blank experiments were conducted without catalyst, light, $CO_2$, and without water.

Reactors being batch or continuous makes a difference in results processing as the batch reaction would have an initial maximum reaction rate, whilst the continuous would have a steady reaction rate. It is typical to use batch mode reactors as product yield is low and makes detection difficult.

#### *2.5.4.2 Temperature and Pressure of Reaction*

In photocatalysis the temperature of the reaction, particularly in the extremes to room temperature (less than 263.15 K and greater than 353.15 K), has an effect on the reaction rate as can be seen in Figure 2.13. As photocatalysis is a catalytic reaction affected by any energy input, it is expected that reaction rate varies with temperature. As low temperatures (below 353.15 K) are approached, reactants and products will be adsorbed more strongly, and as temperatures increase adsorption decreases, inhibiting reactions as they require surface contact [92].

Temperature effects can be challenging to test experimentally as rigs are often not constructed in temperature controlled environments. Particularly in gas phase reactors, temperature may be difficult to measure, as it may be higher at the surface of the catalyst than in the surrounding gas. It is noteworthy that the drawing in Figure 2.13 shows the highest reaction rate coincides with a temperature closer to 253.15 K for alcohol dehydrogenation and alcane-deuterium isotopic exchange [202]. Experimental work to optimize reaction temperature for $CO_2$ reduction found that 423 K was best for $CO_2$

photoreduction because of improved balance between $CO_2$ adsorption and product desorption [144].

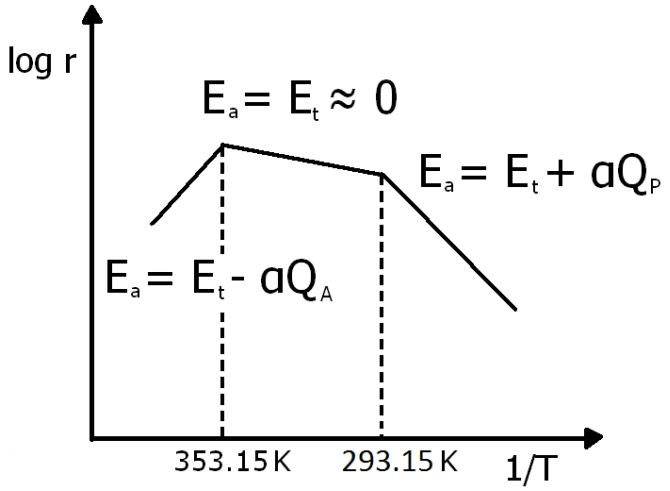


Figure 2.13 plots the changes in reaction rate with time and is dependent on Figure 2.12. The logarithm of reaction rate (r) was found to be a function of inverse temperature (1/T) with three regimes of behavior considering the apparent activation energy ($E_a$) as a function of true activation energy ($E_t$) and the heat of adsorption ($Q_a$) and desorption ($Q_p$) multiplied by constant (α), modified from Herrmann [96, 202].

Photocatalytic reactions can gain thermal energy from light. When the energy of incoming photons is higher than the band gap energy of the semiconductor releasing the excess energy as heat, or the energy of the incoming photon is lower than the band gap energy such that the energy is all converted to heat, unless reflected. The Shockley-Queisser limit of 1.34 eV in this case is also the band-gap energy that produces the least heat [197]. As the energy intake is optimized, the heat output is minimized. This acknowledges that using solar light will heat the catalyst to some extent. Therefore, due to this thermal gain, temperature should be monitored throughout photocatalytic testing or a cooling system used to modulate heat.

Pressure has an impact on the reaction rate in the case of liquid phase reactions, or liquid phase products. In chemical engineering, pressure changes in reactors can be indicative of reaction rate as products form in gas phase [200]. Pressure changes may give information on the nature of products by indicating phase of products. Pressure impacts the rate of the reaction through concentration as the higher the pressure, the higher the $CO_2$ dissolved in liquid phase. Rossetti and colleagues were able to use a high pressure (up to 20 bar) liquid phase photoreactor to improve the production yield with methane production as high as 1.73 mmol per hour and per $kg_{cat}$ at 358.15 K and 20 bar [203]. They attributed this performance improvement to an increase in the amount of dissolved

$CO_2$. Thus, the more $CO_2$ dissolved, the higher the concentration and yield. More specifically, studying the effect of pressure on reaction rates for liquid phase reactions allows for the measure of change in volume going from reactant state to the activated state [204].

## 2.6 Broadening the photocatalytic materials discussion

This chapter covers a wide swath of known, often accepted and agreed $CO_2$ photoreduction ground. The only real possible exception is the proposal of linking modifications more directly to improvement in experimental results. From this common ground, a wider discussion of benchmarking will be built. This wider discussion comes from the disagreement within the field of $CO_2$ photoreduction. It will require revisiting experimental goals and procedure, reporting, and a wide range of published literature. The intent is to be generous with the confusion, to over clarify, and to make many entry points into the discussion. Therefore, it will not have the same materials focus that so much of the literature has. The focus on materials improvements is critical for $CO_2$ photoreduction research, however this thesis departs from that discussion to assist in a more experimentally in-depth way. The end goal of $CO_2$ photoreduction research has many avenues, from fine chemical synthesis, to solar fuels, to $CO_2$ utilization, and all the same challenge. As Nahar *et al.* puts it, "The present situation in this area of research is quite confusing, and comparing the efficiency of the different photocatalysts is also difficult due to the high variability of influencing factors and reaction conditions" [205]. Therefore, this thesis clarifies the distinctions between product formation and efficiency, discussed phenomena, and then goes from there to widen the benchmarking discussion and evaluate an extended normalization result as a possible solution to the dual term problem of quantifying both the photon performance and catalytic performance of the photocatalyst (presented in more detail chapter 3).

Multiple avenues of investigative experimental work are undertaken in this pursuit. As shown in the scope of the thesis work, Figure 2.14, this thesis gives three main packages of experimental work alongside the analysis of current results and parameter influences in $CO_2$ photoreduction experimental work. Initial experiments compare six catalysts based on identical experimental conditions, with the results presented in chapter 4. These results cannot be used to analyze the dual term problem as they do not vary parameters that would enable a distinction between the performance based on the effectiveness of the light, reactor, or catalytic process. Stated another way, the results

being processed into different terms reveals no further information. To enable a comparison of various results analysis the experimental parameters need to be varied. This is done with a design of experiments (DoE) presented in chapter 5, and with a single variable being varied as is common in research presented in chapter 6.

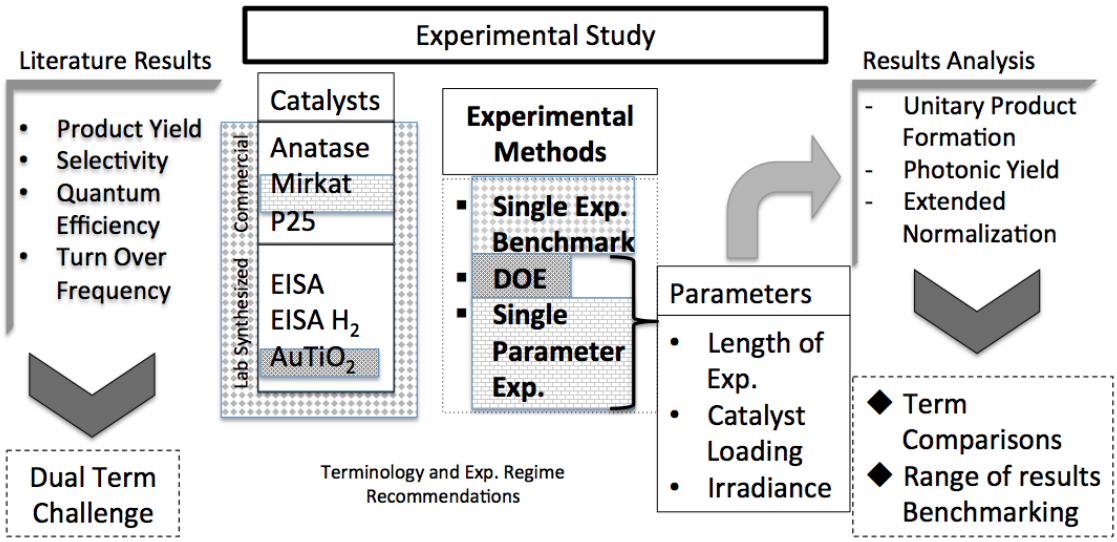


Figure 2.14 Scope of study undertaken in this thesis. The Literature Results are covered in chapter 3 enabling terminology recommendations, all samples compared by typical $CO_2$ photoreduction benchmarking in chapter 4, $AuTiO_2$ DOE experiments in chapter 5, Mirkat experiments varying single parameters in chapter 6 accompanied by regime recommendations to guide experimental work, and then the Mirkat and $AuTiO_2$ results can be analyzed in terms of the dual term problem and the benchmarking problem as covered in chapter 7.

DoE's enable influence of various experimental variables, or factors, to be directly compared as to the effect on an output, or response, and their interactions with each other on that response [206]. They can also be used in model development and for obtaining optimal reaction conditions, however these two purposes require very different experiments [207]. DoE for $CO_2$ photoreduction has been done previously [208]. Delavari and Amin chose a response surface methodology, and varied the reactor geometries of the mesh for catalyst support, the reaction parameters of photocatalyst loading and UV light power and reactant concentrations through feed ratios, along with the material property factor of calcination temperature. The reactant mixture included $CO_2$, $CH_4$, and $N_2$ as a carrier gas, and because of the $CH_4$ the results are challenging to compare to other studies.

In this case, the DoE was chosen because it is another process by which to optimize reaction rate that can enable a wider range of knowledge about factor influence to be investigated with fewer experiments. An optimized response could arguably be used for

benchmarking, either through comparison of conditions to enable a standard rate or through finding a singular performance value. However, in this case, as the experimental rig is limited to the influence of the factors of light intensity, catalyst loading, and reactor time, those are the bounds for which the response can be optimized. For the DoE experimental work the $AuTiO_2$ photocatalyst was used.

This work continues with a set of experiments done with the commercial sample Mirkat 211. These experiments vary light intensity, catalyst loading, and reactor time independently. Taken together, these two sets of data enable a discussion of benchmarking and the dual term problem. As shown in Figure 2.14, these results are all analyzed in terms of unitary product formation or specific rate (the catalytic term), photonic yield (the appropriate photonic performance term), and then the extended normalization that attempts to bridge between these two terms. This is discussed in chapter 7. Therefore, the work elucidates the current challenges to benchmarking and attempts to clarify what is necessary for benchmarking photocatalysts, quantify the effect of limitations to current $CO_2$ photoreduction, and resolve some of the challenges with the proposal of a new result term.

# CHAPTER 3 – ANALYSIS AND COMPARISON OF CARBON DIOXIDE PHOTOREDUCTION ON TITANIUM DIOXIDE BASED PHOTOCATALYSTS

Chapter 3 presents results from literature with a review of terms used in reporting results in section 3.1. These terms that are utilized most often include product yield (section 3.1.1), product selectivity (section 3.1.2), quantum efficiency (section 3.1.3) and turnover frequency (section 3.1.4), with key advantages and disadvantages of these terms and how they are used summarized (section 3.1.5). This is followed by section 3.2, which is a collection of terminology recommendations to clarify how best terms can be utilized to communicate within photocatalysis and externally with other disciplines. Acknowledgement of light and mass transport is incorporated into a process inclusive photocatalytic diagram (section 3.3). Within photocatalytic work there is a dual term problem (section 3.4.1), where the catalytic performance and photonic (light) performance are reported separately. When utilizing the key quantifications of specific rate and photonic performance for photocatalysts it is important to understand the experimental context of the terms (section 3.4.2-4). This chapter concludes with a list of experimental conditions that are recommended to be reported based on the literature review in Section 3.5.

## 3.1 Review of nomenclature in photocatalytic $CO_2$ reduction process and issues for benchmarking

When reviewing the current literature of $CO_2$ photocatalytic reduction, multiple terms are used to report conversion. The most common results given for the photocatalytic process are product formation based, such as yield [45, 62], evolved products and rate [209], or production [44]. Results include a variety of units implicating a lack of standardization in results processing. This is problematic for benchmarking due to the lack of contextual information given, such as information about the light and reactor, which would allow these results to be normalized [90]. These product formation results are then used to calculate other terms such as quantum efficiency, for which these data may not be utilitarian depending on the experimental conditions.

To delve deeper into how to quantify photocatalysts performance for $CO_2$ photoreduction, two aspects have been critically reviewed in detail here; firstly, the conversion measurements reported for photocatalytic reduction of $CO_2$ with $TiO_2$ based

materials; secondly, how the photon and catalytic reporting terms relate to the physical phenomena (what is included in the measurement and what is not). This is followed by recommendations on results terms and a proposal of the minimum information to be reported about the $CO_2$ photoreduction experimental work.

A body of articles, using $TiO_2$ based catalysts for the reduction of $CO_2$, has been reviewed to identify commonly used conversion measurements including chemical conversion and energy yield [56, 118, 119, 129, 132-134, 144, 145, 147-149, 151, 152, 190-195, 210]. Most of the articles describe photocatalysis, except two which are catalysis [118, 119] which are included to assist the discussion of rate based terms. Within photoreduction some studies test photocatalytic behavior or activity, through dye degradation tests [141, 142, 190, 211]. These studies are used to prove photocatalytic activity with the assumption materials will then be applied to processes such as water splitting or $CO_2$ reduction.

Within this review, a variety of definitions are explored to understand the diversity of reporting currently being implemented and point to confusion and identify limitations.

### *3.1.1 Product Yield*

Product yield is commonly reported in results for $CO_2$ photoreduction [129, 145, 149, 150, 193, 195, 212]. Product yield as used in photocatalysis is utilized in an inconsistent way, as described here. Product formation or product yield is reported irrespective of $CO_2$ reactant concentration. The units used vary greatly with product formation most commonly reported in micromole of product per gram of catalyst (μmoles/g) [129, 145, 149, 150, 193, 195, 212]. It has also been reported as only moles [194, 213]. The product yield can be refined and reported in units of micromole per gram of catalyst per hour of testing, i.e. μmole $g^{-1}$ $h^{-1}$ [112, 132, 137, 144, 150, 152, 214]. However, results can also be reported as amount of product/experiment length, without considering the amount of catalyst used [147].

Product yield values are measured most often for methane ($CH_4$) and carbon monoxide (CO), but can include various carbon, hydrogen and oxygen containing molecules, such as methanol ($CH_3OH$) or formaldehyde ($CH_2O$) [156]. Where a commercially available catalyst is used to benchmark, such as Degussa P25, the results provide a measurement that assists in comparing across research [154]. This catalyst benchmark is helpful; however, the effectiveness of such benchmarking has not been assessed. Further action in terms of experimental exploration and further data in terms of

results reporting are recommended to fully understand the photon uptake and then reaction efficiency. The concern is that applications of product yield data are limited when the variation in testing procedures are not reported.

The yield of a product in catalytic tests can be the amount of a product formed per amount of reactant fed into the reactor (Equation 3.1). This is different from conversion, which is the amount of reactant that has been converted per the amount of reactant fed into the reactor (Equation 3.2).

$$yield = \frac{moles\ of\ product\ formed}{moles\ of reactant\ at\ start} \qquad \text{Equation 3.1}$$

$$conversion = \frac{moles\ of\ reactant\ at\ start - final\ moles\ of\ reactant}{moles\ of\ reactant\ at\ start} \qquad \text{Equation 3.2}$$

These yield and conversion values allow for the comparison of the catalyst performance to be based on the catalyst's ability to convert quantifiable amounts of reactants. Product formation or product yield that is reported in $CO_2$ photoreduction is more varied, as the amount of reactants is not routinely measured. In many cases, $CO_2$ reduction tests are performed in excess of $CO_2$ (the reactant), pure $CO_2$ is used with no carrier gas and concentration is not monitored. Therefore, it is common for there to be no measurements of $CO_2$ amounts, and thus, conversion, as defined in Equation 3.2, is not calculated.

To inspect the product yield results another way, many examples of results are tabulated with two "levels" of normalization applied to assess comparability (Table 3.1). In Table 3.1 the specific rate (μmole/$g_{cat}$h) are calculated and then an extended normalization (μmole/$g_{cat}$hmLmW). This new calculation of μmole/$g_{cat}$hmLmW is based on normalizing for the volume of the reactor, the illuminated area of the catalyst (as distinct from specific surface area; with illuminated area specifying the boundary of the catalyst and light interface), and the incident irradiance. Normalization, thus, is being used to focus on the catalyst performance and remove the reactor and light sizing effects from the reported results. This enables wider comparison of results. It is already common to normalize for the catalyst mass [71]. In this way, and extended normalization enables some complexity of the results to be incorporated into the comparison.

The amount of catalyst used and length of experiment are the context reported within the articles included in Table 3.1. For a wider understanding of the context given in the articles contained in Table 3.1, reactor type, light source and product analysis is tabulated in appendix A. As seen in Table 3.1 the experimental context is often lacking making the calculation of the rate normalized by irradiance, volume of the reactor and illuminated area, impossible in seven out of the nine articles surveyed. Even more importantly, it is a combination of materials modification and experimental conditions that leads to the wide variation in results. Consider hydrogen production with a range of 0.42-6250 μmole/$g_{cat}$h and carbon monoxide ranging from 0.67-24000 μmole/$g_{cat}$h, also methane ranges from 0.1-2700 μmole/$g_{cat}$h. These ranges include an order of magnitude of $10^6$. While it is clear that articles are able to make comparisons internally, addressing that one material is performing better than another for the given experimental conditions, there is a loss if the context of the experiment is not taken into account. And $10^6$ gains become something that is not attributable to specific variables including material attributes, therefore, benchmarking has either not occurred, or current benchmarking could be considered "fuzzy".

Table 3.1 Normalized results from articles on $CO_2$ photoreduction covering a wider range of the literature.

| *Reference* | *Reported Result* | *μmole/$g_{cat}$h (rate normalized by catalyst loading)* | *μmole / $g_{cat}$ h mL mW (rate normalized by catalyst loading, volume of reactor, irradiance, and surface area of illuminated catalyst)* |
|---|---|---|---|
| *[149]* | 98μmole/g of hydrogen, 10-40 μmole/g carbon monoxide, 10-20 μmole/g of all hydrocarbons tracking methane, ethane, ethene, propane, propene, butane, butene, and methanol | 6.5 of hydrogen, 0.67-2.67 of carbon monoxide, 0.67-1.33 of hydrocarbons | Cannot calculate due to no irradiance, or illuminated surface area |
| *[194]* | 1-2.5 μmole/g of hydrogen and 17-22 μmole/g of methanol plotted against time in hours | 0.5-0.42 of hydrogen, 8.5-5.5 of methanol | No illuminated surface area |

| *Reference* | *Reported Result* | *µmole/$g_{cat}$h (rate normalized by catalyst loading)* | *µmole / $g_{cat}$ h mL mW (rate normalized by catalyst loading, volume of reactor, irradiance, and surface area of illuminated catalyst)* |
|---|---|---|---|
| *[152]* | 1500 µmole/(g*h) of hydrogen, 110-140 µmole/(g*h) of carbon monoxide, and 5-10 µmole/(g*h) of methane | 1500 of hydrogen, 110-140 of carbon monoxide, 5-10 of methane | No reactor volume or illuminated surface area |
| *[132]* | 0.1-0.145 µmole/(g*h) of methane plotted against time in hours | 0.1-0.145 of methane | Complicated by lumens, no volume or illuminated area |
| *[145]* | 100-1150 µmole/g of carbon monoxide and 150-325 µmole/g of methane | 962 of CO, but for an unknown doping of In $TiO_2$ | 0.00151 for CO for the In/$TiO_2$ (taken from abstract as length of experiments were unclear) |
| *[129]* | 40-70 mmole/g of carbon monoxide and 9-11 mmole/g of methane | 24000-13000 of carbon monoxide, 2700-2000 of methane | No irradiance or illuminated area |
| *[148]* | 0.25-0.4 µmole of carbon monoxide and 1.0-2.2 µmole of methane | 1.25-2 of carbon monoxide, and 5-11 of methane | No irradiance or illuminated area |
| *[151]* | 2250 µmole of hydrogen and 35 ppm/g of methane | 6250 of hydrogen (methane ppm not able to convert) | .00824 for hydrogen |
| *[147]* | 0.075-0.22 µmole/h of carbon monoxide | 0.75-2.2 of carbon monoxide | No volume of reactor |

Considering the higher expectations of more complete reporting from more recent articles this exercise can be completed again as seen in Table 3.2, where the ability to calculate the reactor volume and irradiance normalized result leads to a new range to consider. For specific rate (µmole/$g_{cat}$h) results the four article range is 1.86-5662.5 for CO, a range in magnitude of $10^3$. The range of results for µmole/$g_{cat}$hmLmW now is 6.43 x$10^{-5}$ to 8.89 x$10^{-3}$ and is, therefore, within $10^2$ of each other. Obviously, this is not a large sample size and the comparison is limited by incomplete reporting to two articles. And this incomplete reporting is the same as what has been limiting benchmarking as discussed in section 1.4.1, with particularly the lack of data [81] continuing to be an issue.

Table 3.2 Results from articles in 2016 and 2017 giving reported results, and normalized results as a specific rate, and then normalizing for the volume of the reactor, the illuminated area of the catalyst (as distinct from specific surface area), and the incident irradiance.

| *Reference* | *Reported Result* | *µmole/$g_{cat}$h (rate normalized by catalyst loading)* | *µmole / $g_{cat}$ h mL mW (rate normalized by catalyst loading, volume of reactor, irradiance, and surface area of illuminated catalyst)* |
|---|---|---|---|
| *[209]* | 290 µmole of carbon monoxide for $Sr_2KTa_5O_{15}$ | 58 for carbon monoxide | Unable to calculate, no irradiance or illuminated area |
| *[62]* | 14.91 µmole/g of carbon monoxide, 3.98, 4.11 and 0.41 of methane, ethane, and ethane respectively, for 5 wt% graphene oxide doped oxygen rich $TiO_2$ (UV and vis results) | 1.86, 0.49 for carbon monoxide and methane | 6.43 $x10^{-5}$ for carbon monoxide and 1.72 $x10^{-5}$ for methane |
| *[44]* | 3 µmole/g methanol for $TiO_2/Ti_4O_9/Cu_2O$ | 0.6 for methanol | No reactor volume or illuminated area |
| *[45]* | 11325, 97, 0.74, 2.94, 15.97 and 8 µmole/g for carbon monoxide, methane, ethane, ethane, propene and propane for 1%NiO-3.5% $In_2O_3/TiO_2$ | 5662.5 and 48.5 for carbon monoxide and methane | 0.00889 and 7.62 $x10^{-5}$ for carbon monoxide and methane |

Considering the utility of using specific rate, as discussed in section 2.8, it would be pertinent to discuss work with liquid phase photocatalysis that has been done considering reporting of rate results. Hugo de Lasa *et al.*, argue for apparent reaction parameters to be corrected by either the irradiated volume, area or weight divided by the reactor volume [215]. This is based on calculations conducted in a previous article introducing those factors [216]. The reaction rate, in this case, is multiplied by a ratio characterizing a relationship of irradiated catalyst or space in the reactor. This allowed for the reaction rate that was characterized by the volume of the reactor to then be converted into units that characterized the amount of irradiated catalyst used or irradiated volume. This is simply a correlation to discount inactive portions of the photocatalyst. The challenge in utilizing this correlation for benchmarking is that it does not take into

account the desire to minimize catalyst used, or maximize the effectiveness of the catalyst. To take this into account the mass of catalyst or irradiated volume or area needs to be in the denominator. Therefore, the modifications prove more useful to the purposes of kinetics investigations and process parameters, not analysis of the material performance or benchmarking.

When used as a specific rate, product yield results can be considered in terms of the various parameters affecting photoreduction (as discussed in Chapter 2 section 2.8). Ideally input variables would be optimized and the results normalized to the reactor parameters to isolate material performance. Once the reaction modifications are understood and incorporated into the results though optimization and normalization then the work of understanding the materials modifications can be more directly accomplished (as discussed in with materials matrix, section 2.3.4).

### *3.1.2 Product Selectivity*

Product selectivity can refer to the preferential production of one compound over another [217], and is defined as the amount of a specific product formed per reactant converted [84].

$$Selectivity\ (catalysis) = \frac{moles\ of\ product\ formed}{moles\ of\ reactant\ at\ start - final\ moles\ of\ reactant} \quad \text{Equation 3.3}$$

When the conversion of the reactant gas is not measured, the results can vary more greatly due to uncertainty of measuring all gas products. Collado *et al.* reported product selectivity in photoreduction of $CO_2$ as the moles of a specific product over the total moles of products [149]:

$$Selectivity\ (CO_2\ photoreduction) = \frac{moles\ of\ specific\ product\ formed}{total\ moles\ of\ all\ products\ formed} \quad \text{Equation 3.4}$$

Thus, selectivity is often reported in a way that is product dependent. There is a challenge to ensure all products are accounted for to ensure selectivity is as accurate as possible. Examples of selectivity in the literature include, Collado *et al.* reported the selectivity results for $TiO_2$ anatase as 50.6% for $H_2$ production, 42.9 % for CO and $CH_4$, ethane ($C_2H_6$), ethane ($C_2H_4$), propane ($C_3H_8$), propene ($C_3H_6$), butane ($C_4H_{10}$), butene

($C_4H_8$), and methanol ($CH_3OH$) production selectivities between 3.2-0.1% [149]. This was compared to $TiO_2$ with 3.0 weight percent silver loading giving a selectivity of 74.8% for $H_2$, 6% for CO, and a range of 4.5-0.1% for production of $CH_4$, $C_2H_6$, $C_2H_4$, $C_3H_8$, $C_3H_6$, $C_4H_{10}$, $C_4H_8$, and $CH_3OH$ separately [149]. Tahir *et al.* reported selectivity for CO (25.8%) and $CH_4$ (69%) for a monolith reactor and then in comparing a monolith reactor with In doped $TiO_2$ vs. undoped $TiO_2$ selectivity was reported for CO (94.39% and 34.87% respectively), $CH_4$ (5.44% and 36.27% respectively), $C_2H_4$ (0.034% and 1.22% respectively), $C_2H_6$ (0.147% and 0.64% respectively), and $C_3H_6$ (effectively 0 for both) [145, 193]. Anpo compared tetrahedrally coordinated Ti-oxide single-site catalysts based on their $CH_3OH$ selectivity which ranged from 21-58% [39]. Although the measurement of product selectivity is rare, selectivity is important to compare $CO_2$ reduction endeavors for producing solar fuels.

### *3.1.3 Quantum Efficiency*

The quantum efficiency of a material is a dimensionless number that characterizes a material's ability to absorb photons and then for those photons to be productive depending on the application. In the case of photovoltaic cells, the quantum efficiency is the success rate of a photon exciting an electron across the band-gap energy threshold. In the case of $CO_2$ photoreduction, the electrons are productive when they contribute to $CO_2$ reduction. Quantum efficiency is reported in photocatalysis as a function of the product formation rate or product yield. This is a direct consequence of limited reactants tracking, and instead only measuring products. Lee and colleagues report photoreduction quantum efficiency (PQE); using Equation 3.5 (units are shown in parenthesis) [194]. Equation 3.5 is sometimes referred to as apparent quantum efficiency, and is equivalent to how quantum efficiency is used by Tahir and Amin [145]:

$$PQE = \frac{n_e \times Product\ formation\ rate\ \left(\frac{nmole}{h}\right)}{Incident\ photon\ rate\ \left(\frac{nmole}{h}\right)} \qquad \text{Equation 3.5}$$

The term $n_e$ is defined as the number of electrons needed to reduce the reactant to one product molecule. The numbers of electrons necessary for the formation of products, such as hydrogen, carbon monoxide and methanol, used to calculate PQE are presented in Table 3.3. For $H_2$, the number of electrons is 2, methanol ($CH_3OH$) would

use 6, and CO would require 2 [194]. In the supplementary information supplied by Singh *et al.*, they detail many more species including $CH_4$ formation with 8 electrons, ethane ($C_2H_6$) with 14, ethylene ($C_2H_6$) with 12 and to hexane ($C_6H_{14}$) needing 62 electrons to be formed with this information incorporated into Table 3.3 [33]. This is not indicative of how many $CO_2$ molecules are consumed. These moles of electron values are calculated from electronic stoichiometry where the electronegativity of the molecules relative to their neutral state give the overall oxidation state which is then used to calculate electrons. For example, take ethanol ($C_2H_6O$; $aCH_3bCH_2OH$); in this case, the oxidation state of aC is -3, and bC is -1. To reduce the two $CO_2$ molecules that have an oxidation state of +4, 7 and 5 electrons are necessary respectively to form ethanol and, thus, 12 electrons total are needed.

Table 3.3 Electrons used in formation of products [33, 109, 112, 194, 205].

| *Product Species* | *Formula* | *Electrons per molecule* |
|---|---|---|
| *Hydrogen* | $H_2$ | 2 |
| *Carbon Monoxide* | CO | 2 |
| *Formic Acid* | HCOOH | 2 |
| *Formaldehyde* | HCHO | 4 |
| *Methanol* | $CH_3OH$ | 6 |
| *Methane* | $CH_4$ | 8 |
| *Acetaldehyde* | $C_2H_4O$ | 10 |
| *Ethylene* | $C_2H_4$ | 12 |
| *Ethane* | $C_2H_6$ | 14 |
| *Propylene* | $C_3H_6$ | 30 |
| *Propane* | $C_3H_8$ | 32 |
| *1-Butene* | $C_4H_8$ | 40 |
| *Butane* | $C_4H_{10}$ | 42 |
| *1-Pentene* | $C_5H_{10}$ | 50 |
| *Pentane* | $C_5H_{12}$ | 52 |
| *1-Hexene* | $C_6H_{12}$ | 60 |
| *Hexane* | $C_6H_{14}$ | 62 |

Some of the semi-reactions for the conversion of $CO_2$ used to derive electrons used are equations 2.1-2.9 listed in section 2.3 in the context of redox potentials [81, 107].

The incident photon rate is calculated by Equation 3.6:

$$Incident\ photon\ rate = \frac{I_{int}\left(\frac{W}{m^2}\right) \times A_{proj}(m^2)}{\frac{hc}{\lambda}\left(\frac{J}{number\ of\ photons}\right)} \qquad \text{Equation 3.6}$$

Where $I_{int}$ is the incident light irradiance, $A_{proj}$ is the area of light irradiation, hc is Plank's constant multiplied by the speed of light, and λ is the wavelength of light. The area of light irradiation is taken as the whole area projected onto the reactor. The light intensity, area of light irradiation, and the wavelength of light used are all considerations that need to be clearly reported. The light used for testing could have a specific single wavelength or broad range wavelength spectra. If a wavelength spectrum is used, then these wavelengths may have different intensities, necessitating further integration to calculate the light intensity provided by a broad light spectrum. Reactors can also modify light intensity that reaches the photocatalyst. Variations in the incident photon rate calculated can cause an underestimate or overestimate the quantum efficiency calculated. Therefore, it is important to report clearly how incident photons are calculated, so they can be compared to the radiation spectrum used.

In the case of quantum efficiency which is calculated using photons absorbed by the catalyst, terms used include quantum efficiency [218] or as Anpo calculated, quantum yield [39] (Equations 3.7 and 3.8, respectively).

$$Quantum\ efficiency\ percentage = \frac{product\ formation\ rate\ \times n_e}{number\ of\ photons\ absorbed} \times 100 \qquad \text{Equation 3.7}$$

$$Quantum\ yield = \frac{Number\ of\ photo-formed\ products}{number\ of\ photons\ absorbed} \qquad \text{Equation 3.8}$$

Collado *et al.* report apparent quantum yield (AQY) for $CO_2$ photoreduction studies by Equation 3.9 [149]:

$$AQY = \frac{\sum(product\ formation\ rate\ \times n_e)}{number\ of\ photons} \qquad \text{Equation 3.9}$$

In this case, the sum of products represent the successful conversion of incoming photons, and acknowledgment of limits on product detection analysis needs to be stated.

Conversion is measured with products as a proxy relative to conversion, as seen before in section 3.1.1 based on reactants concentration. This term is then used to calculate Quantum Yield Index (QYI) that attempts to quantify the impact of metal doping (the doping metal was silver in this case) in quantum yield performance (Equation 3.10) [149]. By calculating the quantum efficiency as a function of products without full mechanism analysis the products detected could limit the efficiency calculated.

$$QYI = \frac{AQY\ Ag/semiconductor}{AQY\ semiconductor} \qquad \text{Equation 3.10}$$

Table 3.4 presents values found in current research for the variety of quantum terms described above. The variations in quantum efficiency presented in Table 3.4 show the lack of consensus on quantum efficiency measured from indexing results to internal or external quantum efficiency used. The quantum efficiencies measured are mostly small, as can be seen in Table 3.4; the efficiency is wide ranging from 0.0051% PQE to 20% internal quantum efficiency (IQE), and varied widely compared to the 4.6-6% efficiency of photosynthesis [35].

Table 3.4 Different examples of how photon performance or quantum results values are reported.

| Reference | Reported term | Baseline comparison | Best result from article |
|---|---|---|---|
| ***[149]*** | Quantum Yield Index | Anatase $TiO_2$ with low sulfate content (<0.8%) obtained from Millenium Co. used as benchmark performance, set to 1 QYI | 2.7 QYI for a 3.0 weight percent Ag loaded $TiO_2$ through wet impregnation method |
| ***[145]*** | Quantum Efficiency for CO | Cell type photoreactor with $TiO_2$ 0.0005% QE | Monolith with $TiO_2$ 0.0042% QE, monolith with In 10 weight percent loading on $TiO_2$ 0.10% QE |
| ***[145]*** | Quantum Efficiency for $CH_4$ | Cell type photoreactor with $TiO_2$ 0.0028% QE | Monolith with $TiO_2$ 0.0301% QE, monolith with In 10 weight percent loading on $TiO_2$ 0.022% QE |

| Reference | Reported term | Baseline comparison | Best result from article |
|---|---|---|---|
| *[149]* | Quantum Yield Index | Anatase $TiO_2$ with low sulfate content (<0.8%) obtained from Millenium Co. used as benchmark performance, set to 1 QYI | 2.7 QYI for a 3.0 weight percent Ag loaded $TiO_2$ through wet impregnation method |
| *[194]* | Photoreduction Quantum Efficiency | Single photocatalyst system Pt loaded $CuAlGaO_4$ ($H_2$ generation and $CO_2$ reduction) 0.0019% PQE | Dual photocatalyst system utilizing Pt loaded $CuAlGaO_4$ for $CO_2$ reduction and Pt loaded $SrTiO_3$:Rh for $H_2$ generation and $WO_3$ for $O_2$ generation 0.0051% PQE |
| *[218]* | Quantum Efficiency | Slurry batch annular reactor with 1 weight percent Pd and 0.01 weight percent Rh loaded $TiO_2$ 0.002% QE for methane | Internally illuminated monolith reactor 1 weight percent Pd and 0.01 weight percent Rh loaded $TiO_2$ 0.015% QE methanol 0.047% QE acetaldehyde |
| *[39]* | Quantum Yield | None | 0.3% QY for highly dispersed Ti-oxide catalysts |
| *[33]* | Internal Quantum Efficiency | varied solar irradiance | Over 20 % IQE with platinum doped $TiO_2$ and 1 solar irradiance used |

### *3.1.4 Turnover Frequency*

Turnover frequency (TOF) is a term used to measure the performance of a catalyst. It refers to the number of product molecules that can be produced by a catalyst in a specified amount of time, or the number of catalytic cycles performed in a certain amount of time, equation 3.17 [219]. It is recommended, however, that TOF is appropriate for use on continuous reactions, and not for batch catalytic reaction, as TOF is concentration dependent, and batch reactions need either to vary initial concentration or length to calculate a rate [84]. They argue batch reactions can be utilized, however with great care to vary initial concentrations of all species, and that to report an average from a single

data point does not constitute a rate. Where continuous reactions are possible, the main challenge in calculating TOF for $CO_2$ photoreduction is the identification of active sites. In the case of metal doping sites, metal dispersion (the number of metal atoms on the surface with respect to the total amount,) has been used to calculate the TOF for catalytic reactions [118, 119]. However, in this case, the metal is only a promoter that slows electron hole recombination; therefore, it is of limited utility. Because semiconductors are being used, it may be useful to consider specific surface area when calculating TOF. However, this makes modifications such as metal doping difficult to compare. Serpone and Emeline argued that catalytically active sites need to be defined in the ground state and not excited state [101]. In this way, the TOF value would contain information on the photon uptake and product formation. This is challenging due to lack of consensus on what constitutes a photo catalytic site, and thus, active site identification remains a barrier [100].

$$TOF = \frac{volumetric\ rate\ of\ reaction}{number\ of\ active\ sites/volume}$$
$$= \frac{moles\ product}{time\ moles\ catalyst}\ units: 1/time \qquad \text{Equation 3.11}$$
$$= \frac{r_C}{n_{act\ sites}/_V} = \frac{n_P}{t \cdot n_{cat}}$$

Attempts have been made at calculating catalytic performance by identifying or approximating active sites, as presented in Table 3.5. Presenting articles ranging from catalysis for $CO_2$ reduction to photocatalysis, Table 3.5 gives the best results found in each article. The range of results is broad from 1.04 x $10^{-3}$ $s^{-1}$ TOF of $CH_4$ to 9.12 x $10^{-27}$ s-1 TOF of CO [118, 220]. Most importantly, Table 3.5 identifies active sites used for calculations, and thus, gives options tried for calculation of TOF.

Photocatalytic turnover numbers (TON) have been calculated (equation 3.12) for a liquid catalyst used in $CO_2$ reduction, however, in this case individual catalyst sites were identified by added supramolecules, namely two kinds of Ru(II) complexes [221]. Eaton *et al.* estimated active sites for a photocatalyst through phenyl-phosphonic acid titration, testing the reactivity by photooxidizing benzyl alcohol [222]. This provides information on accessible surface sites.

An insightful review of catalytic measures of photocatalysis for water splitting has been conducted finding surface area or photoactive surface site normalized results to provide insights into bulk and surface variations in photoactivity [223]. This was an

improvement on mass normalized results. This supports the glossary suggestion to use specific surface area when calculating TOF as an improvement to approximate active sites in TOF results [89].

$$TON = TOF \times lifetime\ of\ the\ catalyst\ (dimensionless) \qquad \text{Equation 3.12}$$

Table 3.5 Examples of results from tests reporting catalytic measurements (TOF and TON)

| *Reference* | *Test conducted* | *Best result from reference* | *Material and active site* |
|---|---|---|---|
| *[118]* | Catalytic hydrogenation of $CO_2$ to $CH_4$ (methanation) | 1.04 x $10^{-3}$ $s^{-1}$ TOF of $CH_4$ at 120°C | Photohole-oxidation-assisted fabricated ultra-small Ru clusters (~1.5 nm) on $TiO_2$ loading density roughly $10^{17}$ $m^{-2}$. Active site determined based on metal dispersion. |
| *[119]* | Catalytic methanation | 2.14 x $10^{-3}$ $s^{-1}$ TOF of $CH_4$ at 200°C | Ni nanoparticles immobilized on $TiO_2$ (4.89 weight percent Ni), Ni dispersion 43%. Active site determined based on metal dispersion. |
| *[220]* | Catalytic $CO_2$ hydrogenation | 64.8 x $10^{-25}$ $h^{-1}$ for alcohols and 328.2 x $10^{-25}$ $h^{-1}$ for CO TOF at 200 °C and 275 °C respectively | 3 weight percent Fe and 10 weight percent Cu loaded on bimodal MCM-41 mesoporous silica supports. Active site moles surface metal atoms. |
| *[222]* | Benzyl alcohol photooxidation | 2.1 $h^{-1}$ TOF mole product per mole phenylphosphonic acid bound | $TiO_2$ anatase. Assumed one catalytic active site per titrated site. |
| *[221]* | $CO_2$ photoreduction | 562 TON of HCOOH (produced HCOOH/added supramolecule) | Photocatalyst made of supramolecular complexes consisting of 2 photosensitizer units $[Ru(dmb)_n(BL)_{3-n}]^{2+}$ [dmb = 1,2-bis(4'-methyl-[2,2'-bipyridin]-4-yl)ethane] and 1 catalyst unit $[Ru(dmb)_m(BL)_{2-m}(CO)_2]^{2+}$. Each added supramolecule as active site. |

An interesting term developed has been turn over productivity (TOP, equation 3.13) [58]. This appears to be trying to work towards including process parameters in the assessment, however, it focuses more on the photonic response and does not enable a

calculation of reaction rate. The formulation given is for the whole reactor, which effectively multiplies by one simplifying to equating the TOP with the quantum yield (as it is well established that the ideal gas law is PV = nRT). It is true that for the photocatalyst surface the ideal gas law would not hold, however over the bulk of the reactor in a batch reaction it would.

$$TOP\ (\%) = QY \times \frac{PV}{nRT} \qquad \text{Equation 3.13}$$

It is an intriguing question to consider how to incorporate the reaction parameters such as volume, pressure, and temperature in the analysis. Unfortunately, this is not necessarily accomplished with the TOP term.

### *3.1.5 Summary of Conversion Measurements*

Table 3.6 summarizes the various conversion terms reviewed in this section, with example values from the literature or how these terms are used and the advantages and disadvantages of these terms. Most importantly, it is clear that the terms are not standardized. It can be seen that there are many products to be reported. Product results are then consolidated into the quantum efficiency term that tries to identify the product formation relative to the light input. Lastly, there is the TOF which is not reported currently in $CO_2$ reduction and thus the example comes from catalysis, but is nonetheless important as a term to be reported in the future for benchmarking. Therefore, it can be observed that results all depend on product results and that there is no clear indicator that testing is tailored to assess particular performance. It should be noted that the examples presented in Table 3.6 are picked as typical results ranges found in the literature.

Table 3.6 Advantages and Disadvantages of Terms used to report Conversion

| Conversion Term Reported | Example | Advantages | Disadvantages |
|---|---|---|---|
| ***Product Yield*** | 1500 µmole/(g*h) of $H_2$, 110-140 µmole/(g*h) of CO, and 5-10 µmole/(g*h) of $CH_4$ [152] | ▪ Widely reported<br>▪ Can use commercial benchmark | ▪ Limited comparability<br>▪ Lack of information<br>▪ Lack of normalization |
| ***Product Selectivity*** | For $CH_4$ 3.2-8.1% [149] | ▪ Focus on particular product aids comparison | ▪ Lack of consensus on products to compare<br>▪ Often calculated from products detected |
| ***Quantum Efficiency*** | Monolith with 10 weight percent of In loaded on $TiO_2$, 0.022% QE [145] | ▪ Greater normalization for products<br>▪ Comparing results quantifying photon success rate | ▪ Not often calculated the same way across research<br>▪ Lack of normalization for testing procedure<br>▪ Often calculated from products detected |
| ***Turnover Frequency*** | $1.04 \times 10^{-3}$ $s^{-1}$ TOF of $CH_4$ at 120°C for catalytic hydrogenation of $CO_2$ to $CH_4$ on photohole-oxidation-assisted fabricated ultra-small Ru clusters loaded on $TiO_2$ [118] | ▪ Quantifies catalytic performance | ▪ Challenge in active site identification |

Product yield measurements with units per time can be considered as a specific rate and used to analyze catalytic performance. Experiments used to report selectivity should clarify all products detected and acknowledge the limitations to selectivity when considering results. Photocatalytic quantum efficiency needs to be standardized to express a consistent measurement [89]. For TOF measurements, active sites need to be identified when $CO_2$ reduction mechanisms are understood to a greater extent, or it may be possible to utilize illuminated surface area. Addressing these points would enable wider comparison across research. This is not to exclude other terms that could prove to be useful in the future such as carbon fraction utilization, waste to products ratios, avoided $CO_2$, or energy consumption ratios [224]. Most importantly, these reviewed terms are not

standardized and should not necessarily be used for future work. For future terminology usage, glossaries are recommended such as the IUPAC Glossary of Terms [89] (discussed in Chapter 2), or the list of terms in section 3.2.

### 3.2 Terminology Recommendations

This section lists terms and definitions to clarify terminology and units independently of section 3.1. Here they are presented together as the recommended definitions of terms to be used to report photocatalytic results for $CO_2$ reduction. In many ways, this section is about realigning $CO_2$ photoreduction work with catalysis norms and reintroducing recommended terms because these standard terms enable wider applicability and collaboration. The terms defined here are reaction rate, quantum yield, photonic yield, photonic efficiency, conversion, yield, selectivity, product distribution, turn over frequency, and unitary production, unitary productivity, and conversion molar balance. This may appear repetitive, however, this is to collect terms and clear up confusion that may linger from the literature review section of this chapter (section 3.1). It should also be noted that the goal is larger still. As Bligaard *et al.* point out, the metric goals for benchmarking, or what is "relevant in every study" when discussing catalysis include "reactant scope, rate, yield, selectivity, reaction mechanism, [and] deactivation behavior" [84]. These are relevant to photocatalysis as well, and here the rate, yield, selectivity and photonic results are discussed in terms of a discussion of how to facilitate benchmarking.

A reaction controlled by the *chemical regime* is a necessary condition to calculate reaction rate $r_C$, defined in Equation 3.14:

$$r_C = -\frac{d[A]}{dt} \qquad \text{Equation 3.14}$$

where [A] is limiting reagent concentration and t is reaction time; it can also be expressed as in Equation 3.15:

$$r_C = k_C \cdot [A]^n \qquad \text{Equation 3.15}$$

where $k_c$ is the kinetic constant for the chemical reaction and n is reaction order.

Turning now to mass based metrics, conversion is the amount of limiting reactant that is consumed during the reaction divided by the amount of reactant fed into the system [200]. Conversion, X, (of the limiting reactant) is defined as:

Equation 3.16

$$X_{CO_2} = \frac{n_{CO_{2(0)}} - n_{CO_2}}{n_{CO_{2(0)}}} = 1 - \frac{n_{CO_2}}{n_{CO_{2(0)}}}$$

Where $n_{CO_{2(0)}}$ is the initial amount of $CO_2$, and $n_{CO_2}$ is the final measured amount of $CO_2$, assuming $CO_2$ is the limiting reactant which is certainly true in the case of liquid phase reactors. The *conversion* metric is best suited to the quantification of *$CO_2$ utilization*.

In the case of batch reactions, where the volume does not change the concentration can be used, however, the n designates number molar.

If water is the limiting reactant, which is most likely the case in gas phase reactors, such as those used in this thesis work, the conversion is defined as:

$$X_{H_2O} = \frac{n_{H_2O_{(0)}} - n_{H_2O}}{n_{H_2O_{(0)}}} = 1 - \frac{n_{H_2O}}{n_{H_2O_{(0)}}} \qquad \text{Equation 3.17}$$

There are multiple definitions of yield in the literature. Also, yields can be instantaneous (expressed in rates) or global (expressed in amounts). Instantaneous yields can be derived by dividing by time, thus converting amounts to rates. The most common definition is that yield ($y_p$) is the amount of product P formed per amount of product that could be formed (Equation 3.18).

If A is the limiting reactant, and P is the desired product:

$$y_p = \frac{n_p}{n_{A,(0)}} \left|\frac{\nu_A}{\nu_p}\right|, \left(n_p^{max} = n_{A,(0)} \frac{\nu_p}{\nu_A}\right) \qquad \text{Equation 3.18}$$

Where, the number of moles P measured, ($n_p$), over the initial number of moles limiting reactant, ($n_{A,(0)}$), are multiplied by the stoichiometric ratio of reactants and products, $\left|\frac{\nu_A}{\nu_p}\right|$.

The definition of selectivity ($S_P$) is the total amount of desired product formed per total amount of limiting reactant consumed, alternatively Fogler defines this as yield [200]:

$$S_P = \frac{n_P}{n_{A,(0)} - n_A} \cdot \left|\frac{\nu_A}{\nu_P}\right| \qquad \text{Equation 3.19}$$

A benchmarking recommendation from Bligaard *et al.* for supported and unsupported molecular catalysis, that is equally relevant to photocatalysis is the reminder that "selectivity must be reported with the corresponding conversion" giving the challenge to more accurately track $CO_2$ photoreduction reactants [84]. Another definition from Fogler of selectivity is the moles of desired product, $n_P$, per moles of undesired product, $n_u$ [200], which would be more appropriate for full scale continuous production:

$$S_{P/u} = \frac{n_P}{n_u} \qquad \text{Equation 3.20}$$

Importantly product selectivity should be distinct from product distribution. Product distribution $ is defined as:

$$\$_P = \frac{n_P}{\Sigma n_{P,i}} \qquad \text{Equation 3.21}$$

In the case of turnover number (TON) and TOF (as discussed in section 3.1.4), new terms may be more utilitarian, particularly if the $CO_2$ photocatalytic experimental work is not conducted with a continuous flow process. Where the moles of catalyst or number of active sites are difficult to define or quantify, the recommendation is to use these terms with clarity and appropriate caution respectively;

Unitary production, $U_p$, defined as:

$$U_p = \frac{n_P}{Catalyst\ amount\ (g)} \qquad \text{Equation 3.22}$$

Unitary productivity, $\dot{U}_p$, defined as:

$$\dot{U}_p = \frac{n_P}{Catalyst\ amount\ (g) \cdot time\ (h)} \qquad \text{Equation 3.23}$$

These unitary production and productivity rates could also be calculated using specific surface area multiplied by amount of catalyst used, instead of only grams of catalyst used, to better reflect available active sites. The units utilized need to be clearly expressed. The emphasis with this "unitary" term is a shift to clearly indicate units. Therefore, this collection of terms are referred to as *unitary product formation*.

As the comparisons of terms has unfolded, terms from Fogler have been included in this summary of definitions even though they are more suitable to large scale, chemical engineering processes. This highlights the importance of awareness of terms available alongside process realities, and it enables a recognition of the wider context photocatalysis resides in within reaction engineering and catalysis. When possible $CO_2$ photoreduction research should identify definitions utilized to enable collaboration and understanding in a wider context. In the current case of photocatalysis, the experimental work and research so far has been accomplished as a small scale process, and therefore, it may make more sense to have a conversion molar balance defined as:

$$conversion\ molar\ balance = \frac{n_P}{n_{CO_2,(0)} - n_{CO_2}} \times 100 \qquad \text{Equation 3.24}$$

Currently, $carbon\ molar\ balance = \frac{n_P + n_{CO_2}}{n_{CO_2,(0)}}$, but since $n_{CO_2,(0)}$ is almost equal to $n_{CO_2}$, the metric does not show a significant change with extremely low conversions. As a *conversion molar balance* the term allows for scrutiny of the loss of products or $CO_2$, even at a ppm level, however it should be acknowledged that there are limitations to analytical techniques as follows. Due to the significance of the error relative to the accuracy of the analytical technique, and inherent limitations therein, a 100% molar balance should not be expected. This means a conversion molar balance would give a better indication of the adequacy of the analytics by comparing it with error margins.

### 3.3 A phenomena inclusive photocatalytic diagram

A schematic for photocatalysis which includes the complexities found in experimental work is depicted in Figure 3.1. This figure covers internal and external phenomena at the photocatalytic surface, each characterized by different rates and physical laws. Here $TiO_2$ is considered, as it is the most widely studied material in the discipline. Starting with the external phenomena, A and D are the reactant concentrations in the bulk of the electron acceptor and electron donors, respectively, and R and O are the products concentrations in the bulk (the ad subscript, such as $A_{ad}$, indicates adsorption on the photocatalytic surface). The coinciding external behavior has to do with the light transport to the photocatalytic surface and then absorption.

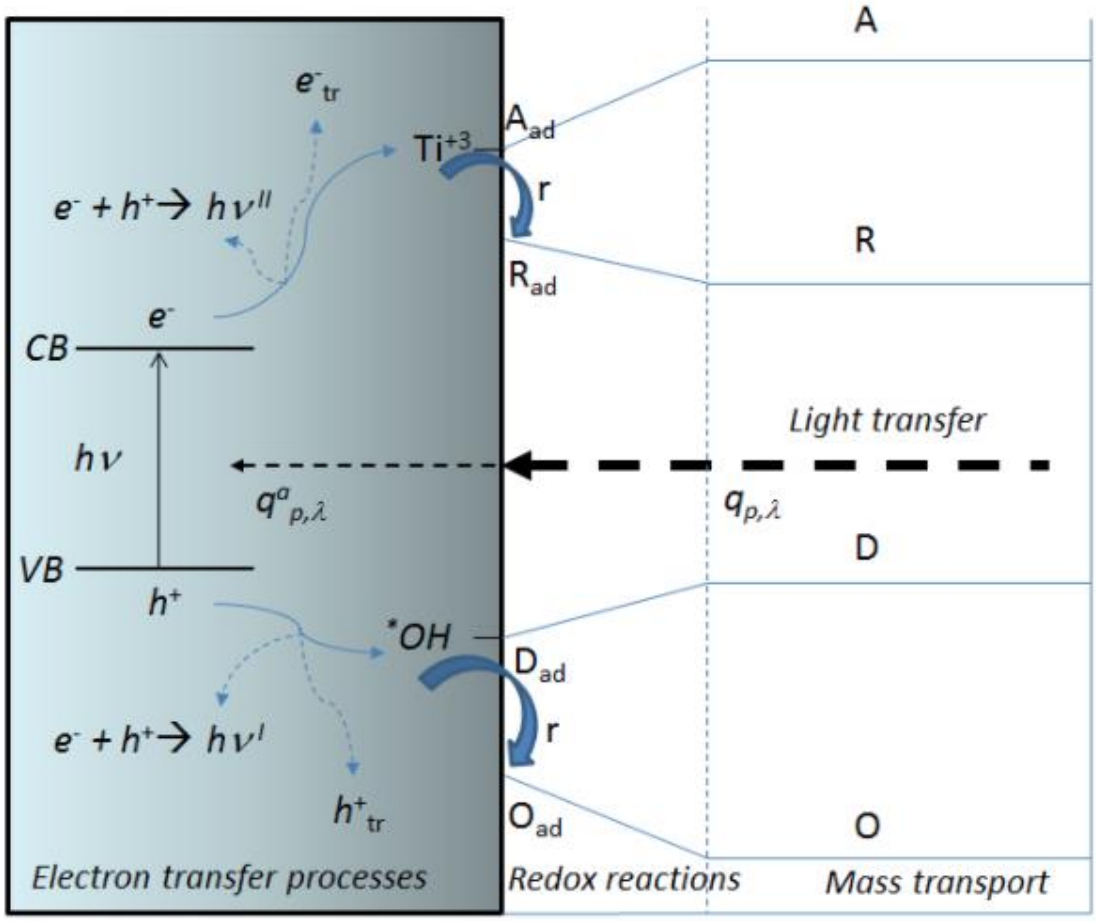


Figure 3.1 Schematic of the photocatalytic process including external (right side) and internal (left side) phenomena relevant to photocatalytic experimental testing on a $TiO_2$ photocatalyst material. Figure made by Dr. Eva Sanchez Fernandez.

Internally, considering titanium dioxide electronic structure, the valence band [VB] is fully occupied by electrons [$e^-$] in ground state. When excited by a photon, electrons can be promoted to the conduction band [CB]. This promotion to an excited state occurs only if the energy [hν] from the absorbed (a superscript) photon (p subscript at a specific wavelength subscript λ) flux [$q^a_{p,\lambda}$] is greater than or equal to the band gap of the semi-conductive material. The excited electrons that did not recombine [$e^- + h^+ \rightarrow h\nu^I$, $e^- + h^+ \rightarrow h\nu^{II}$] with holes ($h^+$), or get trapped [$e^-_{tr}$, $h^+_{tr}$], would then be available to migrate to the surface and react, forming $Ti^{+3}$ and *OH [107]. Once the electron has reached the surface catalytic site, it is available to reduce adsorbed $CO_2$ [a redox reaction, with rate r, $A_{ad}$ (acceptor) to $R_{ad}$ (reduced)], while the hole is available to an oxidation reaction with $H_2O$ [$D_{ad}$ (donor) to $O_{ad}$ (oxidized)].

In summary the phenomena covered in Figure 3.1 are:

- Light transfer from the emission source to the catalyst surface

    - Reactor transmission
    - Material absorption
- Electron transfer processes
    - charge separation
    - electron with hole recombination (dotted blue line)
    - electron and hole trapping in the bulk (dotted blue line)
    - electron migration to the surface (solid blue line)
- Surface redox reactions
- Mass transport
    - Reactants mass transport from bulk to photocatalytic surface and adsorption
    - Products desorption and mass transport to bulk

## 3.4 Carbon dioxide photoreduction quantified by the terms

This section seeks to clarify how the experimental phenomena interact with results reporting. There are currently limitations bounding photocatalytic experimental work alongside limitations in reporting experimental work. However, there needs to be an acknowledgment of the utility to be gained from current terminology. Or put another way, what are the bounds on the current terminology. The information gathered from experimental work is mostly reported in terms of unitary or photonic performance (and by photonic performance it is meant the group of terms: quantum yield, quantum efficiency, photonic yield and photonic efficiency, section 3.2). Therefore, this section works to link terms with the phenomena quantified to identify what parts of the material performance and the experimental conditions are quantified. Because of the unique importance of the specific rate and the photonic performance in reporting these terms will be focused on for in depth discussion. These photonic performance terms will be discussed as a group, representing a body of terms (section 3.2).

### *3.4.1 Dual Term Problem*

As discussed in Chapter 1, section 1.4.1, there are articulated concerns about the comparability and utility of $CO_2$ photoreduction results. One focus of this concern is on evaluating both the rate of the reaction and the effective use of photons. For Kondratenko *et al.* measuring the efficiency of photons to chemical energy was crucial [27], and for Chen *et al.* the concern was the lack of a singular parameter that can be used for

benchmarking [83], possibly an issue of defining a figure of merit; and for discussion purposes it will be referred to as the dual term problem. Put simply, the dual term problem is generated because photocatalysis relies on photons for energy input and this needs to be accounted for in the results. Whereas in catalysis the rate of performance of a catalyst is often benchmarked based on temperature, for photocatalysis there needs to be a logical incorporation of photon behavior into the analysis, even when considering the rate of the reaction.

A first option to the dual term challenge is to accept and report the two terms: quantification of the rate and quantification of the photonic performance. Further options include normalizing the rate by the photonic input, which is distinctly different from current photonic measures that first convert products into their respective numerical electron equivalents; or accept the rate as dependent on the photon flux (and as long as the irradiance is reported), take it on board as an irradiance specific rate measure. To widen the understanding of the implications of these options the current dual terms of photon performance and catalytic performance will be mapped out alongside the comprehensive reaction diagram and practicalities of experimental work.

### *3.4.2 Mapping out the equation of photo performance*

Light is presented to photocatalytic reactors in a directional manner for the most part. Due to the rig containment some light is reflected, or due to the angle of incidence less light may be exciting electrons in the semiconductor photocatalytic material. When excitons are generated they can recombine or electrons can be trapped, however some encounter and promote redox reactions to convert $CO_2$ and $H_2O$ into a vast array of products based on the photocatalytic material and energy levels of the various material interfaces. And all this activity is measured by a bulk reactant and product concentration. The photonic measure of this process is developed from taking the products that can be measured and converting them into the representation of the electrons that had been formed by photons and comparing that to the photons provided to the process.

This performance measure encompasses both the reactor's facilitation of light entering the reactor and transport to the photocatalytic surface alongside the mass transport in the reactor and back to the bulk. Within that context is the materials performance and the effective conversion of $CO_2$.

To focus more intently on the material performance utilizing photons only, absorbed photons would be considered, which would also accompany techniques to

identify reactants and products on the surface. This requires a sophisticated monitoring and measuring system.

Relating to the full photocatalytic diagram, and considering the bulk measurement experimental work, the equation of photonic performance encapsulates the light and mass transport characteristics of the reactor rig and the material conversion. In the case of photonic performance, the time dimension of the process is encapsulated in the amounts of electrons and photons, divided by the relationship of rate and flux. Understanding the development of the photonic performance over the length of the reaction becomes an important goal for reporting, and could be used as a way to quantify deactivation behavior.

### *3.4.3 Mapping out the equation of catalytic performance*

In the case of reaction rate, the reactants must travel from the bulk to the photocatalyst surface and be adsorbed. Then the rare, but statistically possible, promoted electron engages to form a product, or any such collection of complex reaction mechanism sequences must occur with the available electron input. These products then must desorb from the surface, travel back to the bulk and then be detected. The electron availability and behavior becomes bulk quantified with the adsorption and desorption of reactants and products and total photocatalytic performance alongside the mass transport of the reactor. All of this behavior is quantified as a rate of the bulk concentrations. The reaction rate thus, quantifies the photocatalytic material usage of electrons, interactions with reactants, and the reactor mass transport properties. There is no assessment of the usage of the energy source or power provided to the reaction to provide electrons to the process. With the catalytic performance, the electron is a given part of the rate, making reporting of irradiance and illuminated area necessary for efficiency quantification.

In catalysis multiple variables can improve reaction rate. These include increased catalyst surface area, reaction temperature, the pressure in gaseous reactions, and the reactant concentrations. With photocatalysis we add the variable of irradiance. Therefore, as catalysis can be benchmarked by tabulating temperatures utilized to achieve certain rates of performance (or the length of the half-life relative to a specific temperature [225]), so too could photocatalysts be benchmarked by tabulating the power (irradiance multiplied by illuminated surface area) necessary to achieve a rate of performance.

And as shown in Chapter 2 section 2.7, rate measurements are ideal for exploring the many variables that can affect or improve reaction rate. However, the main point to make here is that specific rate is not encompassing of energy efficiency.

### *3.4.4 Normalization for reactor as compared to normalization for material*

Inherent in both the assessments of the photocatalytic performance is the accurate assessment of products. Beyond that, there are many aspects of the reactor that modify the bulk measurements. In particular, the light transport and mass transport within the reactor modify the performance [226]. With current identical experimental condition benchmarking it is assumed that the impacts of these behaviors can be ignored as they are assumed constant across the various materials present. However, even as they may not impact the material comparisons being made, they do have substantial impacts on benchmarking and on reactor characterization.

Therefore, it becomes important to separate the impacts of the materials modifications from the reactor characteristics. To map out normalization for the reactor vs. normalization for the material, the reactor needs to be quantified. It also becomes important to think about the ways in which the material choice can shape the light and mass transport. For example, the photocatalytic material reflectiveness and the macro porosity are ways in which the material has a larger impact on reactor transport. To focus the discussion on the properties of the reactor and interacting photocatalytic material properties refer to Table 3.7. This table presents the conditions and properties in interlinking groups, suggesting what to report and guiding linkages in discussion. For example, the band gap energy of a material is linked to the wavelength of the reactor light provided, and the mass transfer of the reactor is linked to the flow rate.

Table 3.7 Interacting influences in experimental reaction rate and what these properties or conditions characterize (such as the reaction, reactor, or material).

| *Reaction Condition* | *Reactor* | *Photocatalyst* |
|---|---|---|
| *Light: irradiance, wavelength(s)* | Illuminated surface area, transparency (or transmission of light windows), distances of light travel | Light absorption spectrum, band gap energy, crystallinity |
| *Flow rate, pressure* | Mass transfer, volume | Specific surface area, porosity |
| *Temperature, reactant concentrations* | Isothermal, Flow/batch, Product removal | Adsorption, desorption of reactants and products |

Previously in section 3.1.1, extended normalization was used to assess the range of data presented, and the variation in the results reported. In that case, the typical grams of catalyst and length of the experiment were accompanied by the volume of the reactor, the irradiance and the illuminated surface area. This incorporates important aspects of the reaction conditions and the reactor geometry (as shown in Table 3.7). While being unable to quantify the full range of parameters, it can incorporate some element of efficiency. However, this is a bit misleading. Note that the photonic term converts the products into representational electrons (section 3.4.2), and this extended normalization does not. It relies on interpretation, either of selecting and focusing on a single product, a representation of the carbon (and the embodied $CO_2$) in multiple products, or a measure of conversion of reactants. In the spirit of a wider conversation about "how can the benchmarking tools themselves be assessed and improved [84]" this discussion will be returned to in Chapter 7. The result here is to reiterate a need for intentional benchmarking action when reporting experimental work.

### 3.5 Experimental context necessary for benchmarking

Developing an agreed benchmarking metric and method for a singular benchmark will require further academic discussion [84]. Hopefully, based on the discussion of parameters affecting conversion in section 2.8 and terms reported in section 3.1, it has become clear that the reporting of results needs to be more complex to match the complexity of the process.

At minimum, the information necessary for benchmarking $CO_2$ photoreduction includes:

- Temperature
- Pressure
- Time
- Amount of photocatalyst used for experiment
- Irradiance preferably at the material surface, or specifics of where measured and how, and light wavelength(s)
- Illuminated surface area (characterized by the boundary of light contact with the photocatalyst, can be surface area of catalyst if two dimensional layer, or surface area boundary of a three dimensional space based on where light is exposed to catalyst)
- Volume of the reactor

- Reactant concentrations, and reactant based conversion measurements (where possible)
- If a flow reactor then flow rates should be included
- Full disclosure of bounds on product detection, such as if the analytical equipment was unable to track specific products
- If it is a liquid phase reaction, pH

Additional information to this list include reaction parameters, photocatalyst aging and contamination investigations. If possible, evidence of understanding of parameter effects, either optimization or a wide experimental range that then gets focused, are important ways to observe and report photocatalystic investigations. These pieces of information will enable catalyst concentration or catalyst to substrate ratio to be calculated, the specific rate and appropriate light quantification to be determined. The intention is that this list makes more concrete and specific the kinds of suggestions Buriak, Kamat and Schanze espouse [90] and expands on conclusions from Nahar *et al.* [205]. Evidence of life time performance of a photocatalytic material (including the designation of fresh samples, relative to repeat use, cycling, and regenerated samples) is possibly a longer-term goal for benchmarking. Nahar *et al.* and Bligaard *et al.* include activity decay in the metric goals for the catalytic subfields of computational catalysis, electrocatalysis, molecular catalysis, and heterogeneous catalysis [84, 205]. Contamination or cleaning procedure evidence could be considered. Grigioni *et al.* show the presence of carbonaceous impurities from a blank experiment without $CO_2$ and, therefore, develop a protocol for cleaning their photocatalyst [227].

Reflecting on section 2.8 many reaction condition variables can be varied and optimized:

- Catalyst loading (even experimental work with dispersion has been conducted [228])
- Reaction time if it is a batch reaction
- Reactant concentrations, including relative to each other (humidity)
- Temperature of the reaction
- Irradiance
- Pressure is an option with impact on gas phase reactions, and an impact on the amount of dissolved $CO_2$ in liquid phase

It is important to remember that the materials modifications are separate. There are examples of materials properties being optimized for improved performance, for example the varying of drying temperature and time of photocatalysts [187].

Obviously there are reasons to not vary certain reaction conditions, as they would increase energy use. Examples would be utilizing room temperature, or employing a solar standard for irradiance, or running experiments at atmospheric pressure. These are decidedly appropriate decisions to be made, however, this should be clearly stated when reporting results as there is no common practice assumptions to be relied on.

After reviewing the complexity of terms being reported within $CO_2$ photoreduction (section 3.1), recommending future trends in wider or broader terminology usage might be beneficial. For example, titles often include larger terms, such as solar fuels and $CO_2$ utilization. Even terms such as efficiency have been challenging to interpret in article titles.

Terminology should be indicative of terms reported, for example $CO_2$ utilization best describes results of conversion based in measuring $CO_2$ reactant concentrations. And solar fuels best describe yield and product results. This would improve the title accuracy and meaning of papers. And when approaching the term efficiency, it is recommended to be more explicit with the photonic performance term that is applicable to the experimental work conducted. If the full analysis of the energy utilized to power the $CO_2$ photoreduction process is calculated and used to calculate the efficiency as compared to energy encapsulated in the products, then system efficiency is an appropriate term. This, it can be argued, should be considered first in terms of actual energy utilized in the experimental condition, and then again in terms of the light provided in case that same light could be provided from a renewable source. These kinds of calculations are more in line with energy consumption ratios that require further analysis [224]. Coridan *et al.* go further in the photoelectrochemical field creating the term energy-conversion efficiency as the key metric and recognizing that the comparison across solar fuels research requires a component and system level comparison of performance [229]. Moving forward from literature and recommended terms, what those terms encompass, and necessary reporting for benchmarking, the thesis now turns to experimental work.

# CHAPTER 4 – EXPLORATION OF BENCHMARKING UTILIZING IDENTICAL EXPERIMENTAL CONDITIONS AND MULTIPLE MATERIALS

In this chapter, commercial and modified photocatalytic samples are assessed with identical experimental conditions. This is the standard form of benchmarking in $CO_2$ photoreduction. Initially, the experimental set up is described along with the materials and analytical equipment (section 4.1). Then the current benchmark of P25 is discussed with the range of literature results (section 4.2), followed by the commercial samples benchmark testing (section 4.3). Then modified $TiO_2$ materials results are presented (section 4.4). Then a discussion of gold doping in the literature is conducted for comparison with the modified samples (section 4.5). This enables an exploration of P25 as a benchmark of the reactor and reaction parameters relative to material modifications. The identical experimental conditions and multiple materials work is then summarized (section 4.6).

## 4.1 Experimental Set Up

The set up used for experimental work consisted of a gas phase reactor, a vessel for calibration, and recirculation loops to aid in product collection with a Hiden Analytic Mass Spectrometer. The gas phase reactor consisted of two stainless steel lids and a cylindrical pyrex vessel (as seen below in Figure 4.1, left). The vessel was sealed with O-rings and four stainless steel rods secured with wing nuts. Internally a support of a quartz plate, angled by a Teflon ring, were the support for the catalyst. This reactor can, however, be used with various supports, interchanged within the cylinder, and in the past this has included honeycomb ceramic monoliths threaded with optical fibers [218]. In Figure 4.1 (left) the stand and reactor can be seen with a catalyst mounted on a quartz plate inside. The other photoreactor used in the rig is also shown in Figure 4.1 (right). This one was used during calibration as a reservoir, to enable the calibration to have the same pressure as the product gases. These reactors were developed during previous PhD study [230, 231].

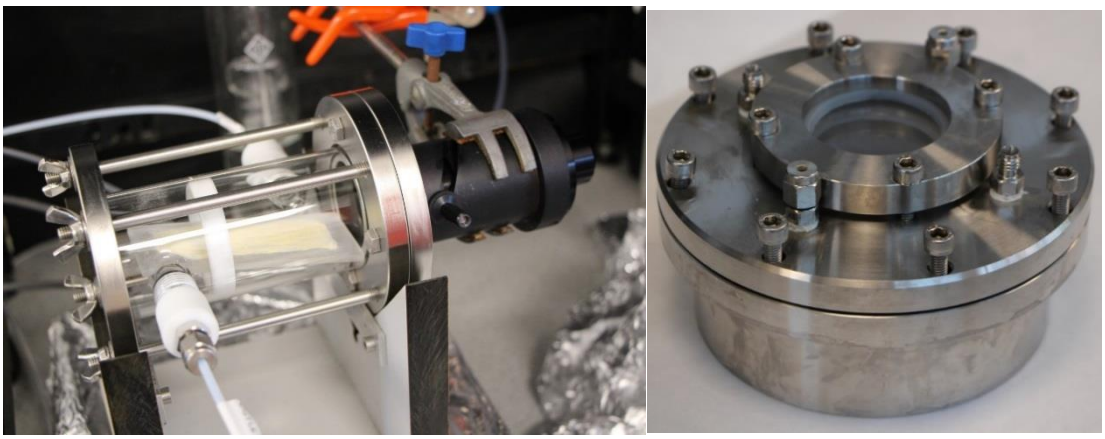

Figure 4.1 Gas phase photocatalytic reactor set up for testing (left). And a liquid phase reactor in this case used as a calibration gas vessel (right).

The internal radius of the cylindrical pyrex reactor is 2.5cm, with a height of 11cm, giving an internal volume of roughly 216 $cm^3$ or mL (as $216 \approx \pi(2.5^2)(11)$ and 1 $cm^3$ = 1 mL). Within the reactor the angle of the quartz plate is 9.46 degrees to the horizontal. The internal volume of the reactor used as a calibration vessel is 353.85 mL.

These reactors were connected together and incorporated into the rig as depicted in Figure 4.2. Gas lines were attached to the rig with a bubbler in line with the $CO_2$ and the helium (He), with an option to bypass the reactor to clear out the line by the analytical intake. Calibration gas was connected to the calibration liquid phase reactor vessel in a loop, with venting, and the option to flush with helium. To connect components of the rig, stainless steel tubing was used with HAM-LET, Parker and Swagelok valves, except for the connections of the bubbler which were in plastic.

Work to prepare the rig for testing most intensely focused on forming an airtight rig and results reproducibility. To improve the rig the replacement of previous plastic tubing to metal for photocatalytic testing was conducted with an expected significant effect. Whereas it was uncertain the exact type of tubing previously being used, it can be assumed the tubing was most likely Nylon, Polyurethane or PTFE. The performance of the types of tubing in terms of permeability, operating temperature, and chemical resistance to weak acids (due to small amounts of $CO_2$ reacting with water to form carbonic acid) is tabulated in Table 4.1. The level of permeability is disconcerting as calculated below.

Table 4.1 Excerpt from Tubing selection Guide from Cole-Parmer giving chemical resistance and permeability data for various plastic and the 316 stainless steel tubing, [232].

| *Formulation* | *Operating Temperature* | *Chemical resistance to weak acids** | *Permeability (approximately at 25°C) Units: {cc-mmsec-cm$^2$-cm Hg} x 10$^{-10}$* | | | |
|---|---|---|---|---|---|---|
| | | | $CO_2$ | $H_2$ | $O_2$ | $N_2$ |
| *Nylon* | -51 to 93°C | A | 20 | 19 | 5.4 | 1.1 |
| *Polyurethane (clear, aqua-tint)* | -40 to 82°C | B | 395 | 66 | 10.5 | 17.1 |
| *PTFE* | -240 to 260°C | A | 6.8 | - | - | 1 |
| *Stainless steel, 316* | -53 to 289°C | A | - | - | - | - |

*Chemical resistance classifications: A – No damage after 30 days of constant exposure, B- Little or no damage after 30 days of constant exposure.

Even in the most stringent case, looking at the performance of PTFE, when considering the gas loading and testing conditions there is significant gas transfer occurring.

The volume of gas that permeates the tubing during loading are roughly 0.17 cc and 0.03cc for $CO_2$ and $N_2$ , and during testing $3.7x10^{-2}$ cc and $5.4x10^{-3}$ cc respectively. Calculation (units in parentheses):

$$volume\ (cc) = \frac{10^{-10}\ \frac{cc-mm}{sec-cm^2-cmHg} \times time\ (sec) \times surface\ area\ (cm^2) \times pressure\ difference\ (cmHg)}{thickness\ (mm)}$$

Where *surface area* refers to the outer surface area of the tubing (permeable surface area); *pressure difference* refers to the difference in pressure across the tubing; and *thickness* refers to the wall thickness of the tubing. For the calculation: the pressure difference across the tubing is 0.5 bar (37.5 cmHg); loading gases takes 30 min (1800 sec), through a length of tubing 3 m long. Considering all the tubing connected to the reactor, to pressure gauges and connections to valves, is 80 cm collectively, with the length of the test being 4 hours (14400 sec). The tubing has an outer diameter of 1/8$^{th}$ inches, giving a circumference of 1cm, and has a wall thickness of .8mm.

In considering the choice of stainless steel tubing it was important to consider how the products would react with the surface of the metal. Acids can degrade stainless steel.

Acid products observed before include acetic acid ($CH_3COOH$) and ethanedioic acid (common name oxalic acid, COOH-COOH) have been observed as products [156] and formic acid (HCOOH) is another possible product. Due to the low concentration of products, 316 stainless steel was chosen for its high corrosion resistance [232, 233].

The metal piped pressurized rig was left overnight with valves v2E, v2F, v2H, v2M open, V3B towards V3A and V3A towards the recirculation, and all other valves closed, and the improvement in permeability was confirmed by the observation of no drop in pressure. When each new sample was added, this required opening and closing the tubing, and therefore the pressurized rig was observed for an hour to confirm no change in pressure. This pressure test was in addition to bubble leak tests at the two main reactor connections upon rig reassembly.

The angle of the sample was created by the use of an o-ring to increase the light available to the sample. In this case, the angle formed was 9.46 degrees to the horizontal plane and was kept constant by two markings to align the quartz plate and the o-ring.

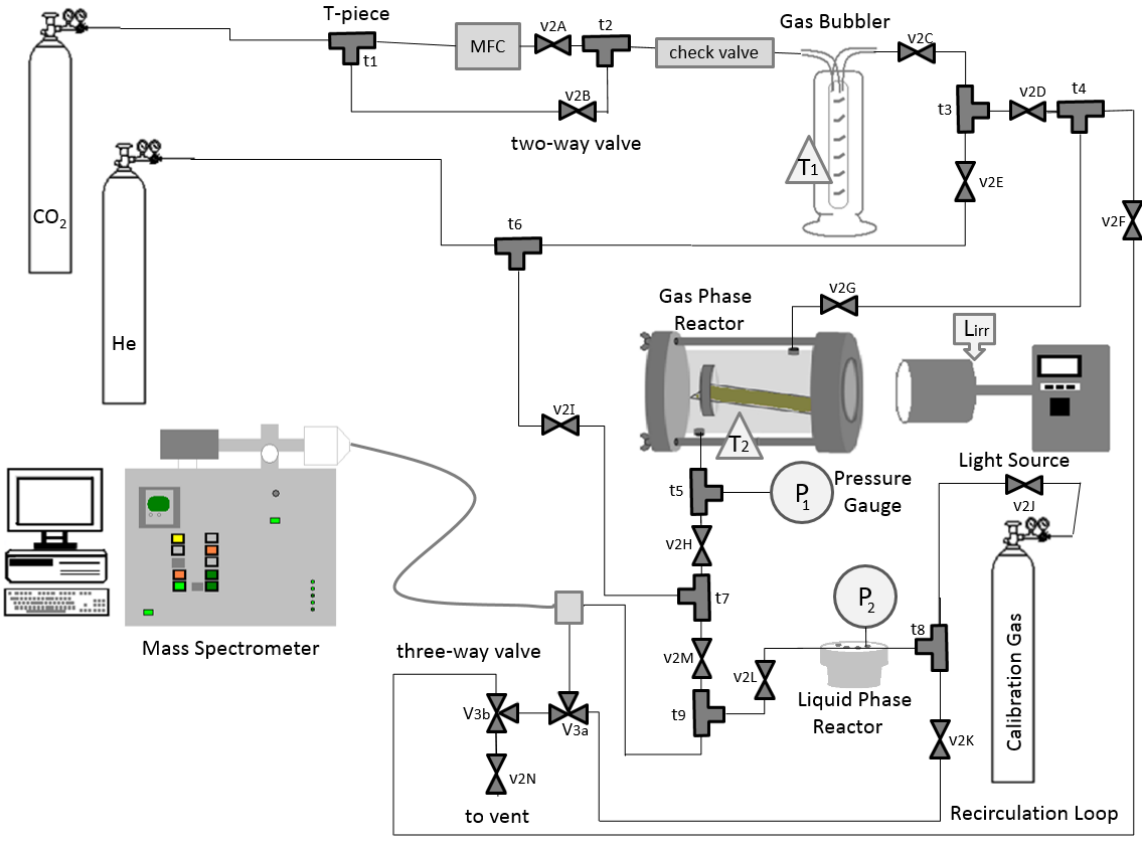


Figure 4.2 Testing Rig showing tubing, and connectors including T-pieces (t#) and valves (v2, being a two way valve, and V3 being a three way valve and further distinctions designated with letters), pressure gauges (P#, in circles), the mass flow controller (MFC), sites of temperature measurement (T# in triangles), site of

light irradiance measurement (Lirr), and the gases used along with reactors, light source, gas bubbler for $CO_2$ humidification, and mass spectrometer (not to scale).

The analytical system used to determine product gases was a Hiden Analytic Mass Spectrometer (MS), HPR-20 QIC system. The samples were delivered to the MS through a 1.5 meter heated capillary line. A pressure gauge was used to determine the pressure within the reactor during testing with two decimal points of accuracy on a digital readout ($P_1$ in Figure 4.2). The mass flow controller had an upper limit of 8 ml/min of flow. The glass bubbler was filled with deionized water. Bubbler and reactor temperature were monitored by means of two glass ethanol thermometers just at the outer surface of each ($T_1$ and $T_2$ in Figure 4.2), error margin of ± 0.5 °C. At room temperature and 8 ml/min flow of $CO_2$ ($Q_{CO_2}$) this provided a ratio of 40 mL $CO_2$ to 1 mL $H_2O$. Water vapor flow rate was calculated using the flow rate of $CO_2$ multiplied by the vapor pressure of water ($p_{H_2O}$, 0.03 atm at room temperature, measured to be 22-23°C) divided by the total pressure ($p_T$) minus the vapor pressure of water (Equation 4.1). The pressure used for all the experiments was 0.5 bar gauge pressure. (When using Equation 4.1 with a carrier gas it is necessary to adjust the concentration of $CO_2$, then sum the two flows, therefore $Q_{CO_2}$ becomes $Q_{Total}$.)

$$Q_{H_2O} = Q_{CO_2} \times \frac{p_{H_2O}}{p_T - p_{H_2O}} \qquad \text{Equation 4.1}$$

The temperature measured was of the bulk after conduction through the quartz reactor. If the light input were not to be converted to electrons and instead the energy were dissipated as heat there would be a substantial heating effect. For example, considering either a 1 hour or 4 hour experiment with a 278 mW/cm$^2$ irradiance input (the highest used experimentally) the expected temperature increase would be 553 and 2215 K respectively. This is considering the 216 mL volume, filled with $CO_2$ and $H_2O$ at a ratio of 40:1, and respective heat capacities of 0.846 and 1.996 J/gK. This scale of heating does not occur, however, because of the semiconductor photocatalytic material. On a fraction of that scale, such as a tenth of the incoming light, there would be 55 K of heating per hour that would then dissipate within the reactor. This possible lamp-heating effect and unmeasured temperature gain at the photocatalyst surface would have been unobservable in the bulk at the outer edge of the reactor. Therefore, the temperature gain

at the photocatalyst surface should be more closely observed, possibly with a thermocouple or optical thermal sensor.

Gas from the photocatalytic reactor was recirculated from the MS intake during sampling, to limit loss of product gases. This recirculation loop of tubing going from the reactor, past the sample inlet, then returning to the reactor is labeled recirculation loop in Figure 4.2. The recirculation line was ineffective in this case, and will need to be developed further with a recirculation pump.

Gases used for experimental work were of high purity; $CO_2$ (99.999%) and He (99.9999%) gases were purchased from BOC Industrial Gases. Calibration gas was 100 ppm each of hydrogen ($H_2$), oxygen ($O_2$), methane ($CH_4$), methanol ($CH_3OH$), ethane ($C_2H_6$), ethylene ($C_2H_4$), acetaldehyde ($CH_3CHO$), and ethanol ($C_2H_6O$) with the remainder being $CO_2$, purchased from Scientific and Technical Gases Ltd. This mixture is used to represent a range of expected products from the photocatalytic reaction [156, 234].

The lamp used was a 200 W mercury lamp, OmniCure Series 2000, with a 365 nm filter, Lumen Dynamics, which had an output range of 6 to 618 mW/cm$^2$ irradiance. The light irradiance was measured with the accompanying UV/vis OmniCure R2000 Radiometer after the optical fiber light guide, but before the optical lens that was located at the quartz window of the reactor ($L_{irr}$ in Figure 4.2). This radiometer was calibrated 4 months before experimentation, with experiments lasting 11 months.

### *4.1.1 Materials and methods of synthesis*

There were three commercial and three lab-produced samples used for $CO_2$ photocatalytic reduction. The commercial samples used were a 99% pure anatase $TiO_2$ purchased from ACROS Organics, a high specific surface area anatase $TiO_2$ (Mirkat 211) from Euro Support, and P25 an anatase and rutile mix purchased from Aldrich Chemistry. The modified samples included $TiO_2$ made by evaporation induced self assembly (EISA), an EISA sample that was then heated at 500ºC with a hydrogen atmosphere (EISA $H_2$), and a gold doped $TiO_2$ photocatalyst ($AuTiO_2$). The EISA samples were synthesized by the author, and the $AuTiO_2$ synthesized by Alberto Olivo [235]. The commercial samples give a range of standard samples with specific surface area and crystal phase modifications, and then the lab synthesized samples cover a range of modifications including specific surface area, calcination in modified atmosphere and doping.

Synthesis of $TiO_2$ can be performed through a variety of methods with the sol-gel technique being the most widely used in $CO_2$ reduction. Other methods include

microemulsion, precipitation, hydrothermal or solvothermal, electrochemical, and even biological synthesis, all described in more detail in a review [236].

The sol-gel process starts with the hydrolysis of the precursors (breaking of bonds through reaction with water). Alcohol can be used as a solvent, and an acid or base can be used to improve hydrolysis by increasing the charge of the solution and thereby increasing ion formation in solution. This is followed by polycondensation reaction, the condensation of the solution to form a gel. After gel formation, the solvent is removed by drying at a relatively low temperature (80-100°C) and then calcined (heating in the presence of oxygen or air). Calcination removes the volatile fraction, promotes thermal decomposition, and drives the phase transition from amorphous to crystalline $TiO_2$ [236]. The popularity of the sol-gel method is due to the economical and energy efficiency advantages of ambient temperature sol preparation and gel processing, homogeneity, and size tuning of the particles [236, 237].

The development of EISA is perhaps best understood as a specialization within the sol-gel process. Therefore, EISA has less exploration history in the field of photocatalytic reduction of $CO_2$. Simply, the EISA process uses a template in the hydrolysis that nucleates organized mesostructures, or complex semi ordered structures [238]. These mesostructures allow for the formation of greater specific surface area. In this case the synthesis route mimics that used for SBA-15 silica, a popular mesoporous high surface area silica [239], however, with P123 (ALDRICH Chemistry), a symmetric triblock copolymer PEG-PPG-PEG, as the template in hydrochloric acid suspension as reported previously [240]. Another sample was developed by modifying an EISA $TiO_2$ by heating to 500C in a hydrogen atmosphere [240]. More specifically the template P123 is a material formed from poly-ethylene oxide (PEO) and polypropylene oxide (PPO) [241] in the proportions $PEO_{21}PPO_{65}PEO_{21}$ (P123). In more detail pure $TiO_2$ from EISA titanium (IV) n-butoxide (6.915 mL, ACROS Organics) was drop added and then thoroughly mixed with 20 mL hydrochloric acid 1N (ACROS Organics), which was then slowly added to a P-123 ethanol mixture of 1.383 g P-123 with 10 mL ethanol (Fisher Chemical). This was then stirred for 3 hours followed by oven drying and heating in oven at 40°C for 6 hours, and then 150°C for 2 hours, and finally 500°C for 1 hour, all done with a ramp of 1°C/min. Thermal pre-treatment was conducted on some of the EISA photocatalyst sample using ChemBET instrumentation to flow 10 ml/min of $H_2$ through the photocatalytic powder sample at 800 °C. This treatment was conducted at the set temperature for 1 hour. A heating rate of 10°C/min was used for reaching a temperature of 800°C.

And lastly a sample with gold doping ($AuTiO_2$) has been used. $AuTiO_2$ was synthesized by precipitation from sulphate salt in sodium hydroxide using nitrogen [70]. The $TiO_2$ was synthesized through precipitation of $TiOSO_4$ salt with the base NaOH, forming $Ti(OH)_4$ which was then calcinated at 400 °C to form $TiO_2$. Then Au was added using deposition precipitation [242]. Reiterated briefly the $AuTiO_2$ synthesis method utilized 1.2 M titanyl sulphate solution, prepared by dissolving 34.55 g of $TiOSO_4$ (Sigma-Aldrich Ti assay > 29 wt. %) in 100 mL of deionized water. Using 36 g of NaOH, Carlo Erba assay > 97 wt. %, in 100 mL of deionized water a 9.0 M NaOH solution is prepared (in an ice bath to overcome extreme exothermicity). In order to keep a neutral pH, both solutions were added concurrently drop wise to 200 mL of distilled water under vigorous stirring (500 rpm), in order to keep a neutral pH, which was monitored with a Metrohm 691 pH meter. The $Ti(OH)_4$ suspension was kept at 60 °C for 20 hours. Then the suspension was filtered and washed with deionized water to remove sulphate ions from the precipitated solid. This was then dried overnight at 110 °C and calcined at 400 °C (with a heating rate 2 °C·min-1) for 4 hours in air flow (30 mL·min-1) to obtain $TiO_2$. This sample is labeled as $TiO_2$-PREC in the corresponding thesis [235]. For gold deposition $TiO_2$ was suspended in an aqueous solution at 60 °C of $HAuCl_4 \cdot 3H_2O$, whose pH is below 2. This pH was then raised by the addition of 0.5 M NaOH (assay > 97% Carlo Erba) and sodium hydroxide solution such that the pH was maintained at 8.6 for 3 hours. The sample was washed with deionized water. The sample was then dried overnight at 35 °C and calcined at 400 °C in air for 1 h. This sample is labelled as Au-$TiO_2$-PREC in the corresponding thesis [235].

When considering materials synthesis within the challenge of comparing different studies difficulties arise from the variation in production methods. As the sol-gel and EISA processes each require mixing of precursors, followed by time to react and then be dried at elevated temperatures to drive out organic components of the precursors, which also drives crystal structure, there is a wide variety in the process. There is also no consistency in washing or washing procedure of catalysts before testing. Thus, the most commonly used benchmark catalysts are commercially available catalysts. In lab sol-gel produced catalysts are used as benchmarks as well, however, lab produced benchmarks provide less of a standardized reference. Therefore, the usage of both commercial and lab produced samples were used for testing comparison.

### *4.1.2 Materials Characterization*

The commercial anatase and Mirkat samples are anatase crystals. P25 is a mix of anatase and rutile crystals. The EISA samples have a mix of anatase and rutile crystals, as assessed by x-ray diffraction [240], while the $AuTiO_2$ is anatase. The commercial anatase is 99% pure, the Mirkat is 85% $TiO_2$, 35-40% anatase and then the remainder is amorphous. Au-$TiO_2$ is anatase, and 0.2 wt% gold. The commercial anatase sample has a specific surface area of 7.52 $m^2/g$ [240]. P25 has a specific surface area of 50 $m^2/g$, and Mirkat one of 217 $m^2/g$. The $TiO_2$ EISA sample has a specific surface area of 66.9 $m^2/g$, with the $H_2$ calcined EISA sample having a specific surface area of 63.2 $m^2/g$. Au-$TiO_2$ has a specific surface area of 110 $m^2/g$. A summary of the specific surface area, band-gap energy, and crystal phase for the samples can be found in Table 4.2 below. Previous work, by the author, has included further characterization including x-ray photoelectron spectroscopy and specific surface analysis [240].

Table 4.2 Specific surface area and band-gap energy of commercial.

| | *Specific Surface Area ($m^2/g$)* | *Band-Gap Energy (eV)* | *Crystal Phase* |
|---|---|---|---|
| *Anatase $TiO_2$* | 7.5 | 3.19 | anatase |
| *P25* | 50 | 3.21 | anatase and rutile |
| *Mirkat 211* | 217 | 3.34 | anatase |
| *EISA* | 66.9 | 3.16 | anatase and rutile |
| *EISA $H_2$* | 63.2 | 3.10 | anatase and rutile |
| *Au $TiO_2$* | 110 | - | anatase |

The Anatase $TiO_2$ was found to have a crystal size of 23.25 nm [240]. The P25 has a 21-nm particle size and contains 0.5% or less trace metals. Mirkat 211 has a variation in pore size suggesting macro and meso-pores mainly at 4nm and 25nm. Mirkat 211 has a pore volume or 0.27 cc/g with $N_2$ at 77K. $TiO_2$ (wt%) 85 and sulphur content is 1.5%, with 15% made from hydroxide. P25 was calculated to have a band gap energy of 3.21 eV, compared to 3.38 found in the literature [228].

### *4.1.3 Experimental methodology*

The experimental procedure for the identical experimental conditions testing were as follows:

To load the photocatalyst on the quartz plate support, 0.02 g photocatalyst was suspended in 2mL isopropanol and then mixed in an ultrasonic bath for an hour. Then the solution was dripped onto a heated quartz plate at 110°C, followed by baking in an oven at 110°C for at minimum an hour to remove the solvent completely. For catalyst loading a template system was adopted (Figure 4.3). The template area loaded with catalyst was 12cm$^2$ (2 cm by 6 cm). This template was placed under the quartz plate during loading as a guide for distribution of the solution.

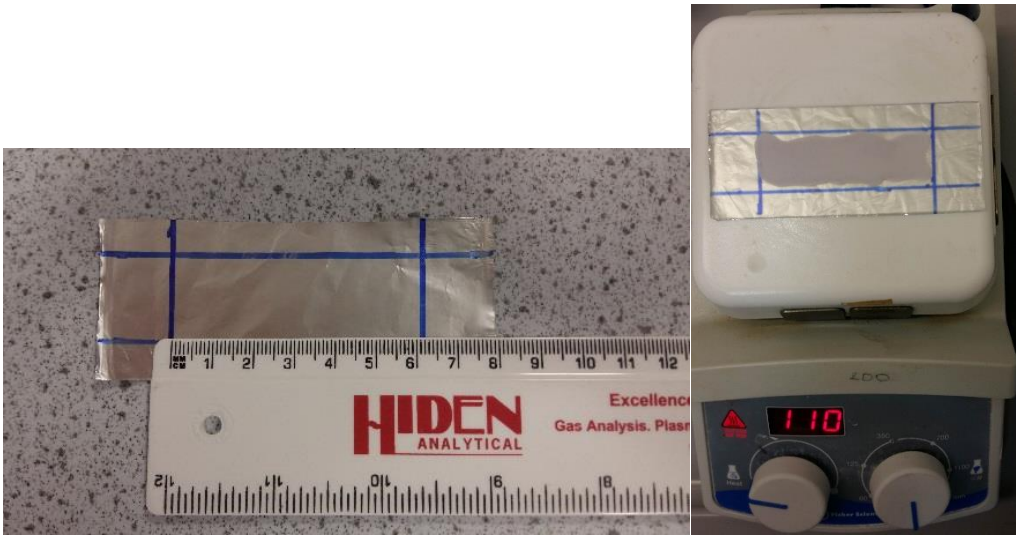


Figure 4.3 Template development showing foil template (left) and in use beneath transparent photocatalyst loaded quartz plate (right).

Background values were obtained by running helium overnight, to clear MS lines and limit background, through the reactor at 1 ml/min, taking readings the next morning before the test. Calibration was conducted right after the background values were obtained. This was done by purging the liquid phase reactor vessel with calibration gas. Then the vessel was brought up to pressure of 0.5 bar gauge. Then the gas was analyzed with the MS, also in a loop or recirculation configuration. The irradiance of the lab was measured at the end of the optical fiber light guide after the calibration.

The reactor was purged with an 8mL/min flow of $CO_2$ bubbled through water for 45 min, followed by that continued flow as the reactor was brought up to 0.5 bar gauge pressure. Then an initial reading was taken of the contents of the reactor through MS

analysis, then the pressure was brought to 0.5 bar gauge and the light turned on to begin the experiment. Final results were taken and then the initial contents subtracted to determine conversion. The analysis with the MS was always taken at twenty minutes, which lead to a 0.45 bar final pressure reading.

Blank tests were conducted to verify the photocatalytic behavior and included: (1) blank tests without light that verify the presence of a light driven process; (2) blank tests without catalyst that demonstrate a catalytic enhancement of reaction rates or enabling of the reaction; (3) blank tests with no $CO_2$, which prove that the resultant gases originate from the $CO_2$ and (4) blank experiments without water to confirm hydrogen source.

#### *4.1.3.1 Considerations in experimental work for solvent drying in catalyst loading and the use of foil during experiments along with irradiance calculations*

While conducting this experimental work the solvent removal, residual from catalyst loading, became an important factor to consider. Solvent removal is vital, as seen from Figure 4.4 showing the results of baking the 80mg loaded sample for 1 vs 2 hours. Baking after two hours left no detectable smell or scent, and this accompanies a drop observed for carbon based products as shown in Figure 4.4, coinciding with the effective removal of solvent. For lesser quantities of catalyst, the 1 hour drying results were not outside of the experimental error margin.

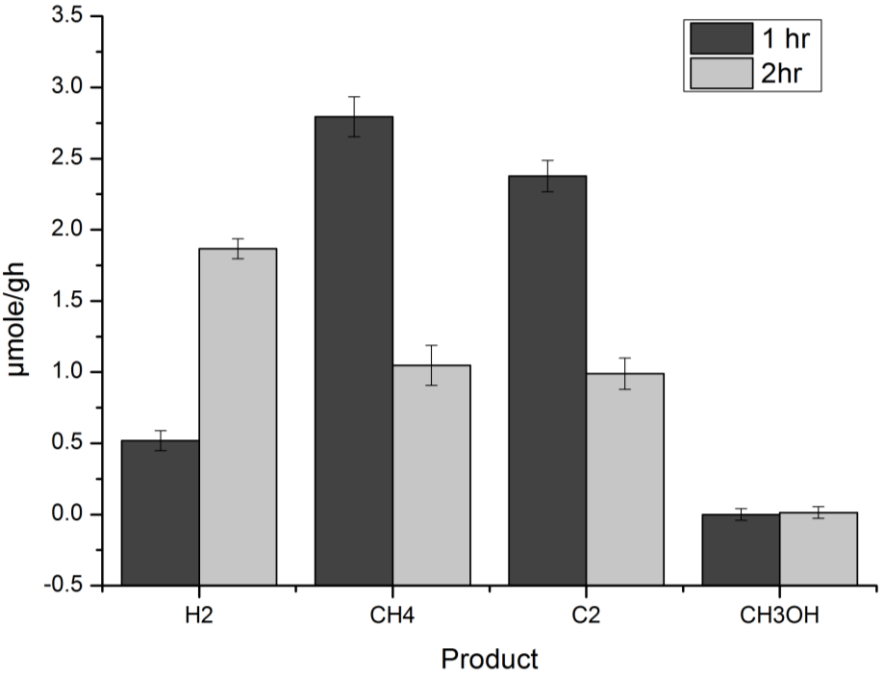


Figure 4.4 Isopropanol drying times from plating catalyst and impact on products. Experiments conducted at room temperature with 0.08g of Mirkat catalyst, for 4 hours, and a light intensity of 278 mW/cm$^2$.

The practice in the lab was to wrap the reactor in aluminum foil to prevent exposure to UV light; however it also was a reflective surface, enhancing light utilization in the reactor. To investigate the light irradiance impact of the foil experiments were conducted with and without foil with the results as shown in Figure 4.5. The use of foil clearly improves the light transfer in the reactor as seen in the increased unitary production. The increased products come from the foil reflecting some of the photons that then assist in more reactions, as these photons would otherwise escape.

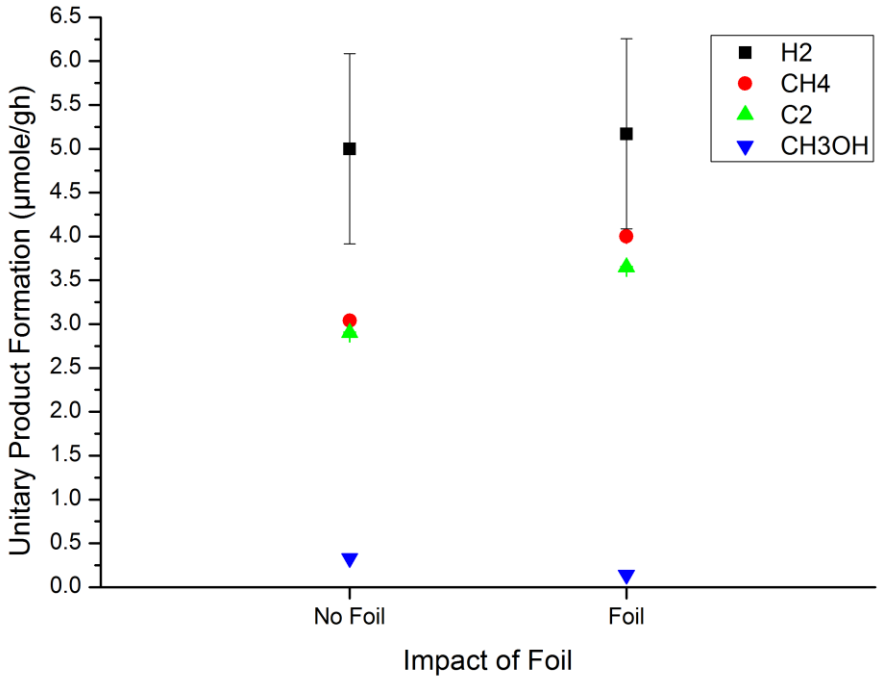


Figure 4.5 Product variation due to the intensity change of reactions with and without foil. Experiments conducted at room temperature with 0.04g of $AuTiO_2$ catalyst, for 2 hours, and a light intensity of 278 $mW/cm^2$.

The irradiance measured (with the UV/vis OmniCure R2000 Radiometer) was the incident irradiance. Due to the angle of the quartz plate, of 9.46 degrees to the horizontal, the light that reached the surface was reduced; and in the case of the screening experiments the 186 $mW/cm^2$ irradiance would have been 31 $mW/cm^2$, correcting for the angle of incidence based on trigonometry. Considering this is UV light, and only 4% of the solar spectrum, as discussed in section 2.5.1.1, and using $1000W/m^2$ as the irradiance of the sun on the earth's surface, then 31 $mW/cm^2$ ($310W/m^2$) is equivalent to 7.75 the expected solar UV irradiation (40 $W/m^2$ or 4 $mW/cm^2$).

### *4.1.4 Quadrople Mass Spectrometer analytical background and technique*

Mass spectrometry can be used to quantify elemental composition, amount, and even aspects of molecular structure of materials that can be excited into gas phase ions [243]. The quadrupole mass spectrometer works by ionizing sample gases through electron impact, magnetically separating the ions and sending then to a detector to quantify the

change in signal for the various mass charge ratios. A simple schematic for this process can be seen in Figure 4.6. Samples enter and are charged and then pass through a magnet where too light and too heavy molecules fall away into the magnet leaving a single mass charge to strike the detector.

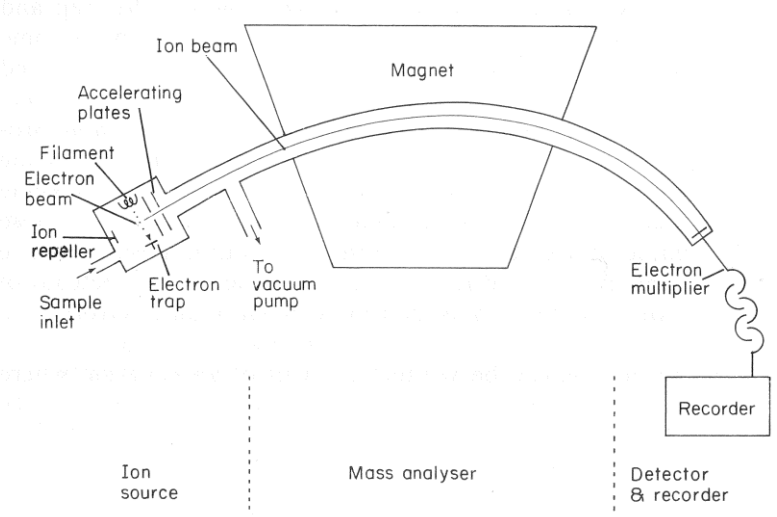


Figure 4.6 Drawing of a single focusing mass spectrometer showing key features, from Davis and Frearson [244].

For the analysis the magnet used was a quadrupole (Figure 4.7). The analytical system used to determine product gases was a Hiden Analytic Mass Spectrometer (MS), HPR-20 quartz inert capillary (QIC) system utilized with the accompanying MASsoft 7 Professional software. Detector readings can be displayed as tables and graphs of the partial pressures of the molecules by time (referred to as multiple ion detection (MID) mode in manufacturer's literature) or as positions of different mass charge peaks by partial pressure in Torr or % (referred to as Bar Mode). Analysis for experiments were conducted in MID mode.

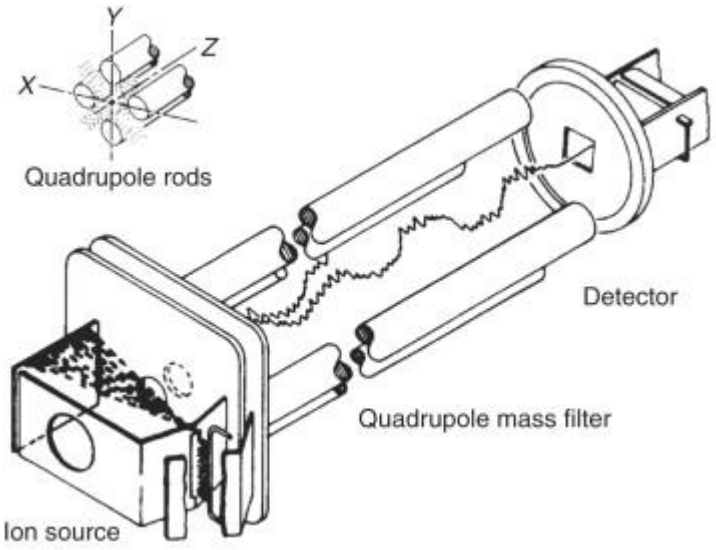


Figure 4.7 Drawing of the quadrople magnetic filter for the ion separation in a mass spectrometer from Sparkman *et al.* [245].

The MS has a faraday detector and a secondary electron multiplier (SEM) detector. The faraday detector has a detection limit of $10^{-11}$ and a maximum operating pressure of 1 x $10^{-4}$ Torr and gives results as a percentage of total pressure. SEM detector has a detection limit of down to $10^{-14}$-$10^{-13}$ Torr and a maximum operating pressure of 1 x $10^{-6}$ Torr and can give results of less than 1% giving parts per million (ppm).

The samples were delivered to the MS through a 1.5 meter heated capillary line. The MS tracked specific mass charge ratios to allow for quantitative analysis. The MS tracked the relative pressure of $H_2$ at the mass/charge peak of 2, $CH_4$ at the mass peak of 15, $C_2$ based compounds at mass peak 26, $CH_3OH$ with mass peak 31, $O_2$ at mass peak 32, Ar with mass peak 40, and $CO_2$ with mass peak 44. All mass peaks were tracked with the SEM detector except for the $CO_2$ at 44. The only values that were converted into ppm values, by means of calibration, are the $H_2$, $CH_4$, $C_2$ compounds, $CH_3OH$ and $O_2$. The MASsoft programing for this calibration and experimental test work can be seen in screen shots given in Appendix C. The mass spectrometer was chosen for the ability to give highly accurate results at the low detection necessary for photocatalysis for $CO_2$ reduction.

In the case of the Quadrupole MS, the CO peak was not tracked due to overlaps with the other product peaks. This is due to fragmentation of the molecule. The MS ion source is an Appearance Potential Soft Ionization (APSI), and ion generation is by electron bombardment, which gives the molecules charge, but also fragments them. This

means that the gas is subjected to an electron beam to charge the gas molecules and then ions of specific mass to charge ratios are directed by magnetism to the detectors. As seen in Appendix A, Table A.1, much of the available literature utilizes a gas chromatograph (GC) with a flame ionization detector. The GC is able to separate molecules through diffusion and adsorption/desorption along a packed column. A GC-MS with the capacity to separate molecules and then quantify them individually would limit the challenges of overlapping molecule fragments greatly by separating the gas presented to the MS. As CO is often considered an initial product at the start of the reduction process this limits results to detection of further developed products, however this was acceptable as the detection of solar fuel production was the goal of experimental work.

To minimize error, calibrations were performed within hours of the experiment as part of the experimental preparation. This is in accordance with the recommendation to complete frequent calibration as MS detectors are sensitive to previous exposures and fluctuation in temperature and pressure and humidity [246, 247]. Thus, the use of overnight flows through the MS and experimental pressures held constant at 0.5 bar gauge were also done. Error analysis was done through calculating the standard deviation divided by the square root of the number of experimental runs, from experimental results done in triplicate for all screened photocatalysts in a singular test (error margins are tabulated by product in Table 4.3 for Mirkat and $AuTiO_2$) [248]. The conditions of the Mirkat error experiments were 0.04 g photocatalyst loading, 4 hour experiment length and 278 $mW/cm^2$. The conditions of the $AuTiO_2$ error experiments were decided by the design of experiment structure midpoint, and were 0.03 g photocatalyst loading, an experimental length of 2 hours and a light intensity of 124 $mW/cm^2$.

Table 4.3 Error margins for Mass Spectrometer detection experiments done in triplicate with Mirkat and $AuTiO_2$ samples for unitary product formation (µmol/gh).

| *Product* | *Mirkat error (µmol/gh)* | *$AuTiO_2$ error (µmol/gh)* |
|---|---|---|
| $H_2$ | 0.14 | 2.17 |
| $CH_4$ | 0.28 | 0.03 |
| $C_2$ products | 0.22 | 0.02 |
| $CH_3OH$ | 0.08 | - |

### *4.1.5 Results calculations demonstrated*

Due to the importance of units and calculations for benchmarking, and to this thesis work, here is included examples of results calculation utilized in the following experimental chapters:

The method by which all results were converted from the output of the MS, which was ppm's, into μmole values (that are then used to calculate all other terms) is presented here with an example. If the MS reading was 8 ppm $CH_4$ with the reactor at 0.45 bar guage (1 bar ≈ 1 atm), due to time and pressure loss with MS reading, room temp 25°C. Reactor volume is 216 ml.

$$1\ ppm = \frac{1\ gas\ volume}{10^6\ headspace\ volume} = \frac{1\ \mu mole\ gas}{1\ mole\ headspace\ gas} \qquad \text{Equation 4.2}$$

Utilizing the Ideal gas law:

$$n = \frac{PV}{RT} = \frac{1.5 atm\ \times 0.216 l}{0.08206\ \frac{l \cdot atm}{mole \cdot K} \times 298.15\ K} = 0.01324\ mole \qquad \text{Equation 4.3}$$

$$8\ ppm\ CH_4 = \frac{8\ \mu mole\ CH_4}{1\ mole\ headspace\ gas} \times 0.01324\ mole\ headspace\ gas = 0.10594\ \mu mole \qquad \text{Equation 4.4}$$

$$\frac{0.10594\ \mu mole}{0.02\ g_{catalyst}\ \times 4\ hr} = 1.324\ \frac{\mu mole}{g \cdot h}\ CH_4 \qquad \text{Equation 4.5}$$

For the calculation of $\frac{\mu mole}{g \cdot h \cdot mL \cdot mW}$ results the unitary product formation $\left(\frac{\mu mole}{g \cdot h}\right)$ was divided by the volume of the reactor (216 mL), the irradiance (mW/cm$^2$), and the illuminated surface area (12 cm$^2$).

For the calculation of photonic yield moles were converted into elections per time, and the light irradiance converted to photons per time. For example:

$$photonic\ yield = \frac{\frac{summed\ products\ (\mu mole \cdot electrons)}{length\ of\ experiment\ (h, converted\ to\ seconds * 3600)}}{\frac{irradiance\ \left(\frac{W}{m^2}\right) \times area \times time \times wavelength\ (m)}{h\ \left(6.626E-34\ \frac{joule}{s}\right) \times c\left(300000000\ \frac{m}{s}\right) \times\ N_A\ \left(6.022E+23\ \frac{molecules}{mole}\right)}}$$

(Equation 4.6)

Where h is Plank's constant, c is the speed of light, and $N_A$ is Avogadro's number. As discussed in section 3.1.3, $H_2$ molecules correspond to 2 electrons, $CH_4$ with 8 electrons, $CH_3OH$ with 6, and the $C_2$ compounds ($C_2H_6$ with 14 electrons, $C_2H_4$ with 12 electrons, $CH_3CHO$ with 10 electrons, and $C_2H_6O$ with 12 electrons) are analyzed together, therefore, the electron equivalents are averaged to 12. The wavelength is 365 nm, and therefore 0.000000365 m.

### 4.2 P25 and the current "fuzzy" benchmark

To start to analyze the significance of the results comparison by identical test conditions, which is current common practice, first P25 results for $CO_2$ photoreduction from literature are investigated. This provides a context of other P25 results to initially assess whether the experimentally found results match the literature. Comparing P25 results also allows an exploration of the experimental conditions influence on the results. The literature reviewed includes 14 articles [60, 61, 66-69, 71, 78, 80, 183, 184, 186, 187, 228, 249, 250]. To compare the articles, it was chosen to focus on $CH_4$ results, as product based detection is most common. From the literature, the range of $CH_4$ specific rate or unitary product formation results is 0.019-1.106 μmol/gh [61, 66-69, 71, 78, 80, 183, 184, 186, 228, 249, 250]. Because of the variation in reporting some results could not be directly compared in this way, such as results reported in percentage of relative products [60], and ppm results without enough context to be converted into moles [187]. Table 4.4 presents a summary of literature results and then the given or calculated specific rate for articles where the $CH_4$ results enabled comparison. It is most crucial to realize that the material utilized in these comparisons is identical. There are no modifications to P25. Therefore, the variation in results observed is all due to the reactor and experimental parameters.

Based on the data given, and the principles of photocatalysis, the expected behavior would be that the results of all products are proportional to irradiance. This can be confounded however, by light distribution in the reactor. Ideally, the data provided

would be more complete when assessing the comparison photonic performance. When irradiation is not measured, or included in reporting, this hinders the ability to investigate these larger anticipated trends. The irradiance, however, only gets the comparison process so far. In this case, comparison is also hindered by the lack of characterization of the illuminated surface area. The irradiance measurement is power per square centimeter, so this information would have to be included for comparison. Only Fang *et al.* report the illuminated surface area, 3.14 $cm^2$, such that a calculation of the specific rate can be normalized by the power provided [78]. Therefore, 0.23 µmol/gh divided by 62.8 mW gives an extended rate normalization of 0.0037 µmol/ghmW.

Table 4.4 Results as reported for articles where a specific rate normalized by time and amount of catalyst can be calculated. (NA – not available)

| *Article* | *Length of Experiment (hours)* | *Catalyst loading (grams)* | *Light irradiation ($mW/cm^2$)* | *$CH_4$ result* | *units* | *$CH_4$ µmol/gh* |
|---|---|---|---|---|---|---|
| *[69]* | 8 | 0.5 | 1.7 | 2 | µmol/g | 0.25 |
| *[249]* | 20 | 0.1 | NA | 0.264 | µmole | 0.132 |
| *[183]* | 6 | NA | 8.5 | 0.129 | µmol/g | 0.0215 |
| *[228]* | 24 | 0.1 | NA | 11 | µmol/g | 0.46 |
| *[184],[185]* | 1 | NA | 8.5 | 0.025 | µmol/gh | 0.025 |
| *[80]* | NA | NA | NA | 0.019 | µmol/gh | 0.019 |
| *[66]* | 16 | 0.1 | NA | 10 | µmol/g | 0.625 |
| *[78]* | 24 | 0.01 | 20 | 0.23 | µmol/gh | 0.23 |
| *[67]* | 5 | 0.04 | NA | 0.5 | µmol/g | 0.1 |
| *[68]* | 1 | 0.1 | 50 | 1 | µmol/gh | 1 |
| *[186]* | 8 | NA | NA | 8.85 | µmol/g | 1.106 |
| *[250]* | 22 | NA | NA | 3 | µmol/g | 0.14 |

P25 results were collected experimentally under the conditions of 0.02 grams catalyst loading, for 2 hours experimental time, and 185 $mW/cm^2$ irradiance. The results were 0.2323 µmol/gh. This falls within the results range from literature. As the illuminated area was 12 $cm^2$, the specific rate normalized for power can be calculated and is 0.00011 µmol/ghmW. This result, while being within the range of results from literature and providing an acceptable benchmark, demonstrates drastically different performance

than that found by Fang *et al.*, when compared in terms of power utilization (extended normalization). This presents a situation where experimental procedure and reporting must become more sophisticated. Where it is possible to normalize for irradiance the range of results for this literature set becomes 0.0025-0.02 (µmol $cm^2$/g h mW) meaning the magnitudes in the range of results becomes 10, which does appear to be more unified as opposed to the $10^2$ range for the unitary product formation results range (µmol/gh). The implications of normalizing for irradiance alone is unclear. This result range variation must come from the experimental parameters and the reactor modifications of light and mass transport.

To consider comparing between rigs based on the P25 results, Table 4.5 was compiled including all products. The variation in the P25 results should be based in the reaction conditions of the experiment, the geometry of the reactor including illuminated surface area, distance of light source to catalyst, and volume, and the analytical detection capabilities of products. Key observations from Table 4.5 is the lack of reporting of key influences such as reactor geometry. This compounds the problem of reaction parameters reporting on discussing results across the literature. The ranges of products vary throughout Table 4.5. The hydrogen unitary product results range spans from 0.386-217.6 µmol/gh. An extended normalization can be applied to the experimental and [78] hydrogen results giving 0.098 and 0.0126 µmol/ghmW respectively. However even with this level of detail it is not possible to probe the reactor geometries. Could the product distributions have a relationship to the reactor geometry? The sense from the data is so much is untold and there is so much to discuss; a larger three-dimensional discussion that has been limited and confounded. The benchmark is often left without context, showing a range of results, and therefore with limited meaning, can thus be called "fuzzy".

Table 4.5 P25 results of various products detected from articles and experimental work (Exper.), conducted for this thesis, giving the reaction parameters of experimental length, catalyst loading and light irradiation, alongside reactor geometries such as illuminated surface area and reactor volume.

| *Article* | *Length of Exper. (hours)* | *Catalyst loading (grams)* | *Light irradiation ($mW/cm^2$)* | *Illum. surface area ($cm^2$)* | *Reactor Volume (mL)* | *Product result* | *units* |
|---|---|---|---|---|---|---|---|
| *[69]* | 8 | 0.5 | 1.7 | NA | 500 | $CH_4$ 2 | µmol/g |
| | 8 | 0.5 | 1.7 | NA | 500 | $CH_3OH$ 9 | µmol/g |
| | 8 | 0.5 | 1.7 | NA | 500 | HCHO 4 | µmol/g |

| *Article* | *Length of Exper. (hours)* | *Catalyst loading (grams)* | *Light irradiation ($mW/cm^2$)* | *Illum. surface area ($cm^2$)* | *Reactor Volume (mL)* | *Product result* | *units* |
|---|---|---|---|---|---|---|---|
| *[249]* | 20 | 0.1 | NA | 20 | NA | $CH_4$ 0.264 | µmole |
| | 20 | 0.1 | NA | 20 | NA | CO 1.4 | µmole |
| *[183]* | 6 | NA | 8.5 | NA | NA | $CH_4$ 0.129 | µmol/g |
| *[228]* | 24 | 0.1 | NA | NA | NA | $CH_4$ 11 | µmol/g |
| | 24 | 0.1 | NA | NA | NA | $H_2$ 100.9 | µmol/g |
| | 24 | 0.1 | NA | NA | NA | CO 2.5 | µmol/g |
| *[184], [185]* | 1 | NA | 8.5 | NA | NA | $CH_4$ 0.025 | µmol/gh |
| *[80]* | NA | NA | NA | NA | NA | $CH_4$ 0.019 | µmol/gh |
| | NA | NA | NA | NA | NA | CO 0.24 | µmol/gh |
| *[66]* | 16 | 0.1 | NA | NA | 100 | $CH_4$ 10 | µmol/g |
| | 20 | 0.1 | NA | NA | 100 | $H_2$ 170 | µmol/g |
| *[78]* | 24 | 0.01 | 20 | 3.14 | 11 | $CH_4$ 0.23 | µmol/gh |
| | 24 | 0.01 | 20 | 3.14 | 11 | $H_2$ 0.79 | µmol/gh |
| | 24 | 0.01 | 20 | 3.14 | 11 | CO 1.99 | µmol/gh |
| *[67]* | 5 | 0.04 | NA | NA | NA | $CH_4$ 0.5 | µmol/g |
| | 5 | 0.04 | NA | NA | NA | $H_2$ 1.93 | µmol/g |
| | 5 | 0.04 | NA | NA | NA | CO 1.1 | µmol/g |
| | 5 | 0.04 | NA | NA | NA | $CO_2$ conv.1.6 | µmol/g |
| *[61]* | 5 | 0.04 | 10 | NA | NA | CO; UV 18 | µmol/g |
| | 5 | 0.04 | NA | NA | NA | CO; vis 3 | µmol/g |
| *[68]* | 1 | 0.1 | 50 | NA | 70 | $CH_4$ 1 | µmol/gh |
| | 3 | 0.1 | 50 | NA | 70 | $CH_4$ 1.5 | µmol/g |
| *[71]* | 5 | 0.05 | 420 | NA | NA | CO 10 | µmol/g |
| | 5 | 0.05 | 420 | NA | NA | CO 550 | µmol/ $cm^2$ |
| *[186]* | 8 | NA | NA | NA | NA | $CH_4$ 8.85 | µmol/g |
| *[250]* | 22 | NA | NA | NA | NA | $CH_4$ 3 | µmol/g |
| | 22 | NA | NA | NA | NA | $H_2$ 42 | µmol/g |
| *Exper.* | 2 | 0.02 | 185 | 12 | 216 | $CH_4$ 0.00929 | µmol |
| | 2 | 0.02 | 185 | 12 | 216 | $H_2$ 8.704 | µmol |
| | 2 | 0.02 | 185 | 12 | 216 | $C_2$ 0.00039 | µmol |
| *[69]* | 8 | 0.5 | 1.7 | NA | 500 | $CH_4$ 2 | µmol/g |

Before moving on it is pertinent to note that it can be argued that P25 is an ineffective benchmark. Focusing specifically on the production of $CH_4$ for example, Li *et al.* state that "Under either UV or UV-vis illumination, P25 $TiO_2$ exhibited insignificant

catalytic activity for methanation of $CO_2$, with $CH_4$ production rate lower than 1 μmol/gh" [68]. They are working with $CO_2$ and $H_2O$ vapor as many of the articles are. And Li *et al.* cite Xie *et al.* and Zhai *et al.* as reaching the same conclusion [251, 252]. Based on the threshold Li *et al.* put forward, very few of the results from the literature are significant. This provides a wonderful opportunity for the kind of academic discussion and assessment questioning that Bligaard *et al.* encourage [84]. The perspective of this thesis is a benchmarking material is better than no benchmarking material. However, there is room to propose a new commercial photocatalytic material to take P25's place.

### 4.3 Experimental context for benchmarking, discussion of the current practice of single experiment comparison with commercial samples

The various commercial materials utilized in this experimental work included Anatase $TiO_2$, P25, and Mirkat 211. The Anatse $TiO_2$ is similar to laboratory produced samples with no modification, often used for comparison to observe the improvement due to modification. P25 is a commonly utilized benchmark, and the Mirkat photocatalyst has a very high surface area. To benchmark the commercial materials performance these three samples were screened all at 0.02 g catalyst loading, for 2 hours, and 185 $mW/cm^2$ irradiance. These settings represented a relatively low catalyst loading, a moderate length of experiment, and a relatively high light intensity, all chosen to increase product formation.

The results of the commercial sample benchmarking are shown in Figure 4.8, which shows the unitary product formation of $CH_4$, $C_2$ products, and $H_2$. The behavior of the Mirkat sample appears to be more similar to the behavior of the anatase sample, with P25 favoring $CH_4$ and $H_2$ production. This is to be expected as both the Anatase $TiO_2$ and the Mirkat samples used contain the anatase crystal phase of $TiO_2$, whereas P25 is a mixture of both anatase and rutile. In the literature, anatase $TiO_2$ has been reported to produce $CH_3OH$, however, this was not observed [253]. The P25 results are less than other $CH_4$ results reported, however in the case of Tu *et al.* and Huo *et al.* they also reported CO, and Huo's work confirms the much larger $H_2$ to $CH_4$ ratio [228, 254, 255]. Mirkat results are unlike those found in literature, with the results gathered here being lower values; however, it does show similar trends. For example, Olivo *et al.* found the Mirkat 211 to produce more $CH_4$ than $H_2$ that was also observed here; however, there was

no report of $C_2$ compounds [70]. Crystal phase appears to be the most significant influence for the results under these reaction conditions.

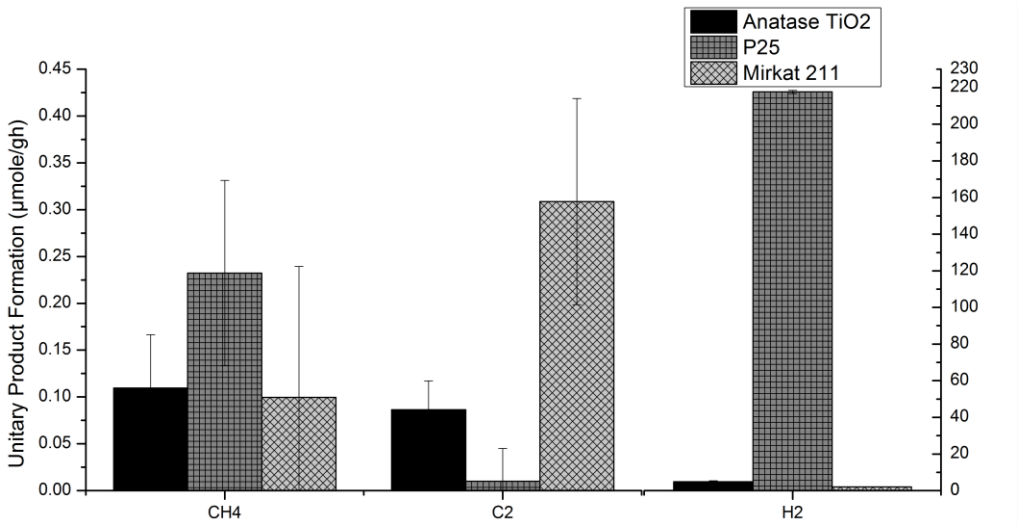


Figure 4.8 Carbon based products detected for commercial samples P25 and Mirkat 211 compared to commercial anatase $TiO_2$ (left axis). Hydrogen results for commercial samples (right axis). These experiments were conducted with 0.02 g of catalyst for 2 hours with 185 mW/cm$^2$ irradiance.

When comparing the P25 results products distributions and proportions from the experimental results to the literature results reviewed in section 4.2, there are a surprising number of articles that report $CH_4$ and or CO production [60, 61, 66-69, 71, 78, 80, 183, 184, 186, 187, 228, 249, 250]. Matejova *et al.* however, report $CH_4$ and $H_2$ results giving a similar trend of greater $H_2$ production that $CH_4$ production as seen with the experimental results here, however the scale of improvement of the $H_2$ production over the $CH_4$ production is only roughly 17 fold as opposed to these experimental results where the $H_2$ production is significantly better being well over 800 fold [250].

Clearly, the materials properties can be used to normalize the rate. Also, the volume of the reactor could be appropriate to assist comparison between labs as shown below in Table 4.6. In this case, the specific surface area revises the trend in performance seen in the product formation. A greater than 5 fold increase in specific surface area, from P25 to Mirkat, can produce a roughly 3 fold improvement in product formation when normalized for illuminated surface area, whereas an initial roughly 10 fold increase in specific surface area from anatase $TiO_2$ to P25 had minimal effect. Therefore, there appears to be no relation between specific surface area and product results.

Table 4.6 Rate results from commercial samples benchmarking experiments conducted at room temperature for 2 hours with 0.02g catalyst and a light intensity of 185 mW/cm$^2$ for all carbon products.

| | *µmole carbon* | *Unitary Product Formation µmole/gh* | *µmole/m$^2$h using specific surface area* | *µmole/gm$^2$h using illuminated surface area* |
|---|---|---|---|---|
| *Anatase $TiO_2$* | 0.011 | 0.282 | 0.038 | 235 |
| *P25* | 0.010 | 0.252 | 0.005 | 210 |
| *Mirkat 211* | 0.029 | 0.717 | 0.003 | 598 |

From the commercial photocatalytic samples performance considering $CO_2$ reduction, it can be observed (

Figure 4.8) that P25 produces the most $CH_4$, however the error margins of all three samples overlap. In contrast, Mirkat produces the most $C_2$ products even considering the error. Due to the higher $CO_2$ embodied in the $C_2$ products further testing was conducted with Mirkat as described in Chapter 6.

## 4.4 Experimental context for benchmarking, discussion of the current practice of single experiment comparison with modified samples

Tests were conducted with modified samples. These samples included EISA produced samples, one of which was further treated with a $H_2$ atmosphere at elevated temperatures after calcination, and an Au doped anatase $TiO_2$. These samples were all tested at 0.02 g catalyst loading, for 2 hours, and 185 mW/cm$^2$ irradiance. The results of the benchmarking experiments are shown in Figure 4.9. The experimental results in Figure 4.9 show that these samples vary greatly in their selectivity toward hydrogen or methane, however not significantly in their production of $C_2$ products. The $H_2$ heat treated EISA sample has a significant increase in $CH_4$ unitary product formation relative with unmodified EISA. Mirkat, here included for comparison, is outperformed by the $AuTiO_2$. EISA $CO_2$ photoreduction results with $TiO_2$ based materials are rare. An example with a $TiO_2 – SiO_2$ composite made by EISA, with a ratio of Ti to Si of 6:4, gives a roughly 0.05 µmole/gh unitary product formation [256]. This is similar to the experimentally found EISA result, however in the literature the comparison is with the composite with a Ti to Si ratio of 8:2, unitary product formation of 0.25 µmole/gh that was very likely due to improved mass transfer as the 8:2 material had a larger mean pore size [256].

Comparing the Au modified samples from literature, there are no examples with the same low weight percent of 0.2 for the experimental sample, but the rates found for $CH_4$ unitary product formation (µmole/gh) include 0.18 for 0.4 wt% Au [250], 0.28 for an unknown wt% of Au (reported with CO results, but no $H_2$ ) [72], 1.5 for 0.5 wt% Au

(with no corresponding $H_2$ products) [186], and 8 for 0.29 wt% Au [257]. The $H_2$ unitary product formation was higher in the literature, 2.27 μmole/gh for 0.4 wt% Au [250], and 9.5 μmole/gh for 0.29 wt% Au [257]. From these results the experimental $AuTiO_2$ performance appears to be within, as is the case with the $CH_4$ results, or near to, as is the case with $H_2$ results, these literature benchmarks. A wider range of Au modified samples from literature are discussed in more detail below in section 4.5 based on $CH_4$ product formation.

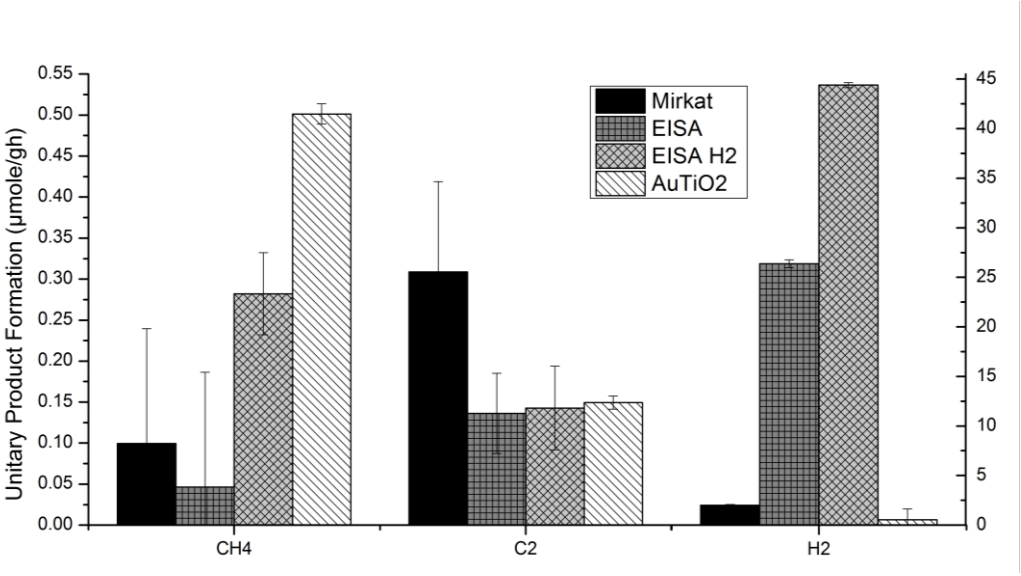


Figure 4.9 Mirkat 211 results as compared to modified $TiO_2$ samples and their detected carbon products (left axis). And Hydrogen results from modified $TiO_2$ samples (right axis). Experiments conducted at room temperature with 0.02 g catalyst, for 2 hours at 185 $mW/cm^2$ irradiance.

The $CO_2$ conversion performance of the samples and the experimental and reactor context results are tabulated below (Table 4.7). All the carbon based products have been summed based on their representative utilization of $CO_2$ and the specific rate is compared to normalization based on the specific surface area of the photocatalytic material and then compared to the reactor illuminated surface area. As compared to the commercial samples, these modified samples have a much more consistent performance proportional to the specific surface area of the material. The defect generation of the $H_2$ atmospheric treatment and the gold doping show slight improvements in performance when specific surface area is controlled for. These kinds of normalizing procedures help identify if modifications have a cumulative impact on performance or if the various modifications impact on the reaction mechanisms involved and limit each other.

Table 4.7 Specific rate results from modified samples benchmarking experiments conducted at room temperature for 2 hours with 0.02g catalyst and a light intensity of 185 mW/cm$^2$ for all carbon products.

| | *µmole carbon* | *Unitary Product Formation µmole/gh* | *µmole/m$^2$h using specific surface area* | *µmole/gm$^2$h using illuminated surface area* |
|---|---|---|---|---|
| *Mirkat 211* | 0.029 | 0.717 | 0.003 | 597 |
| *EISA* | 0.017 | 0.421 | 0.006 | 351 |
| *EISA $H_2$* | 0.023 | 0.567 | 0.009 | 473 |
| *AuTi$O_2$* | 0.032 | 0.800 | 0.007 | 666 |

From the modified samples results, in terms of $CO_2$ reduction, it can be observed (Figure 4.9) that while the Mirkat is still highest in $C_2$ based products, the $CH_4$ unitary product formation for the Au doped $TiO_2$ is the highest. Therefore, the $AuTiO_2$ sample was chosen for further experimental work in chapter 5.

## 4.5 Experimental context for benchmarking, discussion of gold doped $TiO_2$ samples from the literature

Modifications utilizing gold are a common way to improve catalytic and photocatalytic performance. The literature reviewed includes 7 articles [58, 72, 79, 186, 187, 250, 257]. Considering a wide range of articles utilizing Au/$TiO_2$ materials they can be compared based on $CH_4$ production, (Table 4.8) [58, 72, 79, 186, 250, 257, 258]. The unitary product formation results for $CH_4$ production give a range of 0.18-58 µmole/gh. The $10^3$ range of the results is inexplicable due to incomplete reporting. With these gold $TiO_2$ material results the influencing factors challenging benchmarking include modifications to the materials, the reaction parameters, and the reactor geometries. Additionally comparisons of photocatalytic structure including the nanotube arrays, 58.47 $CH_4$ µmol/gh [79], as relative to nanowires 30 $CH_4$ µmol/gh [58] become challenging even as they appear similar and comparable in quantity.

Table 4.8 $AuTiO_2$ materials and their $CH_4$ results where specific rate can be calculated. Various pieces of data were not available (NA).

| *Article* | *Time (hour)* | *Catalyst loading (grams)* | *Light irradiation ($mW/cm^2$)* | *$CH_4$ result* | *units* | *$CH_4$ µmol/gh* |
|---|---|---|---|---|---|---|
| *[79]* | 8 | NA | 100 | 58.47 | µmol/gh | 58 |
| *[72]* | 5 | NA | NA | Anatase 0.28 | µmol/gh | 0.28 |
| *[72]* | 2-5 | NA | NA | Rutile 0.27 | µmol/gh | 0.27 |
| *[186]* | 8 | NA | NA | 23.1 | µmol/g | 2.9 |
| *[257]* | 4.5 | 0.1 | 71.7 UV | 8 | µmol/gh | 8 |
| *[250]* | 22 | NA | NA | 4 | µmol/g | 0.18 |
| *[58]* | NA | 0.01 | NA | 30 | µmol/gh | 30 |

Three of the articles, [186, 187, 250] include both P25 results and a modified Au $TiO_2$ sample results. The results and experimental results are presented below in Table 4.9. These three articles enable a benchmarked comparison allowing for identical laboratory conditions to be assumed to be enumerated in the P25 result. Both the reactor geometries and the experimental conditions are constant for comparing across the gain from modifications. Ideally, the P25 would be a gauge of the reactor conditions, and then the modified photocatalytic material performance would be attributable to the modification alone resolving the relations discussed in Section 3.4.3. Therefore, to assess this material improvement, the gain of the modification performance is divided by the P25 performance. This should remove the effects of reaction parameters and reactor geometries.

Table 4.9 P25 and $AuTiO_2$ samples and their $CH_4$ results from the articles with P25 benchmarking, including experimental results (Exper.). The gold modified materials include doped samples and a three dimensionally ordered macroporous photocatalyst with 6.6 wt. % Au (3DOM $Au_8/TiO_2$).

| *Article* | *Catalyst* | *Specific Surface Area ($m^2/g$)* | *Illuminated surface area ($cm^2$)* | *Light irradiation ($mW/cm^2$)* | *Product result* | *units* | *$CH_4$ µmol/gh* |
|---|---|---|---|---|---|---|---|
| *[186]* | P25 | -- | NA | NA | $CH_4$ 8.85 | µmol/g | 1.10625 |
| *[186]* | 3DOM $Au_8/TiO_2$ | 36 | NA | NA | $CH_4$ 23.1 | µmol/g | 2.8875 |
| *[250]* | P25 | 50 | NA | NA | $CH_4$ 3 | µmol/g | 0.1364 |
| | | 50 | NA | NA | $H_2$ 42 | µmol/g | - |
| *[250]* | $AuTiO_2$ 0.4 wt % | 84 | NA | NA | $CH_4$ 4 | µmol/g | 0.1818 |
| | | 84 | NA | NA | $H_2$ 60 | µmol/g | - |
| *[187]* | P25 | 50 | NA | NA | $CH_4$ 90 | ppm | |
| | | 50 | NA | NA | $CH_4$ 135 | ppm | |
| *[187]* | 1.5 mol% $Au/TiO_2$ | -- | NA | NA | $CH_4$ 503 | ppm | |
| *Exper.* | P25 | 50 | 12 | 185 | $CH_4$ 0.00929 | µmol | 0.2323 |
| | | 50 | 12 | 185 | $H_2$ 8.704 | µmol | |
| | | 50 | 12 | 185 | $C_2$ 0.00039 | µmol | |
| *Exper.* | $AuTiO_2$ 0.2 wt % | 110 | 12 | 185 | $CH_4$ 0.02005 | µmol | 0.5013 |
| | | 110 | 12 | 185 | $H_2$ 0.021 | µmol | |
| | | 110 | 12 | 185 | $C_2$ 0.00597 | µmol | |

The gain in performance from the benchmark P25 to the gold enhanced photocatalytic material is inconsistent. The gains between the two photocatalytic materials are roughly 2.6 [186], 1.3 [250], and 5.3 [187] for the gold modified performance over the P25 results. The gain for the experimental results is 2.16. In terms of materials modifications there are varying amounts of gold loading and specific surface areas used, as shown below (Table 4.10). It can be observed in Table 4.10 that there is no meaningful relationship between the gold content and the results. It appears that normalizing by specific surface area may have more significance, but it is a small set of

results for comparison. Insights from gain normalized for gold will be nuanced as any dopant can increase activity or block irradiation, decrease surface area or act as recombination centers [259].

Table 4.10 Gain in product results for articles containing both P25 benchmarks and gold modified samples with examples of normalizing the gain.

| *Article* | *Amount of gold* | *Specific Surface Area ($m^2/g$)* | *Gain in performance* | *Gain normalized for gold* | *Gain normalized for specific surface area* |
|---|---|---|---|---|---|
| *[186]* | 6.6 wt% | 36 | 2.6 | 0.4 | 0.07 |
| *[250]* | 0.4 wt% | 84 | 1.3 | 3.25 | 0.02 |
| *[187]* | 1.5 mol% | NA | 5.3 | 3.53 | NA |
| *Exper.* | 0.2 wt% | 110 | 2.16 | 10.8 | 0.02 |

Challenges to this type of benchmarking may occur if it can be proven that the reactor set up and parameters have unique interactions with the material that influence performance. An example would be a material modification changing the mass transport in the reactor. With a wider set of compete data each modification or parameter could be used to comprehensively rank the effects. Unfortunately, with current literature the cause of the variation, this cannot be investigated due to incomplete reporting.

### 4.6 Benchmarking reactors and photocatalytic materials

Chapter 4 has reviewed and discussed identical experimental benchmarking, presenting opportunities for normalization that can be expanded, the limited literature comparisons, and the importance of reporting comprehensive data sets. The experimental results show similar trends as literature, including that crystal phase and specific surface area appear to be important material characteristics when comparing across modifications. P25 may be a limited benchmark, however it is better than no benchmark. The literature range for unitary product formation results for $CH_4$ production using P25 as the photocatalyst is 0.019-1.106 µmol/gh. The range of unitary product formation results for the Au modified samples was 0.18-58.47 µmol/gh of $CH_4$. Of the commercial samples Mirkat 211 had the largest $CO_2$ reduction results and, therefore, is used for further exploratory testing varying

experimental parameters. Of the modified samples the Au $TiO_2$ had the largest $CO_2$ reduction results, thus, it is investigated further with design of experiments analysis. A way to use benchmark materials to assess materials modifications improvements by scaling across different reactors is shown, and may be promising especially when results are normalized for specific surface area, however very few publications have enough information to enable this kind of comparison. Most crucially, the conclusion can be made that all three areas of the experimental work; the reactor geometries, reaction parameters and materials characterization, need to be comprehensively reported.

Starting from this discussion of photocatalytic comparisons, this thesis will now move into single material explorations. Further testing presented in Chapters 5 and 6 detailing Mirkat and Au doped $TiO_2$ photocatalytic performance with a single rig will enable a wide scope of discussion for the benchmarking challenge. Au doped $TiO_2$ will be investigated implementing the design of experiments and proposed regime tools utilized with Mirkat to focus experimental work. Therefore, a new opportunity will be created where a singular experimental rig and investigation will generate a range of results from modifying reaction parameters. This will allow for a comparison of the range of results from a single rig with the variability across multiple rigs, a comparison of which reaction parameters have the largest impacts on results, a more nuanced discussion of the dual term challenge, and an attempt to quantify the effectiveness of current "fuzzy" benchmarking.

# CHAPTER 5 – UTILIZING THE DESIGN OF EXPERIMENTS; EXPERIMENTS WITH GOLD DOPED TITANIUM DIOXIDE

Here the results from modified $AuTiO_2$ sample are presented. These results include those from the design of experiments (DoE) investigations. Experimental set up is covered in section 5.1. The variables investigated within the photoreduction system three factor DoE are the catalyst loading, light irradiance, and length of experiment (section 5.2). A two factor DoE, varying reaction length and a wider irradiance range, was also investigated (section 5.3). The output responses investigated were $CH_4$ unitary product formation results (µmole/gh), photonic yield, and extended rate normalization; And $CO_2$ unitary product formation calculated from the sum of carbon containing products measured, the photonic yield of the total products, and the extended normalization of carbon summed products. Insights from this analysis is discussed in section 5.4 in terms of maximum results (section 5.4.1), interaction effects (section 5.4.2), and variation in results terms (section 5.4.3).

## 5.1 Experimental methodology and materials for design of experiments

The experimental plan and material used for the DoE are described in detail below.

### *5.1.1 Experimental method for design of experiments*

In the experimental work for the testing $AuTiO_2$ for the design of experiments, the procedures were changed slightly from the procedure described in chapter 4, section 4.1.3. $AuTiO_2$ was chosen as the modification for intense experimental investigation by design of experiments because of the increased $CH_4$ production compared to the other modified materials tested (Chapter 4, section 4.4). In this case, catalyst loading was done with 1mL suspension. The other significant change to the previously reported methodology was in this case the overnight flow and background readings were done using $CO_2$ bubbled in water instead of helium. These changes were implemented due to better adherence of the catalyst to the quartz plate surface as observed visually, and an improvement in the analytical procedure for products quantification through a reduction in variation in calibration values.

In this case, because a batch reactor is being utilized, there is already a need for many experiments to explore performance to map out a time response, particularly in the investigation of kinetics. To limit the number of experiments a two level factorial was utilized. In particular, the two level factorial is appropriate for understanding the behavior

of the system [260]. Surface response designs assist with further optimizations [208], [260]. This limits the analysis because this type of factorial is best suited to linear behavior. Using a two level factorial is acceptable for this PhD work because it is utilized to gather a reasonable data set from lab variations from $AuTiO_2$ for a benchmarking assessment, it broadens the $CO_2$ photoreduction discussion into DoE experiments further, and it highlights interaction effects in experimental work. In the future, exploration of kinetics would be more expediently conducted with flow reactions, which would allow the complexity of the DoE to increase without extending experimental time drastically.

Experiments done following a DoE for this thesis, used an experimental layout generated using Minitab 17, for a three factor, two level, full factorial; high and low with a three-measurement midpoint, and experiments randomized. It is used to investigate the effect of factors on the response. The midpoint triplicate enables error analysis. The significance of factors to be measured comes from the comparison of the regressed linear function and the p-values. The design matrix of the experiments can be seen in Table 5.1, where the randomized run order and various high (1), low (-1) and midpoint (0), designations can be observed.

Table 5.1 The coded design matrix of experiments using the Au doped $TiO_2$.

| *Standard Order* | *Run Order* | *Catalyst Loading (g)* | *Light Intensity (irradiance, $mW/cm^2$)* | *Length of Experiment (hours)* |
|---|---|---|---|---|
| *1* | 11 | -1 | -1 | -1 |
| *2* | 1 | 1 | -1 | -1 |
| *3* | 10 | -1 | 1 | -1 |
| *4* | 6 | 1 | 1 | -1 |
| *5* | 8 | -1 | -1 | 1 |
| *6* | 3 | 1 | -1 | 1 |
| *7* | 4 | -1 | 1 | 1 |
| *8* | 5 | 1 | 1 | 1 |
| *9 (midpoint)* | 2 | 0 | 0 | 0 |
| *10 (midpoint)* | 9 | 0 | 0 | 0 |
| *11 (midpoint)* | 7 | 0 | 0 | 0 |

The high and low settings were set to 0.04 and 0.02 g of photocatalyst, 3 and 1 hours, and then 185 and 62 mW/cm$^2$ irradiance. Thus, the midpoints were 0.03 g catalyst loading, 2 hours reaction time, and 124 mW/cm$^2$ irradiance. Settings were based on results from prior testing. In particular, the length of experiment were shortened due to higher products observed at lower times, the catalyst loading varied around what appears to be an optically thicker catalyst layer and thinner layer however all are visible, and lastly light intensity was chosen for a range to enable investigation of the irradiance influence on the unitary product formation.

An extended DoE was also conducted to explore the factor ranges further relative to anticipated main effects, and as a two factor extension of the initial DoE utilizing the midpoints. This enabled a wider range of light intensities to be investigated. For these experiments, 0.03 g catalyst loading was used, varying the length of experiment and the reaction time as shown (Table 5.2), along with the experimental randomized run order. The high low values chosen were 3 and 1 hours reaction time, and 241 and 6 mW/cm$^2$ irradiance, giving a much wider range in power provided to the $CO_2$ photoreduction reactions.

Table 5.2 The coded design matrix of the design of experiments for the extended two variable investigation.

| *Standard Order* | *Run Order* | *Light Intensity (irradiance, mW/cm$^2$)* | *Length of Experiment (hours)* |
|---|---|---|---|
| *1* | 4 | -1 | -1 |
| *2* | 3 | 1 | -1 |
| *3* | 1 | -1 | 1 |
| *4* | 2 | 1 | 1 |

As there is a triplicate midpoint an error term can be generated. This is used in the production of Pareto charts, as the error term is used to calculate the confidence level minimum as 1-α/2. The significance level, α, is set at 0.05 and sets the probability of rejecting the null hypothesis, if it is true. The models generate a p value which is the probability of obtaining data if the null hypothesis is true, with the discrimination of results significance being that the p value is less than α.

### *5.1.2 Material review of $AuTiO_2$ as material used in the design of experiments testing*

$AuTiO_2$ was synthesized by precipitation from sulphate salt in sodium hydroxide using nitrogen [70]. The $TiO_2$ was synthesized through precipitation of $TiOSO_4$ salt with the base NaOH, forming $Ti(OH)_4$ which was then calcinated at 400°C to form $TiO_2$. Then Au was added using deposition precipitation [242]. $AuTiO_2$ was measured to have a band gap of 3.21 eV, and at roughly 560 nm surface plasmon resonance was observed. $AuTiO_2$ also has a specific surface area of 110 $m^2/g$ and anatase crystallinity.

## 5.2 Design of experiments investigating Au $TiO_2$ product formation as influenced by light intensity, catalyst loading and length of experiment; three factor design of experiments

To optimize the reaction response for the experimental parameters or factors a DoE is a significant tool to find optimum conditions and investigation of interactions. The MS is calibrated to give ppm results. These results were then used to calculate specific rate of unitary product formation, photonic yield and an extended normalization of the unitary product formation. This is because the response should be understood relevant to reaction parameters which were all observed relative to a specific rate response in Chapter 2, section 2.8.

The model from the DoE is presented below in three parts including the Pareto Chart of standardized effects, main effects plots and interactions plots. The Pareto Chart is significant in that if the effect of a factor is not greater than the reference line it is not a significant factor and is not an important contributing factor to the result analyzed. The main effect plots show the variable effect between high and low points along with the center point. The interaction plots show this variable effect in relation to another factor. Perpendicular lines indicate a strong interaction. These plots do not include error margins instead relying on the p value determination to assess significance.

In this case, two responses have been considered, including the $CH_4$ and the representation of $CO_2$ as calculated from summing product contributions, both in $\mu mole/g_{cat}h$ units. The experimental layout is given here with the $CH_4$ unitary product formation (µmole/gh) results from the three variable DoE (Table 5.3).

Table 5.3 The experimental layout with µmole/gh results of the three factor design of experiments using the Au doped $TiO_2$.

| *Standard Order* | *Catalyst Loading (g)* | *Light Intensity (irradiance, mW/cm²)* | *Time (hours)* | *$CH_4$ Unitary product formation (µmole/gh)* |
|---|---|---|---|---|
| *1* | 0.02 | 62 | 1 | 0.6307 |
| *2* | 0.04 | 62 | 1 | 0.2357 |
| *3* | 0.02 | 185 | 1 | 0.2655 |
| *4* | 0.04 | 185 | 1 | 0.0763 |
| *5* | 0.02 | 62 | 3 | 0.0885 |
| *6* | 0.04 | 62 | 3 | 0.0011 |
| *7* | 0.02 | 185 | 3 | 0.1659 |
| *8* | 0.04 | 185 | 3 | 0.1117 |
| *9 (midpoint)* | 0.03 | 124 | 2 | 0.0331 |
| *10 (midpoint)* | 0.03 | 124 | 2 | 0.0951 |
| *11 (midpoint)* | 0.03 | 124 | 2 | 0.0088 |

The Pareto chart red dashed line is the reference line of significance. This Pareto chart, Figure 5.1, shows the length of experiment, catalyst loading and the interaction of the irradiation and time to be the significant effects. This model includes the effects of catalyst loading, irradiance, reaction time, and the interaction of irradiance and reaction time. Investigations and analysis done previously using ppm results had only shown one effect to be statically significant. Normalizing appears to highlight the importance of a parameter to the process as more factors have become significant in the model.

Pareto charts of both the photonic yield and extended normalization for the $CH_4$ results are presented together in Figure 5.1, middle and bottom. Here the results have been calculated in terms of efficiency of the use of photons to produce products with the products being represented by their necessary constituent electrons, and a power normalization of products. As recommended by IUPAC, the term photonic yield for incident light with a singular wavelength, is utilized for experimental work (Chapter 2, section 2.5.2). Here, the extended normalization discussed and implemented in section 3.1 is revisited utilizing the DoE.

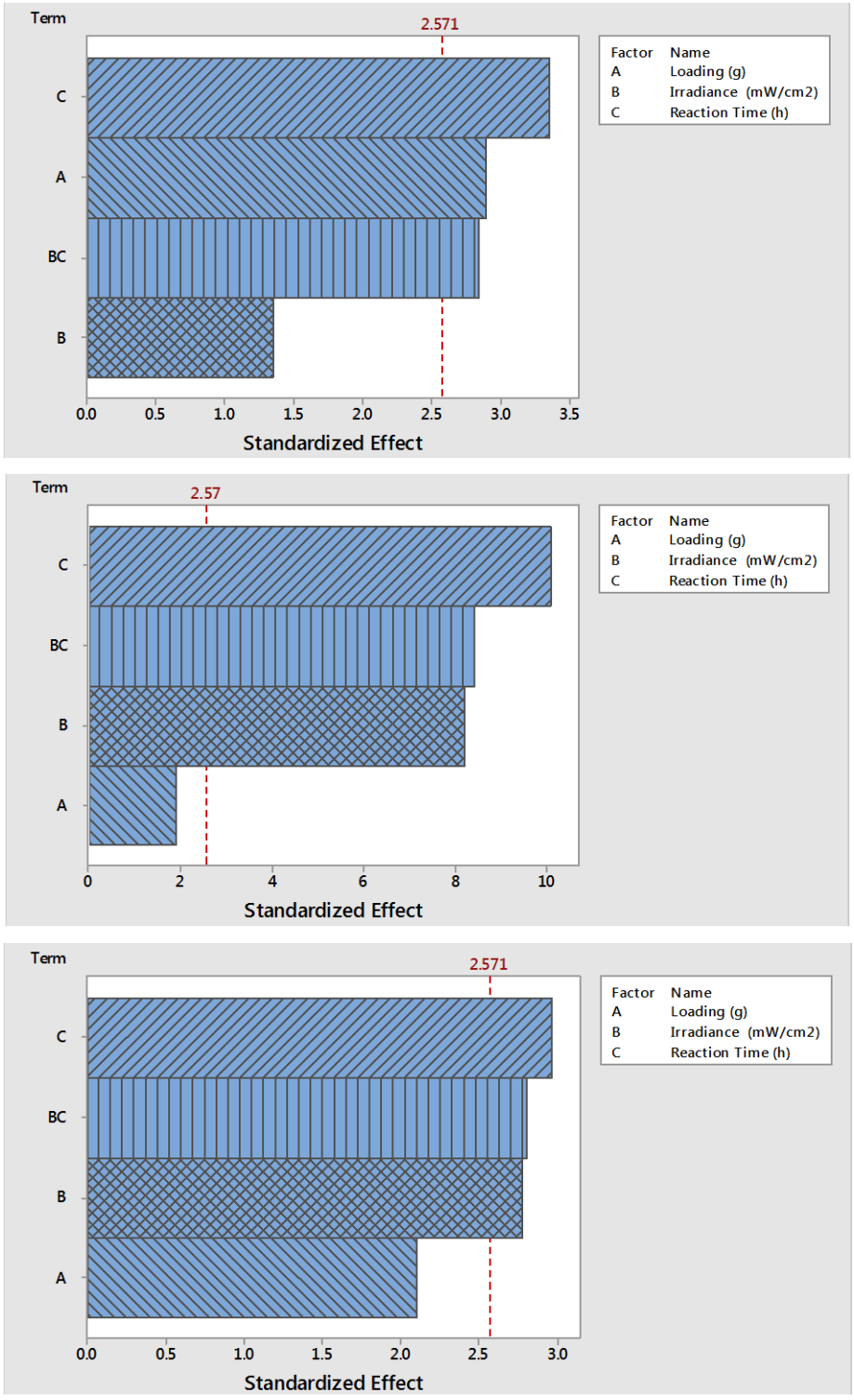


Figure 5.1 Pareto Chart of the standardized effects of the $CH_4$ response for the three factor design of experiments calculated in terms of unitary product formation (µmole/gh), where $\alpha = 0.05$ (top). Pareto chart of the standardized effects of the photonic yield response of the $CH_4$ for the three factor design of experiments (middle). Pareto chart of the standardized effects of the extended normalization (µmole/ghLW) $CH_4$ results for the three factor design of experiments (bottom).

The Pareto charts, Figure 5.1, shows that in both cases the reaction time is the most significant factor, followed by the interaction of irradiance and reaction time, then

the irradiance. When observing the photonic performance and the extended normalization performance, in this case, the photocatalyst loading is not statistically significant. It could be that the amount of photocatalyst utilized for the reaction were all within the light saturated range (Chapter 2, section 2.8.1). This behavior is not what was seen with the three factor $CH_4$ specific rate results (Figure 5.1, top), where the irradiance had not been statistically significant, however the catalyst loading had.

The main effects are plotted in Figure 5.2. The main effects plot shows the response at the low and high conditions, blue dots, and then fitting a linear model line between the results, and giving the midpoint response with a red square. Here the main effects are showing that a lower loading, lower irradiance, and lower reaction time correspond to higher $CH_4$ μmole/gh results. This is unexpected. Therefore, the extended DoE is revisited as it gives a wider irradiation range. Note that in this case, the rate is normalized for the catalyst loading. Therefore, the observation is of whether the further increase of time or photocatalyst leads to further increases in product formation, which it is observed that it does not.

The main effects plot, Figure 5.2, shows that increasing the parameters of irradiance and reaction time lowered the $CH_4$ photonic yield and extended normalization. This is the same as was observed for the $CH_4$ unitary product formation results. This could be due to a high catalyst loading that light is unable to access the whole mass.

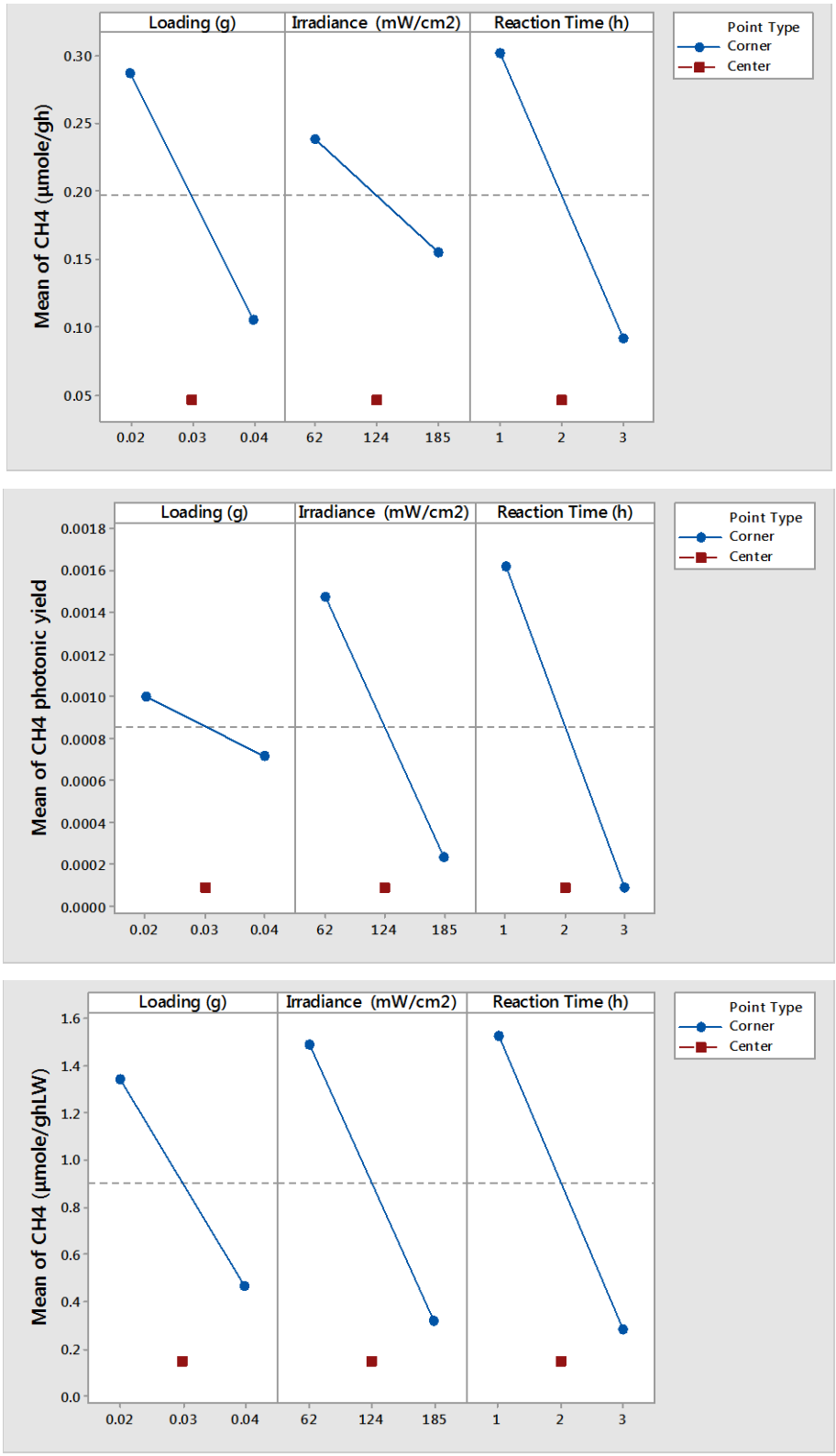


Figure 5.2 Main effects plot for $CH_4$ unitary product formation results (µmole/gh) for the three variable design of experiments (top). Main effects plots of the $CH_4$ photonic yield from the three factor design of experiments (middle). Main effects from the extended normalization $CH_4$ results for the three factor design of experiments (bottom).

The interaction effect can be seen in Figure 5.3, which plots one variable along the x-axis, and another is represented by each line. Therefore, in Figure 5.3, the x-axis

shows the low and high values of irradiance, and the blue line represents the low value for the length of the experiment as 1 hour, and the green line the results for the high value for the length of the experiment at 3 hours. At a low irradiance and low reaction time the largest unitary product formation (μmol/gh) of $CH_4$ was observed. In this case, the interaction plots are showing a moderate interaction, as the lines are clearly not parallel, however they are not perpendicular either. Interestingly, the high irradiance in both time conditions gives very similar unitary product formation results. This is contrary to the expectation that triple the amount of irradiation (the high relative to the low irradiance condition) when at a one hour condition would be roughly equivalent, at least energy input wise to the low irradiance for three hours. Interestingly at one hour, higher irradiance does not increase the product formation, however for the three hour experiment length it does.

The interaction plot for $CH_4$ photonic yield and the extended normalization, Figure 5.3 middle and bottom, shows a limited interaction effect. What is observed is that the level of irradiance appears to have no influence at the three hour reaction time (green dotted line), and the low reaction time with low irradiance result in a high photonic yield. At the lower reaction time, fewer photons can be utilized more effectively than the higher irradiance flux with more photons. But at the three hour time period the proportionalities are constant, the incoming photons appear proportional to the product embodied electrons. This response could be due to photocatalytic degradation occurring causing a steady maximum [261]. It appears that normalizing with the irradiance and illuminated surface area can provide similar information to the photonic efficiency quantification.

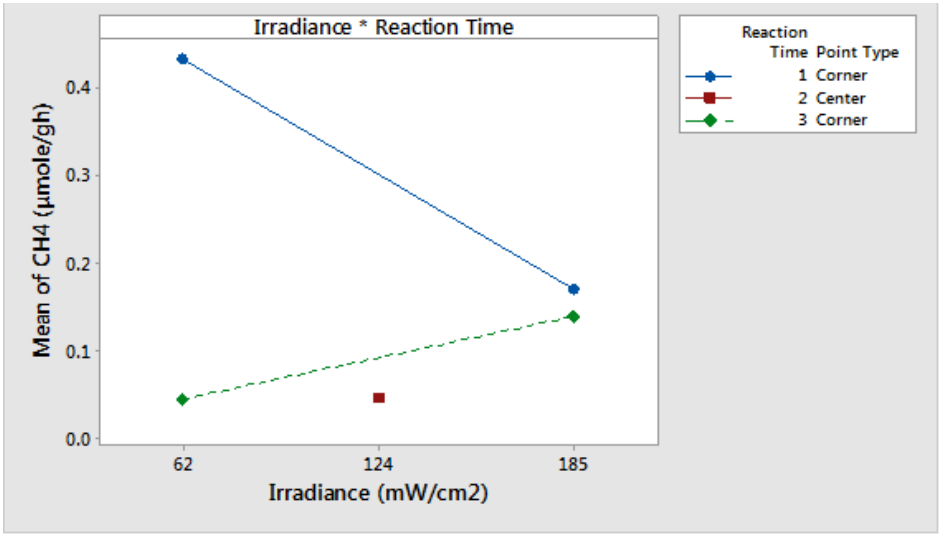


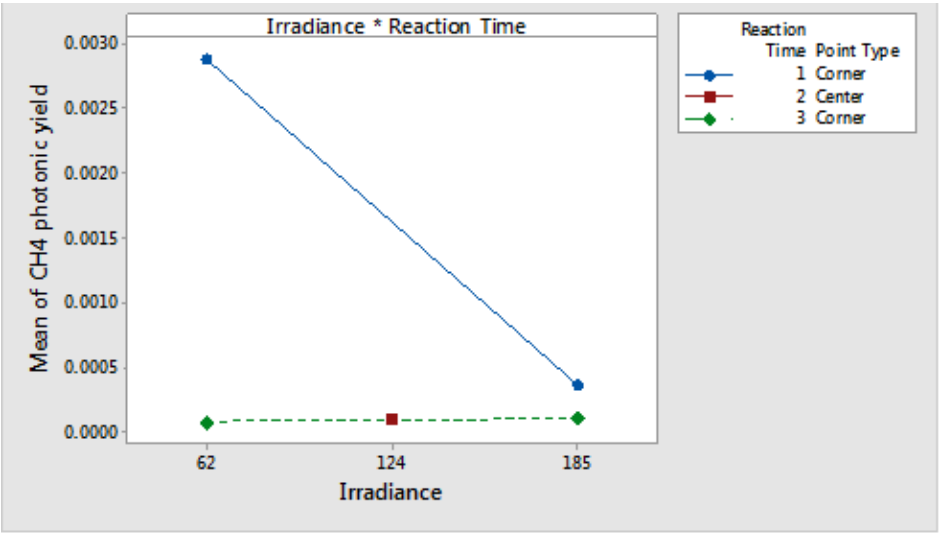



Figure 5.3 Interaction plot for three factor DoE $CH_4$ unitary product formation (µmole/gh) results, of irradiance and time (top). Interaction plot of the $CH_4$ photonic yield response from the three factor design of experiments (middle). Interaction plot of the extended normalization $CH_4$ results for the three factor design of experiments (bottom).

Comparing the specific rate (μmole/gh) response to the photonic yield response in terms of the dual term problem we can compare the $CH_4$ results, for the three factor DoE. The main effects and interaction is relatively similar and shows the same general trends. The largest difference between the terms is what factors are deemed significant. The reaction time is the most significant factor in every case. Then they start to diverge, with the interaction of irradiance and reaction time being significant to the photonic yield and extended normalization, and photocatalyst loading for unitary product formation. And finally, they differ on the last significant factor, with the interaction of irradiance and reaction time being significant for the unitary product formation, which is normalized by catalyst loading, and then the irradiance being significant for the photonic yield and the extended rate normalization. The photocatalyst loading relationship to irradiance (Ch. 2 section 2.5.1.1) may be coming across in different ways depending on the result term.

The three factor DoE was also analyzed considering multiple product summed results. The Pareto charts of all carbon products analyzed in terms of unitary product formation, all the products for the photonic yield performance, and all products in terms of the extended normalization in the three factor design are given in Figure 5.4. It can be seen, that the length of the experiment is significant in all cases. The interaction of the catalyst loading and irradiance is a significant effect for the unitary product formation and extended normalization results. The interaction of irradiance and reaction length and irradiance alone are significant factors to the photonic yield results (Figure 5.4, middle). Then the extended normalization has the greatest number of significant factors including irradiance and photocatalyst loading (Figure 5.4, bottom center). This is interesting as the photocatalyst loading had not played a significant role in the $CH_4$ unitary product formation results case, and is now seen to have an interaction influence.

The main effects again show decreasing results for increasing catalyst loading, irradiance and reaction time (Figure 5.5) for all combined product results. The incorporation of more of the factors into the units appears to highlight this behavior, in fact the extended normalization highlights this the most with all factors being significant (Figure 5.4), and shown at a large slope in the main effects plot (Figure 5.5) as the additional catalyst loading, provided irradiance, and reaction time do not lead to proportional gains in the extended normalization results. The increased total carbon products, representing $CO_2$, corresponds to low loading and decreased time as shown in the main effects plot (Figure 5.5, top). The influence of irradiance is clearly minimal from the main effects plots explaining the low position in the Pareto chart (Figure 5.5, top).

The irradiance is showing minimal impact, even though it is the source of photons to power the reaction. This ends up being one of the more striking main effects plots.

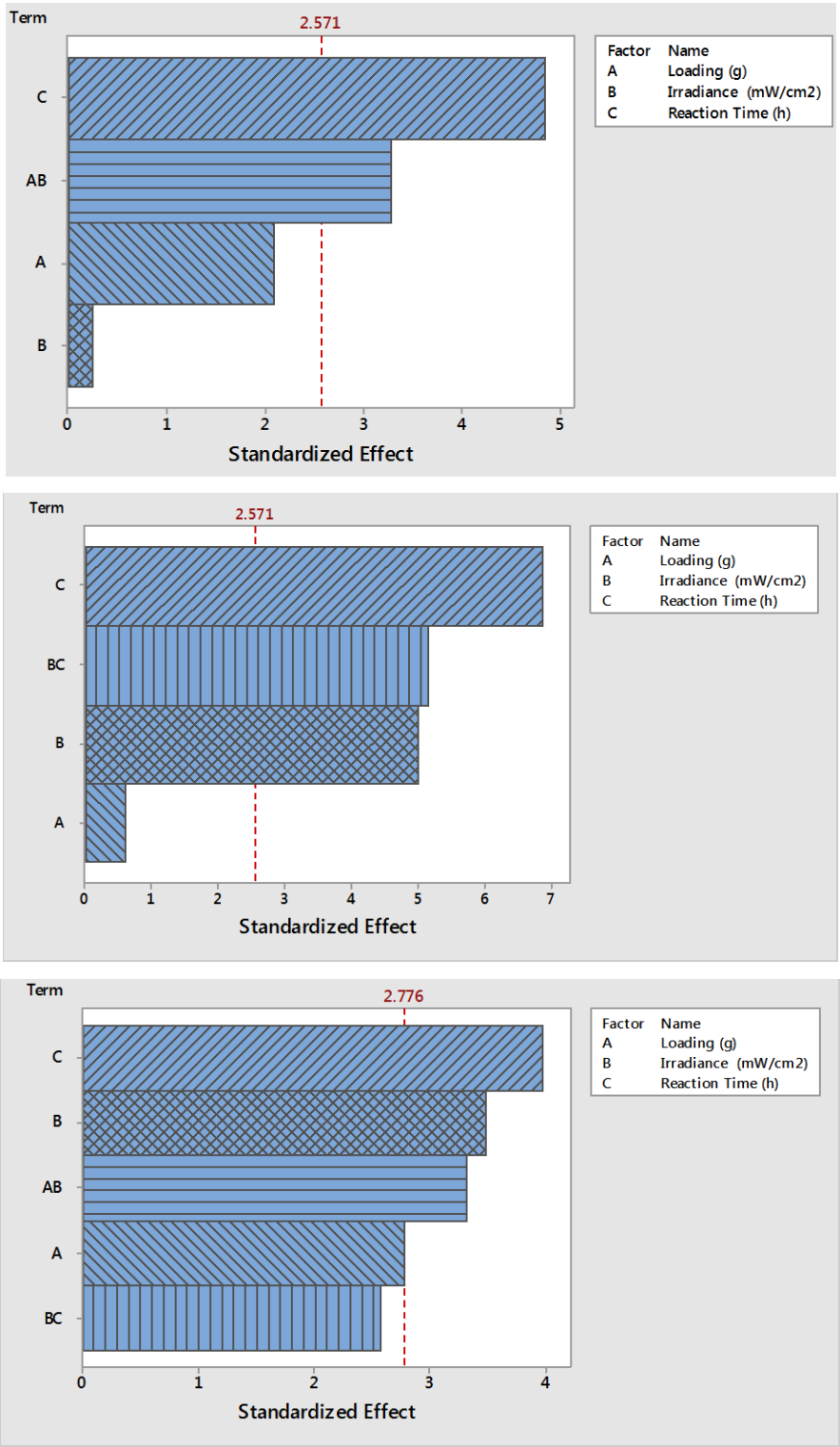


Figure 5.4 Pareto chart (top) of the standardized effects of the unitary product formation (µmole/gh) response of $CO_2$ as calculated from summing contributions of carbon products for the three variable design of experiments, $\alpha = 0.05$. Pareto chart of the standardized effects of the photonic yield calculated for all detected products from the three factor design of experiments (middle). Pareto chart of the extended normalization results from summing all products from the three factor design of experiments (bottom).

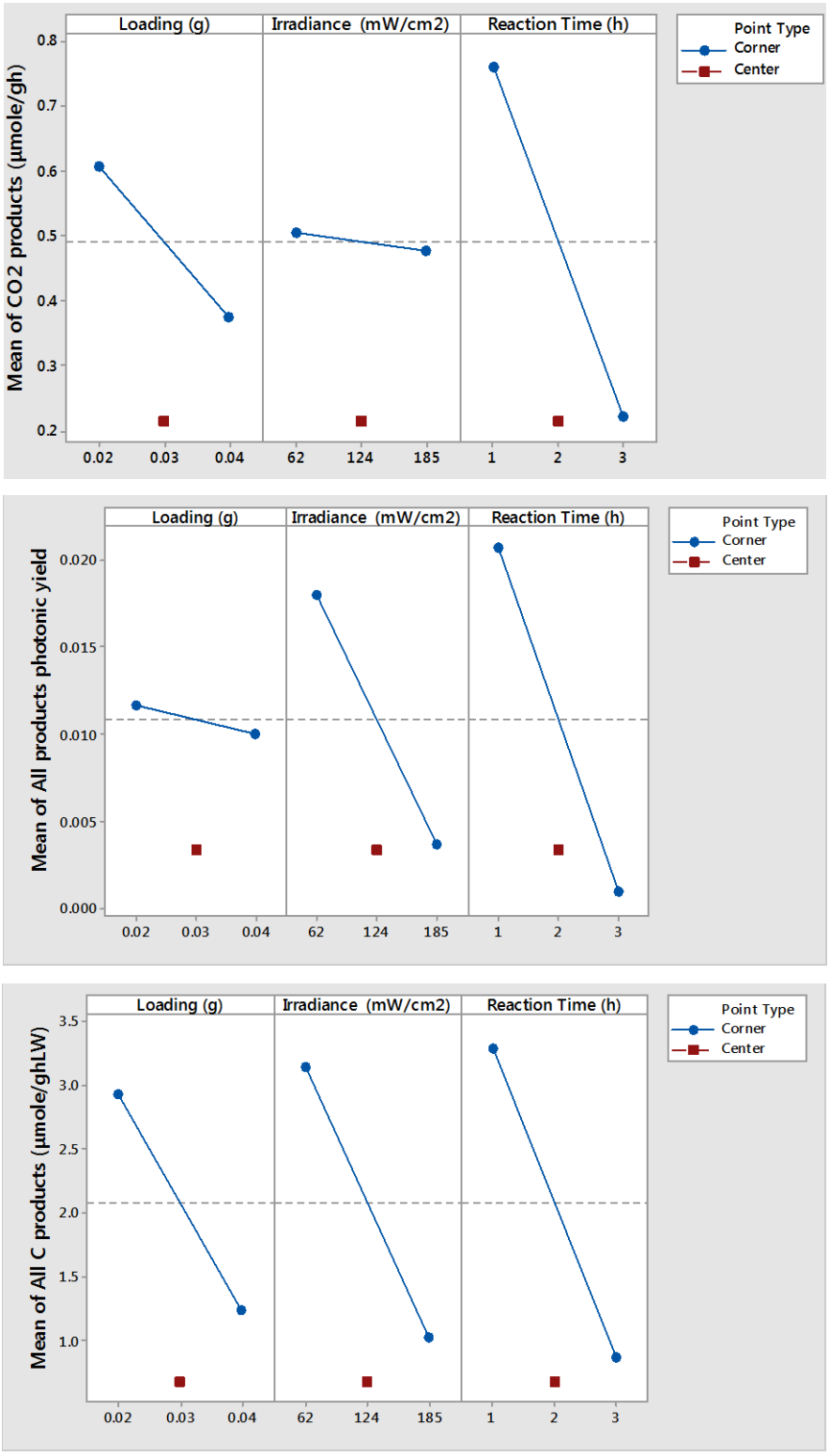


Figure 5.5 Main effects plot for combined products in terms of the unitary product formation (µmole/gh) response of $CO_2$ as calculated from summing carbon product contributions for the three variable design of experiments (top). Main effects plot of the photonic yield calculated for all detected products from the three factor design of experiments (middle). Main effects plot of the extended normalization results from summing all products from the three factor design of experiments (bottom).

The interaction effects plots for the summed products three factor DoE are shown in Figure 5.6. It can be observed that the interactions shown are diverse with the unitary

product formation and extended normalization both having significant interactions of loading and irradiance, but with different trends. The interaction of two variables is shown by the relative angles of the loading and irradiance, and irradiance and reaction time interaction lines for the various results for the carbon or all products (Figure 5.6, bottom). Because there were two interactions included in the DoE model for the extended normalization specific rate carbon products this interaction plot has two graphs (Figure 5.6, bottom). However, the only statistically significant one is the interaction of the photocatalyst loading and the irradiance.

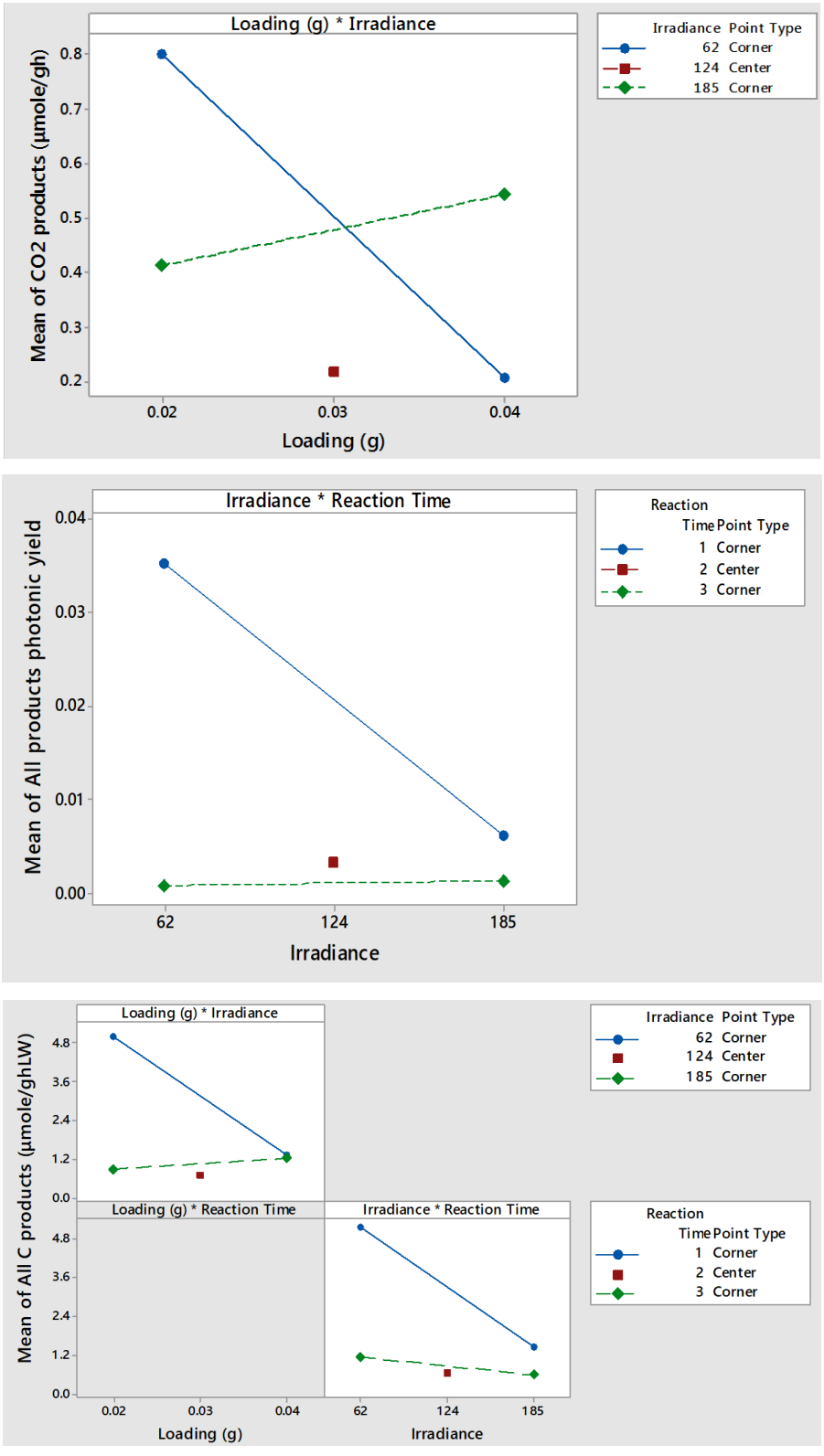


Figure 5.6 Interaction plot (top) for the unitary product formation (µmole/gh) response of $CO_2$ as calculated from summing carbon product contributions for the three variable design of experiments. Interaction plot (middle) of the photonic yield calculated for all detected products from the three factor design of experiments. Interaction plots (bottom) from the extended normalization response calculated from summing all products from the three factor design of experiments.

The three factor DoE has shown increasing significance of parameters with increasing normalization or results sophistication. And the extended normalization appears to nicely bridge the dual term challenge with the $CH_4$ results, however, it behaves more uniquely when a sum of products is analyzed.

## 5.3 Design of experiments investigating Au $TiO_2$ product formation as influenced by light intensity and length of experiment; two factor design of experiments

Here the influence of the factors on the response of $CH_4$ and C products results are assessed. The $CH_4$ unitary product formation results and experimental conditions of the two factor DoE are given in Table 5.4. Again the results were analyzed with linear models, which may be inappropriate in this wide of an irradiance range (Ch. 2, section 2.5.2). This can be seen in the lack of significant factors.

Table 5.4 The experimental layout of the design of experiments for the extended two variable investigation with µmole/gh responses.

| *Standard Order* | *Run Order* | *Light Intensity (irradiance, $mW/cm^2$)* | *Length of Experiment (hours)* | *$CH_4$ µmole/gh* |
|---|---|---|---|---|
| *1* | 4 | 6 | 1 | 0.0044 |
| *2* | 3 | 241 | 1 | 0.3054 |
| *3* | 1 | 6 | 3 | 0.0236 |
| *4* | 2 | 241 | 3 | 0.0914 |
| *midpoint* | | 124 | 2 | 0.0331 |
| *midpoint* | | 124 | 2 | 0.0951 |
| *midpoint* | | 124 | 2 | 0.0088 |

The $CH_4$ unitary product formation, photonic yield, and extended normalization Pareto charts are given in Figure 5.7. The $CH_4$ µmole/gh results do not have a statistically significant influence from reaction length or irradiance (Figure 5.7, top). Before, in the three factor DoE, time and then loading was shown to have the largest impact, followed by an interaction of irradiance and time. Removing a variable and extending the range of light intensity has made these unitary product formation results unable to produce a statistically significant model. Interestingly, the ppm results, or non-normalized results,

were influenced by the interaction of intensity and reaction time. This could be due to the nonlinear behavior that is anticipated in Chapter 2, section 2.7 from experimental mechanisms. For the large irradiance, there is an expected shift in photonic yield response (Figure 5.7, middle) as this is additional photons or energy input in to the process. As shown in the Pareto chart (Figure 5.7, middle and bottom), the $CH_4$ the photonic yield and extended normalization of the rate give only the interaction of the reaction time and the irradiance as a statistically significant parameter.

It is important to note that the range taken for the extended DoE was an intensity of 6 $mW/cm^2$ to 300 $mW/cm^2$ as compared to the previous range of 60 to 185 $mW/cm^2$. The result is does not obviously follow the relationship predicted [96]. With the wide range, the impact of intensity should be obvious. It could be that the linear model fit is unsuited this irradiance range.

The significant interaction effects of the $CH_4$ photonic yield and extended normalization are plotted in Figure 5.8. The highest results in both cases are for the one hour and low irradiance condition. Normalizing for photon or power shifts the plots, with the photonic yield (Figure 5.8, top) favoring a longer reaction time, whereas for the extended normalization (Figure 5.8, bottom) there is a larger ‘penalty’ for the higher irradiance.

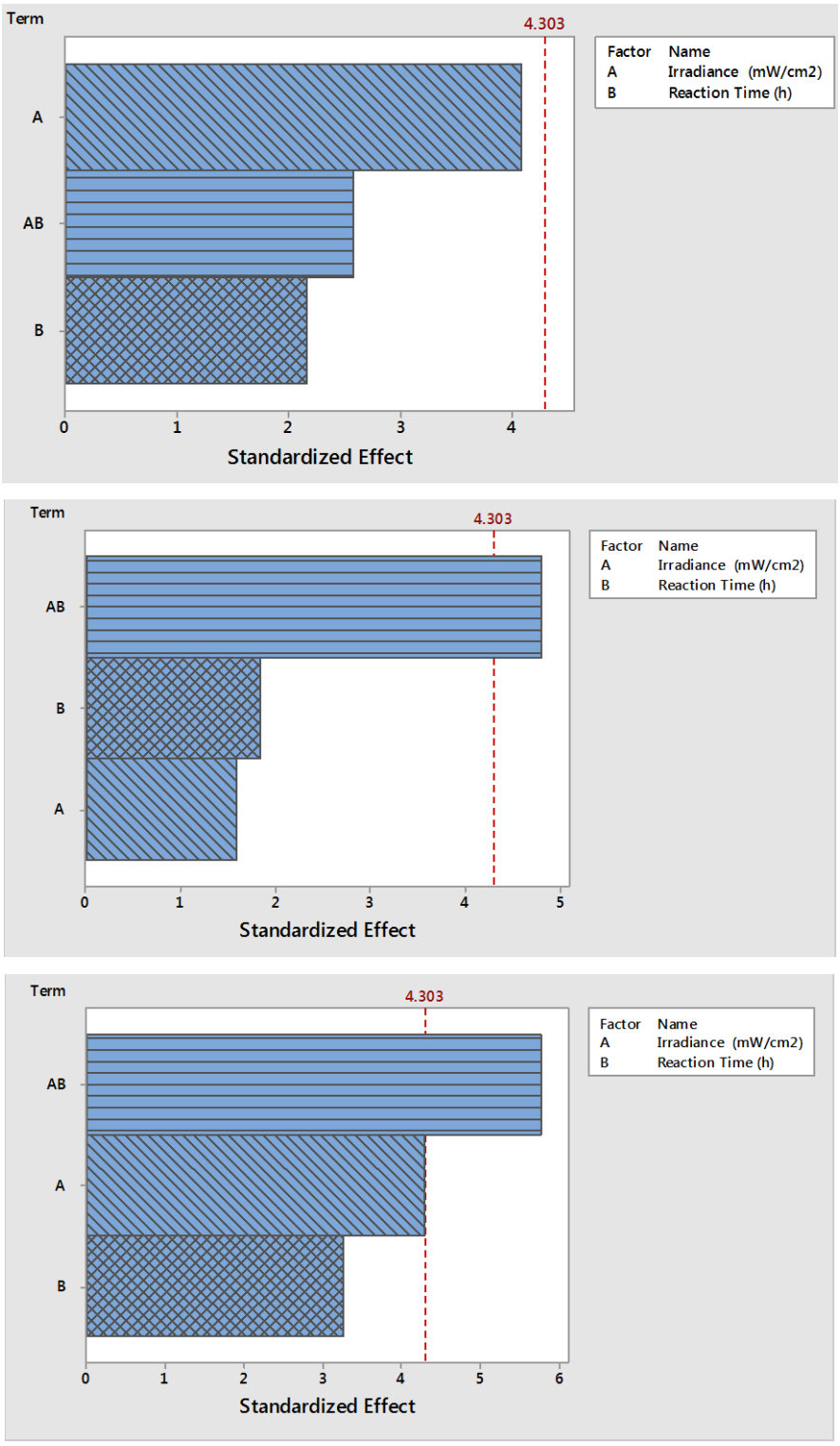


Figure 5.7 Pareto chart of the standardized effects from the analysis of $CH_4$ results in terms of unitary product formation (µmole/gh) for the two variable design of experiments, $\alpha = 0.05$ (top). Pareto chart of the standardized effects of the $CH_4$ photonic yield response from the two factor design of experiments (middle). Pareto chart showing the $CH_4$ extended normalization response for the two factor design of experiments (bottom).

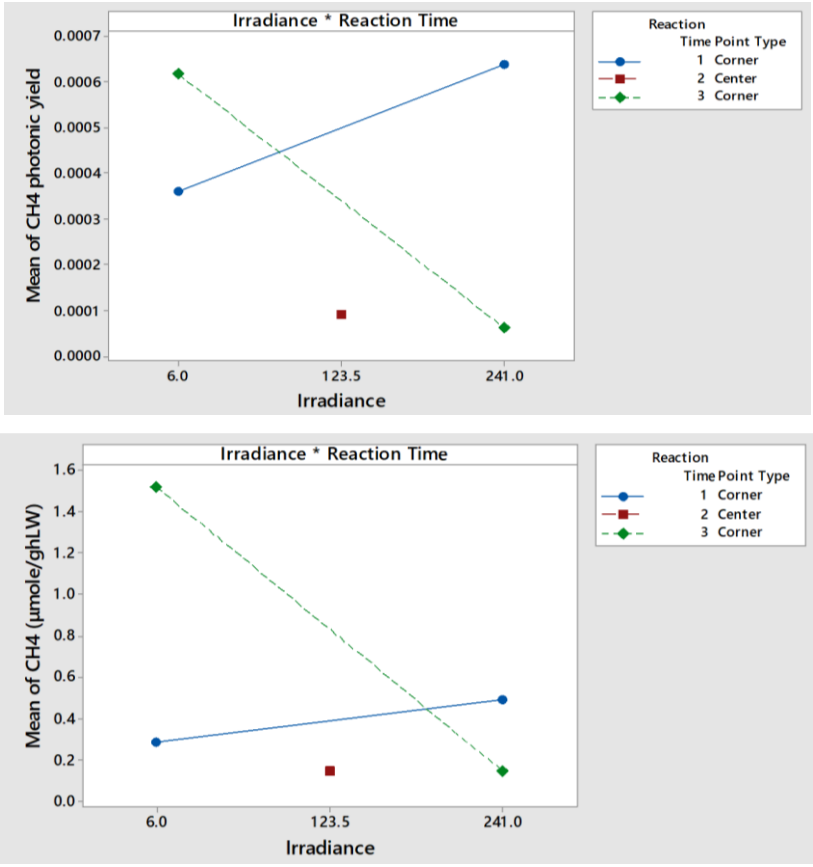


Figure 5.8 Interaction plot of the $CH_4$ photonic yield response from the two factor design of experiments (top). Interaction effects from the $CH_4$ extended normalization response for the two factor design of experiments (bottom).

When investigating the reaction length and irradiance, particularly with a wider irradiance range, the $CH_4$ photonic yield response shows that the statistically significant factor is the interaction of reaction time and irradiance Figure 5.7, middle. This differs from the three factor photonic yield results in that the independent reaction length and irradiance had been significant within the more limited irradiance range. The Pareto chart, Figure 5.9 (top, bottom), shows no statistically significant factors for both the unitary product formation and extended normalization results for the sum of carbon products. The photonic yield of all products (Figure 5.9, middle) shows the interaction of irradiance with reaction time, along with the irradiance, and reaction time, are all significant factors.

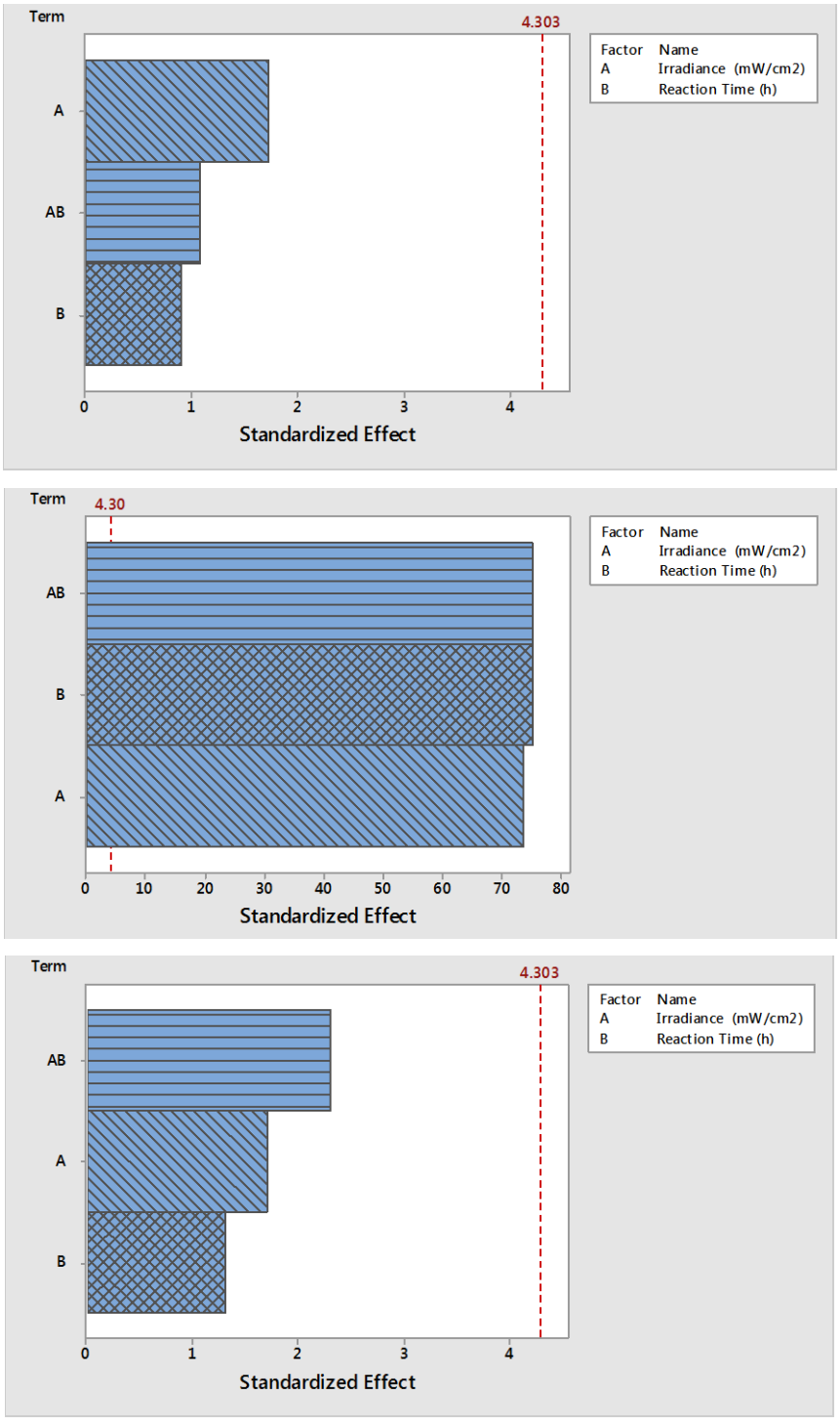


Figure 5.9 Pareto Chart of the standardized effects of the unitary product formation results (µmol/gh) for the carbon product results interpretation of the two variable design of experiments (top). Pareto chart of the standardized effects of the photonic yield as calculated for all detected products from the two factor design of experiments (middle). Pareto chart of the standardized effects of the carbon product extended normalization response from the two factor design of experiments (bottom).

The main effects (Figure 5.10, top) do not resemble the previous three factor response for photonic yield results of increasing factors resulting in decreases in the

photonic yield. Instead, the increased irradiance increases photonic yield. The increase in the reaction time, however, decreases photonic yield. Here the expected relationship with irradiance is observed.

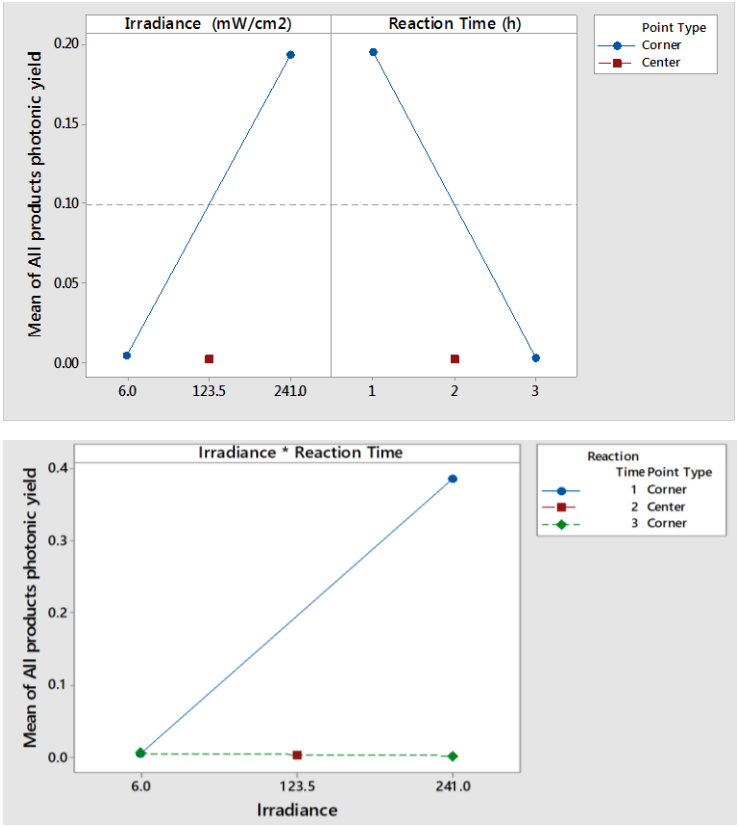


Figure 5.10 Main effects plot for the photonic yield as calculated for all detected products from the two factor design of experiments (top). Interaction plot of the photonic yield as calculated for all detected products from the two factor design of experiments (bottom).

The interaction response plot for the two factor DoE investigating photonic yield for all carbon containing products is also contained in Figure 5.10 (bottom). The interaction plot shows that the low irradiance does not vary the response of the photonic yield as the reaction time is increased. And then the high irradiance appears to significantly decreased photonic yield at the three hour reaction time.

Comparing the two factor DoE to the three factor results, the $CH_4$ photonic yield and extended normalization all show the interaction of irradiance and reaction time as significant in relatively similar patterns. Except for the two factor DoE where the one hour results are higher than typical. It also appears that in the photonic yield all products interaction effects plot that the extended irradiance range reverses the one hour preference for lower radiation and 241 $mW/cm^2$ becomes the high result.

## 5.4 Observations from the design of experiment

The use of the DoE enables the systematic understanding of the importance of experimental factor effects, any variable interactions, and comparisons of results terms within $CO_2$ photoreduction. Here key findings of what conditions give the highest results overall, of interaction implications, and of normalization considerations for the $AuTiO_2$ DoE results are discussed.

### *5.4.1 Design of experiments and the conditions of the maximum results*

The maximum results for the three factor DoE when observing all products (both $CH_4$ and summed products) were found under the conditions of 0.02 g loading, 62 mW/cm$^2$ irradiance, and one hour reaction time. These maximum results were 0.6307 $CH_4$ unitary product formation (µmol/gh), 0.0033 for $CH_4$ photonic yield, and 3.925 $CH_4$ extended normalization. The maximum results found for both DoE experimental sets and all results terms are given in Table 5.5. The maximum dual term results (unitary product formation and photonic yield) for the two factor DoE were found under the different reaction conditions of 0.03 g photocatalyst loading, and one hour reaction time, however the unitary product formation results favored 241 mW/cm$^2$ irradiance, and the photonic yield favored 6 mW/cm$^2$ irradiance. When it comes to the $CH_4$ results of the extended normalization of the 2 factor DoE the maximum result aligns with the maximum results conditions of the photonic yield. However, when comparing the summed product terms of the two factor DoE none of the results terms conditions align. This is a unique case where the extended normalization does not align with either dual term.

Table 5.5 Maximum results for the three results terms for the three and two factor DoE and the corresponding reaction conditions.

| *DoE* | *Product* | *Catalyst loading (g)* | *Irradiance (mW/cm$^2$)* | *Reaction Length (hours)* | *Maximum result* |
|---|---|---|---|---|---|
| Three Factor | $CH_4$ (µmol/gh) | 0.02 | 62 | 1 | 0.6307 |
| | $CH_4$ photonic yield | 0.02 | 62 | 1 | 0.0033 |
| | $CH_4$ extended normalization (µmol/ghLW) | 0.02 | 62 | 1 | 3.925 |
| | C products (µmol/gh) | 0.02 | 62 | 1 | 1.2549 |

| *DoE* | *Product* | *Catalyst loading (g)* | *Irradiance ($mW/cm^2$)* | *Reaction Length (hours)* | *Maximum result* |
|---|---|---|---|---|---|
| | Photonic yield (all detected products) | 0.02 | 62 | 1 | 0.0410 |
| | C products extended normalization (µmol/ghLW) | 0.02 | 62 | 1 | 7.809 |
| Two Factor | $CH_4$ (µmol/gh) | 0.03 | 241 | 1 | 0.3054 |
| | $CH_4$ photonic yield | 0.03 | 6 | 3 | 0.00064 |
| | $CH_4$ extended normalization (µmol/ghLW) | 0.03 | 6 | 3 | 1.518 |
| | C products (µmol/gh) | 0.03 | 241 | 1 | 0.3054 |
| | Photonic yield (all detected products) | 0.03 | 6 | 1 | 0.38557 |
| | C products extended normalization (µmol/ghLW) | 0.03 | 6 | 3 | 1.518 |

Interestingly for the DoE, the reaction time, which was a function of being a batch reaction, was the overwhelmingly most significant factor in all the DoE analysis. Then the irradiance was the next most significant, which is appropriate as it is the energy source. Then would come catalyst loading. It is also crucial to see that the overall trend for the three factor DoE was that for increasing units of time, photocatalyst and irradiance, there was not a proportional increase in product formation. It is in the wider irradiance range of the two factor DoE that the irradiance or reaction time is increasing the extended rate normalization, but not in a directly statistically significant way, instead it is in the interaction of these effects when observing the $CH_4$ results behavior.

While the DoE analysis does show variation in how the results interact with the data, there is a great amount of overlap and congruence. Further DoE work with a range of experiments at a lower irradiance range, photocatalyst loading, and reaction time would be interesting to investigate if this unity of maximum results continues to align for the dual terms. These unitary product formation results can be compared to the parameter effects that are expected as discussed in Chapter 2, section 2.8. For example, catalyst loading behavior appears to be irradiance dependent. And the low catalyst loading behavior relative to irradiance appears to be a saturated response, possibly where photoreforming was occurring. The high photocatalyst loading behavior relative to irradiance, showed an unsaturated response with increased response to increasing irradiance.

### *5.4.2 Design of experiments results considering interaction effects*

The most common statistically significant interaction was of the irradiance and reaction time, being significant for the $CH_4$ products in all results term cases and in both the three and two factor DoEs, except for the two factor DoE case of the unitary product formation result in which no factor was significant. The reaction time and irradiance interaction was also significant for the photonic yield results for the carbon-based products in both the two and three factor DoEs. Then the next significant interaction was catalyst loading with irradiance. This interaction was significant in the case of the unitary product formation and extended normalization for the carbon-based products from the three factor DoE.

The interaction effects can be explained through the relationships of the factors. For example, with the irradiance and reaction time, as irradiance is a measure of all incoming photons and this is occurring over the time of the reaction, perhaps what is observed by the DoE is that interaction of photon flux and reaction progression. It appears that there is a stabilizing effect where the rate of product formation levels out by three hours particularly observed for the $CH_4$ three factor DoE main effects interaction plots. As the other example, there is the irradiance and catalyst loading, where the photocatalyst availability to incident light is a key interaction that could be generating the observed interaction effects. The two factor DoE is also an opportunity to observe the extreme behavior of the irradiance. Interestingly, some of the terms to quantify the results were ineffective at these wider ranges of irradiance, including the $CH_4$ and C products specific rate (μmole/gh). In the $CH_4$ products case, the photonic yield and extended normalization had a statistically significant response, for the interaction of irradiance and reaction time.

Then for all summed products photonic yield was the only term to ‘make sense of’ or produce significant factors.

### *5.4.3 Design of experiments results considering normalization and results terms*

It is also important to observe how the normalization of the parameters affects interpretation. The DoE is such an interesting tool to utilize in a benchmarking exercise because it allows for a wider range of terms to be easily visualized and compared. So, when unitary product formation is used the only term not being normalized for in the results analysis is the irradiance. This can then be compared to the extended normalization in which all varied parameters are being normalized in the analysis. So, there is a shift from just observing a growth in the product relative to catalyst loading and reaction time, to assessing if irradiance inputs produce gains beyond the initial product output found for the lowest input conditions. It is a way of interrogating the use of energy resources when normalization is utilized. In the experimental work conducted for the three factor DoE the additional catalyst loading, irradiance, and time did not increase upon the low level conditions performance in most cases. However, with the wider irradiance range of the two factor DoE the high irradiance condition leads to a higher unitary product formation, and the lower irradiance leads to a higher photonic yield and extended normalization result.

How these shifts in data processing affected the analysis is interesting. One case is the significance of photocatalyst loading. The photocatalytic loading was a statistically significant factor in the $CH_4$ unitary product formation response for the three factor DoE and for the carbon products in the extended normalization of rate for the three factor DoE (Figure 5.1 (top) and Figure 5.4 (bottom) respectively). Then the photocatalytic loading was statistically significant for the interaction with irradiance in the case of the carbon products unitary product formation and the carbon products extended normalization response of the three variable design of experiments (Figure 5.4). This influence appears to be lost when further normalization is introduced to the $CH_4$ measure. This influence appears to be more observable in terms of the interaction with irradiance in the case of the sum of all carbon products extended normalization. For the most part increasing normalization preserves or highlights trends and is only confounded in the summed products two factor DoE case.

The extended normalization results relative to the dual terms challenge gives an interesting third option. In the case of $CH_4$ results, the three factor DoE based on the extended normalization gave the similar main effects and interaction as the previous two,

as in general they were alike, with the same significant factors as the photonic yield. This appears to be a good compromise between the terms. For the two factor DoE the $CH_4$ extended normalization the wider irradiance trends relative to the $CH_4$ photonic yield response both give the statistically significant factor of the interaction of irradiance and reaction time. This did not hold with summed product analysis where for the three factor DoE the interaction of photocatalyst loading and irradiance was shared by unitary product formation and extended normalization. Thus the extended rate normalization appears to be an appropriate 'straddling' of the dual term divide.

While it is challenging to unpack the density of DoE information provided, it is clear that the factors can be ranked in terms of significance; reaction time, irradiance, then photocatalytic loading. It is also clear that interaction effects are present between irradiation and reaction time and between irradiation and photocatalyst loading. And lastly, while the extended normalization may uniquely quantify the $CO_2$ photoreduction process varying whether catalytic or photonic trends are being shown, in smaller irradiance ranges it holds close to dual term trends.

# CHAPTER 6 – TESTING REGIMES AND SINGLE VARIABLE VARIANCE EXPERIMENTS WITH MIRKAT SAMPLES

In this chapter results from the commercial sample Mirkat 211 are considered. The regime framework is proposed (section 6.1) and used for testing. Inspiration for the regime approach to $CO_2$ photoreduction has come from photovoltaics (section 6.1.1) and catalysis (section 6.1.2). An explanation of the regimes is given in section 6.1.3. Therefore, single variable variance experiments are conducted to identify testing regime and reaction rate information for Mirkat 211. Experimental methodology and material is reviewed in section 6.2. The single variable experiments include variation in catalyst loading (section 6.3), length of experiment (section 6.4), and light intensity (section 6.5). For further results terms analysis beyond unitary product formation (section 6.6) the Mirkat regime data is then converted to photonic yield (section 6.6.1) and extended rate normalization (section 6.6.2). The chapter ends with a discussion of benchmarking Mirkat results and the conditions of maximum results, in section 6.7.

## 6.1 Testing Regimes Proposed

As shown in section 3.1.1 and chapter 4, the context of reactions are not generally given in the current literature, and focus is not placed on comparing rates, or investigating operational parameters effect on rates of conversion. Reporting that enable these endeavors are necessary to benchmarking across multiple labs and reactor setups. To facilitate the consideration of experimental work that benchmarking requires, here inspiration from photovoltaics and catalysis are discussed. These considerations were fundamental to structuring the testing regime framework addressing operational parameters and metrics, that is proposed in this section.

### *6.1.1 Considering photovoltaics and light*

In photovoltaics, separate tests are run to either determine the efficiency of the device or identify the quantum efficiency of the photovoltaic material alone [262]. This acknowledges a need for multiple experimental strategies to compare performance.

Quantum efficiency (QE) is a figure of merit in photovoltaics. In photovoltaics, quantum efficiency is measured in two different ways. As they are conceptually similar they are sometimes both called quantum efficiency; however, in photovoltaic practice spectral response (Equation 6.1) and quantum efficiency (Equation 3.37) are distinct.

$$Spectral\ Response = \frac{current/_{charge\ of\ one\ electron}}{total\ power\ of\ photons/_{energy\ of\ one\ photon}} = \frac{q\lambda}{hc} QE$$

Equation 6.1

Where q is the radiant energy at the wavelength (or the total from summing various wavelengths), h is the Planck constant, λ is the wavelength (or range of wavelengths), and c is the speed of radiation in a vacuum.

$$Quantum\ Efficiency = \frac{electrons/_{second}}{photons/_{second}}$$

Equation 6.2

Firstly, spectral response is measured in the lab with varying single wavelength of light provided (roughly 0.02 to 1.2 μm), with quantum efficiency being calculated from the spectral response, as shown in Equation 6.1. This can also be discussed as Incident Photon to Charge Carrier Efficiency (IPCE) of the device. This suggests that in photocatalysis the quantum efficiency measurements would benefit from being tested in the linear range of flux of irradiation (as previously explained in Chapter 2, section 2.5.2), and should be reported relative to the wavelengths of irradiation used as this would ensure maximum photon utilization and appropriate energy measures. This forms the basis for establishing the catalyst light performance regime in Table 6.1.

Quantum efficiency measurements are distinctly separated from the efficiency of the device as a whole unit. To enable measurement of the entire device, energy output relative to the input energy from the sun (to enable comparability), different tests are run. In photovoltaics, there are strict standards keeping the testing spectrum, intensity and temperature the same across different lab tests, namely AM 1.5, 298.15 K (25°C). The input power for the efficiency calculation is 1 kW/m$^2$ or 100 mW/cm$^2$. Applying a similar concept to photocatalysis would result in tests performed in the standardized conditions reactor performance regime in photocatalysis with an asterisk (*) indicating that temperature and pressure would be standardized at 298.15 K and 1 atmosphere to minimize energy input.

### *6.1.2 Considering catalysis and transport phenomena*

As discussed in section 2.5.3, there are a variety of reactor options affecting flow and mass transport. These choices impact the photocatalytic performance and are highlighted in the testing regimes to enable testing improvements. Here, reactor performance in catalysis is discussed in more detail to explain why consideration of mass transport and $CO_2$ photoreduction results are needed.

In catalysis, the Damköler number is used in reactor design to characterize reactor performance. This dimensionless number is derived to ensure that the mass transport in the reactor is more than sufficient to provide reactants to the catalyst and then remove products (Equation 6.3).

$$Damköler\ number = \frac{reaction\ rate}{mass\ transport\ rate} = \frac{reaction\ rate\ (photocatalyst)}{mass\ transport\ rate\ (reactor)} \quad \text{Equation 6.3}$$

When the Damköler number is significantly lower than one, the reaction is limited by the performance of the catalyst and not the mass transport of the reactor.

Mass transport is influenced by many factors including properties of the gases, such as diffusivities or viscosity of liquids, but it can be managed through reactor design. This has significant implications for photocatalysis for the reduction of $CO_2$. In the case of photocatalysis, there are two inputs that limit the catalytic reaction rate, namely consideration of mass transport and reactants access to the catalysts, and the light transport or access to the catalyst. Clearly, the reaction rate performance of the catalytic material, required to determine performance quantified by catalyst site performance such as turn over frequency, needs to be measured without mass or light transport limiting the materials performance. Testing conducted considering sufficient mass transport and an excess supply of light for the catalyst used would give the catalyst kinetic performance, as stated below in Table 6.1.

### *6.1.3 Testing Regimes*

Table 6.1 summarizes novel testing regimes based on the identification of the rate determining process (either mass transport or photocatalytic reaction), their dependence on experimental parameters, and the intent of the experimental work. The proposed testing regimes also suggest metrics for each regime. For these testing regimes it is assumed that tests are run at relatively low pressures near 1 bar, and room temperature. The six regimes presented in Table 6.1 vary depending on the light provided, the amount

of catalyst used, and the mass transport within the reactor. To understand the proposed regimes it can be useful to review the parameters affecting $CO_2$ photoreduction from Chapter 2, section 2.5.

Table 6.1 Proposed testing regimes based on mass transport and light conditions, and light interactions with photocatalytic loading, with accompanying results terms recommended for analysis.

| *Testing Regimes* | *Mass transport* | *Light Intensity* | *Catalyst Loading* | *Measurement with IUPAC Glossary Term [89]* |
|---|---|---|---|---|
| *Efficiency of Light Harvesting Regime* | Greater than reaction rate | Fixed value in the range of intensities where reaction rate is proportional to radiance flux | Linear range (where varying amount of catalyst used linearly changes reaction rate) | Quantum yield, quantum efficiency, photonic yield or photonic efficiency, and TON or TOF |
| *Catalyst Loading Optimized Performance Regime* | Greater than reaction rate | Varied ranges | Fixed unstandardized light source with mass of catalyst used optimized to light provided | Unitary product formation, photocatalytic efficiency, effective radiation catalytic activity, or radiation-chemical yield |
| *Catalyst Kinetic Performance Regime* | Greater than reaction rate | Fixed in the range where reaction rate proportional to the square root of radiance flux | Saturated (where varying amount of catalyst used does not change reaction rate) | Reaction rate (catalyst) |
| *Mass transport Regime* | Less than reaction rate | Optimized where surface reaction rate is proportional to the square root of radiance flux | Saturated (where varying amount of catalyst used does not change conversion) | Mass transport rate (reactor) and Damköler number |
| *Standardized Conditions Reactor Performance* | Known (can use information from Mass transport Characterization or calculated value) | Solar Standard 1.5 AM* | Mass of catalyst used optimized | Device performance that is comparable to other devices measuring efficiency |
| *Model Validation Conditions* | Chosen ranges (limits to validate models) | Chosen ranges | Chosen ranges | Device performance as a function of light provided measuring efficiency |

The first three regimes (light harvesting, loading optimized, and catalyst kinetic) consider different experimental parameters affecting surface photocatalytic $CO_2$ photoreduction; the fourth considers mass transport; the fifth (reactor performance) represents comparison between results from different experimental testing setups while the sixth regime (model validation) represents testing conditions in which a device response to modeling is sought and it is not necessary to investigate separately a single parameter of the whole process.

The regimes or conditions of testing determine what metric should be used based on what inputs are limiting the photocatalytic process and what the goal of experimental work is.

As presented in Table 6.1 the regimes can be explained further:

- Efficiency of Light harvesting regime isolates the catalyst performance through measurement of quantum efficiency and is conducted when mass transport on the reactor does not limit the reaction rate, the light intensity varies proportionally to rate, and the light provided is less than required for all superficial sites' photoactivation. In this way, all photons are available for surface reaction. These measurements should be taken at equilibrium: in this way reactant adsorption on the surface and light absorption have already reached steady-state. As this is useful for quantum yield determination, it won't provide a faithful determination of reaction kinetic dependence on light. Also, catalyst loading should not affect the reaction rate.
- Catalyst loading optimized performance testing regime identifies the catalyst performance through product terms and is conducted when the mass of the catalyst used for testing is optimized to the light provided in the reactor, the light intensity is varied, and the mass transport is sufficiently great so as not to control the reaction rate. These measurements should be taken at equilibrium.
- Catalyst kinetic performance testing regime provides information on the catalyst performance through the reaction rate and is conducted when the mass transport within the reactor is adequate to allow the reaction rate to be catalytically controlled, the rate varies proportionally to the square root of light intensity, and the light provided is more than sufficient for the amount of catalyst used.
- Mass transport regime measures the reactor performance through assessing mass transport within the reactor and is conducted when the mass transport on the reactor limits the reaction rate, the rate is optimized with respect to irradiance

intensity, and the light provided is more than sufficient for the amount of catalyst used.

- Standardized reactor performance testing condition finds information on the device performance through overall efficiency and is conducted when the mass transport is unknown, the mass of catalyst is optimized, and the light provided is standardized to 1.5 air mass coefficient (AM), as used in photovoltaic standard measures [262]. Efficiency here is the useful energy delivered or bound over the energy supplied [89]. These measurements should be taken at equilibrium, when the conversion has plateaued, and possibly maintaining irradiance. This is an important way to benchmark reaction systems as devices.
- Model validation testing condition provides information on the device performance through the overall efficiency and is conducted when the mass transport and light provided are either specified or not quantified and ranges of irradiance are selected. These measurements should be taken at equilibrium. These experiments can be used for model verification.

A way to work though regimes and conditions would be to go through them one by one to assess the material and the reactor and develop models to then be verified experimentally, as described here. The assumption is that to start photoreduction experiments something about mass transport is known, whether it be derived from a model or experimentally found.

Firstly, catalysts would be compared by testing them in the regime for efficiency of light harvesting. Thereby, allowing the best performing material to be selected. Then the catalyst loading optimized performance experiments would give the best conditions of experimental testing for a given irradiation intensity, being a good regime to look at the dependence of the reaction rate on irradiance. Therefore, the mass of catalyst used is optimized relative to the light provided in the photoreactor [188] and this is essential if trying to calculate quantum efficiency. In this way light intensity then mass of photocatalyst is optimized.

Next experiments in the catalyst kinetic performance regime would be conducted to measure kinetics, ideally to explore the dependence of the reaction rate on reactant concentration. Next the mass transport regime or standard conditions reactor performance experiments can be conducted for benchmarking the overall process. And lastly, experiments in model validation conditions would be conducted to compare experimental results with various theoretical predictions.

The most significant aspect of the testing regimes and conditions is that they separate measurement of the photocatalytic material from reactor and experimental conditions through intentional regime choice. The only two regimes that measure the material alone are the catalyst kinetic performance and the efficiency of light harvesting. Catalyst loading optimized performance is optimized to the reactor. Then standardized conditions reactor performance and model validation conditions are clearly reactor modified performance.

Building upon testing regimes, a wider materials screening process would be useful. For example, intentionally testing within the efficiency of light harvesting regime would give metrics capable of assessing that either light absorption or charge carrier lifetimes have been increased. Catalyst kinetic performance regime would provide assessment of the hydrophilic behavior, which could be verified by Fourier transform infrared spectroscopy (FTIR). When these testing and results are used to identify material performance and compared to anticipated modification improvement it will be apparent if the modification was successful in its aim. An important component of this will be identifying where the material fits into the matrix given in Table 2.2.

The regimes proposed are general for use in a wider context within photocatalytic $CO_2$ reduction. For the context of this thesis engagement with approaching Mirkat experimental work initiates at the first two testing regimes and, due to batch reactions, an exploration of time. The terms investigated associated with the regimes are unitary product formation and photonic yield. The priority is to focus on methane results for the purpose of forming solar fuels.

### 6.2 Materials and Experimental Methodology for $CO_2$ photoreduction testing

Experiments varying single parameters (such as length of experiment, catalyst loading, and light intensity) were conducted with Mirkat 211 $TiO_2$ purchased from Euro Support Manufacturing. This material was chosen for its high specific surface area and anatase phase, and higher $CO_2$ reduction for the commercial samples (Ch. 4, section 4.3).

The procedures used were changed slightly from the procedure described in Chapter 4, section 4.1.3. In this case, catalyst loading was done with 1mL suspension. The other significant change to the previously reported methodology was the use of $CO_2$ bubbled in water for overnight flow and background readings instead of helium. These changes were implemented due to better adherence of the catalyst to the quartz plate surface and an improvement in the analytical procedure for products quantification. These modifications in experimental procedure were also in place at the time of the low light

intensity experiments that were conducted with the Mirkat and $AuTiO_2$ samples (results in the Appendix C).

### 6.3 Regime exploration by varying catalyst loading

Figure 6.1 shows the results from the experiments varying loading of the catalyst using loadings of 0.01, 0.02, 0.04 and 0.08 grams of Mirkat 211. For these experiments the light intensity used was 278 $mW/cm^2$ and length of the experiment was 4 hours. These settings were chosen for experiments based on prior expertise [230]. Figure 6.1 gives the specific rate, or unitary product formation response. A catalyst loading of 0.02 g shows a significant increase in $H_2$ formation, however this declines at higher loadings. As discussed previously in section 2.5.1.1, with catalyst loading the behavior expected is a leveling off of reaction rate with increased loading over a saturated level. The behavior is not observed for $H_2$ nor $CH_3OH$ where a drop in the unitary product formation is found above a catalyst loading of 0.02 g. The behavior of $CH_2$ and $C_2$ compounds is more similar to the expected behavior.

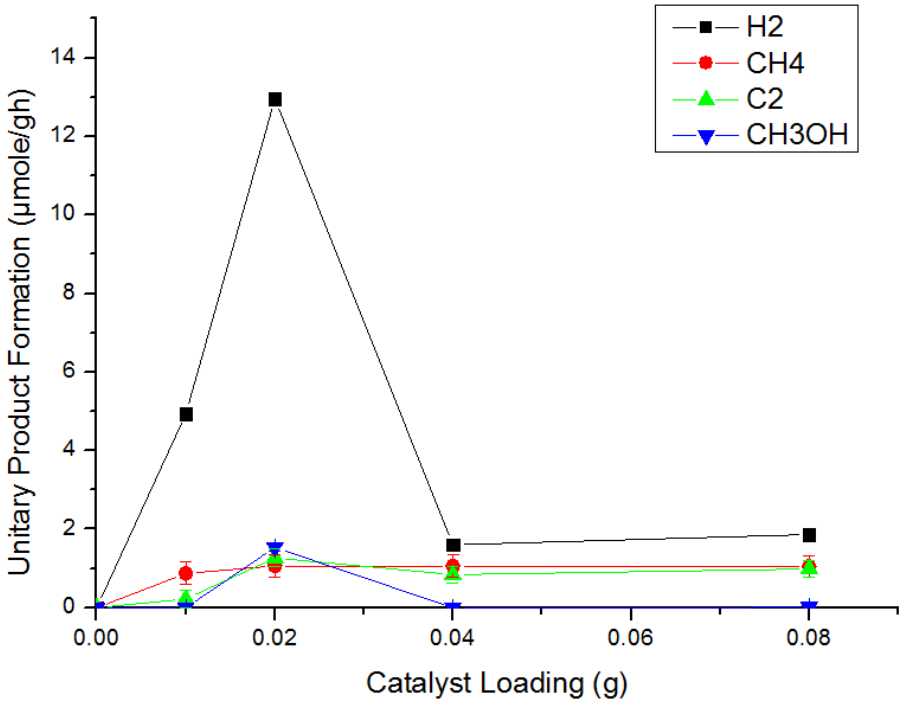


Figure 6.1 All products detected with varying catalyst loading between 0.01, 0.02, 0.04, and 0.08 g. Experiments were conducted at room temperature, for 4 hours with an incident light intensity of 278 $mW/cm^2$.

The plot in Figure 6.2 gives the results for $CH_4$ and $C_2$ compounds relative to catalyst loading. This has been shown along with the $CO_2$ utilized, calculated from summing the proportional contribution of the $CH_4$ and $C_2$ product formation results. The results show a relative increase of carbon based products between a loading of 0.01 g and

0.02 g and would suggest and optimum loading of 0.02 g. The expectation is for a saturated amount of catalyst loading to be reached where the production varying by loaded catalyst reaches a plateau which is observed in this case for $CH_4$ [96, 215].

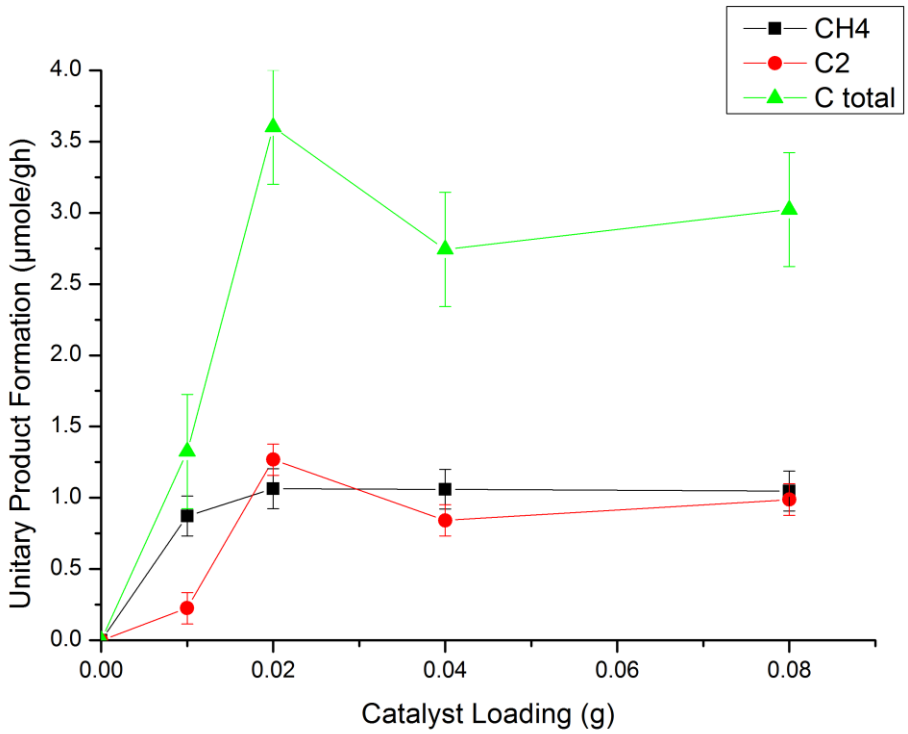


Figure 6.2 Results from varying catalyst loading between 0.01, 0.02, 0.04, and 0.08 g, showing $CH_4$ and $C_2$ products, along with the approximation of $CO_2$ utilized. $CO_2$ total was calculated by adding the moles of $CH_4$ to double the $C_2$ moles. Experiments were conducted at room temperature, for 4 hours with an incident light intensity of 278 mW/cm$^2$.

As shown in Figure 6.2 the $CH_4$ behavior nicely fits the expected parameter behavior. Figure 6.2 shows that the majority of the results are in the saturated range where varying the amount of catalyst does not vary the rate of reaction, as relating to the testing regimes (Table 6.1). What this means for the regimes of testing is that the 0.02 g of catalyst loading can be used for Mirkat as saturated, and it indicates that 0.01 g can be considered in the linear range (Table 6.1). However, when considering all the results collected experimentally for Mirkat $CH_4$ the highest unitary product formation was found for a sample loading of 0.04 g. Therefore, the sample loading was revisited with a model fit to the data.

The Langmuir Hinshelwood model is applied, as in the technical report [91] (Equation 13 a), reproduced here as equation 6.1:

$$R^{\text{in}} = \frac{A\,[\text{TiO}_2]}{(1 + B[\text{TiO}_2])} \qquad \text{Equation 6.1}$$

Where $R^{\text{in}}$ is the initial rate of substrate disappearance, and A and B are constants, and [$TiO_2$] is the concentration of $TiO_2$ in g/L. In this case, the model will be applied to the amount of $CH_4$ produced.

As shown below, in Figure 6.3, the experimental results fit the model even as the data points are within the plateau. When the model is applied the optimum photocatalyst loading mass ($m_{opt}$) is 0.04 g. More would need to be done to assess whether $m_{opt}$ is irradiance dependent, and it may be prudent to investigate the linear range of the performance more thoroughly.

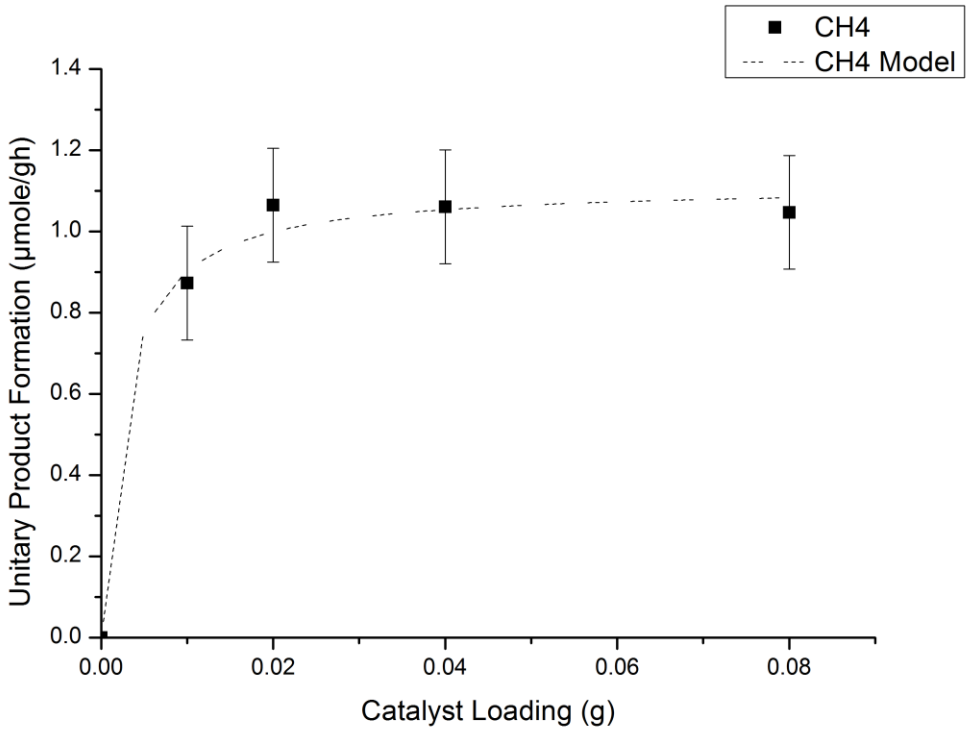


Figure 6.3 $CH_4$ products, varying catalyst loading with inclusion of Langmuir Hinshelwood model, shown by a dashed line. Experiments were conducted at room temperature, for 4 hours with an incident light intensity of 278 mW/cm$^2$. A = 490 µmole/g$^2$h, and B = 440 1/g, with the $R^2$ error being 0.0067.

The 0.04 g optimum mass, as shown in Figure 6.3, means that 0.04 g photocatalyst loading and above would then be considered saturated, and again 0.01 g would be in the linear range.

### 6.4 Varying length of experiment investigation reaction rate

In the length of the experiment investigation the experiments were varied from 1-8 hours. For these experiments the catalyst loading was always 0.04g and the light intensity was maintained at 278 mW/cm$^2$. Results can be seen in Figure 6.4 which shows the unitary product formation, or specific rate, measured for each experiment. The results show a significant increase in unitary product formation at 2 hours. This is similar to behavior others have observed [80].

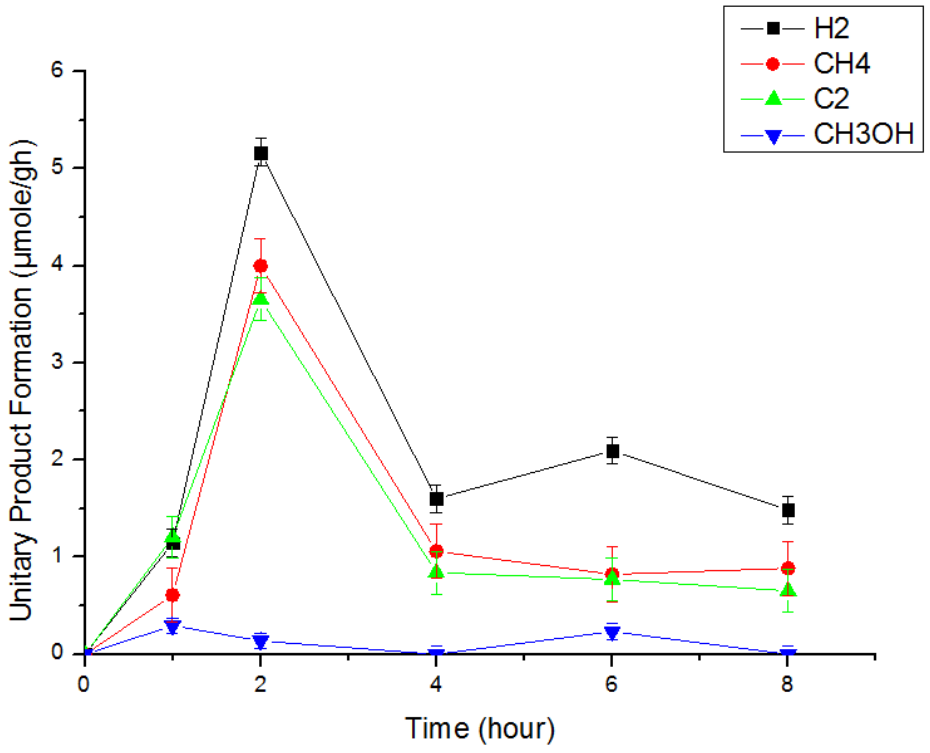


Figure 6.4 All product results as detected with the MS for Mirkat 211 at various experimental lengths of 1, 2, 4, 6 and 8 hours. Experiments were conducted at room temperature with a 0.04g catalyst loading and 278 mW/cm$^2$ incident irradiance.

The two hour experiment was conducted twice to verify product results and increased unitary product formation at that time. This trend suggests a threshold concentration from which hydrocarbons and electrons are then available to oxidation or photoreforming [263, 264], or a set of subsequent reactions (Section 2.4). This could indicate any number of reaction mechanisms. Otherwise a steady state behavior would have been observed where unitary production would have leveled off and remained steady. For the purposes of investigating variation in time for optimum rate response, two hours has the best methane unitary product formation result.

### 6.5 Regime investigation through varying light intensity

Two sets of experiment for varying only light intensity were conducted. Presented here are the three experiments that were conducted with a length of experiment of 2 hours and the catalyst loading was 0.04 g. To see the results from the other set of three experiments refer to appendix C. In the case presented here, light intensity ranged from 92.7-278 $mW/cm^2$ the results of the varied light intensity are shown in Figure 6.5 for all products detected. In Figure 6.5 the expected increase with increasing light intensity can be seen with the $CH_4$ and $C_2$ compounds, however the trend is not maintained as strongly with $H_2$ production.

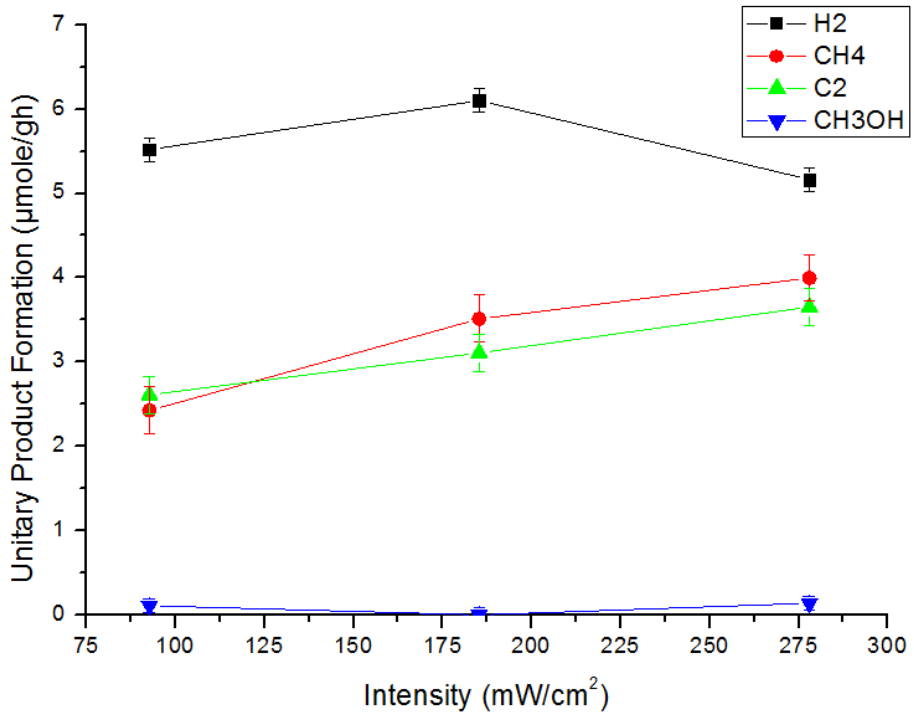


Figure 6.5 All MS detected products varying light intensity between 92.7, 185.3, and 278 $mW/cm^2$. Experiments were conducted at room temperature for 2 hours with a catalyst loading of 0.04 g.

The light intensity behavior is assessed for similarity to Herrman's figure, as discussed in Chapter 2, and thus the methane results are analyzed more closely [96]. Either the relationship is proportional to irradiance, or proportional to the square root of light irradiation (to the power of ½). The relationship is between the reaction rate and the light intensity, however in this case, unitary production is used as an appropriate proxy for reaction rate. For irradiance ranging from 92.7-278 $mW/cm^2$ the relationship found is

shown below in Figure 6.6 using a simple model of $R=A(irr^{1/2})$. At these intensities in the relationship is demonstrated a proportionality to the square root of irradiance as shown in the fitted curve [92]. It is not quite a fit to the data as the error margins on the 278 irr data point do not encompass the model. This means that when it comes to the testing regimes (Table 6.1), that the light intensity is possibly within the range corresponding to catalyst kinetic performance regime, however further experimentation and data points would be necessary to ensure this were true.

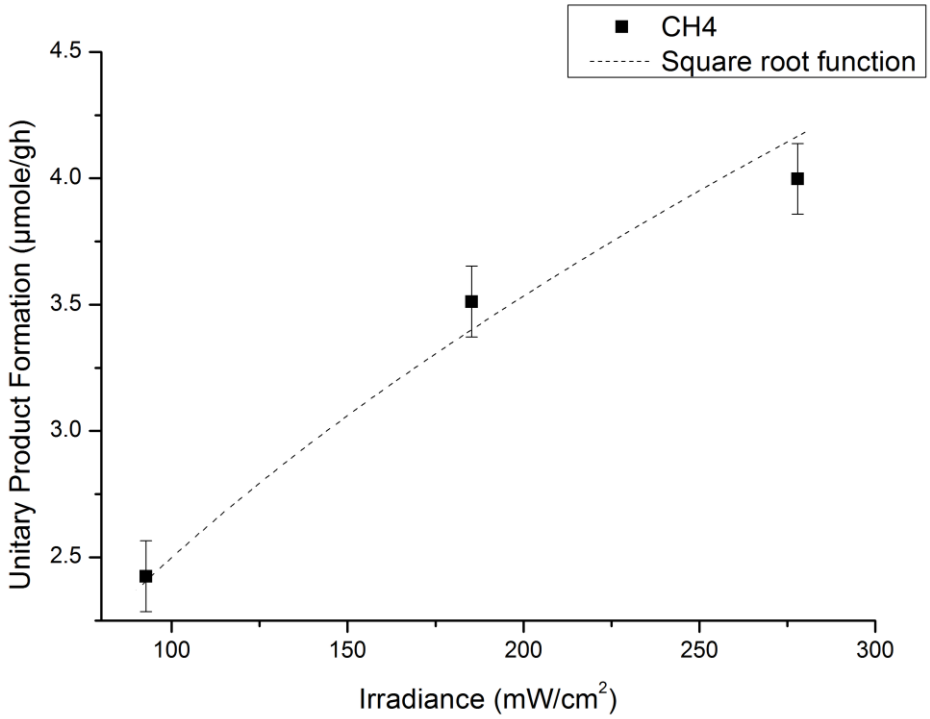


Figure 6.6 Methane production at varying light intensity between 92.7, 185.3, and 278 mW/cm$^2$ with curve fit as a function of the square root of irradiance. Experiments were conducted at room temperature for 2 hours with a catalyst loading of 0.04 g. A = 0.2499 and the error was 0.015.

Further investigations at lower irradiance (Appendix C) were conducted at 6.2, 18.5 and 30.9 irradiance mW/cm$^2$, for one hour with 0.03 g photocatalyst loading for both the Mirkat and the $AuTiO_2$ samples. However, a clear linear trend was not observed in the Mirkat case. Therefore, further irradiance investigation would need to be conducted to establish if Mirkat lower irradiance behavior aligns with expected behavior.

### 6.6 Further results terminology exploration with Mirkat regime data

To enable discussion of the dual term problem and observe the impact of the extended normalization within Mirkat results photonic yield and extended rate normalization were

calculated and presented here. The photonic yield adjusts the results from varying reaction length and irradiance. The extended normalization only adds additional information in terms of the experiments varying irradiance.

### *6.6.1 Photonic yield and Mirkat results in terms of electrons and photons*

Relative to the design of experiments plots in Chapter 5, where the variables have individual plotted expressions, it is challenging to plot a three variable input to the photonic yield. This is because the length of the experiment and irradiance impact the incoming photons and the catalyst loading enabled multiple product observations for similar photonic input. To plot photonic yield results generated with three input variables, the photonic yield was plotted as a ratio of rates; the denominator for the x-axis and the numerator as the z-axis, therefore the product electrons/time by incident photons/time (Figure 6.7). The y-axis being photocatalyst loading.

Considering first constant catalyst loading and varying incident photons the response to incident photons can be observed. Incoming photons increase the rate of product production up until roughly the 0.10 photons/sec point, at which a higher incoming photon rate does not increase product formation rate with results lowering and roughly plateauing at 0.15 photons/sec incident light. Then considering the catalyst loading varying with respect to a constant incident photon rate, it is also observable that the increase in photocatalytic loading increases the product electron rate. The summed carbon product results can be compared to the results of all carbon containing products (Figure 6.8), giving similar trends in behavior.

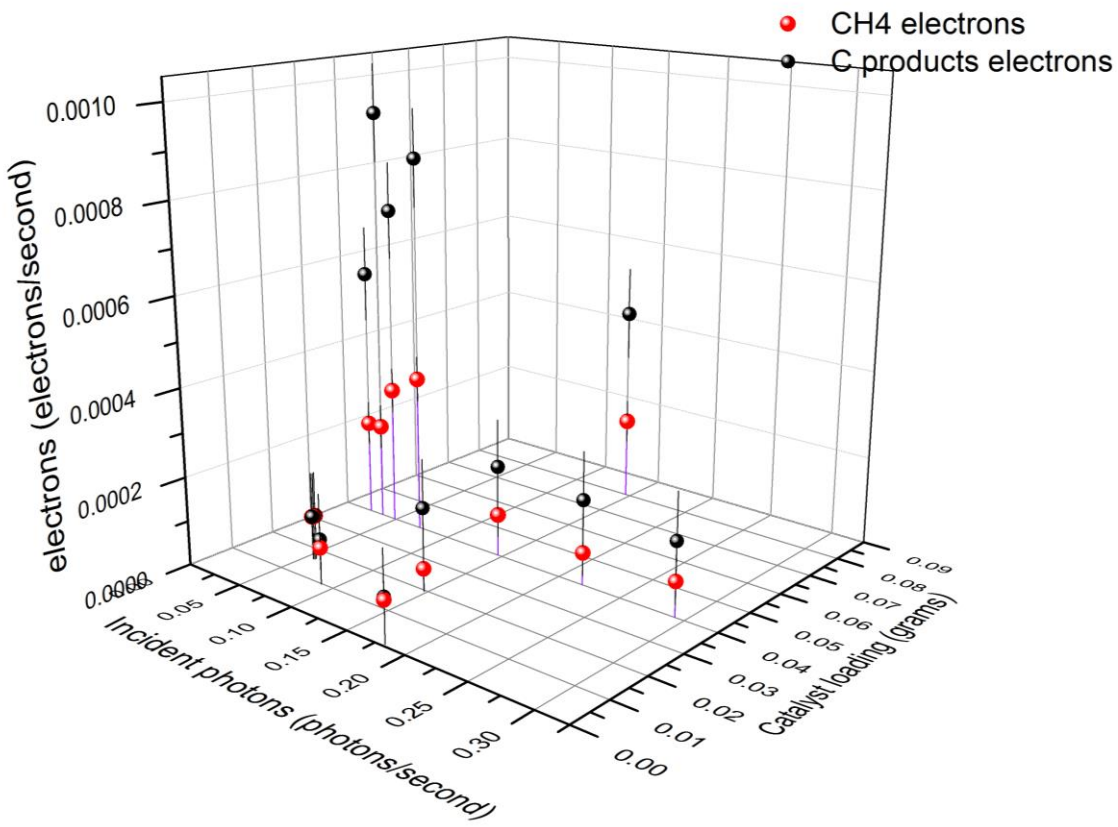


Figure 6.7 $CH_4$ and summed carbon products photonic yield plotted by electron rate found at various photon rates, with catalyst loading and black error bars. Colored drop lines are provided to anchor the rate within the incident photon rate and catalyst loading; gray for the carbon products, and purple for $CH_4$ results.

To compare the influence of including all the products with the $CH_4$ results, Figure 6.8 includes the photonic yield rates for all products summed. The widest uncertainty or change in results is displayed along the electrons and catalyst loading plane within the low irradiance conditions where the high hydrogen results make the blue drop line visible. Considering constant catalyst loading and varying incident photons the trends for $CH_4$ appear to hold for further products. The ability to observe hydrogen in Figure 6.8 is distinctly an observation of the larger photocatalytic reduction process, and not the $CO_2$ conversion alone. Most of the gains are minimal, but in the low photon rate case the hydrogen gains are substantial. The 0.02 g of photocatalyst loading case does appear to be an unusual response, particularly at the 0.05 incident photon rate, and at the 0.15 incident photon rate line this 0.02g high result makes for a jagged pattern along the incident light rate for all products, but an increasing curve for carbon products as observed before (Figure 6.2, in terms of unitary product formation). It becomes clear that the additional catalyst increased the products, when considering constant incident photons and varying catalyst loading, because the phonic yield is not normalized for photocatalyst loading, therefore it is interesting to compare to Figure 6.1 of the unitary product

formation results for the detected products. This comparison is made however at 0.15 incident photonic rate and varying loading from 0.01 to 0.08 g photocatalyst, and the trend is found generally to be the same. In terms of following the 0.04 g catalyst loading line there is a sense for the results given from varying the length of the reaction.

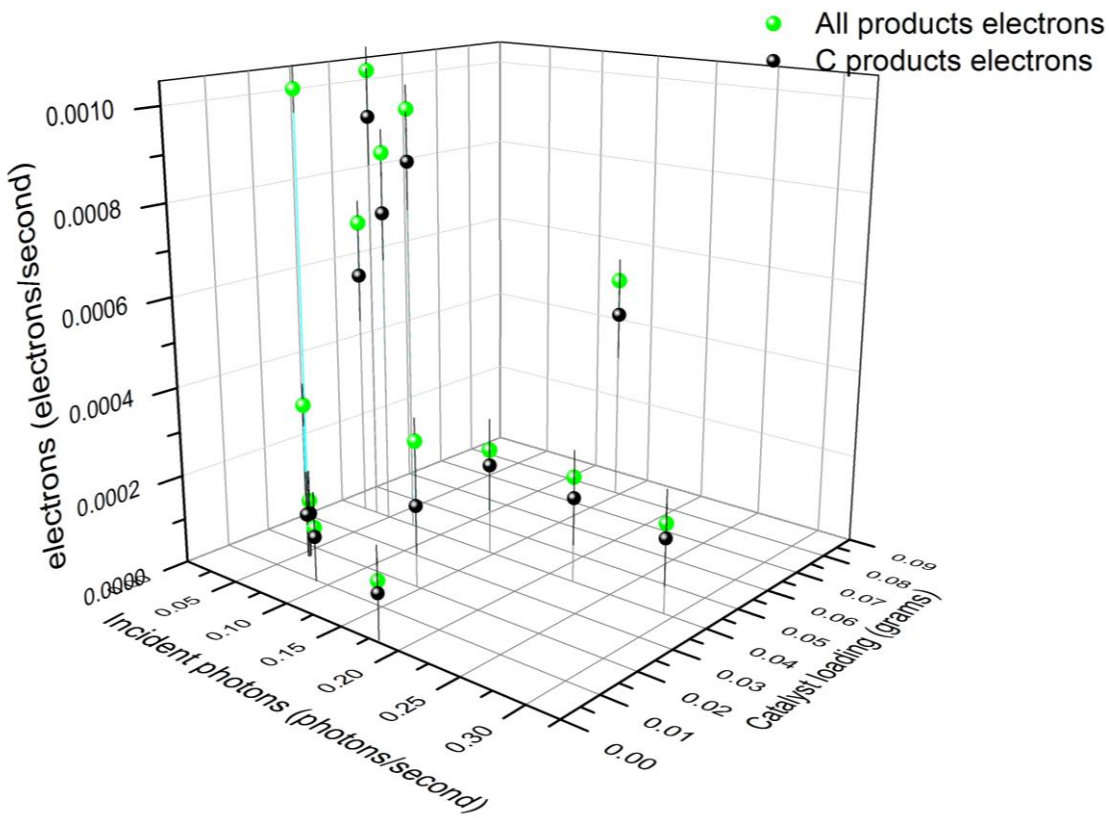


Figure 6.8 Carbon products and all products photonic yield plotted by electron rate found at various photon rates, with catalyst loading and black error bars. The blue colored drop lines correspond to the green all products data, and grey the black carbon products data with many drop lines overlapping.

To compare the photonic yield from catalyst loading and varying time the photonic yield has also been plotted simply as a function of these varied variables. In the case of varying catalyst loading a linear behavior appears characterized by $y = 0.016x$, and a $R^2$ value of 0.99895 as shown in Figure 6.9. This is distinctly different from the saturated behavior observed with unitary product formation or specific rate (μmol/gh) in section 6.3. And therefore, also highlights the dual term challenge. The extended normalization of the specific rate would not have the photonic perspective on the results

as the experimental conditions were constant and it would only proportionally shift the original unitary product formation result.

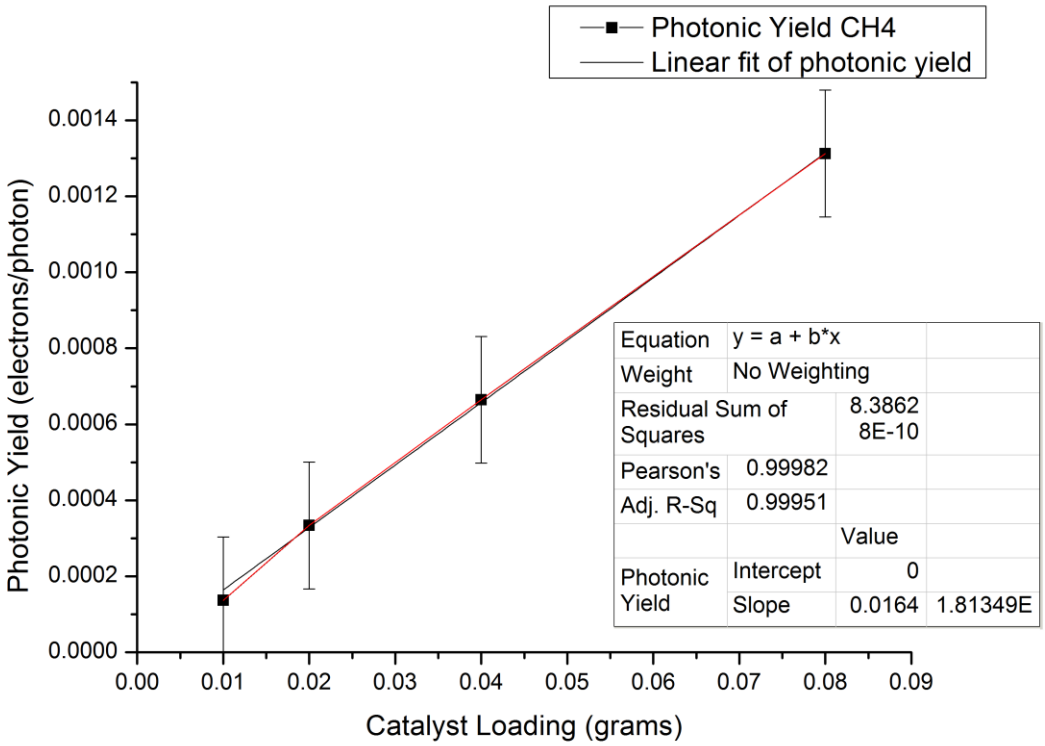


Figure 6.9 The $CH_4$ photonic yield results for varied catalyst loading between 0.01, 0.02, 0.04, and 0.08 g. Experiments were conducted at room temperature, for 4 hours with an incident light intensity of 278 $mW/cm^2$.

The photonic yield is plotted by varying reaction time in Figure 6.10. In this case, the behavior is rather similar to the unitary product formation results in Figure 6.4. The general trends line up with one exception of the one hour reaction time having a much higher photonic response than catalytic response. The photonic yield and catalytic unitary product formation rate are in alignment in their general trend, particularly at higher reaction times (which would also agree with the extended normalization that would be a proportional shift of the unitary product formation).

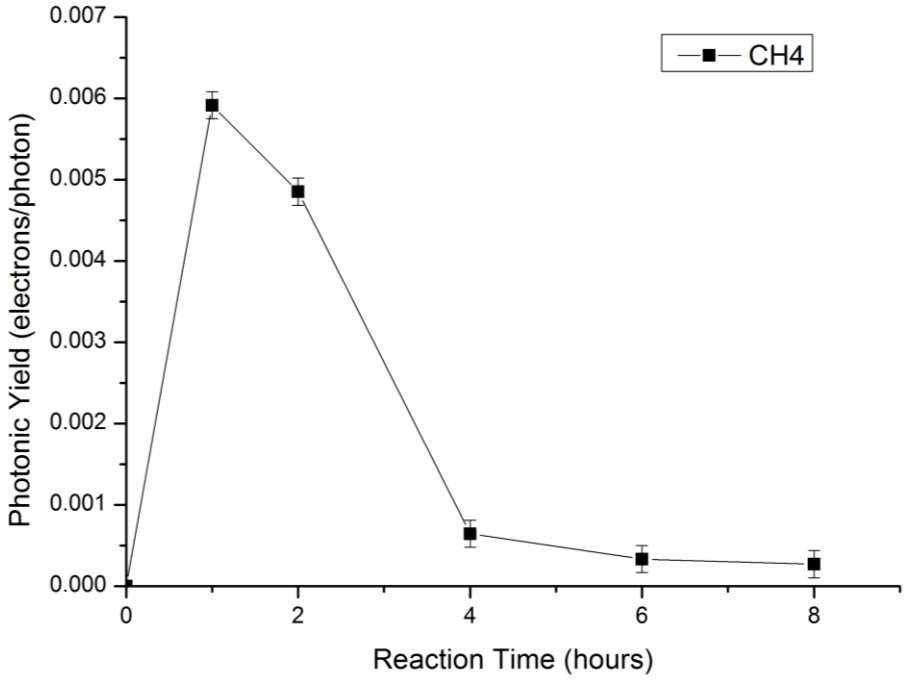


Figure 6.10 $CH_4$ photonic yield varying reaction time for experiments conducted at room temperature with a 0.04g catalyst loading and 278 mW/cm$^2$ irradiance.

The photonic yield plotted by varying irradiance is presented in Figure 6.11. It shows decreasing product embodied electrons per increased photon flux. This signifies a larger penalty for increasing irradiance than unitary product formation results analysis in Figure 6.6.

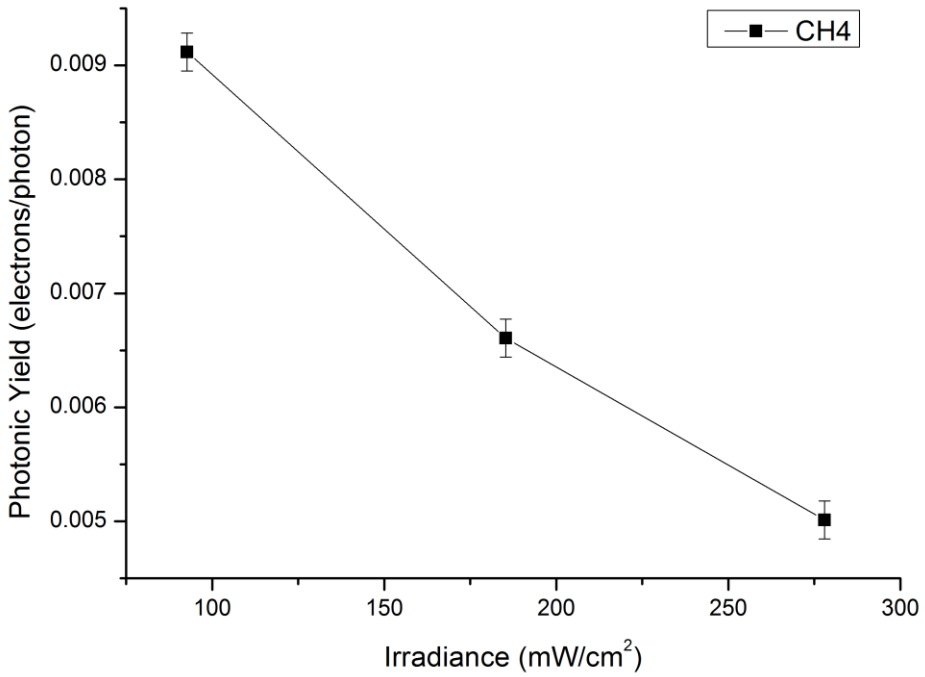


Figure 6.11 Photonic yield $CH_4$ results for the experiments with varying light irradiance, conducted with at room temperature, for 2 hours, with a catalyst loading of 0.04 g and irradiances of 92.7, 185.3, and 278 $mW/cm^2$.

Photonic yield results analysis has allowed a wider range of information to be processed together through the conversion of products into their respective electrons. It enables a system wide consideration of the data and makes it possible to compare low and high irradiance results across the variation in reaction length.

### *6.6.2 Further normalization of Mirkat regime results*

As discussed in Chapter 3 normalization by volume of reactor, light intensity and the surface area of the incoming light on the catalyst and extended normalization can provide more information from a singular result. The extended normalization calculation for the varying experimental irradiance is plotted (Figure 6.12).

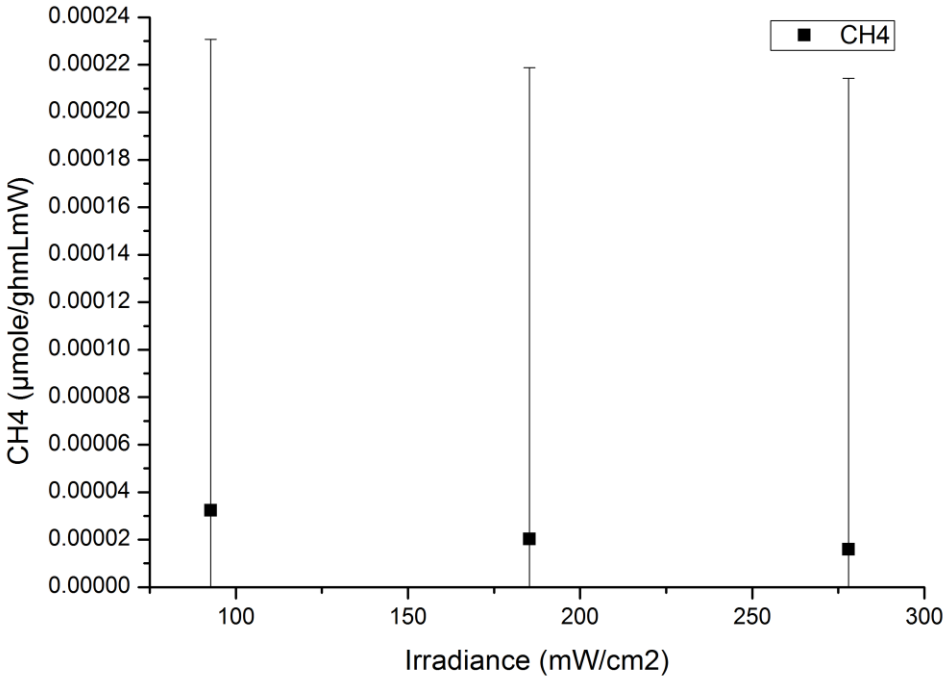


Figure 6.12 Extended normalization of results for varying light intensities, for the experiments conducted with at room temperature, for 2 hours, with a catalyst loading of 0.04g and irradiances of 92.7, 185.3, and 278 mW/cm$^2$.

In converting the result to the extended normalization the error is significant. When the irradiance energy input is considered within normalization of specific rate results, it is clear in Figure 6.12 that the additional energy is not furthering product formation, particularly in the case of $CH_4$ production, however to be certain of this trend further experimental work would need to be conducted. To compare the photonic yield consider Figure 6.11 where the trend is almost identical. This behavior is also unlike that of the unitary product formation in Figure 6.7, with the square root of the irradiance being proportional to unitary product formation. Instead we are seeing this inverted trend which agrees with the decrease seen in photonic yield.

The three cases of parameter variance showed different aspects of the extended rate normalization. With varying photocatalyst loading the extended normalization agreed with the unitary product formation response. In the experiments varying reaction length all 3 terms were in basic agreement in trends. Then in the case of varied irradiance the extended normalization was in agreement with the photonic yield trends. Thus, there was a balance in how the extended normalization analyzed results. This result is an argument that extended normalization could bridge the gap in normalizing the photocatalytic response across the dual terms.

### 6.7 Mirkat 211 Benchmarking Experimental Results and Analysis

When considering the regime for these experiments, mass flow is constrained by diffusion as the experiments are conducted in batch. This means that for the reaction the mass transport is characterized by the diffusion of $H_2O$ in $CO_2$, which is 0.138 $cm^2/s$ [265]. Ranges of performance in terms of catalyst loading and light intensity were identified, with 0.04 g catalyst loading and above being saturated, and the light intensity in the square root range.

The regime approach to photocatalytic experiments is straight forward. It is easy to get kinetic data by varying the initial concentration of reactants or the measurement from various times during the reaction process. The usefulness of the regime analysis and varying single experimental parameters is limited by the lack of data on the interaction effects. To investigate the interaction effects with the single variable variance, it would be necessary to intentionally study two factors together as demonstrated by Delavari and Amin, particularly in the supplementary materials [208]. In this case, they present Fig. S6. giving the photocatalyst loading and time and find no interaction effect for $CO_2$ conversion. Further experiments such as these exploring a wider range of parameters would enable interaction effects to be investigated. However this would require more experiments than a DoE.

The maximum results found for the unitary product formation, photonic yield, and extended rate normalization are given for $CH_4$ and C products in Table 6.2. There is an agreement on 0.04 g photocatalyst loading for maximum results. And in general an agreement amongst the results terms for a lower reaction length, one or two hours. The irradiance range shift in maximum results is the most notable. For $CH_4$ products the Mirkat results agree in terms of photonic yield and extended normalization. For the sum of all carbon products the extended normalization does not agree with the dual terms. This could be because the second highest photonic yield for the sum of carbon products occurred in the conditions the extended normalization is highest for. The extended rate normalization appears to be slightly more strongly weighted to irradiance efficiency than even the photon metric.

Table 6.2 Maximum results for the three results terms for the Mirkat experiments and the corresponding reaction conditions.

| *Product* | *Catalyst loading (g)* | *Irradiance ($mW/cm^2$)* | *Reaction Length (hours)* | *Maximum result* |
|---|---|---|---|---|
| *$CH_4$ (µmol/gh)* | 0.04 | 278 | 2 | 3.998 |
| *$CH_4$ photonic yield* | 0.04 | 92.7 | 2 | 0.0088 |
| *$CH_4$ extended normalization (µmole/ghLW)* | 0.04 | 92.7 | 2 | 10.09 |
| *C products (µmol/gh)* | 0.04 | 278 | 1 | 13.25 |
| *Carbon products photonic yield* | 0.04 | 278 | 1 | 0.0256 |
| *C products extended normalization (µmole/ghLW)* | 0.04 | 92.7 | 2 | 32.27 |

In the case of comparing trends across the single variable variance experiments, the dual terms were in disagreement, twice where the extended rate normalization was balanced, matching the catalytic trend in varying photocatalyst loading, and then matching the photonic trend with varied irradiance. Then with varied reaction time the three terms were in agreement. Thus the extended normalization may be an appropriate bridge between the dual terms with unclear overall implications due to the significant error.

# CHAPTER 7 – GOLD DOPED TITANUIM DIOXIDE AND MIRKAT PERFORMANCE; DISCUSSION OF APPLICABILITY AND PROCEDURE LIMITATIONS

This chapter builds upon the previous literature and results comparisons, discussing the results from the $AuTiO_2$ and Mirkat in relation to each other, thereby facilitating a quantification and comparison of the fuzziness of the benchmarking. The dual term challenge, and the appropriateness of the extended normalization are discussed in terms of figure of merit in Section 7.1. This is separated into Mikat results discussion (section 7.1.1), $AuTiO_2$ results discussion (section 7.1.2) and then a combined discussion (section 7.1.3). Then the current benchmarking is quantified in Section 7.2. A wider discussion of experimental procedure in Section 7.3, is followed by a brief consideration of reaction rate in Section 7.4. The chapter concludes with Section 7.5 covering the main insights from the experimental work.

## 7.1. Results applicability and terms

In Chapter 3 there was a developing understanding of challenges with benchmarking. In particular, the challenge of the dual term problem and a possibility for a combined figure of merit. This was developed by reviewing the reporting of results (section 3.1), the recommended standardized terminology options (section 3.2), and by giving a fuller picture of what photoreduction within the experimental process looks like (section 3.3). This story of benchmarking terms, or figure of merit, ended with the acknowledgment of the dual term challenge, an explanation of what the terms mean, and presenting the option for extended rate normalization (section 3.4). Since that discussion, many results have been investigated. These included the benchmarking of P25, identical experimental conditions within literature and experimental results (Chapter 4), the design of experiments results of the Au doped $TiO_2$ (Chapter 5), and the single variable variance Mirkat results inspired by proposed regimes that are intended to assist in considering intent before initiating experimental direction and parameters (Chapter 6). Here this dual term, or figure of merit, discussion is returned to in light of the experimental results gathered.

### *7.1.1 Mirkat results considering figure of merit*

The experimental conditions range for the Mirkat testing was 0.01 to 0.08 grams of photocatalyst, 6.2 to 278 mW/cm$^2$ irradiance, and 1 to 8 hours. The highest and lowest unitary product formation for methane: 3.998 µmole/gh was obtained at 0.04 g catalyst loading, 278 mW/cm$^2$ and 2 hours; and 0.00885 µmole/gh was obtained at 0.03 g catalyst loading, 6.2 mW/cm$^2$ and 1 hour respectively. The optimum unitary product formation conditions are at a much higher irradiance than the optimum photonic yield conditions. The highest and lowest photonic yield for $CH_4$; 0.0088 electrons/photon was obtained at 0.04 g catalyst loading, 92.7 mW/cm$^2$ and 2 hours; and 0.00009 electrons/photon was obtained at 0.02 g catalyst loading, 185 mW/cm$^2$ and 2 hours respectively. The photonic yield maximum and minimum results align with those of the extended normalization. The highest and lowest extended normalization results for $CH_4$; 10.09 µmole/ghLW were obtained at 0.04g catalyst loading, 92.7 mW/cm$^2$ and 2 hours; and 0.207 µmole/ghLW was obtained at 0.02 g catalyst loading, 185 mW/cm$^2$ and 2 hours. This shows the extended normalization term agreeing with photonic yield conclusions. The maximum and minimum results from the Mirkat results terms are tabulated below for clarity (Table 7.1). When the results term ranges, as evidence of the extended normalization agreeing with photonic yield are considered, the extended normalization appears as a photon dependent figure of merit in results conclusions.

Table 7.1 Presents the maximum and minimum for all results from Mirkat experiments.

| | *Catalyst loading (g)* | *Irradiance (mW/cm$^2$)* | *Reaction Length (hours)* | *Result* |
|---|---|---|---|---|
| *Maximum $CH_4$ (µmol/gh)* | 0.04 | 278 | 2 | 3.998 |
| *Minimum $CH_4$ (µmol/gh)* | 0.03 | 6.2 | 1 | 0.00885 |
| *Maximum $CH_4$ photonic yield* | 0.04 | 92.7 | 2 | 0.0088 |
| *Minimum $CH_4$ photonic yield* | 0.02 | 185 | 2 | 0.00009 |

| | *Catalyst loading (g)* | *Irradiance ($mW/cm^2$)* | *Reaction Length (hours)* | *Result* |
|---|---|---|---|---|
| *Maximum $CH_4$ extended normalization (µmole/ghmLmW)* | 0.04 | 92.7 | 2 | 10.09 |
| *Minimum $CH_4$ extended normalization (µmole/ghmLmW)* | 0.02 | 185 | 2 | 0.207 |

In this case, the modeled $m_{opt}$ of 0.04 g photocatalytic loading and the 2 hour optimum length of experiment do give the highest unitary product formation result. The highest unitary product formation result comes from the conditions of being proportional the square root of irradiance and the mass of catalyst loading being saturated. Interestingly, the photonic yield that is highest does come from the linear range of irradiance, however it also comes from the mass saturated range of catalyst loading, and therefore could potentially be improved, however the photonic performance metric does not encompasses photocatalytic loading.

The Mikat work covered the widest ranges for the experimental work. Even as it appears that the extended normalization may make an appropriate figure of merit for benchmarking, it remains true that the results also argue for separate terms for separate experimental regimes, as they highlight different conclusions, as exemplified by separate trends in Chapter 6 results.

### *7.1.2 Gold doped Titanium Dioxide results considering figure of merit*

The experimental conditions range for the $AuTiO_2$ testing was 0.02 to 0.04 g of photocatalyst, 6.2 to 241 $mW/cm^2$ irradiance, and 1 to 3 hours. The maximum and minimum of all the results terms with their corresponding reaction conditions are tabulated. As can be seen in Table 7.2 the highest and lowest unitary product formation for methane: 0.7503 µmole/gh was obtained at 0.02 g catalyst loading, 62 $mW/cm^2$ and 1 hour; and 0.0011 µmole/gh was obtained at 0.04 g catalyst loading, 62 $mW/cm^2$ and 3 hours. Relative to the Mirkat $CH_4$ unitary product formation results this range is smaller and shows a much clearer penalty of additional photocatalyst loading and time. The

highest and lowest photonic yield for $CH_4$: 0.0039 electrons/photon was obtained at 0.02 g catalyst loading, 62 mW/cm$^2$ and 1 hour; and 0.000004 electrons/photon was obtained at 0.04 g catalyst loading, 62 mW/cm$^2$ and 3 hours (the same conditions for the high and low unitary product formation). The highest and lowest extended normalization results for $CH_4$: $4.6x10^{-5}$ µmole/ghmLmW was obtained at 0.02 g catalyst loading, 62 mW/cm$^2$ and 1 hour; and $6.9x10^{-9}$ µmole/ghmLmW was obtained at 0.04g catalyst loading, 62 mW/cm$^2$ and 3 hours. Again the conditions are the same as each other showing dual term agreement. This is uniquely unified relative to the Mirkat results that show a dual term problem where the unitary product formation and the photonic yield highest output results do not align.

Table 7.2 Presents the maximum and minimum for all results from Au $TiO_2$ experiments.

| | *Catalyst loading (g)* | *Irradiance (mW/cm$^2$)* | *Reaction Length (hours)* | *Result* |
|---|---|---|---|---|
| *Maximum $CH_4$ (µmol/gh)* | 0.02 | 62 | 1 | 0.7503 |
| *Minimum $CH_4$ (µmol/gh)* | 0.04 | 62 | 3 | 0.0011 |
| *Maximum $CH_4$ photonic yield* | 0.02 | 62 | 1 | 0.0039 |
| *Minimum $CH_4$ photonic yield* | 0.04 | 62 | 3 | $4x10^{-6}$ |
| *Maximum $CH_4$ extended normalization (µmole/ghLW)* | 0.02 | 62 | 1 | 4.66 |
| *Minimum $CH_4$ extended normalization (µmole/ghLW)* | 0.04 | 62 | 3 | 0.006 |

Based on significant interaction and main effects plots from the $AuTiO_2$ DoE experiments in Chapter 5, the extended normalization appeared to be able to cover the same main effects in the three factor DoE considering $CH_4$ results. This was a smaller

range in irradiance had more agreement between the results terms as they all shared main effects. With the two factor DoE the wider irradiance range the $CH_4$ extended normalization results aligned with the photonic yield. However with the summed products the extended normalization model was confounded and no significant effects were present. Therefore, as a figure of merit, the extended normalization is observed to be usually appropriate, however occasionally emphasizing other conclusions.

Because the range of experimental work for the $AuTiO_2$ was smaller, there was not as noticeable variation in the results based on different terms. The DoE also does not facilitate regime analysis. It was observable that there are interaction affect to be investigated within the $CO_2$ photoreduction process, namely between irradiance and reaction length, and irradiance with photocatalyst loading.

### *7.1.3 Performance and Characterization, exploring the material surface and the performance of Mirkat and $AuTiO_2$*

Considering the Mirkat and $AuTiO_2$ results all together, the dual term challenge is visible as the catalytic and photonic aspects of the process are characterized differently. In many of these cases the extended rate normalization was able to incorporate further information so as to bridge the terms, showing both catalytic and photonic analysis trends. Do to the limits of the analysis the extended rate normalization is recommended for further investigation as a possible figure of merit for the $CO_2$ photoreduction process.

To compare the performance of the samples relative to each other based on their physical properties discussion now turns to investigating their performance relative to their characterization. As both samples were anatase and experiments were conducted with the same illuminated surface area the substantial shifts between these materials are mainly through the specific surface area and the Au doping. In this case, the results are normalized for the specific surface area of the photocatalyst (Table 7.3). It is clear that a substantial portion of the performance of increase of the Mirkat sample over the Au $TiO_2$ sample is due to the almost twice as great specific surface area of Mirkat. The further difference in the results for $CH_4$ is likely due to the increased hydrophilicity of Au $TiO_2$ observed by FTIR as discussed elsewhere [235].

Table 7.3 Specific surface area normalized results for Mirkat and Au $TiO_2$ samples and their maximum unitary product formation, photonic yield, and extended normalization results.

| | *$CH_4$ (µmol/gh)* | *$CH_4$ (µmol/h$m^2$)* | *$CH_4$ photonic yield* | *CH4 photonic yield by surface area of the sample ($m^{-2}$)* | *$CH_4$ extended normalization (µmole/ghmLmW)* | *$CH_4$ extended normalization including specific surface area (µmole/hmLmW$m^2$)* |
|---|---|---|---|---|---|---|
| *Mirkat* | 3.998 | 0.0184 | 0.0088 | 0.0010 | 10.09 | 0.0465 |
| *Au $TiO_2$* | 0.7503 | 0.0068 | 0.0039 | 0.0009 | 4.66 | 0.0424 |

It is important to remember that the variation in the unitary product formation comes both from reaction conditions and materials variation. As the photonic yield and the extended normalization incorporate more of the experimental conditions in the quantification, the results differences observed can be most attributable to the materials modifications. It may be more clear to consider Table 7.4 giving the unitary product formation results with the experimental conditions pointing out the substantially higher irradiance utilized and higher proportion of photocatalyst and reaction time. It becomes clear the Au doping generates only a small shift in the performance overall.

Table 7.4 Maximum $CH_4$ specific surface area normalized unitary product formation results for Mirkat and Au $TiO_2$ samples with experimental conditions.

| | *Catalyst loading (g)* | *Irradiance (mW/$cm^2$)* | *Reaction Length (hours)* | *$CH_4$ (µmol/gh)* | *$CH_4$ (µmol/h$m^2$)* |
|---|---|---|---|---|---|
| *Mirkat* | *0.04* | *278* | *2* | 3.998 | 0.018423963 |
| *Au $TiO_2$* | 0.02 | 62 | 1 | 0.7503 | 0.006820909 |

**7.2 Benchmarking quantified from experimental results and literature comparisons**

Current benchmarking will be assessed through comparing the literature variations with the experimental variations explored in this thesis. This will be done considering P25 as representative of literature ranges and the variation due to experimental parameters and

reactor geometries. The experimental results for Mirkat and $AuTiO_2$ represent variation due to experimental parameters. And the literature results ranges in $Au/TiO_2$ based materials encompass the experimental parameters and reactor geometries and materials modifications variation.

As discussed in Chapter 4, P25 is demonstrated to have a "fuzzy" benchmark (0.019 to 1.106 μmole/gh of $CH_4$) due to the variance in experimental setups and reaction conditions. The Au range from literature is 0.18-58.47 μmole/gh of $CH_4$ quantifying both the variation between experimental work and the materials modifications. This however was of limited insight across the four P25 to Au samples gain examples avalible (Chapter 4, section 4.5). The Mirkat unitary product formation results range of 0.00885-3.998 and $AuTiO_2$ range of 0.0011-0.7503 μmole/gh of $CH_4$, are based in varying reaction parameters. The range of Mirkat results is larger than the P25 range by more than double. Mirkat results are also well above the 1 μmole/gh threshold of significance [68]. The limit of P25 as a benchmark appears clear, irrespective of if only the best P25 results are being used, and therefore shrinking the results range. According to this comparison Mirkat has a wider ability or range of performance to represent the experimental variation than P25 and may be able to be used to scale performance against modifications more effectively. For the Au samples the literature range is wider at $10^3$ and the experimental range observed is smaller at $10^2$. This could be accounted for as variation from materials modification. The suggestion from the experimental results is that the materials perform differently within the same reactor system based on experimental parameters. And this should be investigated more systematically.

Just based on reactor conditions the relative performance of materials can change. The initial experimental comparison from 0.02 grams of catalyst loading, 185 $mW/cm^2$ and a 2 hour reaction time the results of the μmole/gh of $CH_4$ results for Mirkat and $AuTiO_2$ were 0.0995 and 0.5013 respectively (Ch. 4). This can be compared to the Mirkat result at 0.04 g photocatalyst loading, 185 $mW/cm^2$ irradiance and 2 hours giving 3.5 μmole/gh of $CH_4$ relative to the 0.1117 or 0.076 μmol/gh for the 0.04 g catalyst loading, 185 irradiance and 3 or 1 hour reaction time. In this case, the observed performance has shifted with the Mirkat outperforming the Au doped catalyst. Therefore, the experimental parameters can be found to alter the benchmarking conclusion, even when all else is equal.

This then becomes impetus to be clear about the benchmarking conditions and use options such as the standardized conditions reactor performance (Table 6.1) regime to identify a common goal in the benchmarking requirement, such as solar light utilization

to drive the significance of the results. Another option is to utilize optimization and a commercial benchmark to isolate peak performance.

### 7.3 Experimental procedure and the regime and design of experiment tools

A preferable approach to further experimental work would initiate experiments with regime testing. This regime testing would then be followed by DoE work in specific ranges of behavior to explore interaction effects. One particular delineator would be the linear and square root ranges of irradiance. If these ranges were identified and then used to formulate a DoE the significance of the DoE insights would be improved. Particularly if a considering a model based DoE, allowing for the optimization and interaction effects in a regime space to be clarified and not conflated.

The complexity of light as a parameter in a reaction is clear from the discussion in Chapter 3, and remains an important consideration. In this thesis, work was constrained to 365 nm as discussed in Chapter 4. Therefore, considering results in terms of band gap energy relative to utilized photons was not appropriate. The quantum efficiency relative to the band gap provides an assessment of the effectiveness of any band gap variations. However, if experiments are conducted with a range of wavelengths then reactants and products could be assessed for if they directly absorb those wavelength energies enabling photoreforming.

In Chapter 6, section 6.1.2, the choice of what to optimize first was presented as part of regime testing optimizing first for irradiance then mass. However, the interplay of irradiance and catalyst loading are not fully explored yet. In trying to simplify the testing it would be nice to rely on a parameter like the optimum mass of catalyst and to use it in all experiments. To enable this it is necessary to know if the optimum mass is irradiation dependent. To visualize this comparison Figure 7.1 presents a singular optimum mass to the left, and a varying optimum photocatalyst mass loading to the right. Currently it is unknown which is the case, and it could possibly be explored for multiple photocatalysts to also observe if it is material dependent, before definitive agreement is found.

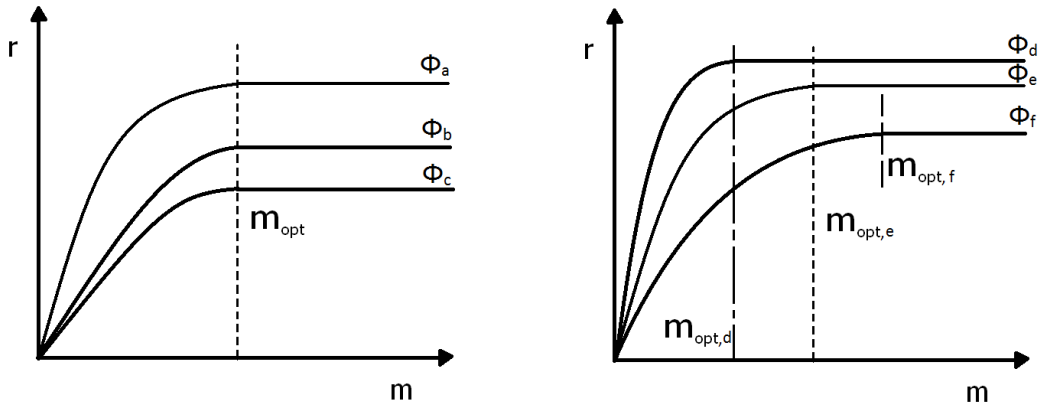


Figure 7.1 Possible challenges to optimizing the mass of a material in a photocatalytic reactor includes the consideration of optimum mass as irradiation dependent. Left drawing depicts varying irradiation (a, b and c) has no effect on optimum mass of catalyst used. Right drawing depicts optimum masses for specific irradiation (d,e and f).

For the experimental work presented the main goal was to enable a benchmarking discussion. Therefore, this possible functional dependence of $m_{opt}$, was not explored further. However, it may be pertinent depending on the experimental plan.

### 7.4 Considering reaction rate

Much of this work utilizes unitary product formation for results analysis and benchmarking discussion. It is accepted that a normalized rate is appropriate for benchmarking. However, for reactor scale up research into characterizing the $CO_2$ photoreduction process with a rate equation would be more likely. There are some current proposals as to what are the important factors to include in the reaction rate characterization. For example, de Lasa *et al.* propose the following equation, reproduced here as Equation 7.1. When looking at the equation proposed by de Lasa *et al.*, reaction rate in photoconversion they indicate three variables upon which it depends [215]:

$$r'''_{i,in} = f_1(C_{i,in}) f_2(C_C) f_3(P_a) \qquad \text{Equation 7.1}$$

In this equation $r'''_{i,in}$ is the overall apparent initial reaction rate, $f_1(C_{i,in})$ is the function of the initial concentration of the chemical species, $f_2(C_C)$ is the function of the catalyst concentration, and $f_3(P_a)$ is the function of the rate of absorbed photons indicating information about the catalyst photon performance.

When considering this equation in terms of the results gathered it can be observed that the light intensity most likely is the single most important function and contributor to the reaction rate, modified both by catalyst loading and photon absorption. This was

particularly clear with the DoE results highlighting the interactions of irradiance with reaction time, and irradiance with photocatalyst loading.

Interactions integrated into the function require that it be rewritten as in Equation 7.2:

$$r = f(C)(m)(I) \qquad \text{Equation 7.2}$$

C stands for concentration of reactants, m is the mass of the catalyst and I, irradiance. Unfortunately, at this stage how to formulate the equation is not obvious from this thesis work. Instead, the DoE has highlighted that interactions are occurring. Hopefully this benchmarking discussion has been a small stepping stone to enable a stronger rate discussion for gas phase $CO_2$ photoreduction in particular.

### 7.5 Insights from experimental work

Mirkat is a possible future commercial benchmark for $CO_2$ photoreduction experiments as the performance clearly adjusts to reaction conditions and has significant results. The dual term challenge has been observed with different trends and significant factors highlighted by unitary product formation compared to photonic yield. The extended normalization acts as a unique bridge between the terms highlighting aspects of both, and in some cases forming independent conclusions. In retrospect, regime testing insights, followed by DoE analysis would be a beneficial method to approach a singular photocatalytic material. Caution is suggested when approaching optimization of photocatalyst loading in gas phase $CO_2$ photoreduction as the optimum mass may be irradiance dependent. And this work suggests a rate function of multiple interacting variables.

# CHAPTER 8 – CONCLUSIONS AND FUTURE WORK

This thesis identifies the parameters influencing $CO_2$ photoreduction results, contextualizes the results reported and resolves issues in benchmarking through a testing regime framework, proposed results term, and insights from experimental procedure. Conclusions in Section 8.1 include what is necessary for benchmarking (section 8.1.1), major conclusions from experimental work (section 8.1.2), and finally the conclusions from the dual term challenge and benchmarking quantification (section 8.1.3). Future work is proposed from conceptual discussions of how best to benchmark materials modifications, and for specific experimental rig improvements for this unique set up (section 8.2).

## 8.1. Conclusions

The complexity of the $CO_2$ photoreduction process and unique experimental set ups may mean that there will be limited benchmarking, however, thorough clear reporting the ability to assess causes of performance improvements will improve. What this thesis has presented is a myriad of ways to engage more thoughtfully with the $CO_2$ photoreduction testing procedure to embrace and acknowledge more fully the system parameters and conditions that are relevant to producing research that facilitates benchmarking. Thus the first objective to understand and assess current practice has led to a description of what benchmarking, or really reporting, need to entail going forward.

The second objective, to quantify current benchmarking, has led to experimental work focused on varying parameters which are incorporated in important quantifications of the photoreduction process, such as irradiance and reaction time. This experimental work has included the DoE analysis, and single variable variance. This has culminated in regime proposals for testing, and the comparisons of the range of results in literature with that which can be generated in one lab for the purpose of proposing a new benchmark material.

### *8.1.1 What Benchmarking entails going forward*

A main conclusion has been that more needs to be disclosed about the experimental work for benchmarking to occur. It is essential to consider and report the material characterization, the reactor rig geometries, and the experimental parameters for $CO_2$ photoreduction. To review what this entails, a list of the considerations for the experimental parameters and reactor geometry are given in Chapter 3, section 3.6.

It can be agreed that benchmarking is a major concern for $CO_2$ photoreduction as improvements to the reactor systems, photocatalytic materials, and even ideal reaction parameters are unclear. Thus, for materials it is important to link modifications and outcomes, ensuring that appropriate care is taken to explore the photocatalytic reaction. Experimental exploration will allow reaction mechanisms to be more widely understood, and requires an acknowledgment of the detection limitations on the products observed. Reaction parameters been proven to have a wider influence through producing a wider range of results with Mirkat than P25 results observed in the literature. Experimental parameters were also was used to alter which material is observed to have higher results between Mirkat and Au $TiO_2$ experimentally. Thus Mirkat may prove to be a more significant benchmark with the ability to encompasses variations in experimental conditions and set up.

As well as considering the surface photocatalytic reaction, to develop experimental tests on $CO_2$ photoreduction other physical processes need to be considered as they happen at the same time in the photocatalytic system (i.e. mass and light transfer). Consideration of regimes testing can assist with this approach. With comprehensive disclosure there is an opportunity to optimize the conditions and the photocatalytic materials. This is because using the reaction rate allows for the influence of experimental conditions and materials modifications to be explored and 'benchmarking' will improve in meaning.

### *8.1.2. Testing Regimes and multivariable work conclusions from experimental work*

In many ways, the DoE results prove that the work has only begun in understanding the interaction of the reaction parameters. The main interactions observed were reaction time with irradiance, and photocatalyst loading with irradiance. This would be interesting to investigate with multiple materials, particularly if there is observed to be a stronger material dependence on optimum performance. The factors varied can be ranked based on level of significance to the DoE analysis. Time was found to be the most significant factor, followed by irradiance, and lastly photocatalyst loading. The rankings signify a large effect in using batch reactions, an appropriate acknowledgement of the essential nature of irradiance to the reaction, and the relationship of irradiance with photocatalyst loading.

The regimes are provided to enable discussion and hopefully wider collaboration from incorporating key concepts from photovoltaics and catalysis. In $CO_2$ utilization, there are many related fields and the insights can be more widely articulated and shared

if appropriate terminology, such as the recommended terms (section 3.2), are worked with. This use of regimes and recommended terminology would assist in overcoming the current limitations of benchmarking.

### *8.1.3. Dual term challenge and quantified benchmarking*

There is also the challenge of results terms. It is clear from this work that experimental work needs to be designed to enable both the photonic and catalytic performance by both varying the rate, either by varying reaction length or initial concentration in a batch reaction, and by also varying photons provided through varying irradiance. Even as various terms are appropriate for various experimental conditions, it is also a challenge for benchmarking to find a singular figure of merit. Arguably a possible candidate is the extended normalization of unitary product formation or specific rate (Section 3.1.1). This term incorporates reactor geometry in the form of reactor volume and illuminated surface area, and reaction parameters such as irradiance and catalyst loading. It has been found to hold a middle ground with the Mirkat single variable variance experiments. The extended normalization term agreed with both the photon and catalytic quantification when reaction length was varied. And then the observed trends sided with unitary product formation in relation to varying photocatalyst loading, and then with photonic yield when irradiance was varied. In terms of the DoE analysis the interactions were more nuanced with more trends aligning with photonic yield. However, in the three factor DoE observing $CH_4$ results the main effects were of the same trends for all three terms. Due to the extent to which the terms were bridged by the further normalization and the opportunity to incorporate important reaction parameters into the result the extended rate normalization is recommended for further investigation as to its appropriateness as a figure of merit for $CO_2$ photoreduction benchmarking.

## 8.2. Future Work

Here recommendations for future work are presented, considering both larger parameters to be investigated and more effective testing utilizing the rig and set up from this thesis work:

- Rig improvements for future work include:
  - Incident light angle would be improved by ensuring it is perpendicular to the photocatalytic surface. This could possibly be achieved by catalyst loading on membrane or mesh.
  - Control of $CO_2$ concentration with adding to inlet gas inert carrier gas; The recommendation for the current set up is to attach He to a mass flow

controller in tandem with the $CO_2$ coming from the bubbler, at the inlet of the reactor.

- Analysis Improvements to track the $CO_2$ with the more analytically sensitive SEM detector to enable analysis of $CO_2$ reduction through conversion using 22 mass per charge peek (more detail in Appendix E).
- Continuous reactions would shorten the time necessary to assess kinetics. With a flow based reaction system, it would be practical to integrate model based DoE analysis that can quantify the various influences on reaction rate. Considering the number of factors necessary to investigate and marching it to the appropriate DoE design is important and challenging. Jones, Schoen and Montgomery discuss the options for four to six two-level factor options [266].
- Investigate if the optimum mass loading for gas phase reactors is irradiance dependent.
- Utilize the regime testing procedure to fully quantify a reactor system and photocatalyst. Then employ the DoE experimental work in specific ranges. The results can then be used to identify optimum results within appropriate regimes, thereby verifying proposed regimes (Table 6.1). Use results to explore the extended rate normalization.
- Comprehensively report findings using Section 3.5 as a checklist.

# APPENDIX A: Supporting table from Chapter 3

Table A.1 presents a sample of typical product yield results from articles testing modified $TiO_2$ catalysts for $CO_2$ photocatalytic reduction. The product formation results illustrate the variation in units, as well as covering a wide range of values. As can be seen in Table A.1, the product yield results are not normalized for the experimental conditions. For example, the results cannot accommodate the use of variations in participant species, distinction in light source, and change of reactor type.

Table A.1 Summary of representative articles on $CO_2$ photocatalytic reduction emphasizing different reporting of product yield results.

| *Reference* | *Rector* | *Catalyst Modifications* | *Photocatalyst* | *Light source* | *Reductant* | *Product analysis* | *Product Yield reported* |
|---|---|---|---|---|---|---|---|
| *[149]* | gas phase on glass microfib-er filter | metal doping, silver | $TiO_2$, Ag | Philips Actinic BL TL 8W | water | gas chromatograph with thermal conductivity detector, flame ionization detector and methanizer | ~98µmole/gcat of hydrogen, ~10-40 µmole/gcat carbon monoxide, ~10-20 µmole/gcat of all hydrocarbons tracking methane, ethane, ethene, propane, propene, butane, butene, and methanol |
| *[194]* | liquid phase twin reactors | two catalysts metal loading, platinum | Pt/$CuAlGaO_4$ for $CO_2$ reduction and Pt/$SrTiO_3$:Rh for Hydrogen ($H_2$) generation | 300 W Xenon lamp | water | gas chromatograph with thermal conductivity detector, flame ionization detector and methanizer | 1-2.5 µmole/g of hydrogen and 17-22 µmole/g of methanol plotted against time in hours |
| *[152]* | gas phase on glass fiber | metal incorporation , silver | Ag/$TiO_2$ | 150 W solar simulator Oriel | water and methanol | gas chromatograph with thermal conductivity detector and flame ionization detector | 1500 µmole/(g*h) of hydrogen, 110-140 µmole/(g*h) of carbon monoxide, and 5-10 µmole/(g*h) of methane |
| *[132]* | gas phase catalyst support unspecif-ied | carbon nanotubes grown on surface | carbon nanotubes on Ni/$TiO_2$ | 75 W visible daylight lamp | water | gas chromatograph with flame ionization detector | 0.1-0.145 µmole/(g*h) of methane plotted against time in hours |

| *Reference* | *Rector* | *Catalyst Modifications* | *Photocatalyst* | *Light source* | *Reductant* | *Product analysis* | *Product Yield reported* |
|---|---|---|---|---|---|---|---|
| *[145]* | gas phase on monolith | metal doping, indium | In/$TiO_2$ | 220W mercury UV lamp | water | gas chromatograph with thermal conductivity detector and flame ionization detector | 100-1150 µmole/g of carbon monoxide and 150-325 µmole/g of methane |
| *[129]* | gas phase on stainless steel | composite | mesoporous CeO-$TiO_2$ | 300 W Xenon lamp | water | gas chromatograph | 40-70 mmole/g of carbon monoxide and 9-11 mmole/g of methane |
| *[148]* | gas phase on Teflon holder | composite | MgO/Pt-$TiO_2$ | 100 W Xenon lamp | water | gas chromatograph with flame ionization detector | 0.25-0.4 µmole of carbon monoxide and 1.0-2.2 µmole of methane |
| *[151]* | gas phase on glass reactor | crystal facet surface control | anatase $TiO_2$ nanosheets with 95% {100} facets | 300 W Xenon lamp | water | gas chromatograph with flame ionization detector and methanizer | 2250 µmole of hydrogen and 35 ppm/g of methane |
| *[147]* | gas phase on glass-fiber filter | bicrystalline phase | anatase-brookite $TiO_2$ | 150 W solar simulator Oriel | water | gas chromatograph with thermal conductivity detector and flame ionization detector | 0.075-0.22 µmole/h of carbon monoxide |

# APPENDIX B: Band Gap Energy Calculations

Band gap energy was utilized to assess the aging of samples and has been included in the appendix due to experimental work utilizing only the 365 nm wavelength and, therefore, the band gap energy is not directly relevant to results analysis.

### *B.1 Ultraviolet-visible spectroscopy analysis*

Optical spectroscopy is based on the relationship of light with energy as it allows for the electronic states of molecules to be investigated based on electron excitation [267]. The Bohr-Einstein frequency relationship ($\Delta E = h\nu$, $\nu$ being the frequency of electromagnetic radiation) simplifies to $E = hc/\lambda$ (plank's constant multiplied by the speed of light over wavelength). The ultraviolet and visible light spectrum is significant as a probe because it corresponds to the electronic states of atoms and molecules and enables chemical investigation [267].

Light can be reflected, absorbed or transmitted through a sample that is in solution, gas phase or crystal form. In the case of solid powder samples the reflected and absorbed light is analyzed as transmission is greatly reduced [268]. The ultraviolet and visible light radiation is directed at the sample in monochromatic increments while the resulting reflected light is detected. Due to the reflection, refraction and diffraction of light in a solid powder, heterogeneous catalyst are analyzed in this thesis as a densely packed powder and the Schuster-Kubelka-Munk radiative transfer theory is applied (also referred to as the Kubelka-Munk Function) [268].

Kubelka-Munk Function [268]: $F(R_\infty) = \frac{(1-R_\infty)^2}{2R_\infty} = \frac{K}{S}$ Equation B.1

Where $R_\infty$ is the diffuse reflection of a sample that satisfies the condition of being infinitely thick, and K is the apparent absorption, and S is the apparent scattering coefficient.

UV-vis analysis was conducted with a Jasco V-670 Spectrometer, used previously [240]. This ISN-723 model contained a 60 mm integrating sphere, used a quarts plate sample holder, and was calibrated using a barium sulphate standard. Approximately 0.05 g of sample was packed into the sample holder, compressed against the quarts plate window. Analysis was taken with the accompanying manufacturers software.

Analysis of the UV-vis data were conducted utilizing the Kubelka-Munk function for a new calculation of band-gap energy. Previously the intersection of the main trend lines was used [240]. With the Kubelka-Munk function (equation B.1) the procedure is

instead to find the intersection of the main trend line with the light wavelength (x) axis. Using the Bohr-Einstein relationship the band gap energy can be calculated from: $E_g = 1240/\lambda$, energy in eV at a particular wavelength in nm.

### *B.2 The calculation of band gap energy for a photocatalyst*

UV-vis analysis is important as decreasing the band-gap of a catalyst is a key way to improve the efficiency of a photocatalyst (as discussed in section 2.5.2). The assumption is that by increasing the range of wavelengths of light that promote an electron to the CB the photocatalytic performance will improve. This is, of course, if the VB and the CB are still sufficiently oxidizing or reductive, respectively.

There are two types of band-gap energy discussed in the literature and a small bit of confusion around energy gaps [269]. One occurs when the photon has enough energy to form an exciton, however, not enough to maintain the separation of the electron and hole pair. The band gap observed at this energy is called the optical band-gap energy. In the typical case, where the photon excites an electron to a higher energy state, the energy level necessary is called the electronic band-gap energy, also referred to as apparent band-gap. This energy gap between the valence band and the conduction band is the electronic band-gap.

Band-gap energy of a catalyst is often estimated using UV-vis spectrum data. These data are analyzed either by introducing trend lines with, or without, being mathematically transposed into a different plot to estimate band-gap energy. Reflectance data is used in the Kubelka Munk function to approximate optical absorbance. To identify the band gap energy then the Kubelka Munk function, as an approximation of the absorption coefficient, is multiplied by the photon energy and then treated to a power function depending on the transition energy of the semiconductor. With the UV-vis spectrum five ways of interpreting the band-gap energy has been found [47, 270, 271].

The first example using two trend lines has been used by Park and colleagues and [270] Zhang and associates [271]. This method uses the raw UV-vis data to estimate the band-gap energy. This method can be contrasted with a single trend line using raw data (called absorption extinction), translations done using the Tauc and Kubelka-Munk functions that also utilize a single trend line. (Kubelka-Munk function as shown above, equation B.1, is a function of reflectance.) Ohtani, however, is concerned as he points out that Tauc plots assume single transition mode of direct or indirect, which can be misleading in multicrystal phase materials [47]. With indirect semiconductors an exponent of ½ is used and with direct semiconductors an exponent of 2 is used. Another

method is to find the band gap from an inversion of diffuse reflectance measurements [272].

Tauc plots have developed based on the relationship [273]:

$$(\alpha h\nu)^n = A(h\nu - E_g) \qquad \text{Equation B.2}$$

Where the absorption coefficient (α) multiplied by the by the energy of the photon calculated by Plank's constant (h) and the photon frequency (ν) is then raised to n which depends on the energy transition of the band gap. This is equivalent to a proportionality constant multiplied by the photon energy minus the band gap energy ($E_g$). The Tauc method has recently been evaluated and recommendations given to improve the accuracy to around ±0.033 eV for single crystal phases [273].

A direct band gap semiconductor has the highest energy of the conduction band and the lowest energy state of the valance band in the same k space (or k vector in Figure B.1 below). Indirect semiconductors have different k values for the energy states for their electrons at the conduction and valance band. This can be seen in Figure B.1 by observing where the energy gap is lowest between the conduction and valence band, highlighted in yellow, and whether this energy maximum and minimum align in k space. $TiO_2$ in the anatase phase is an indirect semiconductor and rutile and brookite phases are direct [274]. For mixed crystal phases determining whether the sample has a direct or indirect band gap is a further challenge to using the Tauc method.

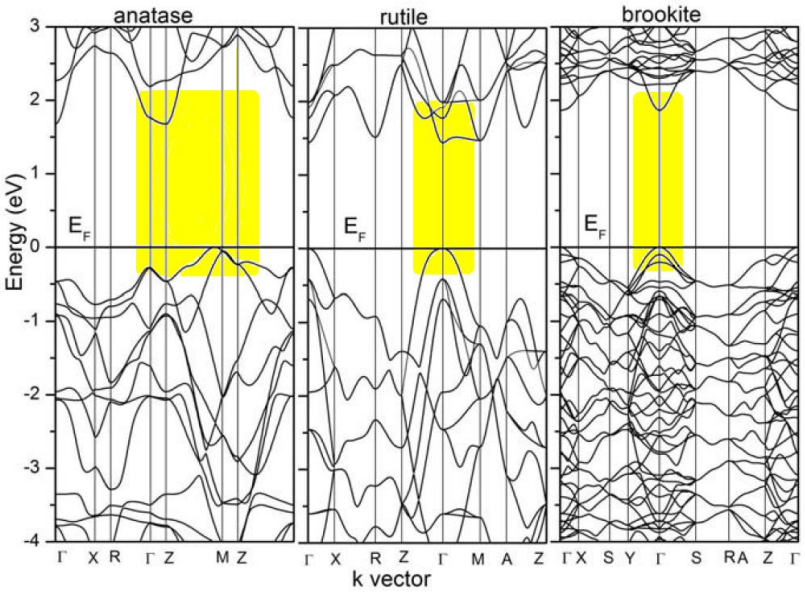


Figure B.1 The calculated band structure of $TiO_2$ in various crystal phases with regards to the Fermi level $E_F$, from Reyes-Coronado *et al.* [274].

Another method is to find the band gap from an inversion of diffuse reflectance measurements [272].

Herrmann argues the need for establishing experimentally the band-gap energy by using monochromatic light and varying the wavelength with an experiment and no longer relying on calculations from UV-vis analysis. However, for this to be successful a rapid and simple reaction would be necessary [92]. An example of the kind of results curve Herrmann desires, giving band-gap energy of $E_G$, is shown below in Figure B.2. With band-gap energy calculations discrepancies, this request for experimental determination appears justified.

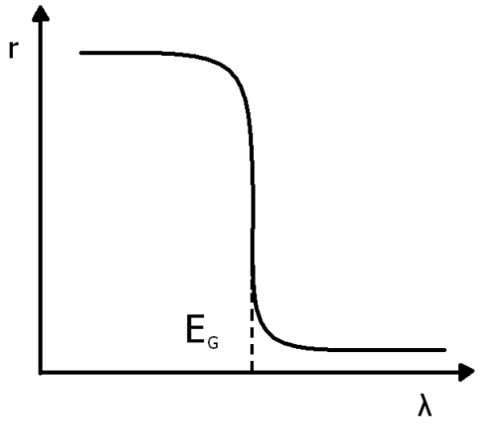


Figure B.2 Expected plot of the rate of reaction as a function of light irradiation wavelength, modified from Herrmann [96].

Toyoda and Tsuboya determined the band-gap energy using a photoacoustic signal [275]. They identified the scattering of $TiO_2$ as a barrier in adequately assessing band-gap energy, and thus, used a signal less sensitive to scattering effects. However, the data are processed similarly as the UV-vis spectra in that results can vary due to human choice in which data points should be included.

The complexity surrounding band-gap energy brings to light a possible need for consensus on processes to identify band-gap energy. It is also a reminder of caution when comparing results. To remove this complexity this thesis works with a single wavelength, thereby not enabling discussion of the improvement of bandgap energy to the photon efficiency performance of the material.

### *B.3 Ultraviolet and visible spectroscopy analysis and band gap energies of photocatalytic samples*

Because some of these samples were produced during the author's MSc thesis, UV-vis analysis was conducted to verify that samples were not aging. Therefore, results are compared with previous work [240], indicating no variation in band-gap energy when

calculated with the identical line intersection method. The results of the band-gap energy calculations that were done with the same method as the master's dissertation, by intersecting trend lines, are compared alongside calculations done using the KM function and a single trend line intersection. These results can be seen in Table B.1. The band-gap energies found using the KM function are all higher than the previous found band-gap energies reinforcing the concern over a need to standardize methods to enable comparisons across the literature.

Table B.1 Band-gap energies of modified samples in eV. Error margin of ±0.05 eV.

| | *Calculated KM band gap energy* | *Intersecting trend lines* | *Repeated trend line calculation with new UV-vis* |
|---|---|---|---|
| *Mirkat 211* | 3.34 | - | - |
| *Commercial Anatase $TiO_2$* | 3.27 | 3.19 | 3.15 |
| *EISA* | 3.16 | 3.05 | 2.96 |
| *EISA500H2* | 3.10 | 3.05 | 2.99 |

# APPENDIX C: Tables of Results and supporting information

## *C.1 Tables of experimental results presented in this thesis:*

Table C.1 Mirkat 211 results from experiments conducted at room temperature and 0.5 bar gauge pressure. Reaction parameters are given in bold. Photonic yield is calculated for the sum of all product electrons.

| *Catalyst loading (g)* | *Irradiance ($mW/cm^2$)* | *time (h)* | *$H_2$ (µmole)* | *$CH_4$ (µmole)* | *$C_2$ (µmole)* | *CH3OH (µmole)* | *photonic yield* |
|---|---|---|---|---|---|---|---|
| **0.01** | **278** | **4** | 0.197 | 0.03493 | 0.00903 | - | 0.00037 |
| **0.02** | **278** | **4** | 1.036 | 0.08519 | 0.10146 | 0.12277 | 0.00223 |
| **0.04** | **278** | **4** | 0.256 | 0.16965 | 0.13466 | - | 0.00165 |
| **0.08** | **278** | **4** | 0.597 | 0.33505 | 0.31612 | 0.00452 | 0.00364 |
| **0.03** | **6.2** | **1** | 0.488 | 0.00026 | - | - | 0.33297 |
| **0.03** | **18.5** | **1** | 1.799 | 0.00066 | - | - | 0.41082 |
| **0.03** | **31** | **1** | 0.058 | 0.00225 | - | - | 0.00922 |
| **0.04** | **92.7** | **2** | 0.441 | 0.19401 | 0.20875 | 0.00889 | 0.02840 |
| **0.04** | **185.3** | **2** | 0.488 | 0.28099 | 0.24872 | - | 0.01766 |
| **0.04** | **278** | **2** | 0.413 | 0.31984 | 0.29222 | 0.01109 | 0.01319 |
| **0.04** | **278** | **1** | 0.183 | 0.09747 | 0.19268 | 0.04727 | 0.02838 |
| **0.04** | **278** | **4** | 0.256 | 0.16964 | 0.13465 | - | 0.00165 |
| **0.04** | **278** | **6** | 0.502 | 0.19746 | 0.18511 | 0.05657 | 0.00108 |
| **0.04** | **278** | **8** | 0.475 | 0.28338 | 0.20928 | - | 0.00067 |
| **0.02** | **185** | **2** | 0.080 | 0.00398 | 0.01235 | - | 0.00097 |

Table C.2 $AuTiO_2$ results from experiments conducted at room temperature and 0.5 bar gauge pressure. Reaction parameters are given in bold. Photonic yield is calculated for the sum of all product electrons.

| *Catalyst loading (g)* | *Irradiance ($mW/cm^2$)* | *time (h)* | *$H_2$ (µmole)* | *$CH_4$ (µmole)* | *$C_2$ (µmole)* | *$CH_3OH$ (µmole)* | *photonic yield* |
|---|---|---|---|---|---|---|---|
| **0.04** | **62** | **1** | 0.395 | 0.00942 | 0.00318 | - | 0.02958 |
| **0.03** | **124** | **2** | 0.405 | 0.00199 | 0.00345 | - | 0.00354 |

| | | | | | | | |
|---|---|---|---|---|---|---|---|
| **0.04** | **62** | **3** | 0.122 | 0.00013 | 0.00106 | - | 0.00094 |
| **0.02** | **185** | **3** | 0.705 | 0.00995 | 0.00225 | - | 0.00184 |
| **0.04** | **185** | **3** | 0.155 | 0.01341 | 0.01009 | 0.00637 | 0.00070 |
| **0.04** | **185** | **1** | 0.294 | 0.00305 | 0.01460 | - | 0.00897 |
| **0.03** | **124** | **2** | 0.103 | 0.00053 | 0.00995 | - | 0.00140 |
| **0.02** | **62** | **3** | 0.018 | 0.00531 | 0.00783 | - | 0.00065 |
| **0.03** | **124** | **2** | 0.544 | 0.00571 | 0.00185 | - | 0.00491 |
| **0.02** | **185** | **1** | 0.109 | 0.00531 | 0.00318 | - | 0.00341 |
| **0.02** | **62** | **1** | 0.514 | 0.01261 | 0.00624 | - | 0.04099 |
| **0.02** | **62** | **1** | 0.121 | 0.01500 | 0.00451 | - | 0.01418 |
| **0.03** | **6** | **3** | 4.928 | 0.00212 | - | - | 0.38557 |
| **0.03** | **241** | **3** | 0.835 | 0.00823 | - | - | 0.00168 |
| **0.03** | **241** | **1** | 0.264 | 0.00916 | - | - | 0.00526 |
| **0.03** | **6** | **1** | 0.006 | 0.00013 | - | - | 0.00513 |
| **0.02** | **185** | **2** | 0.021 | 0.02005 | 0.00597 | - | 0.00078 |
| **0.03** | **18.5** | **1** | 0.013 | 0.00172 | 0.00225 | - | 0.00763 |
| **0.03** | **31** | **1** | 0.309 | 0.00358 | 0.00093 | - | 0.04502 |

Table C.3 Commercial samples experimental results tabulated for experiments conducted at room temperature and 0.5 bar gauge pressure, with 0.02 g of catalyst, 185 mW/cm$^2$ irradiation, for 2 hours. Photonic yield is calculated for the sum of all product electrons.

| *Sample* | *$H_2$ (µmole)* | *$CH_4$ (µmole)* | *$C_2$ (µmole)* | *$CH_4$ (µmole/gh)* | *$CH_4$ $\left(\frac{\mu mole}{g \cdot h \cdot mL \cdot mW}\right)$* | *photonic yield* |
|---|---|---|---|---|---|---|
| *Commercial* | | | | | | |
| *Anatase* | 0.195 | 0.00438 | 0.00345 | 0.1095 | $2.28 \times 10^{-7}$ | 0.00777 |
| *P25* | 8.704 | 0.00929 | 0.00039 | 0.2323 | $4.84 \times 10^{-7}$ | 0.29124 |
| *Mirkat 211* | 0.080 | 0.00398 | 0.01235 | 0.0995 | $2.07 \times 10^{-7}$ | 0.00567 |

Table C.4 Modified samples experimental results tabulated for experiments conducted at room temperature and 0.5 bar gauge pressure, with 0.02 g of catalyst, 185 mW/cm$^2$ irradiation, for 2 hours. Photonic yield is

calculated for the sum of all product electrons. Numbers in parenthesis refer to sample number corresponding with previous work [240].

| *Sample* | *$H_2$ (µmole)* | *$CH_4$ (µmole)* | *$C_2$ (µmole)* | *$CH_3OH$ (µmole)* | *$CH_4$ (µmole/gh)* | *$CH_4$ $\left(\frac{\mu mole}{g \cdot h \cdot mL \cdot mW}\right)$* | *photonic yield* |
|---|---|---|---|---|---|---|---|
| *Au $TiO_2$* | 0.021 | 0.02005 | 0.00597 | - | 0.5013 | $1.04 \times 10^{-6}$ | 0.00078 |
| *EISA (6)* | 1.054 | 0.00185 | 0.00544 | 0.00411 | 0.0464 | $9.69 \times 10^{-8}$ | 0.00630 |
| *EISA500$H_2$ (21)* | 1.775 | 0.01128 | 0.00571 | - | 0.2821 | $5.88 \times 10^{-7}$ | 0.01057 |

### *C.2 Low intensity results from Mirkat experimental work:*

Lower irradiance experiments using Mirkat with catalyst loading of 0.03 g, and length of experiment of 1 hour are shown in Figure C.1. Here the anticipated linear behavior of a proportional relationship is not obvious. While the behavior of the $CH_4$ results seen in Figure C.1 do not lend themselves to curve fitting of a linear or square root function, error margins (repeat experiments) could be investigated further to observe if a linear behavior would result. When a linear curve fit is calculated the $R^2$ value is 0.8924, which is not a good fit, as the fit should be much closer to 1.

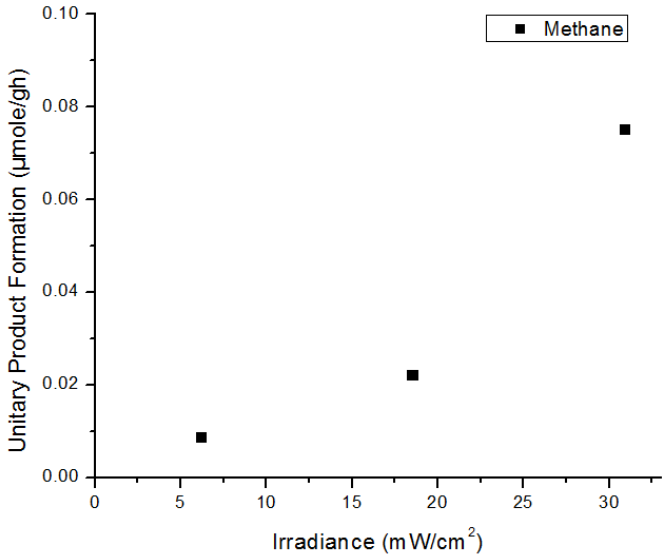


Figure C.1 Methane production from Mirkat at varied intensities of 6.2, 18.5 and 30.9 mW/cm$^2$. Experiments conducted at room temperature for 1 hour with 0.03 g catalyst.

Low light intensity experiments were conducted using $AuTiO_2$. These low intensity experiments were performed with a catalyst loading of 0.03 g, and length of experiment

of 1 hour. The results are shown below in Figure C.2. As opposed to the results for Mirkat from section 6.6.1, these results show a strongly linear behavior. Therefore, these results more obviously fit in to the proportional behavior for light intensity in the regime structure.

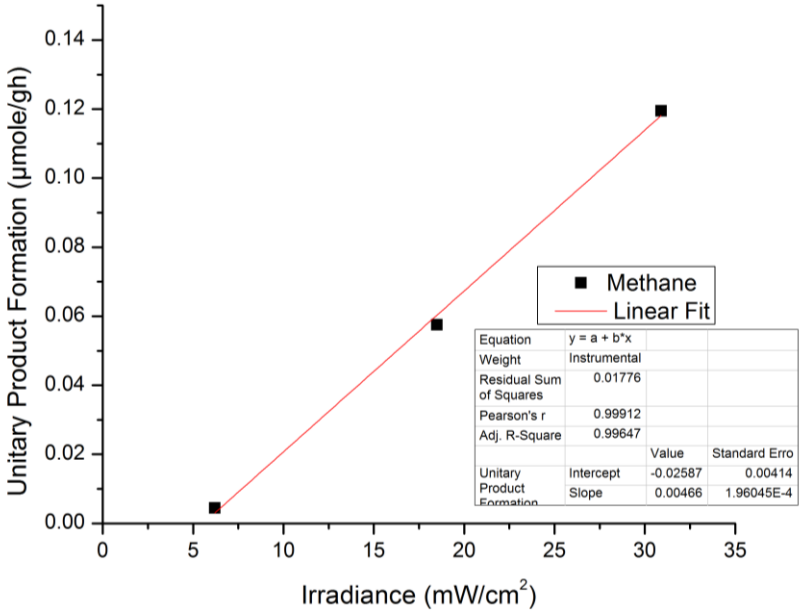


Figure C.2 Low intensity methane production for $AuTiO_2$ varying light intensity from 6.2, 18.5 and 30.9 $mW/cm^2$. Experiments conducted at room temperature with 0.03 g of catalyst, for 1 hour.

## *C.3 Mass Spectrometer MASsoft 7 Calibration and experimental test program instructions*

Calibration:

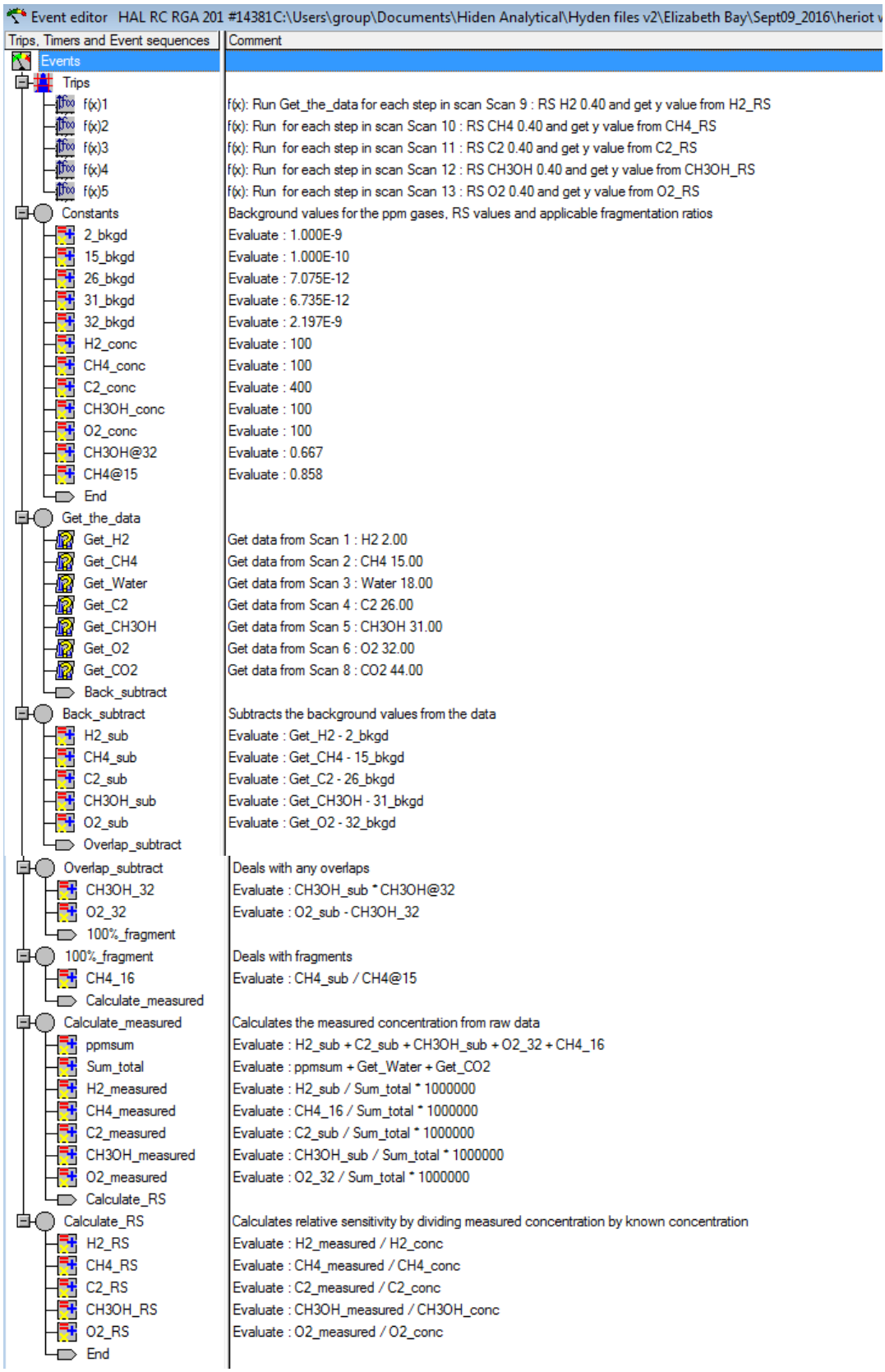

Experimental:

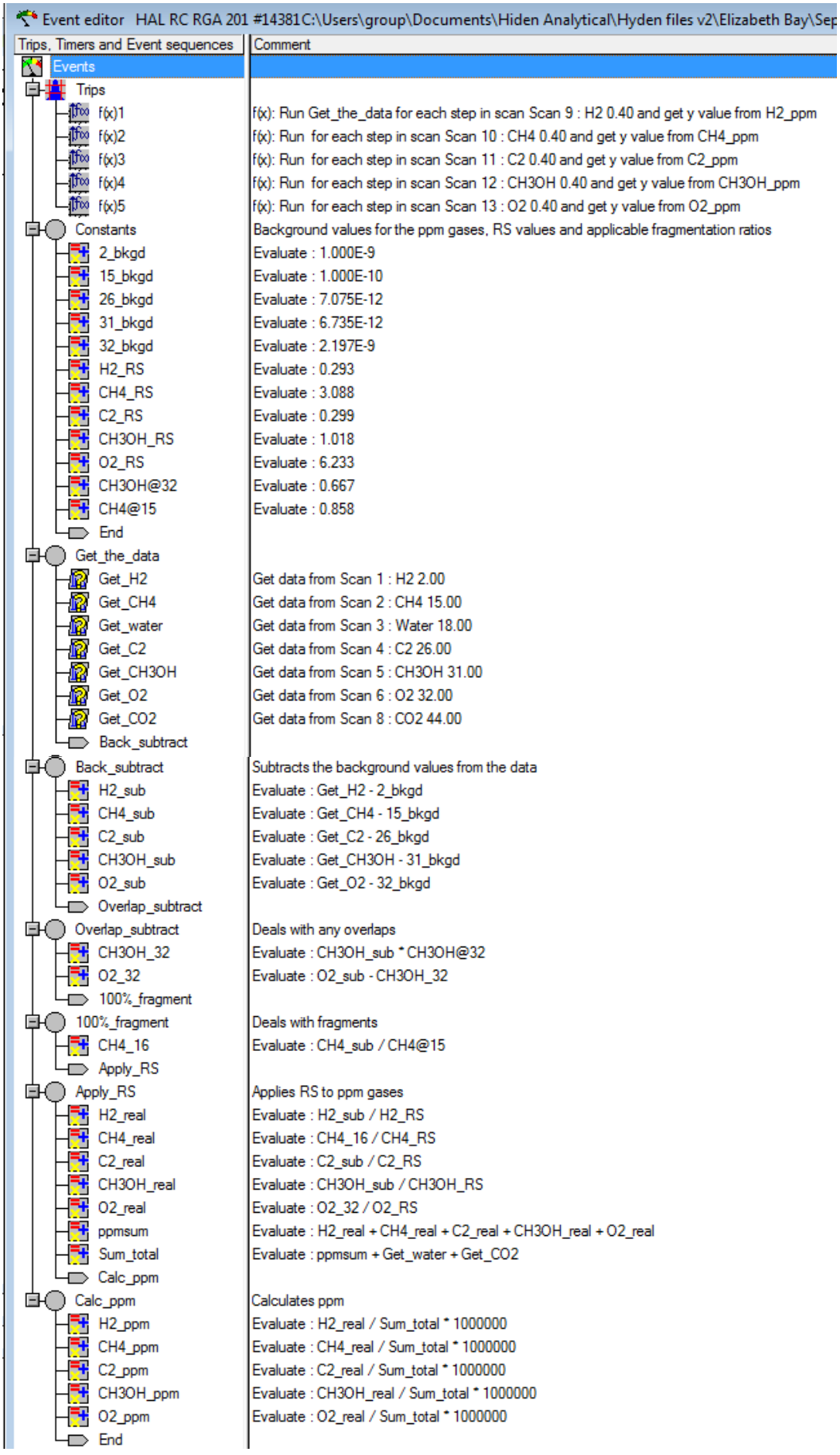

# APPENDIX D: Design of experiments models and P values

To accompany the plots in Chapter 6, here the models generated and their respective P values are included. Note that the p-values bigger than 0.05 were not included in the model.

Three factor DoE

$CH_4$ (µmole/gh) response

Coded Coefficients

| Term | Effect | Coef | SE Coef | T-Value | P-Value | VIF |
|---|---|---|---|---|---|---|
| Constant | | 0.1970 | 0.0314 | 6.28 | 0.002 | |
| Loading (g) | -0.1815 | -0.0907 | 0.0314 | -2.89 | 0.034 | 1.00 |
| Irradiance (mW/cm2) | -0.0841 | -0.0421 | 0.0314 | -1.34 | 0.238 | 1.00 |
| Reaction Time (h) | -0.2103 | -0.1051 | 0.0314 | -3.35 | 0.020 | 1.00 |
| Irradiance (mW/cm2)*Reaction Time (h) | 0.1782 | 0.0891 | 0.0314 | 2.84 | 0.036 | 1.00 |
| Ct Pt | | -0.1509 | 0.0600 | -2.51 | 0.054 | 1.00 |

Regression Equation in Uncoded Units

CH4 (µmole/gh) = 1.122 - 9.07 Loading (g) - 0.00358 Irradiance (mW/cm2)
- 0.2840 Reaction Time (h)
+ 0.001449 Irradiance (mW/cm2)*Reaction Time (h) - 0.1509 Ct Pt

Three factor DoE

$CO_2$ from summed products (µmole/gh) response

Coded Coefficients

| Term | Effect | Coef | SE Coef | T-Value | P-Value | VIF |
|---|---|---|---|---|---|---|
| Constant | | 0.4913 | 0.0555 | 8.85 | 0.000 | |
| Loading (g) | -0.2324 | -0.1162 | 0.0555 | -2.09 | 0.090 | 1.00 |
| Irradiance (mW/cm2) | -0.0266 | -0.0133 | 0.0555 | -0.24 | 0.820 | 1.00 |
| Reaction Time (h) | -0.5378 | -0.2689 | 0.0555 | -4.85 | 0.005 | 1.00 |
| Loading (g)*Irradiance (mW/cm2) | 0.3630 | 0.1815 | 0.0555 | 3.27 | 0.022 | 1.00 |
| Ct Pt | | -0.276 | 0.106 | -2.60 | 0.049 | 1.00 |

Regression Equation in Uncoded Units

CO2 products (µmole/gh) = 2.498 - 48.1 Loading (g)
- 0.00907 Irradiance (mW/cm2)
- 0.2689 Reaction Time (h) + 0.2951 Loading (g)
*Irradiance (mW/cm2) - 0.276 Ct Pt

Three factor DoE

$CH_4$ photonic yield response

```
Coded Coefficients

Term                                  Effect       Coef   SE Coef  T-Value  P-Value
Constant                                        0.000860  0.000076    11.37    0.000
Loading (g)                       -0.000287  -0.000143  0.000076    -1.90    0.116
Irradiance  (mW/cm2)               -0.001240  -0.000620  0.000076    -8.19    0.000
Reaction Time (h)                 -0.001527  -0.000764  0.000076   -10.09    0.000
Irradiance(mW/cm2)*Reaction Time(h) 0.001275   0.000637  0.000076    8.42    0.000
Ct Pt                                       -0.000765  0.000145    -5.28    0.003

Regression Equation in Uncoded Units

CH4      photonic      yield      =      0.006622      - 0.01434 Loading (g)
- 0.000031 Irradiance  (mW/cm2)                   - 0.002043 Reaction Time (h)
+ 0.000010 Irradiance  (mW/cm2) *Reaction Time (h) - 0.000765 Ct Pt
```

Three factor DoE

All products photonic yield response

```
Coded Coefficients

Term                                        Effect      Coef  SE Coef  T-Value  P-
Value   VIF
Constant                                             0.01089  0.00143     7.61
0.001
Loading (g)                                -0.00168  -0.00084  0.00143    -0.59
0.584  1.00
Irradiance  (mW/cm2)                       -0.01431  -0.00715  0.00143    -5.00
0.004  1.00
Reaction Time (h)                          -0.01970  -0.00985  0.00143    -6.88
0.001  1.00
Irradiance  (mW/cm2)*Reaction Time (h)      0.01478   0.00739  0.00143     5.16
0.004  1.00
Ct Pt                                               -0.00754  0.00274    -2.75
0.040  1.00


Regression Equation in Uncoded Units

All    products    photonic    yield    =    0.07716    - 0.084 Loading (g)
- 0.000357 Irradiance  (mW/cm2)
                           - 0.02470 Reaction Time (h)
+ 0.000120 Irradiance  (mW/cm2)
                           *Reaction Time (h) - 0.00754 Ct Pt
```

Three factor DoE

$CH_4$ extended normalization response

```
Coded Coefficients

Term                                    Effect    Coef  SE Coef  T-Value  P-
Value   VIF
Constant                                     0.905    0.209     4.33    0.008
Loading (g)                          -0.878  -0.439    0.209    -2.10    0.090
1.00
```

```
Irradiance  (mW/cm2)                    -1.164  -0.582    0.209    -2.78    0.039
1.00
Reaction Time (h)                       -1.242  -0.621    0.209    -2.97    0.031
1.00
Irradiance  (mW/cm2)*Reaction Time (h)   1.175   0.588    0.209     2.81    0.038
1.00
Ct Pt                                           -0.758    0.401    -1.89    0.117
1.00


Regression Equation in Uncoded Units

CH4 (µmole/ghLW) = 6.99 - 43.9 Loading (g) - 0.02857 Irradiance  (mW/cm2)
                   - 1.801 Reaction Time (h)
+ 0.00955 Irradiance  (mW/cm2)*Reaction Time (h)
                   - 0.758 Ct Pt
```

## Three factor DoE

## All C products extended normalization response

```
Coded Coefficients

Term                                     Effect    Coef  SE Coef  T-Value  P-
Value   VIF
Constant                                          2.082    0.304     6.85    0.002
Loading (g)                             -1.689  -0.844    0.304    -2.78    0.050
1.00
Irradiance  (mW/cm2)                    -2.115  -1.058    0.304    -3.48    0.025
1.00
Reaction Time (h)                       -2.419  -1.210    0.304    -3.98    0.016
1.00
Loading (g)*Irradiance  (mW/cm2)         2.016   1.008    0.304     3.32    0.029
1.00
Irradiance  (mW/cm2)*Reaction Time (h)   1.568   0.784    0.304     2.58    0.061
1.00
Ct Pt                                           -1.404    0.582    -2.41    0.073
1.00


Regression Equation in Uncoded Units

All     C     products     (µmole/ghLW)     =     18.38     - 286.9 Loading (g)
- 0.0919 Irradiance  (mW/cm2)
                             - 2.784 Reaction Time (h) + 1.639 Loading (g)
                             *Irradiance  (mW/cm2)
+ 0.01275 Irradiance  (mW/cm2)
                             *Reaction Time (h) - 1.404 Ct Pt
```

## Two factor DoE

## $CH_4$ (µmole/gh) response

```
Coded Coefficients

Term                                      Effect     Coef  SE Coef  T-Value  P-
Value   VIF
Constant                                          0.1062   0.0225     4.71
0.042
Irradiance  (mW/cm2)                     0.1842   0.0921   0.0225     4.08
0.055  1.00
Reaction Time (h)                       -0.0974  -0.0487   0.0225    -2.16
0.163  1.00
```

```
Irradiance  (mW/cm2)*Reaction Time (h)  -0.1166  -0.0583   0.0225    -2.58
0.123  1.00
Ct Pt                                             -0.0610   0.0344    -1.77
0.219  1.00


Regression Equation in Uncoded Units

CH4 (µmole/gh) = -0.0157 + 0.001776 Irradiance  (mW/cm2)
+ 0.0126 Reaction Time (h)
                 - 0.000496 Irradiance  (mW/cm2)*Reaction Time (h)
- 0.0610 Ct Pt
```

Two factor DoE

$CH_4$, as part of the all carbon products (µmole/gh) response

```
Coded Coefficients

Term                                    Effect     Coef  SE Coef  T-Value  P-
Value   VIF
Constant                                          0.1062   0.0538     1.97
0.187
Irradiance  (mW/cm2)                    0.1854   0.0927   0.0538     1.72
0.227  1.00
Reaction Time (h)                      -0.0974  -0.0487   0.0538    -0.90
0.461  1.00
Irradiance  (mW/cm2)*Reaction Time (h)  -0.1166  -0.0583   0.0538    -1.08
0.392  1.00
Ct Pt                                             0.1089   0.0823     1.32
0.317  1.00


Regression Equation in Uncoded Units

All C Products (µmole/gh) = -0.016 + 0.00178 Irradiance  (mW/cm2)
+ 0.0126 Reaction Time (h)
                           - 0.000496 Irradiance  (mW/cm2)*Reaction Time (h)
+ 0.1089 Ct Pt
```

Two factor DoE

$CH_4$ photonic yield response

```
Coded Coefficients

Term                                       Effect       Coef   SE Coef  T-
Value  P-Value
Constant                                            0.000418  0.000043
9.64    0.011
Irradiance  (mW/cm2)                    -0.000138  -0.000069  0.000043    -
1.59    0.252
Reaction Time (h)                      -0.000159  -0.000080  0.000043    -
1.84    0.208
Irradiance  (mW/cm2)*Reaction Time (h)  -0.000417  -0.000208  0.000043    -
4.80    0.041
Ct Pt                                              -0.000328  0.000066    -
4.95    0.038

Term                                    VIF
Constant
Irradiance  (mW/cm2)                   1.00
Reaction Time (h)                      1.00
Irradiance  (mW/cm2)*Reaction Time (h)  1.00
Ct Pt                                  1.00
```

```
Regression Equation in Uncoded Units

CH4 photonic yield = 0.000212 + 0.000003 Irradiance  (mW/cm2)
+ 0.000139 Reaction Time (h)
                     - 0.000002 Irradiance  (mW/cm2)*Reaction Time (h)
- 0.000328 Ct Pt
```

Two factor DoE

All carbon products photonic yield

```
Coded Coefficients

Term                                        Effect      Coef  SE Coef  T-Value
P-Value   VIF
Constant                                             0.09942  0.00128    77.79
0.000
Irradiance  (mW/cm2)                       0.18841   0.09420  0.00128    73.71
0.000  1.00
Reaction Time (h)                         -0.19188  -0.09594  0.00128   -75.07
0.000  1.00
Irradiance  (mW/cm2)*Reaction Time (h)  -0.19201  -0.09601  0.00128   -75.12
0.000  1.00
Ct Pt                                                -0.09661  0.00195   -49.49
0.000  1.00


Regression Equation in Uncoded Units

All products photonic yield = -0.00954 + 0.002436 Irradiance  (mW/cm2)
                              + 0.00497 Reaction Time (h)
- 0.000817 Irradiance  (mW/cm2)
                              *Reaction Time (h) - 0.09661 Ct Pt
```

Two factor DoE

$CH_4$ extended normalization response

```
Coded Coefficients

Term                                       Effect     Coef  SE Coef  T-Value  P-
Value   VIF
Constant                                            0.6095   0.0683     8.92
0.012
Irradiance  (mW/cm2)                      -0.5845  -0.2922   0.0683    -4.28
0.051  1.00
Reaction Time (h)                          0.4454   0.2227   0.0683     3.26
0.083  1.00
Irradiance  (mW/cm2)*Reaction Time (h)  -0.7879  -0.3940   0.0683    -5.77
0.029  1.00
Ct Pt                                               -0.466    0.104    -4.46
0.047  1.00


Regression Equation in Uncoded Units

CH4 (µmole/ghLW) = -0.357 + 0.00422 Irradiance  (mW/cm2)
+ 0.6368 Reaction Time (h)
                   - 0.003353 Irradiance  (mW/cm2)*Reaction Time (h)
- 0.466 Ct Pt
```

Two factor DoE

All C products extended normalization response

Coded Coefficients

| Term | Effect | Coef | SE Coef | T-Value | P-Value | VIF |
|---|---|---|---|---|---|---|
| Constant | | 0.610 | 0.170 | 3.58 | 0.070 | |
| Irradiance (mW/cm2) | -0.581 | -0.290 | 0.170 | -1.70 | 0.231 | 1.00 |
| Reaction Time (h) | 0.445 | 0.223 | 0.170 | 1.31 | 0.321 | 1.00 |
| Irradiance (mW/cm2)*Reaction Time (h) | -0.788 | -0.394 | 0.170 | -2.31 | 0.147 | 1.00 |
| Ct Pt | | 0.062 | 0.260 | 0.24 | 0.833 | 1.00 |

Regression Equation in Uncoded Units

All C products (µmole/ghLW) = -0.359 + 0.00424 Irradiance (mW/cm2)
+ 0.637 Reaction Time (h)
- 0.00335 Irradiance (mW/cm2)*Reaction Time (h)
+ 0.062 Ct Pt

# REFERENCES


1. Edenhofer, O., et al., *Climate Change 2014: Mitigation of Climate Change*, in *Contribution of Working Group III to the Fifth Assessment Report of the Intergovernmental Panel on Climate Change*, O. Edenhofer, R. Pichs-Madruga, Y. Sokona, E. Farahani, S. Kadner, K. Seyboth, A. Adler, I. Baum, S. Brunner, P. Eickemeier, B. Kriemann, J. Savolainen, S. Schlömer, C. von Stechow, T. Zwickel and J.C. Minx, Editor. 2014, Intergovernmental Panel on Climate Change: Cambridge, United Kingdom and New York, NY, USA.

2. Trenberth, K.E., J.T. Houghton, and L.G. Meira Filho, *The Climate System: an Overview, Climate Change 1995: The science of climate change, contribution of working group 1 to the Second Assessment Report of the IPCC*, L.G.M.F. J.T. Houghton, B.A. Callander, N. Harris, A. Kattenberg and K. Maskell, Editor. 1995, IPCC. p. 51-64.

3. Downing, C., *Assessing Adaptation Knowledge in Europe: Vulnerability to Climate Change*. 2017, European Commission: Avalible online at ec.europa.eu/clima/sites/clima/files/adaptation/what/docs/climate_change_vulnerability_en.pdf [Accessed 2018 05 April]. p. 67.

4. Penistone, A., *2015 UK Greenhouse Gas Emissions, Final Figures*, E.I.S. Department for Business, Editor. 2017: 3 Whitehall Place, London, SW1A 2AW, 1 Victoria Street, London, SW1H 0ET. p. 53.

5. Harvey, L.D.D., *A Guide to Global Warming Potentials (GWPS).* Energy Policy, 1993. **21**(1): p. 24-34.

6. Spokas, K., J. Bogner, J.P. Chanton, M. Morcet, C. Aran, C. Graff, Y. Moreau-Le Golvan, and I. Hebe, *Methane mass balance at three landfill sites: What is the efficiency of capture by gas collection systems?* Waste Management, 2006. **26**(5): p. 516-525.

7. Suberu, M.Y., N. Bashir, and M.W. Mustafa, *Biogenic waste methane emissions and methane optimization for bioelectricity in Nigeria.* Renewable & Sustainable Energy Reviews, 2013. **25**: p. 643-654.

8. Montes, F., R. Meinen, C. Dell, A. Rotz, A.N. Hristov, J. Oh, G. Waghorn, P.J. Gerber, B. Henderson, H.P.S. Makkar, and J. Dijkstra, *SPECIAL TOPICS-Mitigation of methane and nitrous oxide emissions from animal operations: II. A review of manure management mitigation options.* Journal of Animal Science, 2013. **91**(11): p. 5070-5094.

9. Le Quéré, C., et al., *Global Carbon Budget 2016.* Earth Syst. Sci. Data, 2016. **8**(2): p. 605-649.

10. Institute, G.C., *The Global Status of CCS: 2016*. 2016, Global CCS Institute: Australia. p. 28.

11. Solomon, S., D. Qin, M. Manning, R.B. Alley, T. Berntsen, N.L. Bindoff, Z. Chen, A. Chidthaisong, J.M. Gregory, G.C. Hegerl, M. Heimann, B. Hewitson, B.J. Hoskins, F. Joos, J. Jouzel, V. Kattsov, U. Lohmann, T. Matsuno, M. Molina,

N. Nicholls, J. Overpeck, G. Raga, V. Ramaswamy, J. Ren, M. Rusticucci, R. Somerville, T.F. Stocker, P. Whetton, and R.A.W.a.D. Wratt, *Climate Change 2007: The Physical Science Basis*, in *Fourth Assessment Report of the Intergovernmental Panel on Climate Change*, S. Solomon, D. Qin, M. Manning, Z. Chen, M. Marquis, K.B. Averyt, M.Tignor and H.L. Miller, Editor. 2007: Cambridge, United Kingdom and New York, NY, USA.

12. Anderson, K. and A. Bows, *Reframing the climate change challenge in light of post-2000 emission trends.* Philosophical Transactions of the Royal Society a-Mathematical Physical and Engineering Sciences, 2008. **366**(1882): p. 3863-3882.

13. Knutti, R., M.R. Allen, P. Friedlingstein, J.M. Gregory, G.C. Hegerl, G.A. Meehl, M. Meinshausen, J.M. Murphy, G.K. Plattner, S.C.B. Raper, T.F. Stocker, P.A. Stott, H. Teng, and T.M.L. Wigley, *A review of uncertainties in global temperature projections over the twenty-first century.* Journal of Climate, 2008. **21**(11): p. 2651-2663.

14. Van Vuuren, D.P., M. Meinshausen, G.K. Plattner, F. Joos, K.M. Strassmann, S.J. Smith, T.M.L. Wigley, S.C.B. Raper, K. Riahi, F. de la Chesnaye, M.G.J. den Elzen, J. Fujino, K. Jiang, N. Nakicenovic, S. Paltsev, and J.M. Reilly, *Temperature increase of 21st century mitigation scenarios.* Proceedings of the National Academy of Sciences of the United States of America, 2008. **105**(40): p. 15258-15262.

15. Hansen, J., M. Sato, P. Kharecha, D. Beerling, R. Berner, V. Masson-Delmotte, M. Pagani, M. Raymo, D.L. Royer, and J.C. Zachos, *Target atmospheric $CO_2$: Where should humanity aim?* 2008.

16. Mac Dowell, N., P.S. Fennell, N. Shah, and G.C. Maitland, *The role of $CO_2$ capture and utilization in mitigating climate change.* Nature Climate Change, 2017. **7**(4): p. 243-249.

17. Stern, N., *The economics of climate change : the Stern review*. 2007: CUP, 2007.

18. DECC, *2012 UK Greenhouse Gas Emissions, Provisional Figures and 2011 UK Greenhouse Gas Emissions, Final Figures by Fuel Type and End-User*, D.o.E.a.C. Change, Editor. 2013: UK. p. 33.

19. MacKay, **D.J.C.**, *Sustainable Energy – without the hot air*. 2008, Available free online from www.withouthotair.com [Accessed 2018 05 April]: UIT Cambridge.

20. Builes, S. and L.F. Vega, *Effect of Immobilized Amines on the Sorption Properties of Solid Materials: Impregnation versus Grafting.* Langmuir, 2013. **29**(1): p. 199-206.

21. Yu, C.-H., C.-H. Huang, and C.-S. Tan, *A Review of $CO_2$ Capture by Absorption and Adsorption.* Aerosol and Air Quality Research, 2012. **12**(5): p. 745-769.

22. Heydari-Gorji, A., Y. Belmabkhout, and A. Sayari, *Degradation of amine-supported $CO_2$ adsorbents in the presence of oxygen-containing gases.* Microporous and Mesoporous Materials, 2011. **145**(1-3): p. 146-149.

23. *$CO_2$ Capture Technologies, Technology Options for $CO_2$ Capture: Report sponsored by the Global Carbon Capture and Storage Institute, produced by Electric Power Research Institute*. 2012, Global CCS Institute: Palo Alto, CA. p. 11.

24. Song, C.S., *Global challenges and strategies for control, conversion and utilization of $CO_2$ for sustainable development involving energy, catalysis, adsorption and chemical processing.* Catalysis Today, 2006. **115**(1-4): p. 2-32.

25. *IPCC Special Report on Carbon Dioxide Capture and Storage Prepared by Working Group III*, O.D. Bert Metz, Heleen de Coninck, Manuela Loos, and Leo Meyer, Editor. 2005, IPCC: Cambridge, United Kingdom and New York, NY, USA. p. 442.

26. Metz, B. and e. al, *IPCC special report on carbon dioxide capture and storage* 2005: Cambridge : Cambridge University Press, for the Intergovernmental Panel on Climate Change, 2005.

27. Kondratenko, E.V., G. Mul, J. Baltrusaitis, G.O. Larrazabal, and J. Perez-Ramirez, *Status and perspectives of $CO_2$ conversion into fuels and chemicals by catalytic, photocatalytic and electrocatalytic processes.* Energy & Environmental Science, 2013. **6**(11): p. 3112-3135.

28. Cheng, J., M. Zhang, G. Wu, X. Wang, J.H. Zhou, and K.F. Cen, *Photoelectrocatalytic Reduction of $CO_2$ into Chemicals Using Pt-Modified Reduced Graphene Oxide Combined with Pt-Modified $TiO_2$ Nanotubes.* Environmental Science & Technology, 2014. **48**(12): p. 7076-7084.

29. Wang, G., H. Wang, Y. Ling, Y. Tang, X. Yang, R.C. Fitzmorris, C. Wang, J.Z. Zhang, and Y. Li, *Hydrogen-Treated $TiO_2$ Nanowire Arrays for Photoelectrochemical Water Splitting.* Nano Letters, 2011. **11**(7): p. 3026-3033.

30. You, Z., W. Deng, Q. Zhang, and Y. Wang, *Hydrogenation of carbon dioxide to light olefins over non-supported iron catalyst.* Chinese Journal of Catalysis, 2013. **34**(5): p. 956-963.

31. Ogden, J.M., *Prospects for building a hydrogen energy infrastructure.* Annual Review of Energy and the Environment, 1999. **24**: p. 227-279.

32. Haryanto, A., S. Fernando, N. Murali, and S. Adhikari, *Current status of hydrogen production techniques by steam reforming of ethanol: A review.* Energy & Fuels, 2005. **19**(5): p. 2098-2106.

33. Singh, V., I.J.C. Beltran, J.C. Ribot, and P. Nagpal, *Photocatalysis Deconstructed: Design of a New Selective Catalyst for Artificial Photosynthesis.* Nano Letters, 2014. **14**(2): p. 597-603.

34. Chancellor, W.J., *Global Energy Flows and their Food System Components.* Invited Paper from International Commission of Agricultural Engineering (CIGR, Commission Internationale du Genie Rural) E-Journal, 2001. **3**: p. 14.

35. Zhu, X.-G., S.P. Long, and D.R. Ort, *What is the maximum efficiency with which photosynthesis can convert solar energy into biomass?* Current Opinion in Biotechnology, 2008. **19**(2): p. 153-159.

36. Barber, J. and P.D. Tran, *From natural to artificial photosynthesis.* Journal of the Royal Society Interface, 2013. **10**(81).

37. Cogdell, R.J., T.H. Brotosudarmo, A.T. Gardiner, P.M. Sanchez, and L. Cronin, *Artificial photosynthesis–solar fuels: current status and future prospects.* Biofuels, 2010. **1**(6): p. 861-876.

38. Izumi, Y., *Recent advances in the photocatalytic conversion of carbon dioxide to fuels with water and/or hydrogen using solar energy and beyond.* Coordination Chemistry Reviews, 2013. **257**(1): p. 171-186.

39. Anpo, M., *Photocatalytic reduction of $CO_2$ with $H_2O$ on highly dispersed Ti-oxide catalysts as a model of artificial photosynthesis.* Journal of $CO_2$ Utilization, 2013. **1**(0): p. 8-17.

40. Liu, C., B.C. Colon, M. Ziesack, P.A. Silver, and D.G. Nocera, *Water splitting-biosynthetic system with $CO_2$ reduction efficiencies exceeding photosynthesis.* Science, 2016. **352**(6290): p. 1210-1213.

41. Vinyard, D.J., G.M. Ananyev, and G.C. Dismukes, *Photosystem II: The Reaction Center of Oxygenic Photosynthesis.* Annual Review of Biochemistry, Vol 82, 2013. **82**: p. 577-606.

42. Sachs, M., E. Pastor, A. Kafizas, and J.R. Durrant, *Evaluation of Surface State Mediated Charge Recombination in Anatase and Rutile $TiO_2$.* Journal of Physical Chemistry Letters, 2016. **7**(19): p. 3742-3746.

43. Ohtani, B., *Photocatalysis A to Z-What we know and what we do not know in a scientific sense.* Journal of Photochemistry and Photobiology C-Photochemistry Reviews, 2010. **11**(4): p. 157-178.

44. Melo, M.A., A. Morais, and A.F. Nogueira, *Boosting the solar-light-driven methanol production through $CO_2$ photoreduction by loading $Cu_2O$ on $TiO_2$-pillared $K_2Ti_4O_9$.* Microporous and Mesoporous Materials, 2016. **234**: p. 1-11.

45. Tahir, M. and N.S. Amin, *Performance analysis of nanostructured NiO-$In_2O_3$/$TiO_2$ catalyst for $CO_2$ photoreduction with H-2 in a monolith photoreactor.* Chemical Engineering Journal, 2016. **285**: p. 635-649.

46. Stechel, E.B. and J.E. Miller, *Re-energizing $CO_2$ to fuels with the sun: Issues of efficiency, scale, and economics.* Journal of $CO_2$ Utilization, 2013. **1**: p. 28-36.

47. Ohtani, B., *Revisiting the fundamental physical chemistry in heterogeneous photocatalysis: its thermodynamics and kinetics.* Physical Chemistry Chemical Physics, 2014. **16**(5): p. 1788-1797.

48. Yang, C.-C., Y.-H. Yu, B. van der Linden, J.C.S. Wu, and G. Mul, *Artificial Photosynthesis over Crystalline $TiO_2$-Based Catalysts: Fact or Fiction?* Journal of the American Chemical Society, 2010. **132**(24): p. 8398-8406.

49. Klaewkla, R., M. Arend, and W.F. Hoelderich, *A Review of Mass Transfer Controlling the Reaction Rate in Heterogeneous Catalytic Systems, Chapter 29, Mass Transfer - Advanced Aspects,* ed. D.H. Nakajima. 2011: INTECH Open Access Publisher.

50. Machado, R.M., *Fundamentals of Mass Transfer and Kinetics for the Hydrogenation of Nitrobenzene to Aniline* 1994, Air Products and Chemicals, Inc.

51. Najafabadi, A.T., *Emerging applications of graphene and its derivatives in carbon capture and conversion: Current status and future prospects.* Renewable & Sustainable Energy Reviews, 2015. **41**: p. 1515-1545.

52. Rao, K.V., R. Haldar, T.K. Maji, and S.J. George, *Porous polyimides from polycyclic aromatic linkers: Selective $CO_2$ capture and hydrogen storage.* Polymer, 2014. **55**(6): p. 1452-1458.

53. Liu, X.H., J.G. Ma, Z. Niu, G.M. Yang, and P. Cheng, *An Efficient Nanoscale Heterogeneous Catalyst for the Capture and Conversion of Carbon Dioxide at Ambient Pressure.* Angewandte Chemie-International Edition, 2015. **54**(3): p. 988-991.

54. Xiao, T., T. Shirvani, O. Inderwildi, S. Gonzalez-Cortes, H. AlMegren, D. King, and P. Edwards, *The Catalyst Selectivity Index (CSI): A Framework and Metric to Assess the Impact of Catalyst Efficiency Enhancements upon Energy and $CO_2$ Footprints.* Topics in Catalysis, 2015. **58**(10-11): p. 682-695.

55. Trudewind, C.A., A. Schreiber, and D. Haumann, *Photocatalytic methanol and methane production using captured $CO_2$ from coal-fired power plants. Part I - a Life Cycle Assessment.* Journal of Cleaner Production, 2014. **70**: p. 27-37.

56. Tahir, M. and N.S. Amin, *Photocatalytic reduction of carbon dioxide with water vapors over montmorillonite modified $TiO_2$ nanocomposites.* Applied Catalysis B-Environmental, 2013. **142**: p. 512-522.

57. Sastre, F., A.V. Puga, L.C. Liu, A. Corma, and H. Garcia, *Complete Photocatalytic Reduction of $CO_2$ to Methane by $H_2$ under Solar Light Irradiation.* Journal of the American Chemical Society, 2014. **136**(19): p. 6798-6801.

58. Tahir, M., B. Tahir, and N.A.S. Amin, *Synergistic effect in plasmonic Au/Ag alloy NPs co-coated $TiO_2$ NWs toward visible-light enhanced $CO_2$ photoreduction to fuels.* Applied Catalysis B-Environmental, 2017. **204**: p. 548-560.

59. Tahir, B., M. Tahir, and N.A.S. Amin, *Photocatalytic $CO_2$ conversion over Au/$TiO_2$ nanostructures for dynamic production of clean fuels in a monolith photoreactor.* Clean Technologies and Environmental Policy, 2016. **18**(7): p. 2147-2160.

60. Lee, K.Y., K. Sato, and A.R. Mohamed, *Facile synthesis of anatase-rutile $TiO_2$ composites with enhanced $CO_2$ photoreduction activity and the effect of Pt loading on product selectivity.* Materials Letters, 2016. **163**: p. 240-243.

61. Liu, L.J., Y.Q. Jiang, H.L. Zhao, J.T. Chen, J.L. Cheng, K.S. Yang, and Y. Li, *Engineering Coexposed {001} and {101} Facets in Oxygen-Deficient $TiO_2$ Nanocrystals for Enhanced $CO_2$ Photoreduction under Visible Light.* ACS Catalysis, 2016. **6**(2): p. 1097-1108.

62. Tan, L.L., W.J. Ong, S.P. Chai, and A.R. Mohamed, *Photocatalytic reduction of $CO_2$ with $H_2O$ over graphene oxide supported oxygen-rich $TiO_2$ hybrid photocatalyst under visible light irradiation: Process and kinetic studies.* Chemical Engineering Journal, 2017. **308**: p. 248-255.

63. Shi, H.F., C.L. Zhang, C.P. Zhou, and G.Q. Chen, *Conversion of $CO_2$ into renewable fuel over Pt-g-$C_3N_4$/$KNbO_3$ composite photocatalyst.* RSC Advances, 2015. **5**(113): p. 93615-93622.

64. Chen, L., M.E. Graham, G.H. Li, D.R. Gentner, N.M. Dimitrijevic, and K.A. Gray, *Photoreduction of $CO_2$ by $TiO_2$ nanocomposites synthesized through reactive direct current magnetron sputter deposition.* Thin Solid Films, 2009. **517**(19): p. 5641-5645.

65. Lo, C.C., C.H. Hung, C.S. Yuan, and J.F. Wu, *Photoreduction of carbon dioxide with $H_2$ and $H_2O$ over $TiO_2$ and $ZrO_2$ in a circulated photocatalytic reactor.* Solar Energy Materials and Solar Cells, 2007. **91**(19): p. 1765-1774.

66. Koci, K., L. Matejova, L. Obalova, L. Capek, and J.C.S. Wu, *Preparation, characterization and photocatalytic performance of $TiO_2$ prepared by using pressurized fluids in $CO_2$ reduction and $N_2O$ decomposition.* Journal of Sol-Gel Science and Technology, 2015. **76**(3): p. 621-629.

67. Wang, H.Q., Z.X. Sun, Q. Li, Q.J. Tang, and Z.B. Wu, *Surprisingly advanced $CO_2$ photocatalytic conversion over thiourea derived g-$C_3N_4$ with water vapor while introducing 200-420 nm UV light.* Journal of $CO_2$ Utilization, 2016. **14**: p. 143-151.

68. Li, H.L., X.Y. Wu, J. Wang, Y. Gao, L.Q. Li, and K.M. Shih, *Enhanced activity of Ag-MgO-$TiO_2$ catalyst for photocatalytic conversion of $CO_2$ and $H_2O$ into $CH_4$.* International Journal of Hydrogen Energy, 2016. **41**(20): p. 8479-8488.

69. Xiong, Z., Y.C. Zhao, J.Y. Zhang, and C.G. Zheng, *Efficient photocatalytic reduction of $CO_2$ into liquid products over cerium doped titania nanoparticles synthesized by a sol-gel auto-ignited method.* Fuel Processing Technology, 2015. **135**: p. 6-13.

70. Olivo, A., V. Trevisan, E. Ghedini, F. Pinna, C.L. Bianchi, A. Naldoni, G. Cruciani, and M. Signoretto, *$CO_2$ photoreduction with water: Catalyst and process investigation.* Journal of $CO_2$ Utilization, 2015. **12**: p. 86-94.

71. Zhao, H.L., J.Y. Xu, L.J. Liu, G.Y. Rao, C.Y. Zhao, and Y. Li, *$CO_2$ photoreduction with water vapor by Ti-embedded MgAl layered double hydroxides.* Journal of $CO_2$ Utilization, 2016. **15**: p. 15-23.

72. Maruo, Y.Y., M. Sasaki, S. Hino, A. Sato, and Ieee, *Effect of $TiO_2$ crystal structure on $CO_2$ photoreduction using Au nanoparticles on $TiO_2$ catalyst.* 2016 Ieee 16th International Conference on Nanotechnology (Ieee-Nano), 2016: p. 559-562.

73. Liang, Y.T., B.K. Vijayan, K.A. Gray, and M.C. Hersam, *Minimizing Graphene Defects Enhances Titania Nanocomposite-Based Photocatalytic Reduction of $CO_2$ for Improved Solar Fuel Production.* Nano Letters, 2011. **11**(7): p. 2865-2870.

74. Wang, T., X.G. Meng, G.G. Liu, K. Chang, P. Li, Q. Kang, L.Q. Liu, M. Li, S.X. Ouyang, and J.H. Ye, *In situ synthesis of ordered mesoporous Co-doped $TiO_2$ and its enhanced photocatalytic activity and selectivity for the reduction of $CO_2$.* Journal of Materials Chemistry A, 2015. **3**(18): p. 9491-9501.

75. Lo, C.C., C.H. Hung, C.S. Yuan, and Y.L. Hung, *Parameter effects and reaction pathways of photoreduction of $CO_2$ over $TiO_2/SO_4^{2-}$ photocatalyst.* Chinese Journal of Catalysis, 2007. **28**(6): p. 528-534.

76. Ola, O. and M.M. Maroto-Valer, *Synthesis, characterization and visible light photocatalytic activity of metal based $TiO_2$ monoliths for $CO_2$ reduction.* Chemical Engineering Journal, 2016. **283**: p. 1244-1253.

77. Ola, O. and M.M. Maroto-Valer, *Copper based $TiO_2$ honeycomb monoliths for $CO_2$ photoreduction.* Catalysis Science & Technology, 2014. **4**(6): p. 1631-1637.

78. Fang, B.Z., Y.L. Xing, A. Bonakdarpour, S.C. Zhang, and D.P. Wilkinson, *Hierarchical CuO-$TiO_2$ Hollow Microspheres for Highly Efficient Photodriven Reduction of $CO_2$ to $CH_4$.* ACS Sustainable Chemistry & Engineering, 2015. **3**(10): p. 2381-2388.

79. Kar, P., S. Farsinezhad, N. Mahdi, Y. Zhang, U. Obuekwe, H. Sharma, J. Shen, N. Semagina, and K. Shankar, *Enhanced $CH_4$ yield by photocatalytic $CO_2$ reduction using $TiO_2$ nanotube arrays grafted with Au, Ru, and ZnPd nanoparticles.* Nano Research, 2016. **9**(11): p. 3478-3493.

80. Wang, Q.L., Z.G. Zhang, X.D. Cheng, Z.F. Huang, P.M. Dong, Y. Chen, and X.W. Zhang, *Photoreduction of $CO_2$ using black $TiO_2$ films under solar light.* Journal of $CO_2$ Utilization, 2015. **12**: p. 7-11.

81. Indrakanti, V.P., J.D. Kubicki, and H.H. Schobert, *Photoinduced activation of $CO_2$ on Ti-based heterogeneous catalysts: Current state, chemical physics-based insights and outlook.* Energy & Environmental Science, 2009. **2**(7): p. 745-758.

82. Dhakshinamoorthy, A., S. Navalon, A. Corma, and H. Garcia, *Photocatalytic $CO_2$ reduction by $TiO_2$ and related titanium containing solids.* Energy & Environmental Science, 2012. **5**(11): p. 9217-9233.

83. Chen, D., X.G. Zhang, and A.F. Lee, *Synthetic strategies to nanostructured photocatalysts for $CO_2$ reduction to solar fuels and chemicals.* Journal of Materials Chemistry A, 2015. **3**(28): p. 14487-14516.

84. Bligaard, T., R.M. Bullock, C.T. Campbell, J.G.G. Chen, B.C. Gates, R.J. Gorte, C.W. Jones, W.D. Jones, J.R. Kitchin, and S.L. Scott, *Toward Benchmarking in Catalysis Science: Best Practices, Challenges, and Opportunities.* ACS Catalysis, 2016. **6**(4): p. 2590-2602.

85. Hodes, G., *Photoelectrochemical Cell Measurements: Getting the Basics Right.* Journal of Physical Chemistry Letters, 2012. **3**(9): p. 1208-1213.

86. Xing, Z., X. Zong, J. Pan, and L.Z. Wang, *On the engineering part of solar hydrogen production from water splitting: Photoreactor design.* Chemical Engineering Science, 2013. **104**: p. 125-146.

87. Chen, Z., T.F. Jaramillo, T.G. Deutsch, A. Kleiman-Shwarsctein, A.J. Forman, N. Gaillard, R. Garland, K. Takanabe, C. Heske, M. Sunkara, E.W. McFarland, K. Domen, E.L. Miller, J.A. Turner, and H.N. Dinh, *Accelerating materials development for photoelectrochemical hydrogen production: Standards for methods, definitions, and reporting protocols.* Journal of Materials Research, 2010. **25**(01): p. 3-16.

88. Ifang, S., M. Gallus, S. Liedtke, R. Kurtenbach, P. Wiesen, and J. Kleffmann, *Standardization methods for testing photo-catalytic air remediation materials: Problems and solution.* Atmospheric Environment, 2014. **91**: p. 154-161.

89. Braslavsky, S.E., A.M. Braun, A.E. Cassano, A.V. Emeline, M.I. Litter, L. Palmisano, V.N. Parmon, N. Serpone, O.M. Alfano, M. Anpo, V. Augugliaro, C. Bohne, S. Esplugas, E. Oliveros, C. von Sonntag, R.G. Weiss, and M. Schiavello, *Glossary of terms used in photocatalysis and radiation catalysis (IUPAC Recommendations 2011).* Pure and Applied Chemistry, 2011. **83**(4): p. 931-1014.

90. Buriak, J.M., P.V. Kamat, and K.S. Schanze, *Best Practices for Reporting on Heterogeneous Photocatalysis.* ACS Applied Materials & Interfaces, 2014. **6**(15): p. 11815-11816.

91. Serpone, N. and A. Salinaro, *Terminology, relative photonic efficiencies and quantum yields in heterogeneous photocatalysis. Part I: Suggested protocol (technical report).* Pure and Applied Chemistry, 1999. **71**(2): p. 303-320.

92. Herrmann, J.-M., *Fundamentals and misconceptions in photocatalysis.* Journal of Photochemistry and Photobiology A-Chemistry, 2010. **216**(2-3): p. 85-93.

93. Li, H.X., Z.F. Bian, J. Zhu, Y.N. Huo, H. Li, and Y.F. Lu, *Mesoporous Au/$TiO_2$ nanocomposites with enhanced photocatalytic activity.* Journal of the American Chemical Society, 2007. **129**(15): p. 4538-+.

94. Bruner, L. and J. Kozak, *Information on the photocatalysis I The light reaction in uranium salt plus oxalic acid mixtures.* Zeitschrift Fur Elektrochemie Und Angewandte Physikalische Chemie, 1911. **17**: p. 354-360.

95. Baly, E.C.C., I.M. Heilbron, and W.F. Barker, *Photocatalysis. Part I. The synthesis of formaldehyde and carbohydrates from carbon dioxide and water.* Journal of the Chemical Society, 1921. **119**: p. 1025-1035.

96. Herrmann, J.-M., *Photocatalysis fundamentals revisited to avoid several misconceptions.* Applied Catalysis B-Environmental, 2010. **99**(3-4): p. 461-468.

97. Serpone, N., A.V. Emeline, S. Horikoshi, V.N. Kuznetsov, and V.K. Ryabchuk, *On the genesis of heterogeneous photocatalysis: a brief historical perspective in the period 1910 to the mid-1980s.* Photochemical & Photobiological Sciences, 2012. **11**(7): p. 1121-1150.

98. Ohtani, B., *Revisiting the Original Works Related to Titania Photocatalysis: A Review of Papers in the Early Stage of Photocatalysis Studies.* Electrochemistry, 2014. **82**(6): p. 414-425.

99. Shkrob, I.A., T.W. Marin, H. He, and P. Zapol, *Photoredox Reactions and the Catalytic Cycle for Carbon Dioxide Fixation and Methanogenesis on Metal Oxides.* Journal of Physical Chemistry C, 2012. **116**(17): p. 9450-9460.

100. Serpone, N., A. Salinaro, A. Emeline, and V. Ryabchuk, *Turnovers and photocatalysis - A mathematical description.* Journal of Photochemistry and Photobiology A-Chemistry, 2000. **130**(2-3): p. 83-94.

101. Serpone, N. and A.V. Emeline, *Suggested terms and definitions in photocatalysis and radiocatalysis.* International Journal of Photoenergy, 2002. **4**(3): p. 91-131.

102. Jiang, Z., T. Xiao, V.L. Kuznetsov, and P.P. Edwards, *Turning carbon dioxide into fuel.* Philosophical Transactions of the Royal Society a-Mathematical Physical and Engineering Sciences, 2010. **368**(1923): p. 3343-3364.

103. Wang, W.N., J. Soulis, Y.J. Yang, and P. Biswas, *Comparison of $CO_2$ Photoreduction Systems: A Review.* Aerosol and Air Quality Research, 2014. **14**(2): p. 533-549.

104. Emeline, A.V., V.K. Ryabchuk, and N. Serpone, *Photoreactions occurring on metal-oxide surfaces are not all photocatalytic - Description of criteria and conditions for processes to be photocatalytic.* Catalysis Today, 2007. **122**(1-2): p. 91-100.

105. Childs, L.P. and D.F. Ollis, *Is Photocatalysis Catalytic.* Journal of Catalysis, 1980. **66**(2): p. 383-390.

106. Nguyen, C.C., N.N. Vu, and T.O. Do, *Recent advances in the development of sunlight-driven hollow structure photocatalysts and their applications.* Journal of Materials Chemistry A, 2015. **3**(36): p. 18345-18359.

107. Habisreutinger, S.N., L. Schmidt-Mende, and J.K. Stolarczyk, *Photocatalytic reduction of $CO_2$ on $TiO_2$ and other semiconductors.* Angewandte Chemie (International ed. in English), 2013. **52**(29): p. 7372-408.

108. Mohapatra, L. and K. Parida, *A review on the recent progress, challenges and perspective of layered double hydroxides as promising photocatalysts.* Journal of Materials Chemistry A, 2016. **4**(28): p. 10744-10766.

109. Li, K.F., X.Q. An, K.H. Park, M. Khraisheh, and J.W. Tang, *A critical review of $CO_2$ photoconversion: Catalysts and reactors.* Catalysis Today, 2014. **224**: p. 3-12.

110. Gázquez, M.J., J.P. Bolívar, R. Garcia-Tenorio, and F. Vaca, *A Review of the Production Cycle of Titanium Dioxide Pigment.* Materials Sciences and Applications, 2014(5): p. 441-458.

111. Davies, E., *Endangered Elements.* Chemistry World, 2011(January): p. 5.

112. Liou, P.-Y., S.-C. Chen, J.C.S. Wu, D. Liu, S. Mackintosh, M. Maroto-Valer, and R. Linforth, *Photocatalytic $CO_2$ reduction using an internally illuminated monolith photoreactor.* Energy & Environmental Science, 2011. **4**(4): p. 1487-1494.

113. Tan, J.Z.Y., Y. Fernandez, D. Liu, M. Maroto-Valer, J. Bian, and X. Zhang, *Photoreduction of $CO_2$ using copper-decorated $TiO_2$ nanorod films with localized surface plasmon behavior.* Chemical Physics Letters, 2012. **531**: p. 149-154.

114. Hashimoto, K., H. Irie, and A. Fujishima, *$TiO_2$ photocatalysis: A historical overview and future prospects.* Japanese Journal of Applied Physics Part 1-Regular Papers Brief Communications & Review Papers, 2005. **44**(12): p. 8269-8285.

115. Mori, K., H. Yamashita, and M. Anpo, *Photocatalytic reduction of $CO_2$ with $H_2O$ on various titanium oxide photocatalysts.* Rsc Advances, 2012. **2**(8): p. 3165-3172.

116. Fujishima, A., X. Zhang, and D.A. Tryk, *$TiO_2$ photocatalysis and related surface phenomena.* Surface Science Reports, 2008. **63**(12): p. 515-582.

117. Fujishima, A. and X.T. Zhang, *Titanium dioxide photocatalysis: present situation and future approaches.* Comptes Rendus Chimie, 2006. **9**(5-6): p. 750-760.

118. Li, C., S. Zhang, B. Zhang, D. Su, S. He, Y. Zhao, J. Liu, F. Wang, M. Wei, D.G. Evans, and X. Duan, *Photohole-oxidation-assisted anchoring of ultra-small Ru clusters onto $TiO_2$ with excellent catalytic activity and stability.* Journal of Materials Chemistry A, 2013. **1**(7): p. 2461-2467.

119. Liu, J., C. Li, F. Wang, S. He, H. Chen, Y. Zhao, M. Wei, D.G. Evans, and X. Duan, *Enhanced low-temperature activity of $CO_2$ methanation over highly-dispersed Ni/$TiO_2$ catalyst.* Catalysis Science & Technology, 2013. **3**(10): p. 2627-2633.

120. Lei, J.Y., H. Li, J.L. Zhang, and M. Anpo, *Mixed-Phase $TiO_2$ Nanomaterials as Efficient Photocatalysts.* Low-Dimensional and Nanostructured Materials and Devices: Properties, Synthesis, Characterization, Modelling and Applications, 2016: p. 423-460.

121. Landmann, M., E. Rauls, and W.G. Schmidt, *The electronic structure and optical response of rutile, anatase and brookite $TiO_2$.* Journal of Physics-Condensed Matter, 2012. **24**(19).

122. Li, J.G., T. Ishigaki, and X.D. Sun, *Anatase, brookite, and rutile nanocrystals via redox reactions under mild hydrothermal conditions: Phase-selective synthesis and physicochemical properties.* Journal of Physical Chemistry C, 2007. **111**(13): p. 4969-4976.

123. Diebold, U., *The surface science of titanium dioxide.* Surface Science Reports, 2003. **48**(5-8): p. 53-229.

124. Chang, X., T. Wang, and J. Gong, *$CO_2$ photo-reduction: insights into $CO_2$ activation and reaction on surfaces of photocatalysts.* Energy & Environmental Science, 2016. **9**(7): p. 2177-2196.

125. Inoue, T., A. Fujishima, S. Konishi, and K. Honda, *Photoelectrocatalytic Reduction of Carbon-Dioxide in Aqueous Suspensions of Semiconductor Powders.* Nature, 1979. **277**(5698): p. 637-638.

126. Pool, R.E., *Molecular orientation at biological interfaces: Water and lipids studied through surface-specific vibrational spectroscopy*, in *Van der Waals-Zeeman Institute*. 2013, University of Amsterdam. p. 130.

127. Clark, J.H., M.S. Dyer, R.G. Palgrave, C.P. Ireland, J.R. Darwent, J.B. Claridge, and M.J. Rosseinsky, *Visible Light Photo-oxidation of Model Pollutants Using $CaCu_3Ti_4O_{12}$: An Experimental and Theoretical Study of Optical Properties, Electronic Structure, and Selectivity.* Journal of the American Chemical Society, 2011. **133**(4): p. 1016-1032.

128. Koning, R.E. *Light*. 1994 [Accessed 2014 May 29]; *Plant Physiology Information Website*].

129. Wang, Y., B. Li, C. Zhang, L. Cui, S. Kang, X. Li, and L. Zhou, *Ordered mesoporous $CeO_2$-$TiO_2$ composites: Highly efficient photocatalysts for the reduction of $CO_2$ with $H_2O$ under simulated solar irradiation.* Applied Catalysis B-Environmental, 2013. **130**: p. 277-284.

130. Tada, H., M. Fujishima, and H. Kobayashi, *Photodeposition of metal sulfide quantum dots on titanium(IV) dioxide and the applications to solar energy conversion.* Chemical Society Reviews, 2011. **40**(7): p. 4232-4243.

131. Wang, C., R.L. Thompson, P. Ohodnicki, J. Baltrus, and C. Matranga, *Size-dependent photocatalytic reduction of $CO_2$ with PbS quantum dot sensitized $TiO_2$ heterostructured photocatalysts.* Journal of Materials Chemistry, 2011. **21**(35): p. 13452-13457.

132. Ong, W.-J., M.M. Gui, S.-P. Chai, and A.R. Mohamed, *Direct growth of carbon nanotubes on Ni/$TiO_2$ as next generation catalysts for photoreduction of $CO_2$ to methane by water under visible light irradiation.* RSC Advances, 2013. **3**(14): p. 4505-4509.

133. Ping, G., C. Wang, D. Chen, S. Liu, X. Huang, L. Qin, Y. Huang, and K. Shu, *Fabrication of self-organized $TiO_2$ nanotube arrays for photocatalytic reduction of $CO_2$.* Journal of Solid State Electrochemistry, 2013. **17**(9): p. 2503-2510.

134. Qin, G., Y. Zhang, X. Ke, X. Tong, Z. Sun, M. Liang, and S. Xue, *Photocatalytic reduction of carbon dioxide to formic acid, formaldehyde, and methanol using dye-sensitized $TiO_2$ film.* Applied Catalysis B-Environmental, 2013. **129**: p. 599-605.

135. Chang, J., Y. Ning, S. Wu, W. Niu, and S. Zhang, *Effectively Utilizing NIR Light Using Direct Electron Injection from Up-Conversion Nanoparticles to the $TiO_2$ Photoanode in Dye-Sensitized Solar Cells.* Advanced Functional Materials, 2013. **23**(47): p. 5910-5915.

136. Jiang, Z., L. Kong, F.S. Alenazey, Y. Qian, L. France, T. Xiao, and P.P. Edwards, *Enhanced visible-light-driven photocatalytic activity of mesoporous $TiO_2$-xNx derived from the ethylenediamine-based complex.* Nanoscale, 2013. **5**(12): p. 5396-5402.

137. Li, X., Z. Zhuang, W. Li, and H. Pan, *Photocatalytic reduction of $CO_2$ over noble metal-loaded and nitrogen-doped mesoporous $TiO_2$.* Applied Catalysis a-General, 2012. **429**: p. 31-38.

138. Qian, J., G. Cui, M. Jing, Y. Wang, M. Zhang, and J. Yang, *Hydrothermal Synthesis of Nitrogen-Doped Titanium Dioxide and Evaluation of Its Visible Light Photocatalytic Activity.* International Journal of Photoenergy, 2012.

139. Matsumoto, T., N. Iyi, Y. Kaneko, K. Kitamura, S. Ishihara, Y. Takasu, and Y. Murakami, *High visible-light photocatalytic activity of nitrogen-doped titania prepared from layered titania/isostearate nanocomposite.* Catalysis Today, 2007. **120**(2): p. 226-232.

140. Liu, S.-H. and H.-R. Syu, *One-step fabrication of N-doped mesoporous $TiO_2$ nanoparticles by self-assembly for photocatalytic water splitting under visible light.* Applied Energy, 2012. **100**: p. 148-154.

141. Parida, K.M. and B. Naik, *Synthesis of mesoporous $TiO_2$-xNx spheres by template free homogeneous co-precipitation method and their photo-catalytic activity under visible light illumination.* Journal of Colloid and Interface Science, 2009. **333**(1): p. 269-276.

142. Xiong, Z. and X.S. Zhao, *Nitrogen-Doped Titanate-Anatase Core-Shell Nanobelts with Exposed {101} Anatase Facets and Enhanced Visible Light Photocatalytic Activity.* Journal of the American Chemical Society, 2012. **134**(13): p. 5754-5757.

143. Martyanov, I.N., T. Berger, O. Diwald, S. Rodrigues, and K.J. Klabunde, *Enhancement of $TiO_2$ visible light photoactivity through accumulation of defects during reduction-oxidation treatment.* Journal of Photochemistry and Photobiology A-Chemistry, 2010. **212**(2-3): p. 135-141.

144. Liu, L., C. Zhao, H. Zhao, D. Pitts, and Y. Li, *Porous microspheres of MgO-patched $TiO_2$ for $CO_2$ photoreduction with $H_2O$ vapor: temperature-dependent activity and stability.* Chemical Communications, 2013. **49**(35): p. 3664-3666.

145. Tahir, M. and N.S. Amin, *Photocatalytic $CO_2$ reduction and kinetic study over In/$TiO_2$ nanoparticles supported microchannel monolith photoreactor.* Applied Catalysis A-General, 2013. **467**: p. 483-496.

146. Noy, D., C.C. Moser, and P.L. Dutton, *Design and engineering of photosynthetic light-harvesting and electron transfer using length, time, and energy scales.* Biochimica Et Biophysica Acta-Bioenergetics, 2006. **1757**(2): p. 90-105.

147. Zhao, H., L. Liu, J.M. Andino, and Y. Li, *Bicrystalline $TiO_2$ with controllable anatase-brookite phase content for enhanced $CO_2$ photoreduction to fuels.* Journal of Materials Chemistry A, 2013. **1**(28): p. 8209-8216.

148. Xie, S., Y. Wang, Q. Zhang, W. Fan, W. Deng, and Y. Wang, *Photocatalytic reduction of $CO_2$ with $H_2O$: significant enhancement of the activity of Pt-$TiO_2$ in $CH_4$ formation by addition of MgO.* Chemical Communications, 2013. **49**(24): p. 2451-2453.

149. Collado, L., P. Jana, B. Sierra, J.M. Coronado, P. Pizarro, D.P. Serrano, and V.A. de la Pena O'Shea, *Enhancement of hydrocarbon production via artificial photosynthesis due to synergetic effect of Ag supported on $TiO_2$ and ZnO semiconductors.* Chemical Engineering Journal, 2013. **224**: p. 128-135.

150. Liu, L., F. Gao, H. Zhao, and Y. Li, *Tailoring Cu valence and oxygen vacancy in Cu/$TiO_2$ catalysts for enhanced $CO_2$ photoreduction efficiency.* Applied Catalysis B-Environmental, 2013. **134**: p. 349-358.

151. Xu, H., S. Ouyang, P. Li, T. Kako, and J. Ye, *High-Active Anatase $TiO_2$ Nanosheets Exposed with 95% {100} Facets Toward Efficient $H_2$ Evolution and $CO_2$ Photoreduction.* ACS Applied Materials & Interfaces, 2013. **5**(4): p. 1348-1354.

152. Liu, L., D.T. Pitts, H. Zhao, C. Zhao, and Y. Li, *Silver-incorporated bicrystalline (anatase/brookite) $TiO_2$ microspheres for $CO_2$ photoreduction with water in the presence of methanol.* Applied Catalysis A-General, 2013. **467**: p. 474-482.

153. Tu, W.G., Y. Zhou, H.J. Li, P. Li, and Z.G. Zou, *Au@$TiO_2$ yolk-shell hollow spheres for plasmon-induced photocatalytic reduction of $CO_2$ to solar fuel via a local electromagnetic field.* Nanoscale, 2015. **7**(34): p. 14232-14236.

154. Ma, Y., X. Wang, Y. Jia, X. Chen, H. Han, and C. Li, *Titanium Dioxide-Based Nanomaterials for Photocatalytic Fuel Generations.* Chemical Reviews, 2014. **114**(19): p. 9987-10043.

155. Jeyalakshmi, V., R. Mahalakshmy, K.R. Krishnamurthy, and B. Viswanathan, *Titania based catalysts for photoreduction of carbon dioxide: Role of modifiers.* Indian Journal of Chemistry Section a-Inorganic Bio-Inorganic Physical Theoretical & Analytical Chemistry, 2012. **51**(9-10): p. 1263-1283.

156. Liu, L. and Y. Li, *Understanding the Reaction Mechanism of Photocatalytic Reduction of $CO_2$ with $H_2O$ on $TiO_2$-Based Photocatalysts: A Review.* Aerosol and Air Quality Research, 2014. **14**(2): p. 453-469.

157. Ollis, D.F., *Kinetic disguises in heterogeneous photocatalysis.* Topics in Catalysis, 2005. **35**(3-4): p. 217-223.

158. Murzin, D.Y., *Heterogeneous photocatalytic kinetics: Beyond the adsorption/desorption equilibrium concept.* Reaction Kinetics and Catalysis Letters, 2006. **89**(2): p. 277-284.

159. Yuan, Y.P., L.W. Ruan, J. Barber, S.C.J. Loo, and C. Xue, *Hetero-nanostructured suspended photocatalysts for solar-to-fuel conversion.* Energy & Environmental Science, 2014. **7**(12): p. 3934-3951.

160. Wu, J.S. and C.-W. Huang, *In situ DRIFTS study of photocatalytic $CO_2$ reduction under UV irradiation.* Frontiers of Chemical Engineering in China, 2010. **4**(2): p. 120-126.

161. Indrakanti, V.P., H.H. Schobert, and J.D. Kubicki, *Quantum Mechanical Modeling of $CO_2$ Interactions with Irradiated Stoichiometric and Oxygen-Deficient Anatase $TiO_2$ Surfaces: Implications for the Photocatalytic Reduction of $CO_2$.* Energy & Fuels, 2009. **23**: p. 5247-5256.

162. Liu, L., H. Zhao, J.M. Andino, and Y. Li, *Photocatalytic $CO_2$ Reduction with $H_2O$ on $TiO_2$ Nanocrystals: Comparison of Anatase, Rutile, and Brookite Polymorphs and Exploration of Surface Chemistry.* ACS Catalysis, 2012. **2**(8): p. 1817-1828.

163. Indrakanti, V.P., J.D. Kubicki, and H.H. Schobert, *Photoinduced activation of $CO_2$ on $TiO_2$ surfaces: Quantum chemical modeling of $CO_2$ adsorption on oxygen vacancies.* Fuel Processing Technology, 2011. **92**(4): p. 805-811.

164. Karamian, E. and S. Sharifnia, *On the general mechanism of photocatalytic reduction of $CO_2$.* Journal of $CO_2$ Utilization, 2016. **16**: p. 194-203.

165. Koci, K., L. Obalova, L. Matejova, D. Placha, Z. Lacny, J. Jirkovsky, and O. Solcova, *Effect of $TiO_2$ particle size on the photocatalytic reduction of $CO_2$.* Applied Catalysis B-Environmental, 2009. **89**(3-4): p. 494-502.

166. Dimitrijevic, N.M., B.K. Vijayan, O.G. Poluektov, T. Rajh, K.A. Gray, H.Y. He, and P. Zapol, *Role of Water and Carbonates in Photocatalytic Transformation of $CO_2$ to $CH_4$ on Titania.* Journal of the American Chemical Society, 2011. **133**(11): p. 3964-3971.

167. Lin, W.Y., H.X. Han, and H. Frei, *$CO_2$ splitting by $H_2O$ to CO and $O_2$ under UV light in TiMCM-41 silicate sieve.* Journal of Physical Chemistry B, 2004. **108**(47): p. 18269-18273.

168. Yang, C.C., J. Vernimmen, V. Meynen, P. Cool, and G. Mul, *Mechanistic study of hydrocarbon formation in photocatalytic $CO_2$ reduction over Ti-SBA-15.* Journal of Catalysis, 2011. **284**(1): p. 1-8.

169. Li, Y., W.N. Wang, Z.L. Zhan, M.H. Woo, C.Y. Wu, and P. Biswas, *Photocatalytic reduction of $CO_2$ with $H_2O$ on mesoporous silica supported $Cu/TiO_2$ catalysts.* Applied Catalysis B-Environmental, 2010. **100**(1-2): p. 386-392.

170. Srinivas, B., B. Shubhamangala, K. Lalitha, P.A.K. Reddy, V.D. Kumari, M. Subrahmanyam, and B.R. De, *Photocatalytic Reduction of $CO_2$ over Cu-$TiO_2$/Molecular Sieve 5A Composite.* Photochemistry and Photobiology, 2011. **87**(5): p. 995-1001.

171. Uner, D. and M.M. Oymak, *On the mechanism of photocatalytic $CO_2$ reduction with water in the gas phase.* Catalysis Today, 2012. **181**(1): p. 82-88.

172. Hou, W.B., W.H. Hung, P. Pavaskar, A. Goeppert, M. Aykol, and S.B. Cronin, *Photocatalytic Conversion of $CO_2$ to Hydrocarbon Fuels via Plasmon-Enhanced Absorption and Metallic Interband Transitions.* ACS Catalysis, 2011. **1**(8): p. 929-936.

173. Rakowski Dubois, M. and D.L. Dubois, *Development of Molecular Electrocatalysts for $CO_2$ Reduction and $H_2$ Production/Oxidation.* Accounts of Chemical Research, 2009. **42**(12): p. 1974-1982.

174. Peng, Y.-P., Y.-T. Yeh, S.I. Shah, and C.P. Huang, *Concurrent photoelectrochemical reduction of $CO_2$ and oxidation of methyl orange using nitrogen-doped $TiO_2$.* Applied Catalysis B-Environmental, 2012. **123**: p. 414-423.

175. Quang Duc, T., J.-Y. Liu, C.-C. Chung, and Y.-C. Ling, *Photocatalytic reduction of $CO_2$ on $FeTiO_3/TiO_2$ photocatalyst.* Catalysis Communications, 2012. **19**: p. 85-89.

176. Qin, S.Y., F. Xin, Y.D. Liu, X.H. Yin, and W. Ma, *Photocatalytic reduction of $CO_2$ in methanol to methyl formate over CuO-$TiO_2$ composite catalysts.* Journal of Colloid and Interface Science, 2011. **356**(1): p. 257-261.

177. Liu, L., C. Zhao, and Y. Li, *Spontaneous Dissociation of $CO_2$ to CO on Defective Surface of Cu(I)/$TiO_{2-x}$ Nanoparticles at Room Temperature.* Journal of Physical Chemistry C, 2012. **116**(14): p. 7904-7912.

178. Abou Asi, M., C. He, M.H. Su, D.H. Xia, L. Lin, H.Q. Deng, Y. Xiong, R.L. Qiu, and X.Z. Li, *Photocatalytic reduction of $CO_2$ to hydrocarbons using AgBr/$TiO_2$ nanocomposites under visible light.* Catalysis Today, 2011. **175**(1): p. 256-263.

179. Varghese, O.K., M. Paulose, T.J. LaTempa, and C.A. Grimes, *High-Rate Solar Photocatalytic Conversion of $CO_2$ and Water Vapor to Hydrocarbon Fuels.* Nano Letters, 2009. **9**(2): p. 731-737.

180. Iizuka, K., T. Wato, Y. Miseki, K. Saito, and A. Kudo, *Photocatalytic Reduction of Carbon Dioxide over Ag Cocatalyst-Loaded $ALa_4Ti_4O_{15}$ (A = Ca, Sr, and Ba) Using Water as a Reducing Reagent.* Journal of the American Chemical Society, 2011. **133**(51): p. 20863-20868.

181. Zhang, Q., T. Gao, J.M. Andino, and Y. Li, *Copper and iodine co-modified $TiO_2$ nanoparticles for improved activity of $CO_2$ photoreduction with water vapor.* Applied Catalysis B-Environmental, 2012. **123**: p. 257-264.

182. Fan, J., E.Z. Liu, L. Tian, X.Y. Hu, Q. He, and T. Sun, *Synergistic Effect of N and $Ni^{2+}$ on Nanotitania in Photocatalytic Reduction of $CO_2$.* Journal of Environmental Engineering-ASCE, 2011. **137**(3): p. 171-176.

183. Tan, L.L., W.J. Ong, S.P. Chai, and A.R. Mohamed, *Noble metal modified reduced graphene oxide/$TiO_2$ ternary nanostructures for efficient visible-light-driven photoreduction of carbon dioxide into methane.* Applied Catalysis B-Environmental, 2015. **166**: p. 251-259.

184. Tan, L.L., W.J. Ong, S.P. Chai, and A.R. Mohamed, *Visible-light-activated oxygen-rich $TiO_2$ as next generation photocatalyst: Importance of annealing temperature on the photoactivity toward reduction of carbon dioxide.* Chemical Engineering Journal, 2016. **283**: p. 1254-1263.

185. Tan, L.L., W.J. Ong, S.P. Chai, B.T. Goh, and A.R. Mohamed, *Visible-light-active oxygen-rich $TiO_2$ decorated 2D graphene oxide with enhanced photocatalytic activity toward carbon dioxide reduction.* Applied Catalysis B-Environmental, 2015. **179**: p. 160-170.

186. Jiao, J.Q., Y.C. Wei, Z. Zhao, W.J. Zhong, J. Liu, J.M. Li, A.J. Duan, and G.Y. Jiang, *Synthesis of 3D ordered macroporous $TiO_2$-supported Au nanoparticle photocatalysts and their photocatalytic performances for the reduction of $CO_2$ to methane.* Catalysis Today, 2015. **258**: p. 319-326.

187. Cybula, A., M. Klein, A. Zielinska-Jurek, M. Janczarek, and A. Zaleska, *Carbon Dioxide Photoconversion. The effect of Titanium Dioxide Immobilization Conditions and Photocatalyst Type.* Physicochemical Problems of Mineral Processing, 2012. **48**(1): p. 159-167.

188. Colina-Marquez, J., F. Machuca-Martinez, and G.L. Puma, *Radiation Absorption and Optimization of Solar Photocatalytic Reactors for Environmental Applications.* Environmental Science & Technology, 2010. **44**(13): p. 5112-5120.

189. Augugliaro, V., V. Loddo, and M. Schiavello, *Heterogeneous photocatalytic reactors: An assessment of fundamental engineering aspects.* Heterogeneous Photocatalysis, 1997. **3**: p. 169-189.

190. Koo, H.-J. and O.D. Velev, *Biomimetic photocatalytic reactor with a hydrogel-embedded microfluidic network.* Journal of Materials Chemistry A, 2013. **1**(37): p. 11106-11110.

191. Mahmodi, G., S. Sharifnia, M. Madani, and V. Vatanpour, *Photoreduction of carbon dioxide in the presence of $H_2$, $H_2O$ and $CH_4$ over $TiO_2$ and ZnO photocatalysts.* Solar Energy, 2013. **97**: p. 186-194.

192. Merajin, M.T., S. Sharifnia, S.N. Hosseini, and N. Yazdanpour, *Photocatalytic conversion of greenhouse gases ($CO_2$ and $CH_4$) to high value products using $TiO_2$*

*nanoparticles supported on stainless steel webnet.* Journal of the Taiwan Institute of Chemical Engineers, 2013. **44**(2): p. 239-246.

193. Tahir, M. and N.S. Amin, *Photocatalytic $CO_2$ reduction with $H_2O$ vapors using montmorillonite/$TiO_2$ supported microchannel monolith photoreactor.* Chemical Engineering Journal, 2013. **230**: p. 314-327.

194. Lee, W.-H., C.-H. Liao, M.-F. Tsai, C.-W. Huang, and J.C.S. Wu, *A novel twin reactor for $CO_2$ photoreduction to mimic artificial photosynthesis.* Applied Catalysis B-Environmental, 2013. **132**: p. 445-451.

195. Wang, Y., Y. Chen, Y. Zuo, F. Wang, J. Yao, B. Li, S. Kang, X. Li, and L. Cui, *Hierarchically mesostructured $TiO_2$/graphitic carbon composite as a new efficient photocatalyst for the reduction of $CO_2$ under simulated solar irradiation.* Catalysis Science & Technology, 2013. **3**(12): p. 3286-3291.

196. de Lasa, H., B. Serrano, and M. Salaices, *Novel Photocatalytic Reactors for Water and Air Treatment*, in *Photocatalytic Reaction Engineering*. 2005, Springer US. p. 17-47.

197. Shockley, W. and H.J. Queisser, *Detailed Balance Limit of Efficiency of P-N Junction Solar Cells.* Journal of Applied Physics, 1961. **32**(3): p. 510-&.

198. Conibeer, G., *Third-generation photovoltaics.* Materials Today, 2007. **10**(11): p. 42-50.

199. Ola, O. and M.M. Maroto-Valer, *Review of material design and reactor engineering on $TiO_2$ photocatalysis for $CO_2$ reduction.* Journal of Photochemistry and Photobiology C: Photochemistry Reviews, 2015. **24**: p. 16-42.

200. Fogler, H.S., *Elements of chemical reaction engineering*. 3rd ed. 1999: Prentice Hall PTR.

201. Corma, A. and H. Garcia, *Photocatalytic reduction of $CO_2$ for fuel production: Possibilities and challenges.* Journal of Catalysis, 2013. **308**: p. 168-175.

202. Herrmann, J.M., *Heterogeneous photocatalysis: fundamentals and applications to the removal of various types of aqueous pollutants.* Catalysis Today, 1999. **53**(1): p. 115-129.

203. Rossetti, I., A. Villa, C. Pirola, L. Prati, and G. Ramis, *A novel high-pressure photoreactor for $CO_2$ photoconversion to fuels.* RSC Advances, 2014. **4**(55): p. 28883-28885.

204. Avery, H.E., *Basic reaction kinetics and mechanisms*. 1974: Macmillan, 1974.

205. Nahar, S., M.F.M. Zain, A.A.H. Kadhum, H.A. Hasan, and M.R. Hasan, *Advances in Photocatalytic $CO_2$ Reduction with Water: A Review.* Materials, 2017. **10**(6).

206. Anthony, J., *Design of experiments for engineers and scientists*. 2nd ed. ed. 2014, London: London: Elsevier. 208.

207. Echtermeyer, A., Y. Amar, J. Zakrzewski, and A. Lapkin, *Self-optimisation and model-based design of experiments for developing a C-H activation flow process.* Beilstein Journal of Organic Chemistry, 2017. **13**: p. 150-163.

208. Delavari, S. and N.A.S. Amin, *Photocatalytic conversion of $CO_2$ and $CH_4$ over immobilized titania nanoparticles coated on mesh: Optimization and kinetic study.* Applied Energy, 2016. **162**: p. 1171-1185.

209. Huang, Z., K. Teramura, S. Hosokawa, and T. Tanaka, *Fabrication of well-shaped $Sr_2KTa_5O_{15}$ nanorods with a tetragonal tungsten bronze structure by a flux method for artificial photosynthesis.* Applied Catalysis B-Environmental, 2016. **199**: p. 272-281.

210. Urasaki, K., Y. Tanpo, Y. Nagashima, R. Kikuchi, and S. Satokawa, *Effects of preparation conditions of $Ni/TiO_2$ catalysts for selective CO methanation in the reformate gas.* Applied Catalysis A-General, 2013. **452**: p. 174-178.

211. Yang, L., P. Liu, X. Li, and S. Li, *The photo-catalytic activities of neodymium and fluorine doped $TiO_2$ nanoparticles.* Ceramics International, 2012. **38**(6): p. 4791-4796.

212. Lin, Y.-C., S.-H. Liu, H.-R. Syu, and T.-H. Ho, *Synthesis, characterization and photocatalytic performance of self-assembled mesoporous $TiO_2$ nanoparticles.* Spectrochimica Acta Part a-Molecular and Biomolecular Spectroscopy, 2012. **95**: p. 300-304.

213. Liu, D., Y. Fernandez, O. Ola, S. Mackintosh, M. Maroto-Valer, C.M.A. Parlett, A.F. Lee, and J.C.S. Wu, *On the impact of Cu dispersion on $CO_2$ photoreduction over $Cu/TiO_2$.* Catalysis Communications, 2012. **25**: p. 78-82.

214. Mao, J., L. Ye, K. Li, X. Zhang, J. Liu, T. Peng, and L. Zan, *Pt-loading reverses the photocatalytic activity order of anatase $TiO_2$ {001} and {010} facets for photoreduction of $CO_2$ to $CH_4$.* Applied Catalysis B-Environmental, 2014. **144**: p. 855-862.

215. de Lasa, H., B. Serrano, and M. Salaices, *Photocatalytic Reaction Engineering*. 2006: Springer US.

216. Salaices, M., B. Serrano, and H.I. de Lasa, *Photocatalytic conversion of phenolic compounds in slurry reactors.* Chemical Engineering Science, 2004. **59**(1): p. 3-15.

217. Morris, A.J., G.J. Meyer, and E. Fujita, *Molecular Approaches to the Photocatalytic Reduction of Carbon Dioxide for Solar Fuels.* Accounts of Chemical Research, 2009. **42**(12): p. 1983-1994.

218. Ola, O., M. Maroto-Valer, D. Liu, S. Mackintosh, C.-W. Lee, and J.C.S. Wu, *Performance comparison of $CO_2$ conversion in slurry and monolith photoreactors using Pd and Rh-$TiO_2$ catalyst under ultraviolet irradiation.* Applied Catalysis B-Environmental, 2012. **126**: p. 172-179.

219. Boudart, M., *Turnover Rates in Heterogeneous Catalysis.* Chemical Reviews, 1995. **95**(3): p. 661-666.

220. Kiatphuengporn, S., M. Chareonpanich, and J. Limtrakul, *Effect of unimodal and bimodal MCM-41 mesoporous silica supports on activity of Fe-Cu catalysts for $CO_2$ hydrogenation.* Chemical Engineering Journal, 2014. **240**: p. 527-553.

221. Tamaki, Y., T. Morimoto, K. Koike, and O. Ishitani, *Photocatalytic $CO_2$ reduction with high turnover frequency and selectivity of formic acid formation using Ru(II) multinuclear complexes.* Proceedings of the National Academy of Sciences of the United States of America, 2012. **109**(39): p. 15673-15678.

222. Eaton, T.R., M.P. Campos, K.A. Gray, and J.M. Notestein, *Quantifying accessible sites and reactivity on titania-silica (photo) catalysts: Refining TOF calculations.* Journal of Catalysis, 2014. **309**: p. 156-165.

223. Wachs, I.E., S.P. Phivilay, and C.A. Roberts, *Reporting of Reactivity for Heterogeneous Photocatalysis.* ACS Catalysis, 2013. **3**(11): p. 2606-2611.

224. Aresta, M., A. Dibenedetto, and A. Angelini, *Catalysis for the Valorization of Exhaust Carbon: from $CO_2$ to Chemicals, Materials, and Fuels. Technological Use of $CO_2$.* Chemical Reviews, 2014. **114**(3): p. 1709-1742.

225. Stockbridge, R.B., C.A. Lewis, Y. Yuan, and R. Wolfenden, *Impact of temperature on the time required for the establishment of primordial biochemistry, and for the evolution of enzymes.* Proceedings of the National Academy of Sciences of the United States of America, 2010. **107**(51): p. 22102-22105.

226. Van Gerven, T., G. Mul, J. Moulijn, and A. Stankiewicz, *A review of intensification of photocatalytic processes.* Chemical Engineering and Processing, 2007. **46**(9): p. 781-789.

227. Grigioni, I., M.V. Dozzi, M. Bernareggi, G.L. Chiarello, and E. Selli, *Photocatalytic $CO_2$ reduction vs. $H_2$ production: The effects of surface carbon-containing impurities on the performance of $TiO_2$-based photocatalysts.* Catalysis Today, 2017. **281**(Part 1): p. 214-220.

228. Huo, P.W., M. Reli, L. Matejova, M. Sihor, L. Obalova, K. Koci, and T. Ltd, *A New Gas Phase Photocatalytic Reactor for $CO_2$ Conversion: Optimal Photoreduction Conditions with $TiO_2$ P25 Photocatalyst.* Nanocon 2015: 7th International Conference on Nanomaterials - Research & Application, 2015: p. 236-241.

229. Coridan, R.H., A.C. Nielander, S.A. Francis, M.T. McDowell, V. Dix, S.M. Chatman, and N. Lewis, *Methods for Comparing the Performance of Energy-Conversion Systems for Use in Solar Fuels and Solar Electricity Generation.* Energy & Environmental Science, 2015.

230. Ola, O., *Effect of Metal Doping and Supports on $TiO_2$-based Catalysts for $CO_2$ Photoreduction*, in *School of Engineering and Physical Sciences*. 2014, Heriot-Watt University. p. 263.

231. Liu, D., *Effects of Metal Modification on Titanium Dioxide for Photocatalytic Reduction of Carbon Dioxide*. 2012, University of Nottingham. p. 215.

232. Cole-Parmer, I.C. *Tubing Selection Guide*. 03/16/17 [Accessed 2015 October 13].

233. ASSOCIATION, B.S.S. *Selection of stainless steels for handling acetic acid (CH3COOH).* [Accessed 2014 January 16].

234. Hong, J.D., W. Zhang, J. Ren, and R. Xu, *Photocatalytic reduction of $CO_2$: a brief review on product analysis and systematic methods.* Analytical Methods, 2013. **5**(5): p. 1086-1097.

235. Olivo, A., *Development of titanium dioxide based photocatalytic systems for $CO_2$ photoreduction* in *Universita Degli Studi di Trieste e Universita Ca' Foscari di Venezia* 2017, Ca' Foscari University of Venice: Venice, Italy. p. 198.

236. Gupta, S.M. and M. Tripathi, *A review on the synthesis of $TiO_2$ nanoparticles by solution route.* Central European Journal of Chemistry, 2012. **10**(2): p. 279-294.

237. Schwenzer, B., L. Wang, J.S. Swensen, A.B. Padmaperuma, G. Silverman, R. Korotkov, and D.J. Gaspar, *Tuning the Optical Properties of Mesoporous $TiO_2$ Films by Nanoscale Engineering.* Langmuir, 2012. **28**(26): p. 10072-10081.

238. Brinker, C.J., Y.F. Lu, A. Sellinger, and H.Y. Fan, *Evaporation-induced self-assembly: Nanostructures made easy.* Advanced Materials, 1999. **11**(7): p. 579-+.

239. Zhao, D.Y., J.L. Feng, Q.S. Huo, N. Melosh, G.H. Fredrickson, B.F. Chmelka, and G.D. Stucky, *Triblock copolymer syntheses of mesoporous silica with periodic 50 to 300 angstrom pores.* Science, 1998. **279**(5350): p. 548-552.

240. Bay, E.R.B., *Synthesis of novel modified-$TiO_2$ photocatalysts and characterization testing for enhanced interaction with $CO_2$ during photoreduction*, in *School of Engineering and Physical Sciences*. 2013, Heriot-Watt University. p. 75.

241. Jansson, J., K. Schillen, M. Nilsson, O. Soderman, G. Fritz, A. Bergmann, and O. Glatter, *Small-angle X-ray scattering, light scattering, and NMR study of PEO-PPO-PEO triblock copolymer/cationic surfactant complexes in aqueous solution.* Journal of Physical Chemistry B, 2005. **109**(15): p. 7073-7083.

242. Pinna, F., A. Olivo, V. Trevisan, F. Menegazzo, M. Signoretto, M. Manzoli, and F. Boccuzzi, *The effects of gold nanosize for the exploitation of furfural by selective oxidation.* Catalysis Today, 2013. **203**: p. 196-201.

243. Watson, J.T. and O.D. Sparkman, *Introduction to mass spectrometry : instrumentation, applications and strategies for data interpretation* 4th ed. ed. 2007, England: John Wiley & Sons.

244. Davis, R. and M. Frearson, *Mass spectrometry: analytical chemistry by open learning*. 1987, Great Britain: John Wiley & Sons. 603.

245. Sparkman, O.D., Z.E. Penton, and F.G. Kitson, *Chapter 4 - Mass Spectrometry Instrumentation*, in *Gas Chromatography and Mass Spectrometry (Second edition)*. 2011, Academic Press: Amsterdam. p. 89-148.

246. Boyd, R.K., J.D. Henion, M. Alexander, W.L. Budde, J.D. Gilbert, S.M. Musser, C. Palmer, and E.K. Zurek, *Mass spectrometry and good laboratory practices.* Journal of the American Society for Mass Spectrometry, 1996. **7**(2): p. 211-218.

247. Turner, P., S. Taylor, E. Clarke, C. Harwood, K. Cooke, and H. Frampton, *Calibration effects during natural gas analysis using a quadrupole mass spectrometer.* Trac-Trends in Analytical Chemistry, 2004. **23**(4): p. 281-287.

248. Patience, G.S., *Chapter 2 - Measurement and Analysis*, in *Experimental Methods and Instrumentation for Chemical Engineers*. 2013, Elsevier: Amsterdam. p. 15-66.

249. Liu, Y., S. Zhou, J.M. Li, Y.J. Wang, G.Y. Jiang, Z. Zhao, B. Liu, X.Q. Gong, A.J. Duan, J. Liu, Y.C. Wei, and L.Q. Zhang, *Photocatalytic reduction of $CO_2$ with water vapor on surface La-modified $TiO_2$ nanoparticles with enhanced $CH_4$ selectivity.* Applied Catalysis B-Environmental, 2015. **168**: p. 125-131.

250. Matejova, L., K. Koci, M. Reli, L. Capek, V. Matejka, O. Solcova, and L. Obalova, *On sol-gel derived Au-enriched $TiO_2$ and $TiO_2$-$OZrO_2$ Photocatalysts and their investigation in photocatalytic reduction of carbon dioxide.* Applied Surface Science, 2013. **285**: p. 688-696.

251. Xie, S.J., Y. Wang, Q.H. Zhang, and W.P. Deng, *MgO- and Pt-Promoted $TiO_2$ as an Efficient Photocatalyst for the Preferential Reduction of Carbon Dioxide in the Presence of Water.* ACS Catalysis, 2014. **4**(10): p. 3644-3653.

252. Zhai, Q.G., S.J. Xie, W.Q. Fan, Q.H. Zhang, Y. Wang, and W.P. Deng, *Photocatalytic Conversion of Carbon Dioxide with Water into Methane: Platinum and Copper(I) Oxide Co-catalysts with a Core-Shell Structure.* Angewandte Chemie-International Edition, 2013. **52**(22): p. 5776-5779.

253. Wu, J.C.S., *Photocatalytic Reduction of Greenhouse Gas $CO_2$ to Fuel.* Catalysis Surveys from Asia, 2009. **13**(1): p. 30-40.

254. Tu, W.G., Y. Zhou, Q. Liu, Z.P. Tian, J. Gao, X.Y. Chen, H.T. Zhang, J.G. Liu, and Z.G. Zou, *Robust Hollow Spheres Consisting of Alternating Titania Nanosheets and Graphene Nanosheets with High Photocatalytic Activity for $CO_2$ Conversion into Renewable Fuels.* Advanced Functional Materials, 2012. **22**(6): p. 1215-1221.

255. Zhou, S., Y. Liu, J.M. Li, Y.J. Wang, G.Y. Jiang, Z. Zhao, D.X. Wang, A.J. Duan, J. Liu, and Y.C. Wei, *Facile in situ synthesis of graphitic carbon nitride (g-$C_3N_4$)-N-$TiO_2$ heterojunction as an efficient photocatalyst for the selective photoreduction of $CO_2$ to CO.* Applied Catalysis B-Environmental, 2014. **158**: p. 20-29.

256. Dong, C.Y., M.Y. Xing, and J.L. Zhang, *Economic Hydrophobicity Triggering of $CO_2$ Photoreduction for Selective $CH_4$ Generation on Noble-Metal-Free $TiO_2$-$SiO_2$.* Journal of Physical Chemistry Letters, 2016. **7**(15): p. 2962-2966.

257. Collado, L., A. Reynal, J.M. Coronado, D.P. Serrano, J.R. Durrant, and V.A.D. O'Shea, *Effect of Au surface plasmon nanoparticles on the selective $CO_2$ photoreduction to $CH_4$.* Applied Catalysis B-Environmental, 2015. **178**: p. 177-185.

258. Liu, L., Z.B. Liu, H.G. Sun, and X. Zhao, *Morphological effects of Au-13 clusters on the adsorption of $CO_2$ over anatase $TiO_2(101)$.* Applied Surface Science, 2017. **399**: p. 469-479.

259. Usubharatana, P., D. McMartin, A. Veawab, and P. Tontiwachwuthikul, *Photocatalytic process for $CO_2$ emission reduction from industrial flue gas streams.* Industrial & Engineering Chemistry Research, 2006. **45**(8): p. 2558-2568.

260. Yi, X.S., W.X. Shi, S.L. Yu, X.H. Li, N. Sun, and C. He, *Factorial design applied to flux decline of anionic polyacrylamide removal from water by modified polyvinylidene fluoride ultrafiltration membranes.* Desalination, 2011. **274**(1-3): p. 7-12.

261. Neatu, S., J.A. Macia-Agullo, and H. Garcia, *Solar Light Photocatalytic $CO_2$ Reduction: General Considerations and Selected Bench-Mark Photocatalysts.* International Journal of Molecular Sciences, 2014. **15**(4): p. 5246-5262.

262. Osterwald, C.R., *Chapter III-2 - Standards, Calibration, and Testing of PV Modules and Solar Cells*, in *Practical Handbook of Photovoltaics (Second Edition)*, A. McEvoy, T. Markvart, and L. Castañer, Editors. 2012, Academic Press: Boston. p. 1045-1069.

263. Caravaca, A., H. Daly, M. Smith, A. Mills, S. Chansai, and C. Hardacre, *Continuous flow gas phase photoreforming of methanol at elevated reaction temperatures sensitised by $Pt/TiO_2$.* Reaction Chemistry & Engineering, 2016. **1**(6): p. 649-657.

264. Puga, A.V., A. Forneli, H. García, and A. Corma, *Hydrogen Production: Production of $H_2$ by Ethanol Photoreforming on $Au/TiO_2$.* Advanced Functional Materials, 2014. **24**(2): p. 240-240.

265. Perry, R.H. and D.W. Green, *Perry's Chemical Engineers' Handbook*. 7th ed. 1997: McGraw-Hill.

266. Jones, B., E.D. Schoen, and D.C. Montgomery, *A comparison of two-level designs to estimate all main effects and two-factor interactions.* Quality Engineering, 2016. **28**(4): p. 369-380.

267. Perkampus, H.-H., *UV-VIS Spectroscopy and Its Applications*. Vol. 1. 1992, Berlin Heidelberg Germany: Springer-Verlag 244.

268. Weckhuysen, B.M., *Ultraviolet-Visible Spectroscopy*, in *In-situ Spectroscopy of Catalysts*, B.M. Weckhuysen, Editor. 2004, American Scientific Publishers. p. 350.

269. Bredas, J.L., *Mind the gap!* Materials Horizons, 2014. **1**(1): p. 17-19.

270. Park, S.-J., Y.C. Kang, J.Y. Park, E.A. Evans, R.D. Ramsier, and G.G. Chase, *Physical Characteristics of Titania Nanofibers Synthesized by Sol-Gel and Electrospinning Techniques.* Journal of Engineered Fibers and Fabrics, 2010. **5**(1): p. 50-56.

271. Zhang, Y.J., W. Yan, Y.P. Wu, and Z.H. Wang, *Synthesis of $TiO_2$ nanotubes coupled with CdS nanoparticles and production of hydrogen by photocatalytic water decomposition.* Materials Letters, 2008. **62**(23): p. 3846-3848.

272. Murphy, A.B., *Band-gap determination from diffuse reflectance measurements of semiconductor films, and application to photoelectrochemical water-splitting.* Solar Energy Materials and Solar Cells, 2007. **91**(14): p. 1326-1337.

273. Viezbicke, B.D., S. Patel, B.E. Davis, and D.P. Birnie, *Evaluation of the Tauc method for optical absorption edge determination: ZnO thin films as a model system.* Physica Status Solidi B-Basic Solid State Physics, 2015. **252**(8): p. 1700-1710.

274. Reyes-Coronado, D., G. Rodríguez-Gattorno, C. Cab, R. De Coss, G. Oskam, and M.E. Espinosa-Pesqueira, *Phase-pure $TiO_2$ nanoparticles: Anatase, brookite and rutile.* Nanotechnology, 2008. **19**(14).

275. Toyoda, T. and I. Tsuboya, *Apparent band-gap energies of mixed $TiO_2$ nanocrystals with anatase and rutile structures characterized with photoacoustic spectroscopy.* Review of Scientific Instruments, 2003. **74**(1): p. 782-784.